Universitat Autònoma de Barcelona

Rapid diagnostic test for the detection of communicable diseases

Alejandra Ben Aissa Soler

Universitat Autònoma de Barcelona

Rapid diagnostic test for the detection of communicable diseases

Alejandra Ben Aissa Soler

Supervisora: Prof. Maria Isabel Pividori

Tesi Doctoral

Programa Doctorat de Química

Departament de Química

Facultat de Ciències
Universitat Autònoma de Barcelona

2020

Thesis submitted to aspire for the Doctor Degree

Alejandra Ben Aissa Soler

Director´s approval:

Dr. Maria Isabel Pividori Gurgo
Departament de Química
Universitat Autònoma de Barcelona

Bellaterra (Cerdanyola del Valles), January 2020

Table of contents

List of Abbreviations and Symbols

Ab	Antibody
AEC	3-amino-9-ethylcarbazole
Ag	Antigen
AIBN	2,2'azobisisobutyronitrile
ATP	Adenosine triphosphate
BIO	Biotin
BIP	Backward Inner Primer
bp	Base pair
BSA	Bovine serum albumin
BSL-2	Biosafety level 2
C2CA	Circle-to-circle amplification
CCD	Charge-coupled device
cDNA	complementary DNA
CFU	Colony-forming unit
CMOS	Complementary metal–oxide–semiconductor
CNF	Cellulose nanofibril
CNPs	Carbon nanoparticles
Cy3	Cyanine 3
Cy5	Cyanine 5
dATP	Deoxyadenosine triphosphate
dCTP	Deoxycytidine triphosphate
dGTP	Deoxyguanosine triphosphate
DIG	Diogoxinin
DNA	Deoxyribonucleic acid
dsDNA	Double stranded DNA
dTTP	Deoxythymidine triphosphate
DTT	DL-Dithiothreitol
EGDMA	Ethylene glycol dimetacrilate
EDS	Energy-dispersive X-ray spectroscopy
EDTA	Ethylenediaminetetraacetic acid
EIA	Enzyme Immunoassay
ELISA	Enzyme-Linked ImmunoSorbent Assay
FACS	Fluorescence-activated cell sorting
FET	Field-effect transistor-based
FIP	Forward Inner Primer
FLU	Fluorescein
Fw	Forward
GNPs	Gold nanoparticles
hCG	Human chorionic gonadotropin
HDA	Helicase-dependent amplification
HIV	Human Immunodeficiency Virus
HRP	Horseradish peroxidase
HUS	hemolytic uremic syndrome

HQ	Hydroquinone
IgG	Immunoglobulin G
IgM	Immunoglobulin M
IMS	Immunomagnetic separation
IVD	In vitro diagnostics
LAMP	Loop-mediated isothermal amplification
LB	Luria-Bertani, Lysogeny broth
LC-MS	Liquid chromatography–mass spectrometry
LFA	Lateral flow assay
LH	Luteinizing hormone
LOD	Limit of detection
LOQ	Limit of quantification
LxWxH	Length x width x height
MALDI-TOF MS	Matrix-assisted laser desorption/ionization time-of-flight mass spectrometer
MES	2-(N-morpholino)ethanesulfonic acid
m-GEC	Magneto- graphite-epoxy composite
MIPs	Molecularly imprinted polymers
MNPs	Magnetic nanoparticles
MPs	Magnetic particles
MPS	3-methacryloxypropyltrimethyloxysilane
MW	Molecular weight
NALF	Nucleic acid lateral flow
NASBA	Nucleic acid sequence-based amplification
NAVF	Nucleic acid vertical flow
NC	Nitrocellulose
NIR	Near-infrared
NIPs	Non-molecularly imprinted polymers
NTA	Nanoparticle Tracking Analysis
PBS	Phosphate-buffered saline
PBSE	Phosphate-buffered saline (electrochemical)
PBST	Phosphate-buffered saline with Tween® detergent
PCR	Polymerase chain reaction
PMF	Peptide mass fingerprint
PoC	Point of care
PoN	Point of Need
PVDF	Polyvinylidene fluoride
PVP	Polyvinylpyrrolidone
QDs	Quantum dots
qPCR	Quantitative polymerase chain reaction
RCA	Rolling circle amplification
RCPs	Rolling circle products
RDTs	Rapid diagnostic tests
RNA	Ribonucleic acid
RPA	Recombinase polymerase amplification
rpm	Revolutions per minute
RT	Room temperature
RT-PCR	Reverse transcription polymerase chain reaction
Rv	Reverse

SCC	Saline-sodium citrate buffer
SD	Standard desviation
SDA	Strand Displacement Amplification
SEM	Scanning electron microscope
SIPs	Surface imprinted polymers
SSB	Single-strand DNA-binding protein
ssDNA	Single stranded DNA
SPE	Screen printed electrodes
SPR	Surface plasmon resonance
STEC	Shiga toxin-producing *E. coli*
Strep-Cy5	Streptavidin-cyanine 5
StreptAv	Streptavidin
StreptAv-AuNPs	Streptavidin gold nanoparticles
SWV	Square wave voltammetry
TAE	Tris base, acetic acid and EDTA buffer
TB	Tuberculosis
TE	Tris EDTA buffer
TEM	Transmission electron microscopy
TEOS	Tetraethoxy silane
TMA	Transcription-mediated amplification
TMB	3,3′,5,5′-Tetramethylbenzidine
Tosyl-MPs	Tosyl Active Magnetic Particles
TSA	Trypticase soy agar
TSB	Tryptic Soy Broth
UCP	Up-converting particles
UTI	Urinary tract infecction
3SR	Self-sustained Sequence Replication
µPADs	Microfluidic paper-based analytical devices
§	Section

CHAPTER 1

Introduction

1. Technological challenges in the detection of communicable diseases

Point of Need (PoN) diagnostics refer to the diagnosis assays able to be performed outside the facilities of a centralized clinical laboratory. Their main goal is to provide, in most of the instances, a rapid result in a low resource setting. To achieve that, it is mandatory to simplify the analytical procedure in order to be performed by non-skilled personnel, and to shorten the time of analysis, bringing them exactly to the point where they are needed. These features provide a considerable save of money by reducing the time and cost of intervention and transport. Besides all these advantages, another key feature of these platforms is the low cost per assay which allows their implementation in disposable formats.

Due to all these added values, this technology has caused a huge impact on myriads of fields such as environmental(1) monitoring or forensics(2) or food industry(3) where they have become essential for the onsite rapid detection of analytes.

The concept of point of need has been more exploited in the field of healthcare than in any other and it is commonly known as point of care (PoC)(4).

PoC testing has skyrocketed in the last 20 years(5). The increasing demand for accurate and fast clinical testing inside and outside the hospital setting is mainly due to population ageing and the subsequent increase in the number of chronic diseases. PoC tests have proven to be a key tool in the monitoring of pathologies such as diabetes mellitus, hypertension, chronic kidney disease or even congestive heart failure either at physician office or at home(6).

Moreover, the rapid provision of results of these tests at low cost are especially valuable for the fast screening of gases in blood and rapid diagnosis of stroke, severe sepsis, urinary tract infections, acute coronary syndrome, thrombosis or hyperkalemia among many others in the emergency department or primary care centres(7).

On the other hand, these devices are especially useful in low-resource settings in which rapid and reliable diagnostic tools operated by non-trained personnel are

strongly appreciated for the early detection of communicable diseases. These diseases are caused by bacteria, virus, protozoa, fungi, multicellular parasites and prions that are spread through contact with bodily fluids, skin contact, insect bites, through the air or even contaminated objects(8). In most of the instances, prevention and treatment with biosecurity measures, rapid detection, antibiotics and vaccines have made major progress in the control of most threatening and deadly communicable diseases in the developed world(9). However, countries under development with scare resources and facilities still have a significant burden of these diseases.

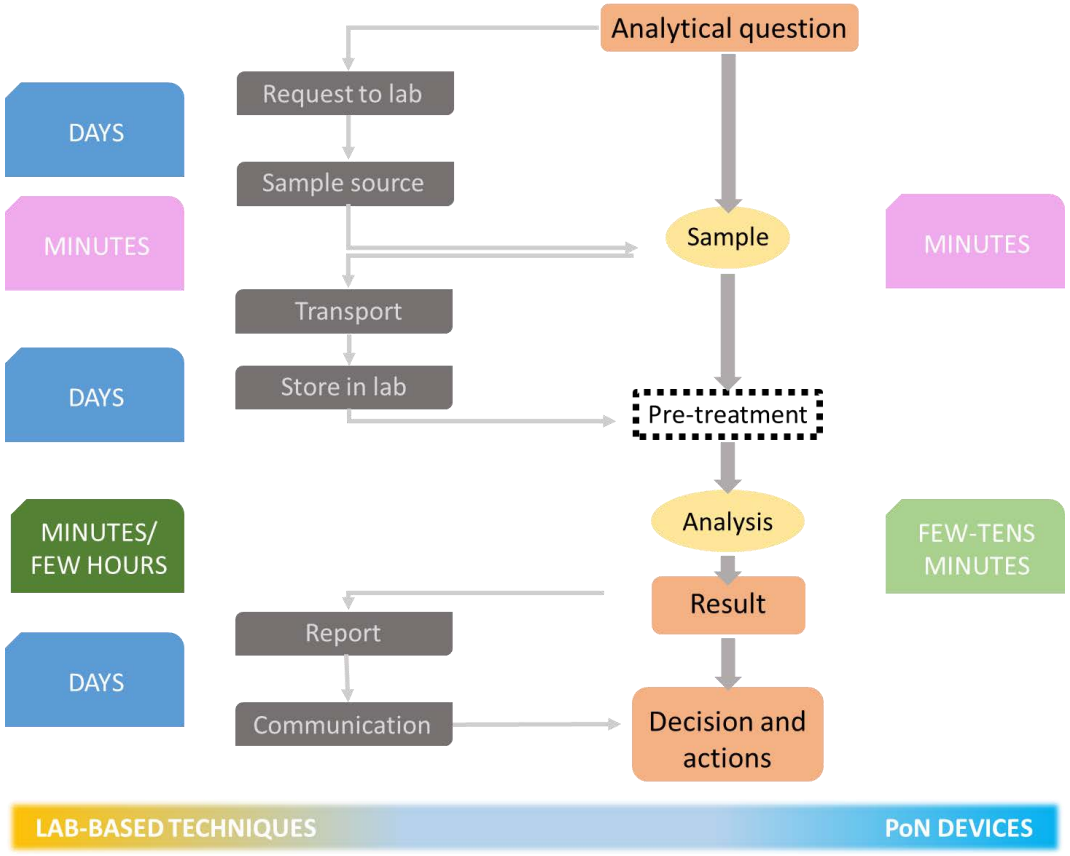

Figure 1.1. Schematic workflow for laboratory-based and for point-of-need testing. Figure adapted from reference(4).

Among these communicable diseases, emerging viral zoonotic diseases transmitted by vectors, for instance mosquitoes, including dengue, chikungunya, yellow fever, Zika or those caused by parasites such as malaria are currently generating outbreaks disregarding borders. Others are transmitted from person to person such

as Ebola, hepatitis or HIV. Most outbreaks generate humanitarian crisis and are responsible for thousands of deaths(10).

Acute respiratory infections are the main cause of morbidity for communicable diseases worldwide(11). Pneumonia is a lower respiratory tract infection, mainly caused by streptococcus, represents one of the main causes of death in children under 5 years of age in developing countries(12). On the other, tuberculosis (TB), caused by Mycobacterium tuberculosis, has caused more deaths in the last hundred years than influenza and HIV combined(13). Millions of people die annually due to TB and drug-resistant TB(14). This disease is spread from person to person through the air and only a few of these germs inhaled are necessary to become infected. However, the risk of falling ill is much higher in immunocompromised people such as HIV infected or malnourished(15).

Besides the zoonotic and person to person communicable diseases, the lack of access to safe food and clean water promote the intoxication with bacteria such as Vibrio cholerae, Listeria, Salmonella or E.coli among many other foodborne pathogens.

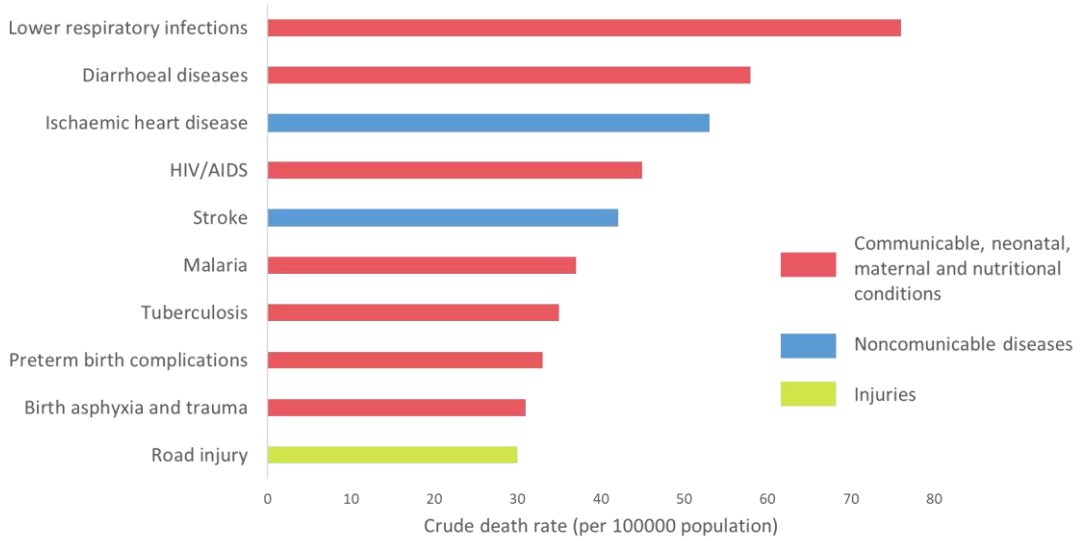

Figure 1.2. Ranking of the top 10 causes of death in low-income countries in 2016. Figure adapted from reference (16).

Cholera is caused by some strains of the bacterium *Vibrio cholerae*. It is spread mostly by unsafe water and unsafe food that has been contaminated with human faeces containing the bacteria. Their symptoms are severe watery diarrhoea,

vomiting and muscle cramps. Diarrhoea can lead to dehydration and electrolyte imbalance, resulting in sunken eyes, wrinkling of the hands and feet that can also turn bluish. Cholera affects an estimated 3–5 million people worldwide and causes 28,800–130,000 deaths a year(17).

Listeria monocytogenes is a species of pathogenic bacteria that can be found in soil, water, decaying vegetation and animals. It causes listeriosis, one of the most serious and severe foodborne diseases which mild symptoms include fever, muscle aches, nausea, vomiting, and diarrhoea. If the more severe form of listeriosis develops, symptoms may include headache, stiff neck, confusion, loss of balance, and convulsions and even death in in very young individuals, the elderly and immune-compromised people, with mortality rates of 20-30%(18).

Salmonella is a group of bacteria that causes salmonellosis. This bacterium can be spread by food handlers, food contact surfaces such as packaging material or cutting tools and from animals to people. Most people with salmonellosis develop diarrhoea, fever and abdominal cramps. More severe cases of salmonellosis may include a high fever, aches, headaches, lethargy, a rash, blood in the urine or stool, and in some cases may become fatal. It is one of the most common causes of diarrhoea globally with above 250000 annually deaths(19,20).

E. coli is harmless bacteria that live in the intestines of people and animals and contribute to intestinal health. However, eating or drinking food or water contaminated with certain types of *E. coli* can cause gastrointestinal illness. Generally, the symptoms include severe stomach cramps, diarrhoea, fever, nausea, and/or vomiting. Some types of pathogenic *E. coli*, such as Shiga toxin-producing *E. coli* (STEC), are life-threatening causing a type of kidney failure called hemolytic uremic syndrome (HUS), high blood pressure, chronic kidney disease and neurologic problems. The average number of deaths per year due to E. coli is 5-10 million worldwide(21).

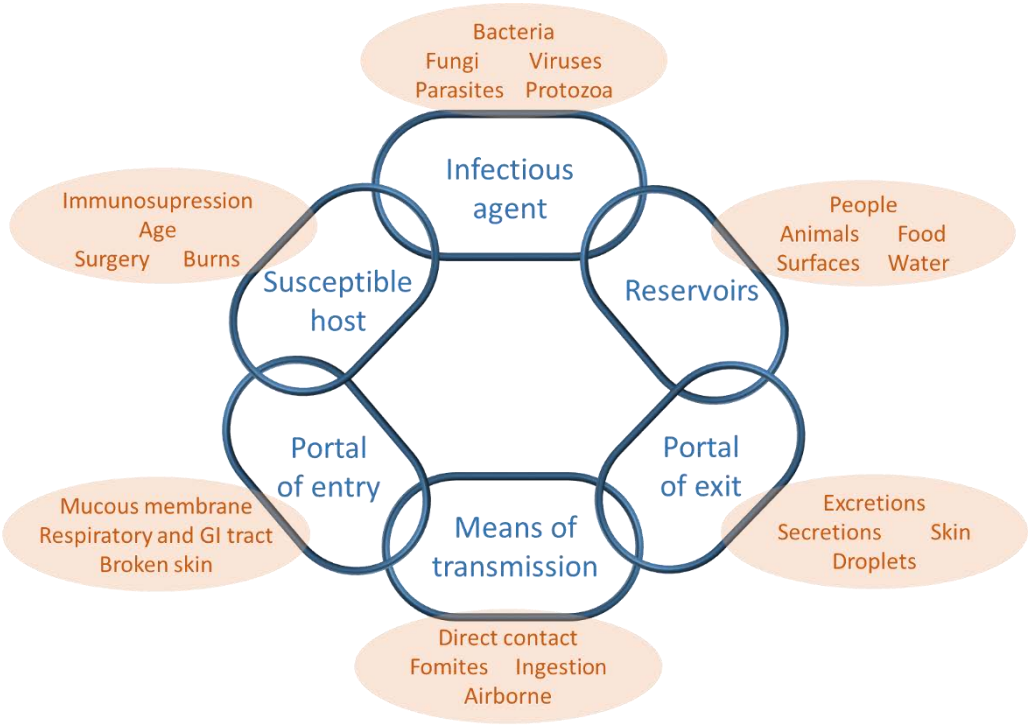

Figure 1.3. Diagram of the chain of infection.

The chain of infection represents the meeting of all the necessary conditions in order for a microbe or infectious disease to be spread from person to person. This process can only occur when all six links in the chain are intact. Therefore, the spread of communicable diseases can be discontinued by interrupting any step of the chain of infection(22). It is, therefore, critical that the scientific research community and international donor agencies continue to increase their efforts with integrated goals of vigilant surveillance, improve treatment and early detection and diagnostic with cost-effective devices even during the incubation period. In that way, transmission to other people, with the consequent economic and personal cost, could be prevented. Next sections address the diagnostic laboratory methods able to disrupt the chain of infection and to prevent the spread of communicable diseases.

2. Laboratory-based techniques

2.1. Microbiological cultures

Culture test, a method created in 19th century(23), still remain as the gold standard for most of the pathogenic agents. This technique uses an adequate medium for the growth of specific microorganism, providing information of the presence, the

amount and the drug effectiveness of that microorganism. The main drawback of this classical method is that it takes a long time to provide a confirmatory result, since the visualization of a colony by a naked eye is the threshold for detection. For instance, it is known to take 2–6 weeks for visual detection of the presence of tuberculosis colonies on the surface of a culture plate. Moreover, the culture test sometimes is extremely dangerous depending on the nature of the microorganism(24).

2.2. Microscopy

Optical microscopy is a technique applied in diagnostics and histology to morphologically determine the presence of pathogens, infectious agents or changes directly from samples like blood, tissues, sputum or food samples. In order to increase the sensitivity and accurate identification of organisms, specific stains or other markers are added to the samples, as well as previous preconcentration steps. Other microscopy techniques such as electron microscopy or AFM have enabled the study of the surfaces and quantitatively probe the interactions between cells(25,26).

2.3. MALDI-TOF

MALDI-TOF MS (matrix-assisted laser desorption/ionization time-of-flight mass spectrometer) is considered the most powerful method for the identification of species as molecular signatures. The sample is mixed with an organic compound which is called matrix. When the sample in the solvent crystallizes, the proteins are ionized with a laser beam. The desorption and further ionization generate singly protonated ions which are then accelerated at a fixed potential. The ionized species are then separated on the basis of their mass-to-charge ratio (m/z)(27). The charged species are then detected and measured using different types of mass analyzers like quadrupole mass analyzers, ion trap analyzers, time of flight (ToF) analyzers, among others. Based on the ToF information, a characteristic spectrum called peptide mass fingerprint (PMF) is generated for analytes in the sample. For microorganism identification, positively charged proteins with a molecular weight between 2000 and 20,000 m/z are used to recognize individual types of bacteria. The identification is done by comparing the individual mass peaks of the PMF from unknown organism with the PMFs contained in the database or by matching the masses of biomarkers

of unknown organism with the proteome database. This technique, which provides very fast results, is limited by the fact that identification of new analytes is only possible if the spectral database already contains peptide mass fingerprints of the type strains of the specific agent(28).

2.4. Molecular methods

Due to the previously discussed disadvantages and limitations of conventional culture techniques, several molecular methods have been increasingly incorporated in laboratories for the detection and characterization of isolates and for the diagnosis of diseases. Molecular biology techniques are common methods used in molecular biology, biochemistry, genetics and biophysics which generally involve manipulation and analysis of DNA, RNA, proteins. The introduction of these timely technologies provides great opportunities for prevention and treatment of infectious diseases. Immunological techniques (§ 2.4) and Nucleic acid-based technologies (§ 2.5) fall in this category. Their main features will be further explained in the next sections.

2.5. Immunological techniques

Immunological methods rely on binding of a specific antibodies (Ab) to an antigens (Ag). The affinity between both components provides the desired high specificity and sensitivity of the immunoassay. Antibodies, also known as immunoglobulins, are molecules generated by the immune system in response to a foreign agent (antigen).

Immunological tests can be designed to detect either an antibody or an antigen. Depending on the pathogen, one of these strategies can be more sensitive than the other. The antigen-antibody complex can be thus detected by labelling either the antigen or the antibody. In the first approach, the specific antibodies (usually IgM and IgG) naturally produced in the patients to combat the pathogen are detected. The IgM is usually considered a biomarker for acute infections. In short, a positive IgM may be a sign of a current, or very recent, infection. On the contrary, IgG is considered a biomarker of past infection, since they are produced once an infection has been going on for a while, and may even be present after the infection has been

completely resolved. In the second approach, the pathogenic agent is directly detected as an antigen, by means of a specific antibody produced by cell culturing or an animal host, which is used as a specific reagent. Next section is focused on the production of antibodies.

2.5.1. Antibody production. Monoclonal and polyclonal antibodies

The classical method of production of polyclonal antibodies, which is now being replaced by animal-friendly approaches, is based on the injection of the antigen for several weeks in animals to produce the specific polyclonal antibodies. The antibodies produced by the animals are collected directly from the blood of the animals. These antibodies are called polyclonal antibodies since they are produced by different B cells clones, producing thus a collection of antibodies with different affinities and binding in slightly different ways to the same antigen. As a result, the final product contains a wide variety of antibodies. On the contrary, a monoclonal antibody is the product of a single B cell clone. The production of monoclonal antibodies is achieved by the combination of B antibody producing cells and immortalized myeloma cells creating immortal hybridoma cells which generates one single type of antibodies in high concentrations. Monoclonal antibodies have higher specificity and lower cross-reactivity than polyclonal antibodies and can be produced indefinitely(29).

When the antigen injected in the animal is an antibody from a second host, the antibodies generated in this case are called antiglobulins. Antiglobulins are thus, developed to recognize a whole antibody class for a specific organism, for instance antibodies against mouse produced in goat.

2.5.2. Fluorescent immunolabeling

Fluorescent immunolabeling is the use of fluorescent dyes for the detection of analytes through their antigen-antibody affinity. A fluorescent dye is conjugated to antibodies to indicate the presence of a particular antigen by the production of fluorescent light under a microscope equipped with a fluorescent light source(30). This labelling can be also applied in immunoassays or immunocytochemistry in

order to confirm the expression and location of target peptides or protein in cells(31).

2.5.3. Enzyme-linked immunosorbent assay

The enzyme-linked immunosorbent assay (ELISA) is a very sensitive method used to detect the presence of antigens or antibodies of interest in a sample. This technique is usually performed in polystyrene microtiter plates where either the antigen or the antibody is immobilized by passive adsorption. The other agent of the immunoassay pair is labelled with an enzyme which in presence of a substrate produces the signal result of this assay. This signal can be directly related to the amount of analyte present in the sample.

ELISA is typically performed using direct, indirect or competitive formats. Direct ELISA involves the passive antigen adsorption onto plate wells by incubation. The unbound excess is removed, and the remaining binding sites of the wells are blocked by using blocking proteins. After, an enzyme labelled antibody is added to the wells and incubated. Again, the excess of reagents is washed away, and the enzyme catalyses the conversion of a substrate into a colorimetric product for a certain time. This reaction is stopped by adding a solution of acid and the resulting colorimetric colour is measured at a specific wavelength(32).

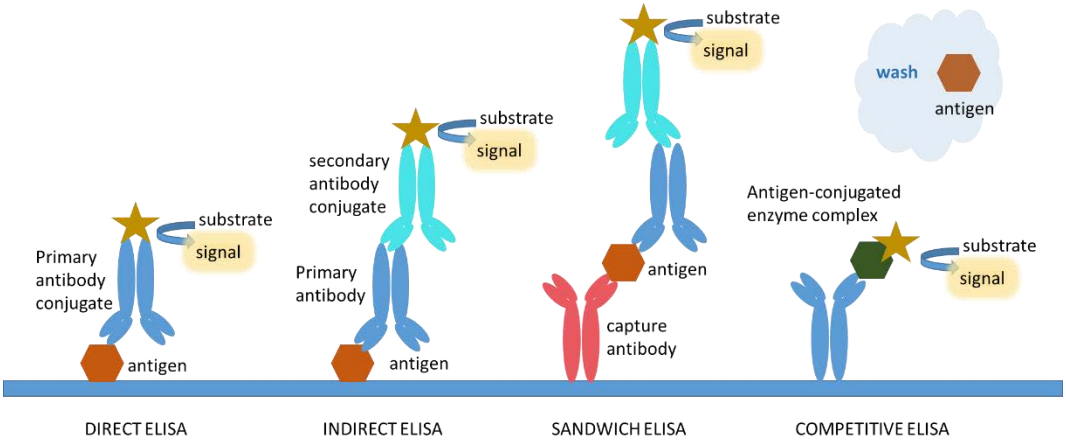

Figure 1.4. Schematic representation of the most relevant ELISAs formats: Direct, Indirect, Sandwich and Competitive immunoassays.

The initial steps in indirect ELISA are very similar to direct ELISA. However, in indirect ELISA, the specific antibody against the antigen is not labelled. In this instance, the labelling involves an additional incubation step performed by a secondary antibody, which is labelled with the enzyme. The secondary antibody specificity is against the immunoglobulins of the species of the first antibody(33). This labelling approach usually increases the sensitivity since many labelled secondary antibodies can bind to each primary antibody molecule(34).

Sandwich ELISA is the most commonly used enzyme immunoassays (EIA) format for the development of a large number of commercial in vitro diagnostics (IVD) kits for the quantification of clinical biomarkers. In a sandwich ELISA, an antibody is immobilized on the microplate and the target analyte binds to it. As in previous formats, the excess of reagents is removed by washing and a second antibody is added and bound to the analyte forming a sandwich immune complex. The sandwich approach can be either direct, if the second antibody is labelled with the enzyme, or indirect if a secondary antibody is used for the readout.

Briefly, in competitive ELISA, the resulting signal is inversely proportional to the concentration of antigen. First the sample is added to the corresponding well and the analyte is bound to the antibody(35). When a labelled control antigen is added a reversible equilibrium is produced. As the analyte is not labelled, the maximum signal will be obtained at its lowest concentrations. This format is usually used for the detection of analytes containing only one epitope, as in the case of the haptens, and therefore was not used in this dissertation.

2.5.4. Western blot

The western blot (also called protein immunoblot) is a technique based on electrophoresis. First, the sample is added to the polyacrylamide gel and separated either by charge and/or size during the electrophoresis. The bands are then electrophoretically transferred onto a nitrocellulose or polyvinylidene fluoride (PVDF) membrane. This membrane is blocked to avoid non-specific adsorption and incubated with enzyme-labelled or radio-labelled antibodies that bind the antigen. After incubation, the bands are revealed with a substrate for enzyme-labelled antibodies or a solution for photographic revealing in case of radio-labelled

substrates. This technique not only allows the separation of the antigen from the sample but also determine its molecular size in order to corroborate its identity(36).

2.5.5. Dot-blot

Dot-blot is the simplification of the western blot technique. The revealing of the proteins is also produced by the addition of labelled antibodies and further incubation with the corresponding substrates. Unlike western blot, in dot blot the previous gel electrophoretic separation is not performed but the sample is directly spotted on the membrane(37). It is a common tool used in genetic testing, for instance in the detection of sickle cell anemia(38) .

2.5.6. Precipitation

Precipitation are based on the reaction of two soluble compounds, such as the antibody and the antigens, producing an insoluble product, which precipitates. When the antigen and the antibody are in optimal ratio, lattices are formed. However, the excess of one of them reduces lattice formation and subsequent precipitation. There are several precipitation methods applied in clinical laboratory for the diagnosis of diseases which can be performed in agar or agarose, or non-gel support media such as cellulose acetate.

The most commonly used serologic precipitation reactions are the Ouchterlony and the Mancini tests. Ouchterlony test is based on double immunodiffusion, a qualitative gel technique that determines the relationship between antigen and antibody whose results can be identity, non-identity, and partial identity(39). Mancini method is based on single radial immunodiffusion, semi-quantitation of proteins by gel diffusion using antibody incorporated in agar(40). The Mancini method results in precipitate ring formation on a thin agarose layer whose diameter correlates with the concentration of proteins in the precipitin(41).

2.5.7. Agglutination

Agglutination test differ from precipitation reactions in the size and solubility of the antigen and in the higher sensitivity of the technique. Agglutination reactions use particulated antigens, usually conjugated to a carrier, such as latex particles, which eventually react with the corresponding serum antibodies generating clumps. The

quality of the result is determined by the time of incubation with the antibody source, amount and avidity of the antigen conjugated to the carrier, and conditions of the test environment. Various methods of agglutination are used in diagnostic immunology and these include flocculation tests(42), latex agglutination(43), direct bacterial agglutination(44), and hemagglutination(45,46).

2.6. Nucleic acid-based techniques

They include many different techniques, based on hybridisations, ranging from amplification techniques, sequencing or DNA/RNA chips and microarrays. All these methods are based on a specific genetic sequence which univocally identify pathogens.

The first step on the ladder of genetics diagnostics was the discovery of DNA. In 1869 Friedrich Miescher identified what he called *nuclein* inside the nuclei of human white blood cells while he wanted to extract the protein content. He realized that he had discovered a new family of substances, equivalent to proteins but with a higher content of phosphorus(47). Some years later, the scientific community started to make the first tentative connections between chromosomes, meiosis, and the inheritance of genes. Around the turn of the 20th century, Albrecht Kossel worked on the study of nuclein Miescher's compound which he renamed deoxyribonucleic acid (DNA) and by 1901 the results of his studies allowed to conclude that DNA was composed of four nitrogen bases: adenine (A), cytosine (C), guanine (G) and thymine (T)(48). Levene was the first to discover the order of a single nucleotide is phosphate-sugar-base, the carbohydrate component of RNA (ribose) and the carbohydrate component of DNA (deoxyribose)In addition, he was the first to correctly identify the way RNA and DNA molecules are put together(49). Later, Avery linked the transformation of bacteria to DNA and demonstrated that genes are composed of DNA(50).

Erwin Chargaff, after developing a new paper-based chromatography method for separating and identifying small amounts of organic material, noticed that DNA composition varies among species and concluded that DNA keeps always an equal proportion of purines and pyrimidines. In detail, the amount of adenine (A) is always

similar to the amount of thymine (T), and the amount of guanine (G) corresponds to cytosine units (C)(51).
This conclusion, together with the image obtained from Rosalind Franklin X-ray crystallography(52), were the keys for the construction of Watson and Crick double-helical modelling of DNA(53).
This discovery and the rapid growth of related technologies have radically transformed biological science and has accelerated progress in forensics, food and medical diagnostics.

2.6.1. DNA amplification techniques

These techniques, which allow the copying of millions of DNA sequences beginning with minute DNA samples, have become routinely laboratory techniques in biochemical and diagnostics laboratories. Polymerase chain reaction and isothermal amplification techniques will be further dicussed in the next sections (§§ 2.6.2 and 2.6.3, respectively).

2.6.2. Polymerase chain reaction

Polymerase chain reaction (PCR) was the first and remains the most popular amplification technology for amplifying and detecting low-abundance nucleic acids. PCR was discovered by Kary Mullis in 1983 while trying to devise a rapid clinical assay for genetic disorders caused by a single nucleotide polymorphism(54). PCR allowed the amplification of DNA obtaining as many copies as needed of the gene of interest. This development of this discovery was awarded the Nobel Prize in Chemistry in 1993.
The performance of PCR requires the presence of the target DNA (also called template), primers, nucleotides, and the presence of DNA polymerase. DNA polymerase is the enzyme that links which extremely high specificity the nucleotides (adenine, thymine, cytosine, and guanine) together to form the final PCR product. Primers are oligonucleotides whose sequences are complementary to the template at different points serving as a frame and a starting point for the elongation of DNA. The resulting PCR product is determined by the position and distance between the annealing sites of the two primers.

The cycles of PCR are performed in thermocyclers based on the Peltier effect, which raise and lower the temperature of the block where the tubes are placed. Different temperatures are the hallmark of each of the cycles, which are repeated during PCR: denaturalization, annealing and elongation(55).

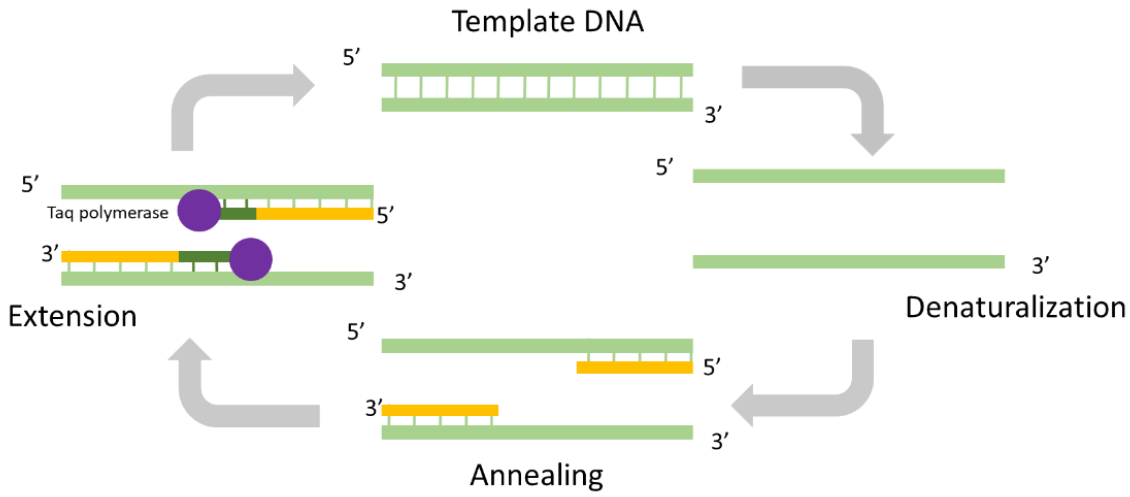

Figure 1.5. Schematic representation of PCR steps based on temperature cycles

The addition of more than one set of primers to the reaction mix enables the multiplex amplification of different sequences of the same target or more than one target in the same sample during one single PCR experiment. For a successful multiplex PCR, the design of primers is critical. Primers not only have to be specific for each sequence but they must have similar Tm and avoid the formation of dimers(56).

Reverse transcription PCR (RT-PCR), implies a previous step where RNA template is first converted into a complementary DNA (cDNA) using a reverse transcriptase. The resulting cDNA is then amplified using PCR(57).

The end-point analysis of the resulting amplicons from PCR is usually performed by gel-electrophoresis. It is a commonly used technique for the separation of charged molecules, like DNA, RNA and proteins according to their size. A potential is applied across the gel (commonly agarose-made). This polarization of the gel provokes the migration of the negatively charged DNA towards the anode. The principle of the technique is that smaller molecules migrate through the gel more quickly and move further than larger fragments. Hence, in electrophoresis of DNA, molecules are separated by length. A DNA marker with fragments of known lengths is usually run

through the gel at the same time as the samples allowing to determine the approximate size of the amplicons by comparing the bands. The visualization is achieved by adding an intercalative dye in the gel composition and using an UV transilluminator(58).

One of the modifications of PCR is real time PCR, also known as quantitative PCR (qPCR)(59). This technique provides information of the amplification during the process allowing the simultaneous quantification of DNA with no need of post-amplification steps. By using fluorescent labels, the thermocycler which contains a light beam, detects the accumulation of amplicons and relates it to the initial amount of DNA(60).

This technique in combination with RT-PCR is widely use for the analysis of genetic disorders and quantification of viral RNA in research and clinical settings(61).

2.6.3. Isothermal amplification techniques

Isothermal amplification techniques replicate nucleic acids normally at a single temperature avoiding the use of thermocyclers. The knowledge in the replication of nucleic acid gained in the last two decades has undoubtedly contributed to the development of isothermal amplification techniques. Nowadays, a wide variety of strategies exist using different enzymes and based in different reactions demonstrating to be a cost-effective and robust solution for the amplification of nucleic acids. Some of them are explained in the following sections.

2.6.3.1. Nucleic acid sequence-based amplification

Nucleic Acid Sequence Based Amplification (NASBA) and Transcription Mediated Amplification (TMA) are very similar amplification methods that amplify RNA from a RNA target. Both techniques mimic the retroviral strategy of RNA to replicate via a complementary DNA (cDNA) intermediate. This RNA amplification technology has been further improved by introducing a third enzymatic activity, RnaseH, to remove the RNA from cDNA without the heat denaturing step. Thus, the thermocycling step has been eliminated, generating an isothermal amplification method named 3SR(62). Figure 1.6 shows a schematic representation of amplification principle of NASBA. First, the first primer hybridises to the RNA which is then converted to complementary DNA (cDNA) by RT and RNaseH. After, a second primer hybridises the resulting cDNA and T7 DNA dependent RNA polymerase produces antisense

sequences to the target RNA which become templates for the initial reverse transcription. Some applications of this technique include the molecular detection of microorganisms such as hepatitis C virus and human immunodeficiency virus.

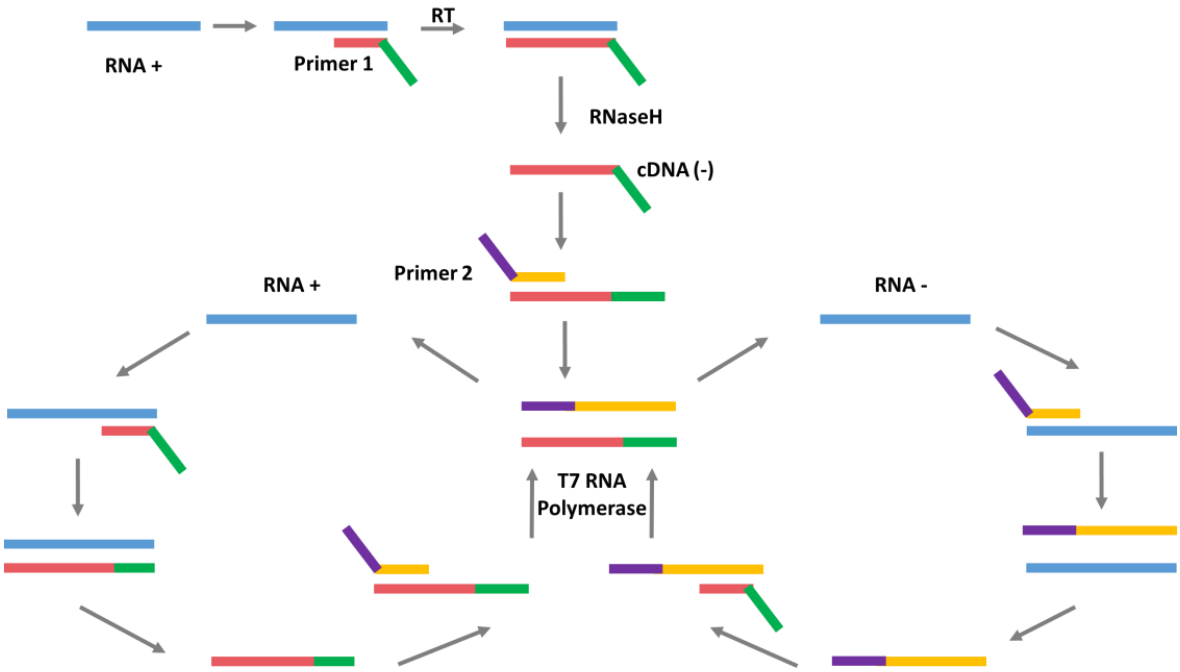

Figure 1.6. Schematic representation of NASBA. Figure adapted from reference (63).

2.6.3.2. Strand displacement amplification

Strand displacement amplification (SDA) employs a restriction endonuclease capable of nicking the unmodified hemiphosphorothioate form of the recognition site. Moreover, the methodology makes use of a DNA exonuclease deficient DNA polymerase which initiates the synthesis extending the 3' end at a nick and displacing the downstream strand.

Therefore, in a first step a target is generated which copies the target sequence flanked by nickable restriction sites. Second, the exponential amplification of these modified target sequences is produced by repeated nicking, strand displacement and priming of displaced strands. SDA is performed at a single temperature and is used to amplify short target sequences(64). Currently this technique is used to detect diseases such as chlamydia and gonorrhoea, among many others(65).

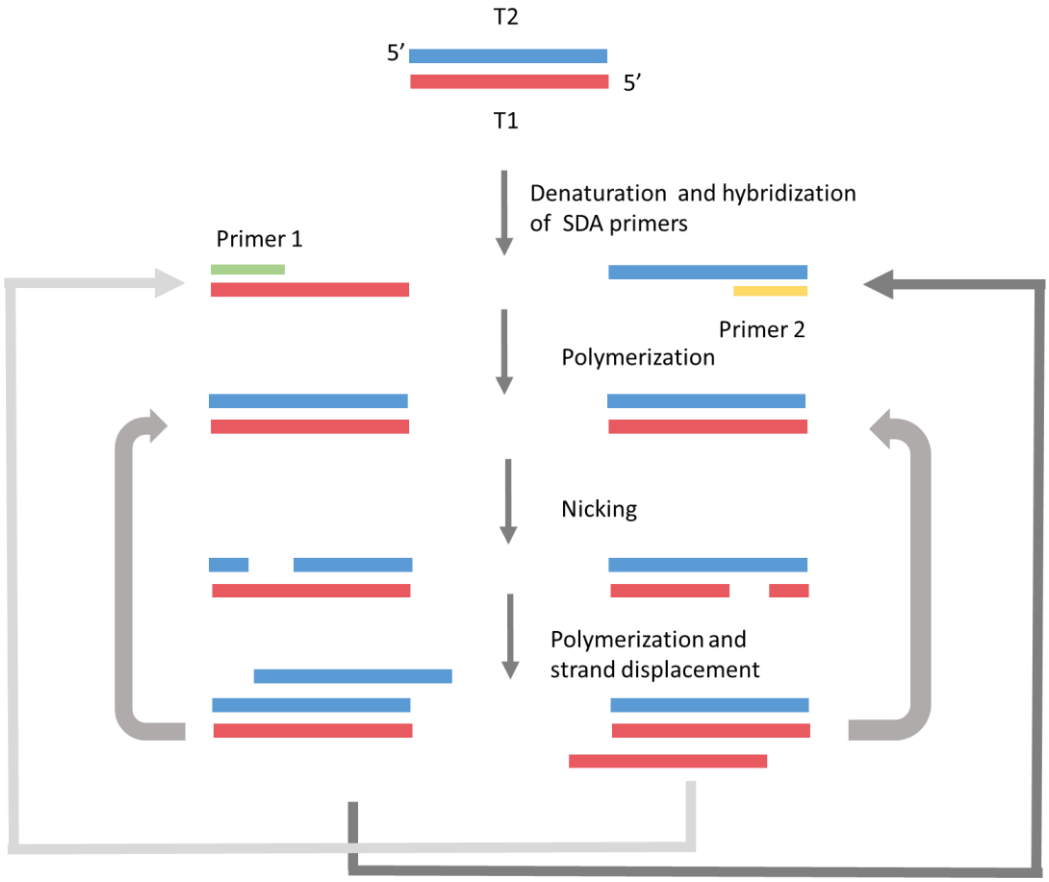

Figure 1.7. Schematic representation of SDA isothermal amplification. Figure adapted from reference Walker et al. 1992(66).

2.6.3.3. Helicase-dependent amplification

Helicase-dependent amplification (HDA) uses a helicase and its cofactors (methyl-directed mismatch repair protein (MutL) and Adenosine triphosphate (ATP) for the separation of the two strands of a DNA duplex. The separated strands are stabilised by single strand binding proteins (SSB) and sequence-specific primers hybridize to the target and are extended by DNA polymerases to amplify the target sequence(67). This process is then repeated amplifying exponentially the DNA. A representation of the process is shown in Figure 1.8. Some commercially available kits detect *Clostridium difficile* or β-hemolytic *Streptococcus* (68),(69).

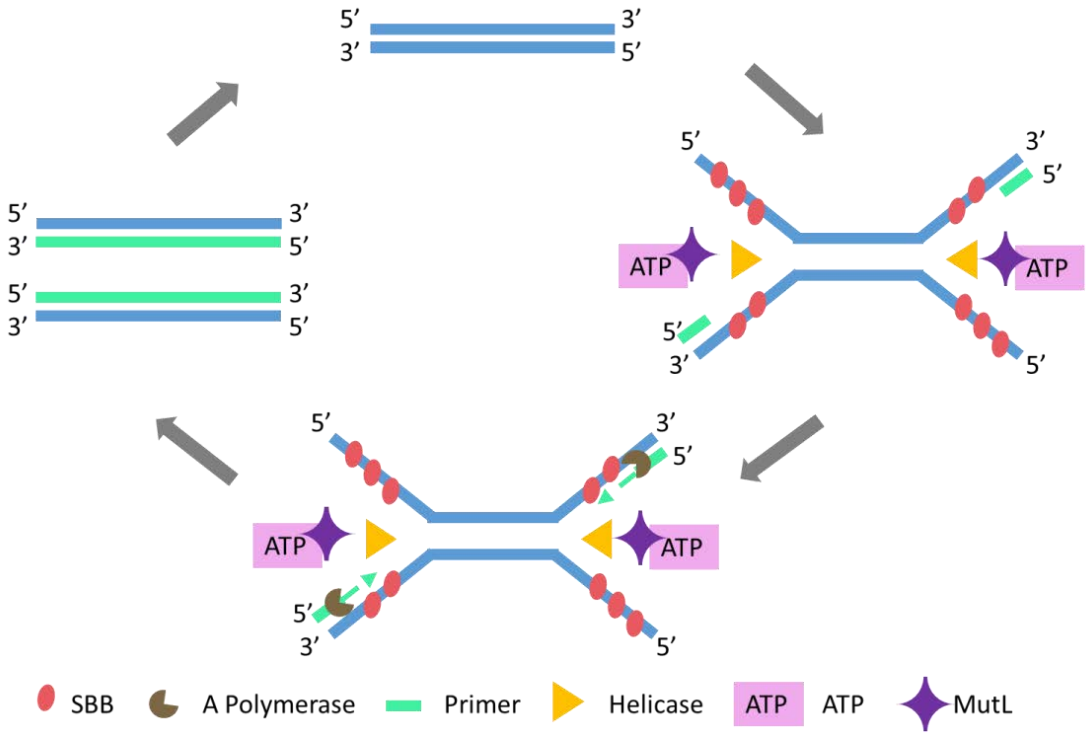

Figure 1.8. Schematic representation of Helicase-dependent amplification (HDA). Figure adapted from reference .(70)

2.6.3.4. Loop-mediated isothermal amplification

The loop-mediated isothermal amplification (LAMP) method is performed at temperatures between 60-65 ºC. It requires a set of at least four specifically designed primers including a forward inner primer (FIP), a backward inner primer (BIP), and two outer primers (F3 and B3), to recognize six different sites at the ends of the amplified DNA sequence.

FIP and BIP contain one sequence for priming extension in the first step and other one for self-priming in the second stage which correspond to the sense and antisense of the target dsDNA respectively. DNA polymerase with strand displacement activity is also required. In LAMP method, the amplification products are stem–loop DNA structures with several inverted repetitions of the template and cauliflower-like structures with multiple loops(71).

This technology has been widely used for the molecular detection of several microorganisms by researchers and it can be a suitable choice for the design and development of rapid molecular tests in the point of need(72)(73)(74).

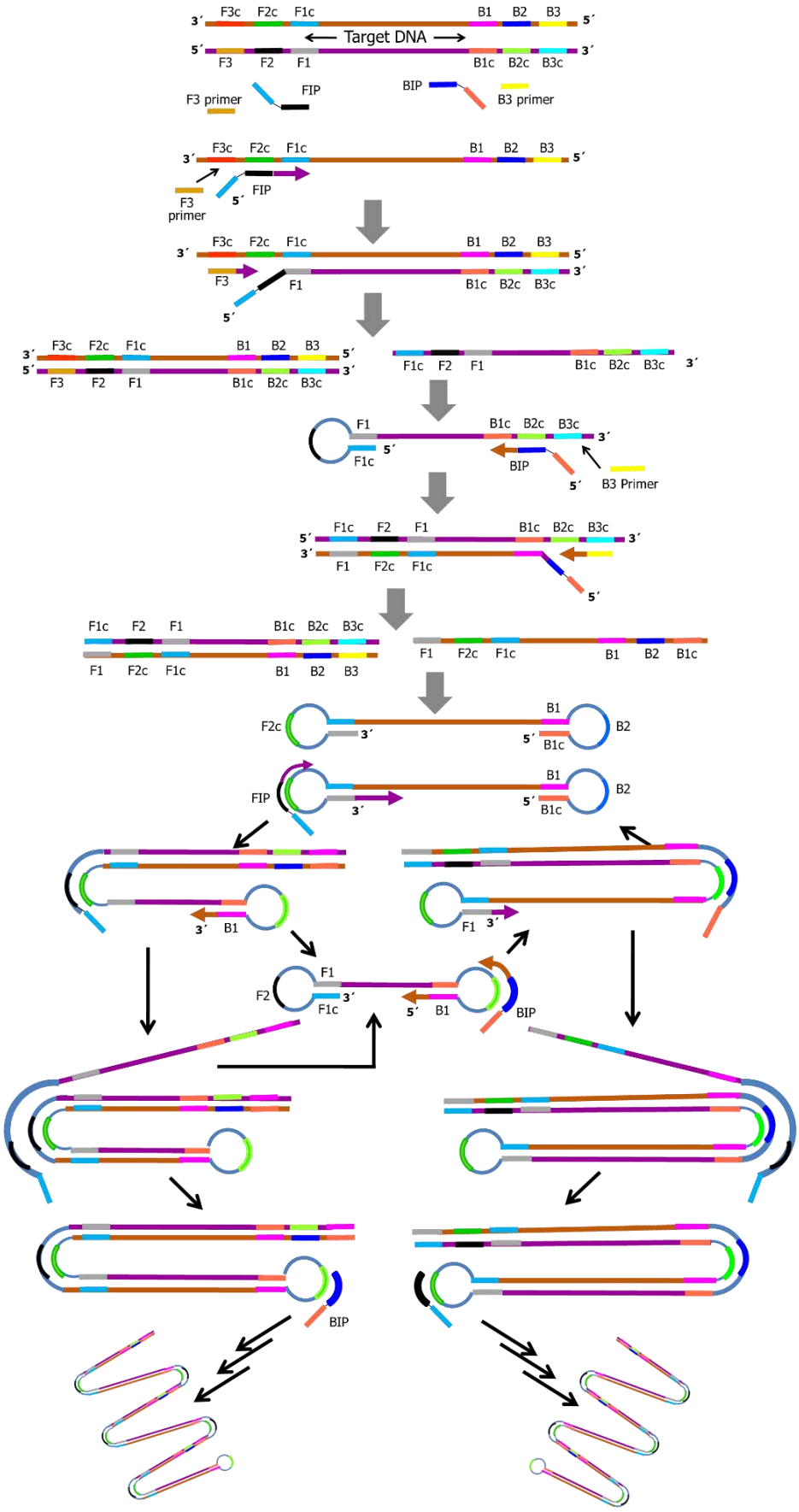

Figure1.9. Schematic representation of LAMP. Figure from reference(74).

2.6.3.5. Recombinase Polymerase Amplification

Recombinase Polymerase Amplification **(**RPA) employs recombinase to catalyze the hybridization of the template with the primer. Then, the recombinase-primer filaments promote the strand exchange at specific zones of dsDNA. The resulting structures are stabilized by ssDNA-binding proteins in order to avoid primer displacement by branch migration. DNA polymerase recognizes the primer 3-ends left by recombinase disassembly and initiates the primer extension reaction. The binding and extension of two opposing primers generates one complete copy of the amplicon together with the original template. This process is repeated and the exponential amplification is achieved at 37-42 ºC(75). This technique is currently used for the detection of several viruses and is available in commercial kits(76).

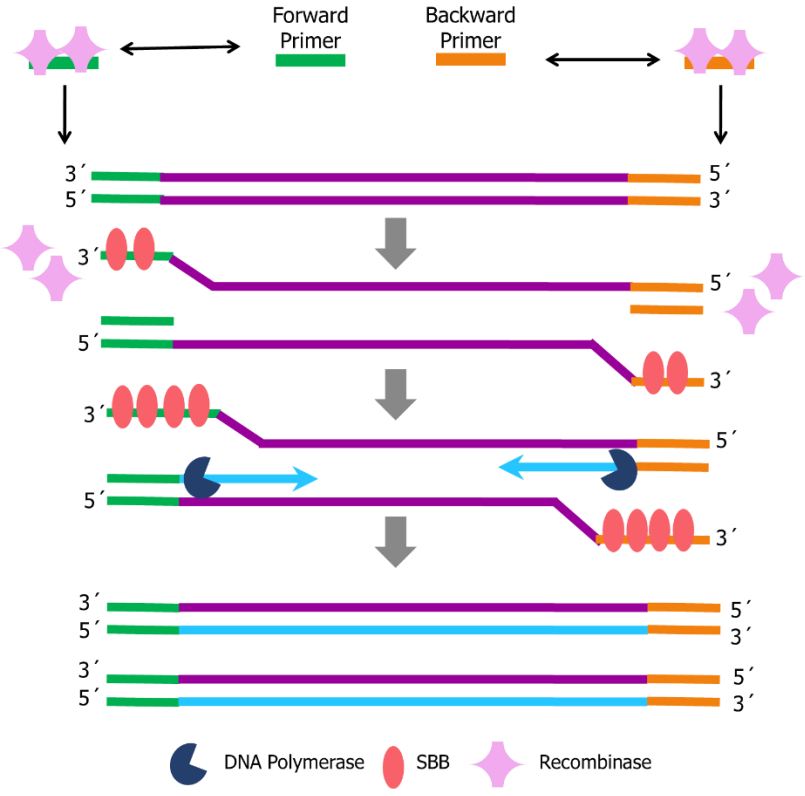

Figure 1.10. Schematic representation of RPA amplification. Figure adapted from reference (76).

2.6.3.6. Rolling circle amplification

The rolling circle amplification (RCA) generates multiple copies of a sequence adapting the in vivo rolling circle DNA replication. RCA uses a primer called padlock

probe, which is a long sequence oligonucleotide whose ends are complementary to adjacent target sequences. The complementary ends, generally called padlock probe arms, are 15-20 bp length while the central part, commonly known as backbone, is usually 60 bp length and links the complementary sequences together. When the padlock probe arms hybridize the target, the padlock probe is closed by ligation by means of the enzyme T4 ligase. Then, Phi29 polymerase, the most common polymerase used in RCA, amplifies the product adding nucleotides to the circular template. The final product consists of hundreds of concatenated circular template copies which can be labelled with hundreds of identical short tagged oligonucleotides that hybridize to the repetitive sequence introduced by the padlock probe backbone. Applications of this technique are found in gene tests, and single-cell analysis(77).

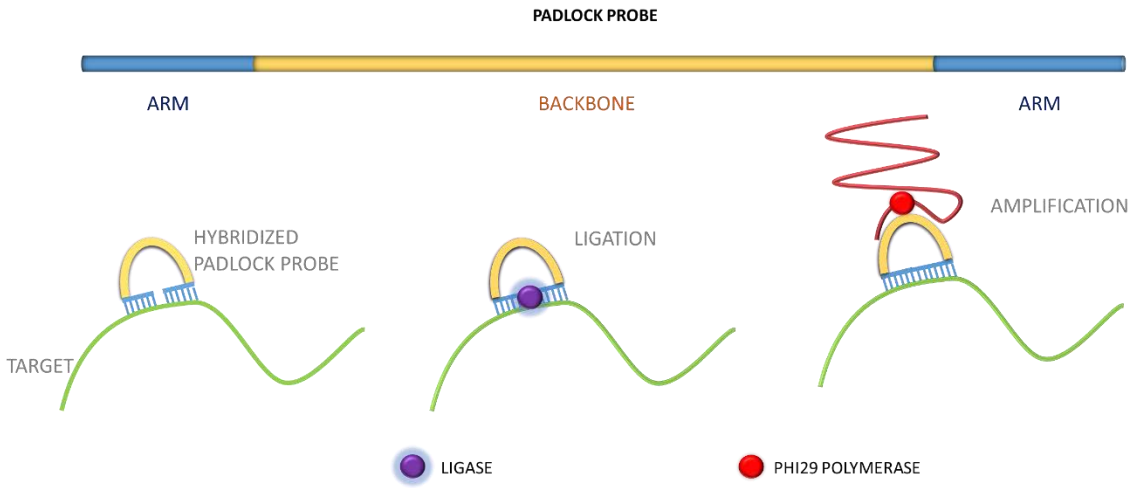

Figure 1.11. Schematic representation of RCA amplification of linear sequence

3. Point of Need diagnostic tests

The accurate identification of patients requiring treatment in low resource settings remains a major stumbling block to disease control due to the lack, in some instances, of rapid, cost effective

diagnostic tests that can be handled for unskilled personnel(78). In this direction, the FDA defines the characteristics that a diagnostic test should ideally have(79).Low complexity for a test includes the final-user interpretation and level

of training required, the number of manual manipulations and intervention steps, and the instrumentation requirements(80).

The desirable features of an ideal point of need test (PoN) is also summarized by WHO under the acronym of ASSURED(81). This acronym defines the requirements that researchers and companies have to consider when developing detection device, which are:

Affordable. The final product should be cheaper than standard method, affordable for public healthcare systems, as well as for users and patients.

Sensitive and specific. Final platforms must be sensitive and specific enough to achieve the LOD required for the specific application improving or at least equalling the limits of detection of traditional tests.

User Friendly. The test should be easily performed and interpreted for the final user after minimal training. It is desirable to present results in a clear and unequivocal way.

Rapid and robust. These tests should be designed to obtain a quick reliable response which allow taking actions on-site. For instance, point of care devices should provide a diagnostic the same day of the visit and eventually start the corresponding treatment as soon as possible if. Moreover, they must resist the transport, extreme temperatures and have a long shelf life.

Equipment-free. Test should be compact, portable and battery powered in order to ensure the access wherever it is needed.

Delivered to those who need it. These tests have to reach the people who need them quickly. For this reason, these devices should not require special transport conditions, it being preferable those that are portable and handheld.

In general, as complexity for a diagnostic test increases (ranging from agglutination test, lateral flow assays, biosensor and microfluidic devices, immunoassays and PCR), the analytical performance and the quality of the analytical information remarkably improve. Unfortunately, the total assay time and the need for complex bench-top instrumentation which requires costly maintenance also increase(82).

The preeminent formats under development as rapid diagnostic tests (RDTs) are lateral-flow, microfluidic devices and biosensors. The lateral-flow assay (LFA) introduced in 1988 by Unipath, is the most common commercially available point of care diagnostic format. Although there are many commercial available examples

including the pregnancy test, the LODs of the test for some applications should be improved. Regarding microfluidic devices, although many breakthroughs have been made(83), the cost of production and the requirement, in most cases, of bench-top equipment for the readout, still constitutes a bottleneck and may put them out of range for end users in the developing world. Finally, and despite the massive use of glucose biosensors with electrochemical transduction, examples of other applications including diagnosis of diseases are currently very limited in the market. Many improvements should be done to achieve analytical simplification. The next sections addresses the enabling technologies (including novel materials such as magnetic particles (§ 3.1.1), biomimetic materials (§ 3.1.2) and hybrid magnetic MIPs (§ 3.1.3), as well as emerging diagnosis platforms, such as biosensors (§ 3.2.1)and lateral flow assays (§ 4)) that have been identified for rapid diagnostic tests (RDTs).

3.1. Enabling technologies for point of need tests. Materials

3.1.1. Magnetic particles

Sample preparation is the initial action of an assay and can be either an extra step or being incorporated in the device. For the separation of biological samples, features such as a high resolution, a high specificity, an easy operation and short analysis time are desirable.

Magnetic particles (MPs) have emerged as great candidates for the development of PoN biosensors allowing to fulfil the sensitivity and specificity requirements. In addition, MPs-based magnetic separation retains the activity of biological samples unlike traditional methods of separation such as centrifugation or filtration that might damage biological samples(84).

Several methods for MPs synthesis have been reported comprising co-precipitation, microemulsion or thermal decomposition among others(85). Although other metals can be used for the synthesis of MPs, the huge majority of MPs used for biosensing applications are made of iron oxide (Fe_3O_4 and ɣ-Fe_2O_3). This material has a great chemical stability, and, at the same time, its surface is easily tuneable. The versatility

of this particles allows several coatings and modifications with groups that promote the covalent binding of bioreceptors such as carboxyl or amino groups in a large surface area (Figure 1.12).

This capability provides two valuable tools for biosensors. First, concentration of analytes from larger volumes of sample increasing the sensitivity. Second, isolation of the molecule of interest from the rest of the sample decreasing considerably the matrix effect and in addition adding specificity to the assay. Both are only possible due to the inherent capability of magnetic particles of responding to a magnetic field and redispersing upon removal of the magnetic separator.

There have been several studies in the literature reporting the use of magnetic particles for the detection of viruses such as hepatitis A virus and B virus(86), influenza(87), chikungunya(88) or HIV(89), as well as for bacteria detection like *Staphylococcus aureus*(90), *Listeria, Ecoli* or *Salmonella*(91).

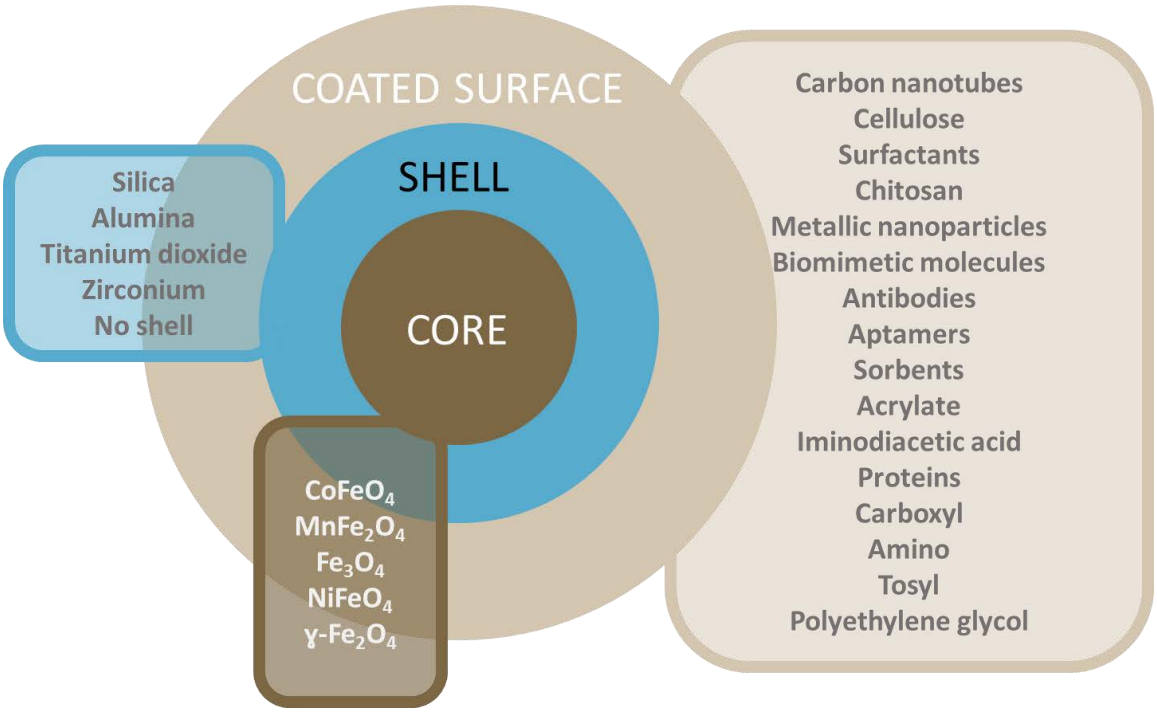

Figure 1.12. Common structure of magnetic particles showing different compositions of their parts: core, shell and coating.

Moreover, magnetic particles are used not only as a solid support for purification and preconcentration, but also as a label for detection in colorimetric and magnetic biosensors(92), contaminant removal from aqueous systems(93), drug delivery(94) or magnetic resonance imaging(95) among many other fields.

3.1.2 Biomimetic materials. Molecularly imprinted polymers

With the aim of simplify and produce cheaper biosensors, a variety of synthetic materials with different possibilities for their immobilization on the transducer have emerged leading, together with the use of nanotechnology, to an increasing number of biosensors. Synthetic receptors have a relatively small molecular weight and are usually more economic and stable than the biological ones. Their main disadvantage and challenge for researchers is their still relatively low biocompatibility compared to biological molecules(96).

The biomimetic approach focusses on generating artificial materials inspired by the nature. In this line, extensive efforts have been devoted to understanding the properties of biomolecules and biomembranes. Among biomimetic materials, artificial polymeric membranes and molecularly imprinted polymers have demonstrated to be excellent biocompatible materials with strong affinity in several applications. Mimicking in artificial polymeric membranes is used to reproduce the functional groups, the structure and morphology of biomembranes in order to achieve their functions such as transport, catalysis, or molecular recognition with specific enzyme or protein onto the membrane(97).

On the other hand, molecularly imprinted polymers are promising materials for molecule recognition due to their inherent re-usability, long-term stability and shelf life, resistance to harsh environment, ruggedness, and low cost. These materials are synthesized in presence of a template which is captured on the cavities during the co-polymerization of functional monomers and cross-linkers. A second step involves the extraction of the template leaving behind the complementary recognition cavities as shown in Figure 1.13. This process provides the ‘‘lock and key’’ mechanism similar to natural receptor–ligand interactions.

This principle has been applied to different material morphologies such us nanoparticles or thin films. The fabrication of MIPs nanoparticles can be achieved

by precipitation, polymerization or solid-phase synthesis. The surface-imprinted polymers (SIPs) are fabricated by soft lithography with stamping of template cells onto polyurethane layers(98).

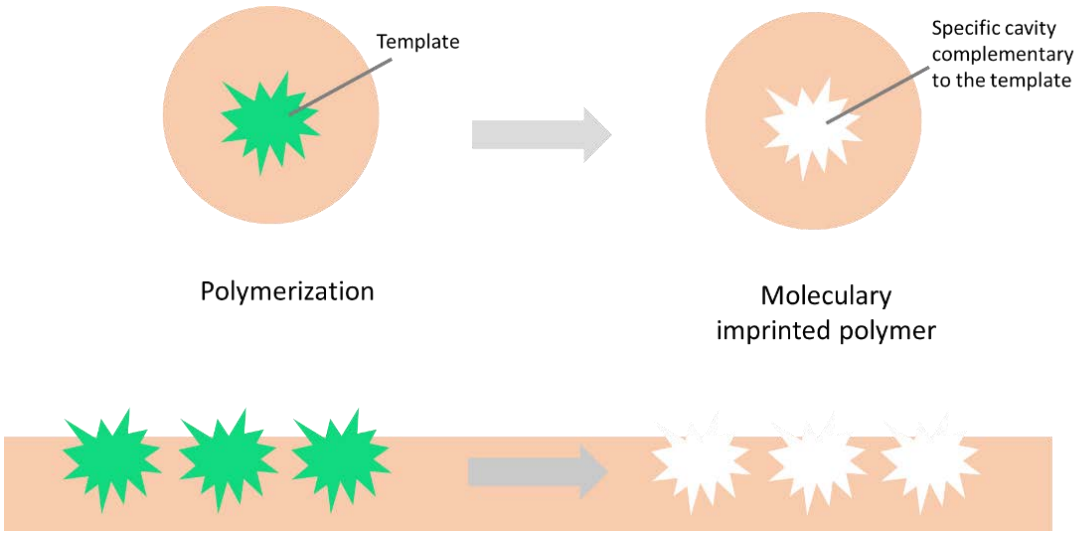

Figure 1.13. Schematic representation of the principle of molecularly imprinted polymers synthesis

A wide range of applications of these materials have been reported during the last years. For instance, a thermal biomimetic sensor in the detection of whole bacteria on surfaces(99) or a combination of the surface cell-imprinting technique for selective macrophages and cancer cell recognition(100)(101) have been recently reported. MIPs have been also used as molecules of biorecognition in the test line of lateral flow strips instead of antibodies(102). Therefore, these materials have demonstrated to be useful for determination and quantification of environmental pollutants, as textile dyes with optical transduction(103) .

3.1.3. Synergic materials. Magnetic molecularly imprinted polymers

The combination of MIPs and magnetic nanoparticles is called magnetic-MIP. The synthesis of this material is based on a core-shell synthesis in which the core was made of magnetite recovered by a shell of the MIP. The combination of MIPs and magnetic nanoparticles properties multiplies the suitable applications for these materials. The robustness and low cost of MIP allow their use in a more extreme environmental conditions. On the other hand, magnetic core enables the manipulation of the material using an external magnetic field, and their uses can be

extended to other areas, including the analysis of industrial effluents or environmental samples. Among other advantages, these hybrid materials offer enhanced selectivity, durability, and the possibility of reuse(104).

3.2. Enabling technologies for point of need test. Diagnostic Platforms

3.2.1. Biosensors

Biosensors have revolutionized the way of diagnosis by allowing early detection of diseases and monitoring of altered amount of body biomarkers using little amounts of biofluids. They have ubiquitous presence in everyday life not only for biomedical applications but also in environmental monitoring or food control enabling the development of several highly sensitive devices for its use as point of need. Leland C. Clark, Jr is considered the 'father of biosensors'(105) as he invented the first biosensor for oxygen detection in 1956 and some years later, the most commercialized biosensor thus far: an amperometric enzyme electrode for the detection of glucose(106). From this moment numerous biosensors have been developed for a very wide range of applications that aim to improve the quality of life.

Biosensors are analytical devices which include a combination of biological detecting elements and a transducer to transform recognition events into measurable signals. This signal is then transduced by passing it to a circuit where it is digitalized. The obtained digital information can be stored in a memory or made accessible via digital communications port. A schematic representation of the basic biodetection principle of biosensors is shown in Figure 1.14.

Biosensors can be classified either by their biorecognition element or by the kind of transducer. The biorecognition can be provided by antibodies, enzymes, cells, nucleic acids, microorganisms or biomimetic molecules among others whereas the transduction can be optical, mechanical or electrochemical(106).

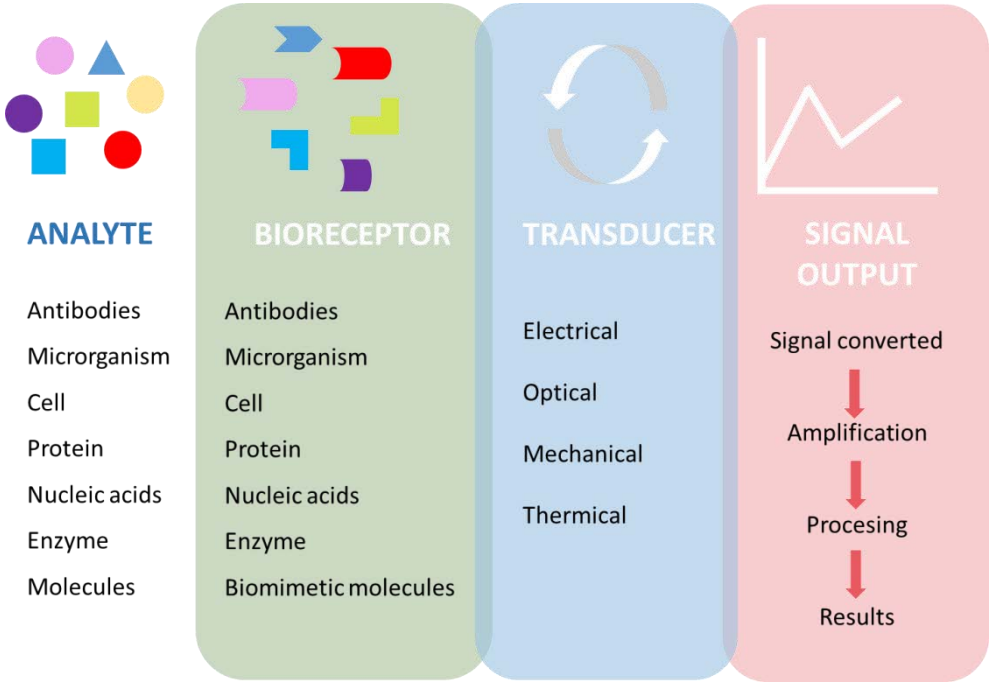

Figure 1.14. Principle of biosensors. Bioreceptor is the molecule that specifically recognises the analyte. The tranducer converts the biorecognition into a measurable signal which is then electronically amplified and converted into a readable format.

A more detailed description of electrochemical biosensors is described hereunder.

3.2.2. Electrochemical biosensors

Electrochemical biosensors transform biochemical information into an analytical measurable electrical signal. The electrochemical biosensor may be further classified as amperometric, potentiometric and conductometric depending on the type of electrochemical parameters measured.

3.2.2.1. Potentiometric biosensors

Potentiometric biosensors measure the difference in the potential of two electrodes in a galvanic cell. One of them, the potential of which is assumed to be constant, is called a reference electrode and the other a working electrode(107).

3.2.2.2. Conductometric biosensors

Conductometric biosensors are based on the measurement of the changes in electrical conductivity as a result of the variation in the concentration of ionic species during biological processes. This measurement is the electrical

conductance/resistance between working and reference electrodes. In impedimetric biosensors, when the bound of the biorecognition element and the analyte is formed, the electrode is coated with a blocking layer and thus the electron transfer resistance increases(108).

3.2.2.3. FET-based biosensors

FET-based biosensors operate by means of an electrical field modulating charge carrier across a semiconductor material converting biorecognition events into electrical signals. The electric current flows along a semiconductor channel connected to a source and a drain electrode. The gate contact, which is coupled to the device through a thin dielectric layer, modulates the conductance between these source and drain electrode. Therefore, FET sensor detects potential changes on the gate surface(109).

3.2.2.4. Amperometric biosensors

An amperometric biosensor measure the resulting current from the exchange of electrons from the electrochemical oxidation or reduction of an electroactive specie at a certain potential fixed at the working electrode. The resulting current is directly correlated to concentration of electroactive species. When the current is measured during a potential scan this technique is called voltammetry. For instance, square wave voltammetry is based on the measuring of current in working electrode while the potential between the working electrode and a reference electrode is increased or decreased linearly in time(110).

Another variant of amperometric technique is known as chronoamperometry, where a square-wave potential is applied to the working electrode and the value of steady state current is measured. Amperometry uses redox molecules as mediators for the direct transfer of electrons to the electrode with no need of reduction of the oxygen co-substrate. These mediators must react rapidly and be soluble in both oxidised and reduced forms. Some examples of good and widely used mediators are hydroquinone or ferrocenes.

Typical configuration of amperometric biosensors have three types of electrodes: a working electrode made of a conductive material (classically gold, carbon or

platinum) where the reaction takes place, a reference electrode made of silver (Ag) or silver chloride (AgCl) having a fixed potential that controls the potential of the working electrode and a counter or auxiliary electrode used to measure current flow(111). Due to the simplicity of the transducer, low cost portable devices are fabricated using this technology and have arisen as essential for applications such as medical diagnostics and environmental monitoring.

The most widely produced and commercialized electrochemical PoC is the enzymatic amperometric glucose biosensor. The principle of the measurement is based on the fact that the immobilized enzyme glucose oxidase, immobilised on a conducting polymer coated electrode, together with its corresponding cofactor catalyse the oxidation of β-D-glucose by molecular oxygen producing gluconic acid and hydrogen peroxide. The resulting H_2O_2 is measured and related with the initial amount of glucose(112).

3.2.2.5. Working electrodes

On the interface between the working electrode and the solution is where the reaction of interest takes place. The rational selection of this component is essential for the performance of the measurement. The material must allow the fast and reproducible electron transfer taking into account the potential range of interest. As wider is the window of potential for the working electrode, a more exhaustive characterization will be possible. The ratio of surface area of working electrode to counter electrode, price, and volume of sample needed for the assay are also factors to be considered when designing the biosensor.

The most commonly used working electrode materials are platinum, gold and carbon(113). Among them, carbon present good conductivity and electrodes made of this material allow scans to more negative potentials than platinum or gold, as well as good anodic potential windows. The most usual form of carbon is graphite.

Graphite composites electrodes have been widely used for analytical laboratory applications. Several examples of combination of graphite with agglutinants such as polyester or polypyrrole have been developed for voltammetric determination(114)(115). In this work graphite epoxy electrodes were prepared and used following the common procedure and previously published method(116).

A schematic representation of the steps for their construction is shown in Figure 1.15.

The graphite is included in a two component paste of epoxy resin and mixed obtaining a curable paste. After the curing polishing and cleaning the electrode is ready to use. The surface obtained can be regenerated after each use polishing it with alumina or 1000-grit sandpaper.

The graphite epoxy electrodes can be functionalized by casting the bioreceptor of interest on the carbon surface and drying. The addition of bioreagents such as avidin (Av-GEC) (117)(118), metal nanoparticles(119) or carbon nanotubes(120) in the paste formulation has been also previously described.

Another modification of graphite-epoxy composite electrodes that has proven applicability for electrochemical biosensors is the incorporation of a magnet in the electrode (m-GEC). Magnetism multiply the analytical possibilities of graphite epoxy electrodes since it allows the integration of magnetic particles and their corresponding advantages in the assay by attracting the magnetic particles to the surface of the electrode(121). The construction of magneto-graphite epoxy electrodes is shown in figure 1.15.

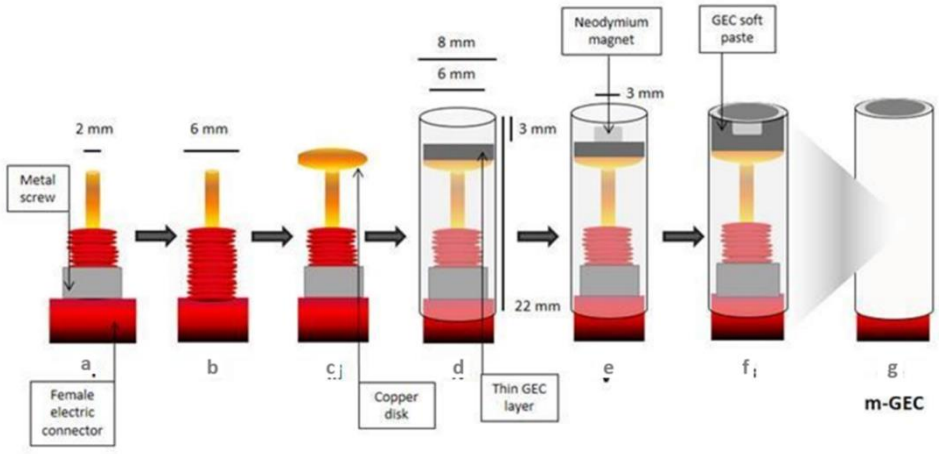

Figure 1.15. Schematic representation of the magneto-graphite epoxy composite (m-GEC) electrodes

The implementation of electrochemical biosensors has been accompanied by the massively fabricated, disposables cheap and well performing screen printed electrodes and the development of portable instruments. The screen printing fabrication of the electrodes is ideal for mass production purposes due to the speed

and reproducibility of the technique, resulting in low unit cost of the electrodes. Normally, they are composed of at least two layers of different inks: the conductive material and the encapsulator (dielectric layer)(122).

3.2.3. Microfluidic devices

Microfluidics is the science of manipulating and controlling little amount of fluids in the range of microliters to picoliters using channels at microscale and often external pumps. Its application in point of care tests as lab-on-a-chip devices has been spotlighted owing to its inherent precision when working with low volumes. This technology enables the integration of sample pre-treatment, preparation, mixing and detection in a single device for small volume samples or continuous sampling for real-time measurements.

Microfluidics is a useful tool for the different combinations of the previously described techniques. For instance, it was reported an integrated and automatized multi-step RCA assay on an all-polymer chip(123). This chip combines phase guides and capillary stop valves to achieve controlled filling of liquids. The sample is handled on-chip using MPs. The setup provides temperature control and automatic manipulation of the MPs using external magnets. The on-chip operations comprise: (i) PLP ligation, (ii) RCA, and (iii) optomagnetic detection obtaining a LOD of 20 pM after 45 min of RCA.

Another example of application of microfluidics at PoC devices is the CyFlow miniPOC, a portable version of benchtop flow cytometers which provide both absolute CD4 counts and CD4% for HIV/AIDS immune status monitoring at primary health centres and remote areas. The system uses dry monoclonal CD4 antibody reagents for capturing/purifying CD4 cells, eliminating any need for a cold chain(124).

Despite the potential offered by microfluidics some improvements are still necessary for the total implementation of this technology in point of need devices. The development of more sophisticated and innovative technologies for designing and manufacturing microfluidic systems is mandatory to launch these devices to the market. Moreover, most of the works published in literature only perform a part of the analysis while requiring additional user interventions and bulky equipment

such as pumps, interfaces and analysers which are not compatible with PoN test format(125).

In order to overcome some of this issues, researchers and engineers are focused on providing simpler electronics for analysers and implementing open source microcontrollers such as Rapsberri Pi or Arduino(126) which not only allow to control the different processes on the chip but also lowers the price of the final device. Moreover, with the same purpose, research is also focused on the implementation of cheap and biocompatible materials such as PDMS, 3D capillary printing polymers or paper for microfluidic devices(83).

3.2.4. Paper-based platforms

The use of paper has become an attractive material for the fabrication of disposable low-cost point-of-care approaches since it provides capillary force to the system. Cellulose, is a linear chain macro- molecule composed of hundreds of glucose units(127), which is hydrophilic, biodegradable and insoluble in water and most organic solvents. Paper-based diagnostics contribute to the affordable, equipment-free, and deliverable-to-end-user aspects.

One key characteristic of most of the paper-based tests is the inclusion of stabilized dried reagents in the device reducing the number of steps for its use and enlarging the shelf life(128). Functional chemical or biological molecules can be immobilized on paper by physical absorption, chemical coupling, and carrier-mediated (e.g., gold particles) deposition(129). The simplest assay is the dipstick format which, as its name indicates, is dipped in the sample and reveals different colours depending on the sample. The most famous example of this test is the pH strip used for instance to reveal kidney damage in urine samples.

Probably the most characteristic feature of paper is its porosity, which promotes the flow of liquid samples through its fibres with analytical purposes. This property provides the possibility of fabricating microfluidic channels including cutting, photolithography, plotting, inkjet etching, plasma etching or wax printing to create channels and barriers in paper(130). These features provide a great potential for its application in many fields in combination with other techniques. For instance,

disposable devices electrochemical detection can be fabricated since electrodes can be easily printed using paper as a substrate(131).

Microfluidic paper-based analytical devices (μPADs) are mainly based on capillary force to drive aqueous fluid movement. They were developed in two-dimensions and three-dimensions by patterning paper with a variety of assay designs(132). Two-dimensional μPADs are made by patterning physical or chemical hydrophobic boundaries to form microchannels on paper by inkjet printing. 3D μPADs are produced by stacking layers of patterned paper in such a way that channels in adjacent layers of paper connect with each other(133). These platforms not only allow filtering processes (134)and chromatographic separations, but also mixing reagents immobilized from different compartments which converge in a reaction zone in the sequential delivery(135). 3D μPAD, compared to 2D format offer the possibility of increasing the complexity of the net of channels therefore multiplying the functionalities.

Despite the great potential of this approach of microfluidics, since it is quite new, more research is still needed, especially when developing devices for quantitative analyses. For this reason, there are few current examples of μPADs on the market, while dipsticks and lateral flow assays LFAs have been successfully commercialized(129).

4. Lateral Flow Assays

Lateral flow tests are prefabricated strips of a carrier material containing dry reagents that are activated by applying the fluid sample. They have an important role for rapid diagnostic purposes such us failure of internal organs infection (136) or contamination with specific pathogens including biowarfare agents (137), presence of toxic compounds in food (138) or the environment (139) and abuse of (illicit) drugs(140,141)

4.1. History of lateral flow – Pregnancy test

The history of lateral flow has gone hand in hand with the development of its best-known example, the pregnancy test.

The first urine based pregnancy test of which there is written-proof is dated in 1350 BC. It is an ancient papyrus which describes the ancient Egyptian equivalent of a pregnancy urine-based test. The document explains that a woman who might be pregnant could urinate on wheat and barley seeds over the course of several days, and depending on the growing of the seeds they could predict the pregnancy (Figure 1.16). This same procedure is referred to in a collection of German folklore from 1699. This theory was tested was tested in 1963 and surprisingly results showed that 70 percent of the time, the urine of pregnant women did promote growth, while the urine of non-pregnant women and men did not. According to scholars this may be due to the elevated levels estrogens in pregnant women's urine.(142)
Over the centuries, numerous methods were reported but the first approach to the study of hormones related with pregnancy is dated in 1903 when Ludwig Fraenkel identified some hormones that had a role in female reproduction, naming the hormone that promoted gestation, progesterone (143).

Figure 1.16. Image of Egyptian ancient papyrus (3500 BC) which contains instructions for a pregnancy test: "*You shall put wheat and barley into purses of cloth, the women shall pass her water on it, every day. It being mixed with dates and sand. If both sprout, she will give birth, if the wheat sprouts, she will give birth to a boy (…) if the barley sprouts, she will give birth to a girl, if they do not sprout, she will not give birth at all*"(144)

During the twenties, scientists recognized that there is a specific hormone (now known as human chorionic gonadotropin (hCG)) that is only found in pregnant women and is thus useful as a biomarker for pregnancy. In 1927, Selmar Aschheim and Bernhard Zondek introduced a pregnancy test (known as the A-Z test) based on the presence of this hormone. A sample of woman's urine was injected into a group

of immature female mice over a period of three days. Afterwards, the mice were sacrificed and autopsied to analyse its ovaries for an estrous reaction. If the woman was not pregnant, there would be no reaction. In the case of pregnancy, the urine would induce ovarian development despite the animal immaturity.

Later, the adoption by the NHS of Xenopus laevis, a toad from South Africa that laid large, visible eggs when injected with human pregnancy urine, allowed to avoid the dissection in the course of a test (145).

In 1960, a "hemagglutination inhibition test" for pregnancy was developed by L. Wide and C.A. Gemzell (146). The test used purified hCG and antibodies directed against hCG mixed with a urine sample. In a positive pregnancy test, the red cells clumped, displaying a particular pattern. This test was much faster and cheaper than the old bioassay, but still relatively scarce predictive, especially for early diagnosis of pregnancy and there was also a pretty high proportion of false-positives due to the cross-reaction with medications. Six years later, in 1966, A. R. Midgley described the first radioimmunoassay for hCG (147). This assay, however, still could not differentiate between hCG and luteinizing hormone (LH).

In the 1970s, tests available to doctors and technicians included Wampole's two-hour pregnancy test. This nine-step kit was composed of two test tubes, a plastic rack, a bottle of "control solution," a bottle of "hCG-antiserum" and a bottle of "cell suspension". (145).

During the next 2 years, hCG was deeply studied identifying two subunits of hCG and found that the beta-subunit is where the immunologic specificity of hCG resides. This study allowed the differentiation of hCG from LH or other hormones (148). Moreover, this discovery led to the development of a specific antiserum for measuring the hormone in humans.

In 1977, the "Error Proof Test." (e.p.t) became the first home pregnancy test kit on the market in the United States and was advertised in major women's magazines with a price of 10 dollars. FDA Approval was also granted to other equivalent tests: Predictor, ACU-TEST, and Answer (Figure 1.17).

The commercialization of this test allowed to protect women privacy and take an active role in their own healthcare either for an early abortion intervention or for starting the prenatal care as soon as possible.

Figure 1.17. A) Image of some of the first home pregnancy tests (e.p.t. and Predictor . B) Instructions for e.pt. Results interpretation in advertisement in "women's journals" C) Image Alison Brie playing Wilder in Glow (Ep8: "Maybe It's All the Disco"). During the episode the tedious method and the corresponding long wait were evidenced.

In 1988, Unipath launched the first pregnancy test as we know today. It was a blue latex lateral flow immunoassay called Clearview. The time for revealing results was three minutes with 99% of accuracy (149).

Figure 1.18. Image of one of the first lateral flow pregnancy test and the last generation of pregnancy tests which includes the weeks indicator

The next generation of home pregnancy tests arrived with the incorporation of a display which generated a result in words and an increase of sensitivity being able to detect pregnancy five days before the missed period(150).

The features of lateral flow format attracted great attentions in the field of Point of care. For many years, the World Health Organization (WHO) and other international health agencies had called for better tools for patient diagnosis to be used by community health workers in low-infrastructure settings. In the nineties, PATH staff focused on the transfer of this technology to a wider range of applications and specimens such us exudates, swabs, spittle or blood (151).

Since then, at least another 500 patents have been created on various aspects of the technology (136) becoming a powerful tool for point of need tests.

4.2. Classical configuration of a lateral flow strip

Lateral flow strips are composed by different layers of different materials overlapping one into another, mounted on an adhesive plastic card, commonly known as backing card, and containing dry reagents which are activated by applying the fluid sample (Figure 1.19). One of the advantages of this kind of assays is that the added sample flows through all membrane by capillary force with no necessity of external pump or other means to move.

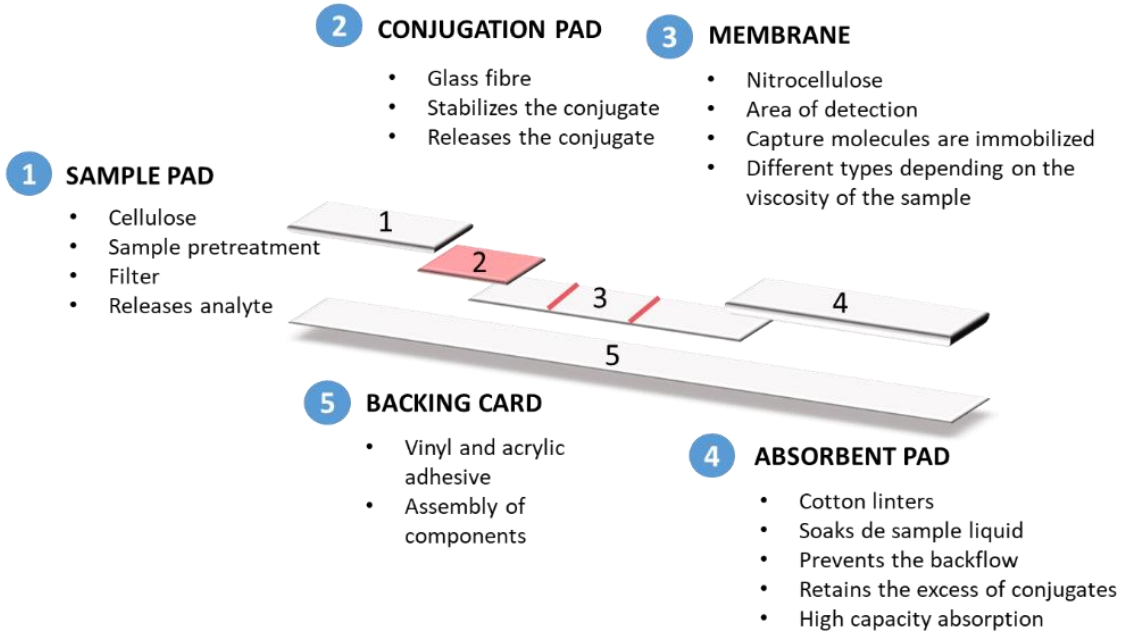

Figure 1.19. Schematic representation of the lateral flow strips components.

The sample is added to the sample pad, close to one end of the strip, which is normally made of cellulose and has a key role in the development of the performance of lateral flow. This part accepts the sample, adapts it to the assay, and releases the analyte in a controlled and

efficient way. The election of the sample pad is conditioned by the kind of sample and the components of the matrix. The structure of the fibers that constitutes the material of the pad allows the separation of particulates or blood cells. Moreover, the pre-treatment of this component of the strip with adequate buffers, surfactants, blocking reagents or additives, not only make the sample compatible with the assay but also improves the sensitivity.

The conjugate pad is in direct contact with the sample pad and is made of hydrophilic substrates, it being glass fibre the most common conforming material. This part contains the conjugate labels which will capture the analyte and will provide the signal of the test (152). During the fabrication, the particles are added and dried together with proteins, surfactants or soluble carbohydrates that ensure the stability of the conjugates during all the shelf life period and their correct release during the assay. Once the sample fluid dissolves the salt-sugar matrix, the conjugates binds the analyte while migrating towards the analytical region (153).

The third capillary bed is a membrane made of nitrocellulose, a material which is produced by partial nitration of cellulose. This process strengthens the porous property of cellulose and changes cellulose from hydrophilic to hydrophobic (127). Nitrocellulose binds specific molecules for the target analytes through a combination of different forces such as electrostatic, hydrogen bonds and hydrophobic forces maintaining their activity over the shelf life of the test. These molecules are deposited on the membrane forming lines or spots where the labels are retained during the assay. Dots can also be used to produce alpha-numeric symbols on the membrane, allowing intuitive result generation. The recognition molecules on the detection zone capture the complex of the analyte binding the conjugation particles generating signal. On the other hand, the reporter on the control zone binds the unreacted particles and ensures the correct perform of the assay since a valid test is considered when the control line appears. The deposition of test and control line require precise instrumentation in order to keep the reproducibility of the resulting product. The most commonly used quantitative dispensers for this purpose are displacement systems and air jetting systems. Positive displacement dispensing systems can be divided in non-contact and contact tips. Non-contact tips are placed at a fixed distance above the membrane while contact dispensing uses a tube made of a flexible plastic which does not damage the membrane during the contact. Both systems are moved at a certain speed through

the membrane surface at the same time as the liquid is dispensed with an optimized flow controlled by a pumping system. On the other hand, air-jetting systems dispense the reagents in aerosol form by pressurized air(154).

In order to avoid non-specific protein binding on the membrane, the remaining unbound sites are blocked using proteins such us casein or bovine serum albumin (BSA). Further, the addition of surfactants to the buffer reagent contributes to a better performance of the assay reducing conjugates agglomeration and hydrophobic interactions (155).

Nitrocellulose membranes of different pore size can be found in the market, however due to the high distribution of the porous size they are catalogued according to the capillary flow rate defined as the time in seconds that takes a fluid to flow through 4 cm of the membrane. The membrane thus has to be selected taking into account this parameter according to the kind of sample as it largely contributes in a successful design of the test. For instance, in order to allow the flow of viscous fluids, nitrocellulose with low value of capillary flow rate should be chosen. However, when lowering this value, the time of contact between analytes and recognition elements is consequently reduced and thus results in decreasing the sensitivity. Moreover, those materials with large porous size lead to a spread of the testing lines over a wider area difficult the read of weak signals. Recently, in order to improve the sensitivity of lateral flow strips, a new signal enhancement strategy based on the use of cellulose nanofibers (CNF) for compacting the pore size only in the detection lines has been reported. This approach allows to keep an adequate flow rate on the strip ensuring an intimate contact between the bioreceptors and the conjugation labels(156).

All in all, the right choice of membrane, the use of precise dispensers, the blocking of membranes as well as the strong immobilization of the capture reagents to the membrane are key elements for the production of sensitive and reproducible assays(157).

Finally, the remaining non bounded particles flow with the sample fluid up to the last pad. This part is composed of cellulose with high absorbent capacity where the fluids are well retained while keeping the capillary force in the correct way avoiding the back-flow.

4.3. Formats of lateral flow assay

There are two binding configurations for lateral flow immunoassays: direct (sandwich) or indirect (competitive) (158). The sandwich configuration, similarly to other immunoassays, is produced when, in presence of analytes, these are bound simultaneously to the detection label and the capture molecule. For this reason, this format is only suitable when the analyte has two different epitopes to be sandwiched for both the test line molecule and the labels producing thus a signal result of the accumulation of this complex in the detection line. Consequently, direct assays produce positive results when signal appear in the test line.

On the contrary, positive results in indirect assays are obtained when there is no signal or it is displaced as more amount of analyte the sample contains (159). This is due to the competitive principle of this format, where initially an immunoprobe is bound at the test line, and when the analyte is present in the sample, due to its higher affinity, it displaces the initial immunoprobe, resulting in a decrease of signal from the test line. This kind of test is adequate when the analytes are small (hapten) or do not have two binding sites to perform a sandwich assay such as pesticides (160), prodrugs (161) or drugs of abuse (162)

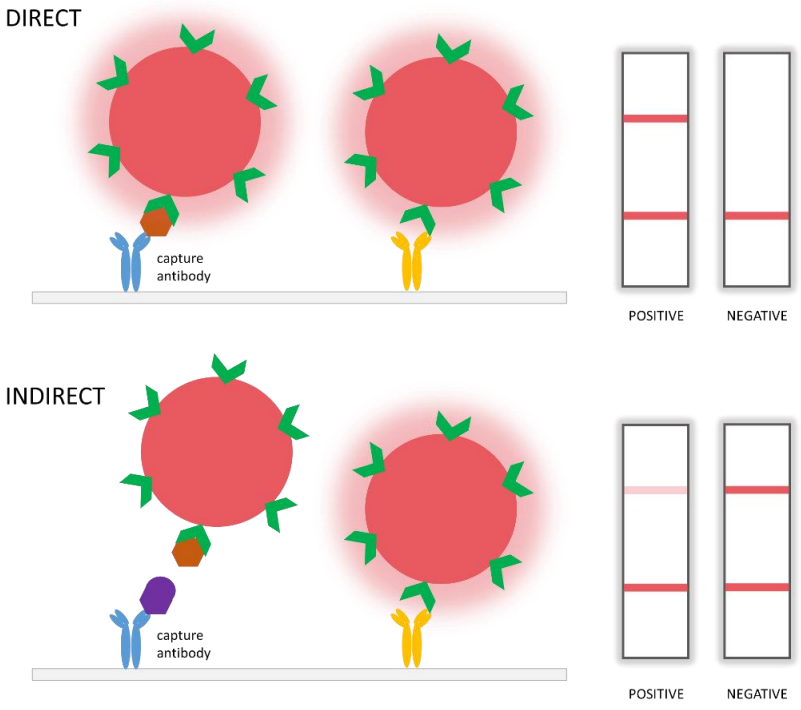

Figure 1.20. Representation of direct and competitive format of lateral flow assays

The results of these assays can be qualitative, quantitative or semiquantitative. Qualitative lateral flow results can be read as positive or negative depending on the apparition of a line (p. eg. common pregnancy test). Quantitative format provides information about the amount of analyte depending on the intensity of the line and usually require the use of readers to obtain data. Semiquantitative test format is based on the comparison of the test line intensity with the signal obtained on the control zone or a card with different colours (p.eg ovulation test).
The complexity of the lateral flow tests can be increased through the use of multiple test lines or using dots instead of lines and different kind of labels in order to detect different antigens within the same sample (163).

4.4. Signal generation systems

4.4.1. Gold nanoparticles

Gold nanoparticles (GNPs) conjugates offer several advantages for its use in diagnostic and medical applications. Their oxide-free surfaces suitable for bioconjugation, biocompatibility and tuneable optical properties are excellent features that make them great candidates for its use in drug delivery (164), cancer imaging and therapy (165,166) and optical and electrochemical biosensors (167,168).

4.4.1.1. Synthesis of gold nanoparticles

The synthesis of GNPs is a fairly studied process, simple and easy to scale-up that has been refined and increasingly diversified during the last years owing to the interest aroused by its potential in the mentioned applications(169). General synthesis methods for AuNPs can be classified in top-bottom and bottom-up approaches.
On the one hand, the top-down approach or descending method is based on the dispersion of a macroscopic material until it reaches the nanometric size. On the other hand, the bottom-up approach or ascending method, also known as reduction method consists in the coupling of atoms or molecules to form larger structures (nanoparticles)(170). The process of nucleation and growth has been described through the LaMer mechanism which can be divided into 3 steps: (i) rapid increase in the concentration of monomers in solution, (ii) burst nucleation which

significantly reduces the concentration of free monomers in solution (III) diffusion of the monomers through the solution generating growth (Figure 1.21) (171).

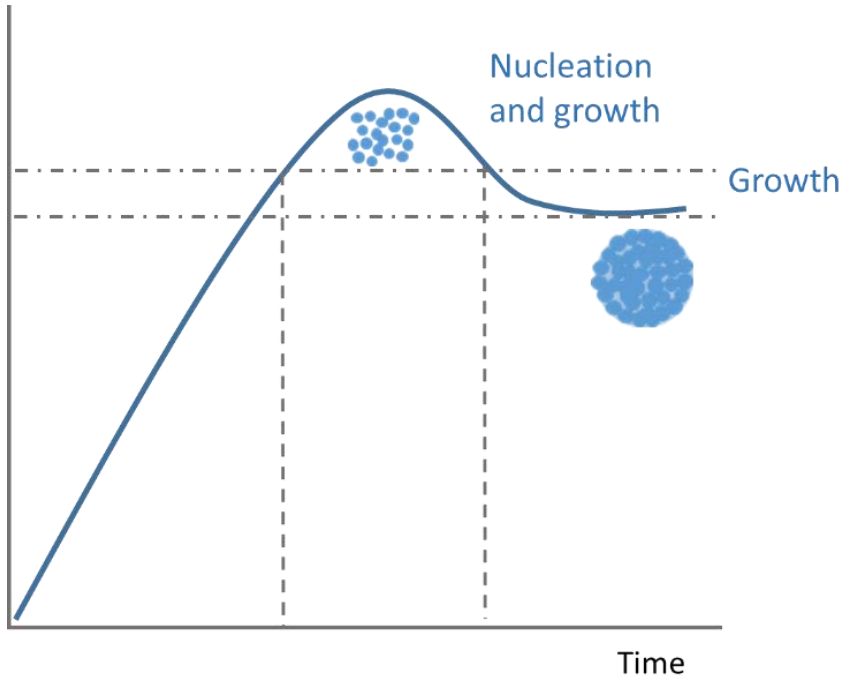

Figure 1.21. Lamer model of the precipitation process for the monodisperse solids formation.

Depending on the shape and the size of the product of interest, different synthesis methods are used. For diagnostic applications the most common method is the bottom-up or ascending approach based on the reduction of a gold salt (HAuCl4) to gold metal (Au (0)) (172). The activated Au (0) species are not thermodynamically stable so they tend to aggregate and eventually form AuNPs. This growing process has to be modulated by controlling the rate of reaction, the concentration of gold and reducing agent, the pH and temperature conditions (173,174). Moreover, the addition of capping agents is also recommendable to inhibit nanoparticle overgrowth and aggregation as well as to control the structural characteristics of the resulted nanoparticles in a precise manner (175) that can be studied by optical techniques as TEM, SEM (176)or NTA(177). Once obtained the desired nanoparticles, stabilizers such as polyethyleneimine or PVP contribute to avoid their aggregation enhancing their shelf life(177).

4.4.1.2. Functionalization of GNPs

Gold nanoparticles as other noble metal nanoparticles are widely used as biolabeling and bioimaging materials(178). Their stable surface for the immobilization of biomolecules with no loss of biological activity, low toxicity and nanometric size similar to lots of biomolecules make them suitable for bioconjugation. The described protocols of functionalization of GNPs open a range of possibilities for the creation of complexes specific for the target of interest. The prevalent methods for GNPs bioconjugation are: (a)passive adsorption(179)(180), (b) conjugation of the ligand on the NP surface(181), (c) conjugation to a small cofactor molecule that the protein can recognize and bind to(182), and (d) direct conjugation to the AuNP surface(183) .

Passive adsorption is produced when the molecules are adhered to the surface of the nanoparticles by weak physical forces of non-covalent nature such as electrostatic interactions. This approach does not require chemical reaction and its simplicity makes it always preferable for AuNP conjugation compared to covalent approach. Nevertheless, the orientation of the molecules is not controlled leading to random conjugation which can reduce the proportion of functional bioconjugated molecules. Moreover, the necessary stabilizing agents such as PEG or BSA can obstruct the target access to the surface decreasing the adsorption yield.

On the other hand, the covalent method allows the control of the chemistry on the surface generating strong bonds that often require a precise control of the stoichiometry. It usually uses metal-thiol bonds directly between AuNPs and biomolecules or cross-linking as the case of the binding of carboxyl groups via EDC reaction on primary amines with sulfo-NHS. AuNPs labelled with NHS esters can react to form covalent bonds with the primary amine of lysine on a protein. AuNPs coated with maleimide groups can react with the thiol of cysteine on a protein(184).

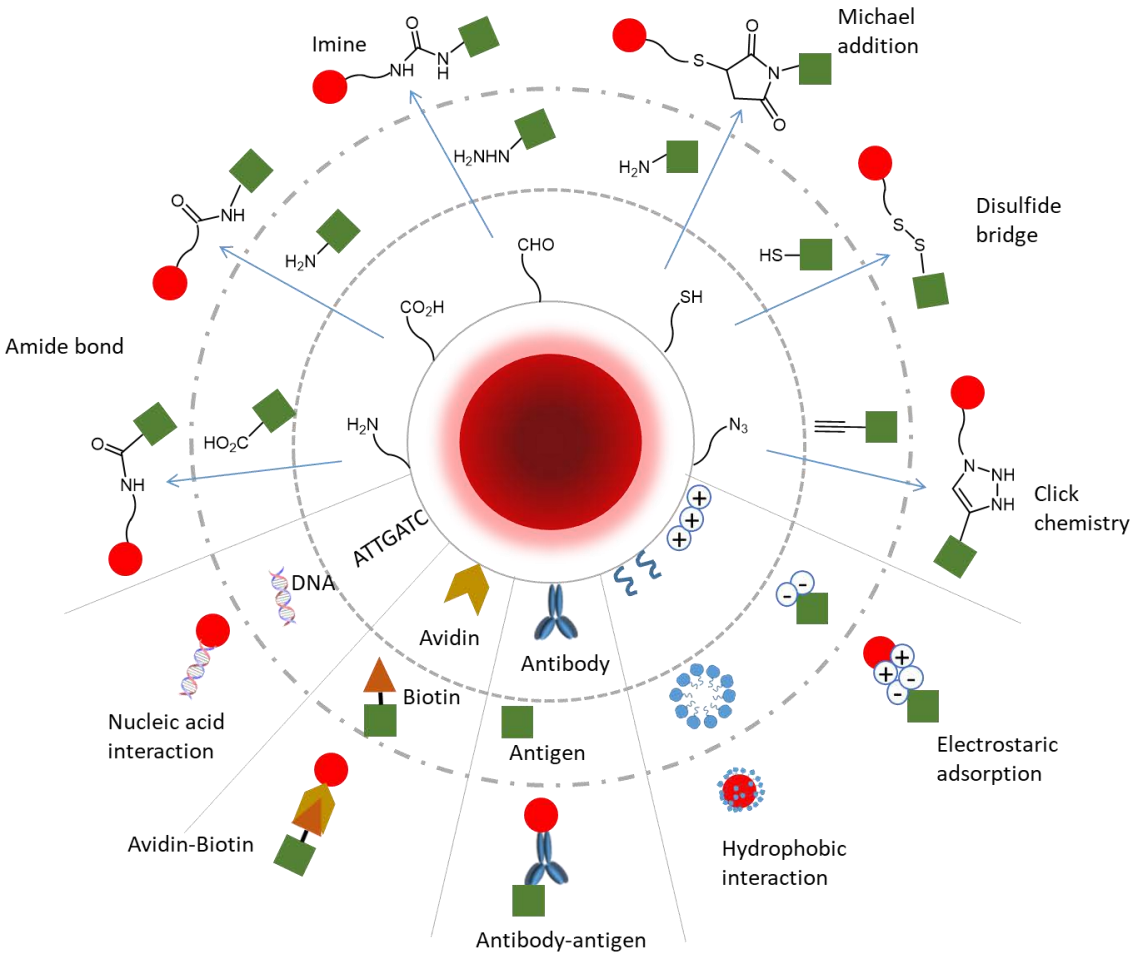

Figure 1.22. Representative bioconjugation protocols of metal noble nanoparticles.

In order to conjugate molecules on gold nanoparticles the direct linking by other affinity reactions is also used, the most common is the union of biotinylated molecules to a streptavidin modified gold nanoparticles and vice versa. This union is as strong as a covalent labelling and several biomolecules can be labelled with biotin.

Finally, the direct reaction of a chemical group on the protein with the AuNPs surface without the use of a linker. It is usually produced during an incubation where the strongly favoured interaction between the gold atoms of AuNP surface and sulphur of thiol groups (-SH) present in the molecules with which it is desired to coat the AuNP is produced(178).

4.4.1.3. Gold nanoparticles in lateral flow strips

The versatility of functionalization and their high signal to noise ratio for visual readouts as well as the optical properties of AuNPs justify their popularity in colorimetric tests.

AuNPs colorimetric assays take advantage of the fact that analytes induce aggregation events that result in measurable changes and shifts in the AuNPs surface plasmon resonance (SPR) bands. AuNPs have an extraordinarily high extinction coefficient, originating from their inherent plasmonic properties. Their optical properties are strongly dependent on the distance between particles, and aggregation causes a massive shift in the extinction spectrum that is manifested as a change in the colour of suspensions from red to purple(185)(168)(186). The clearly distinguishable colour shifts produce a very simple sensor readout that can often be discerned by the naked eye. Most AuNP colorimetric sensors are designed in such a way that binding of an analyte causes particle aggregation accumulation and a consequent attractive colorimetric response for the design of multiple biosensing devices.

One of the first works where gold nanoparticles were used in colorimetric immunoassays was reported in 1981 presenting a sol particle agglutination assay for human chorionic gonadotropin(187). In 1987, it was presented a sol-particle immunoassay for determination of anti-rubella antibodies(188). Not until 20 years later, gold nanoparticles emerged as a labels in lateral flow immunoassays(189).

From then, multiple improvements have been performed in order to solve one of the lateral flow assays main drawbacks: the sensitivity and eventually their accuracy in situations where quantitative results are required.

These strategies are based modifications of the nanoparticles surface and further secondary reactions with other nanoparticles or chemical reagents.

One of the approaches is to increase the density of the gold nanoparticles around the analyte and consequently accumulating more nanoparticles on the test line. This can be achieved interconnecting AuNPs by means of oligonucleotides(190) or antibodies(191) prior to or during the assay. An increase of the density of AuNPs

can be also achieved by assembling AuNPs onto a carrier of larger size such as silica nanorods (192) or dendrimers.

Another strategy is the particles enhancement by the reduction of metals. Silver enhancement is a traditional technique in which colloidal AuNPs act as catalysts to reduce Ag^+ ions to metallic Ag at room temperature in the presence of a reducing agent in acidic pH. Ag atoms are then deposited on the surface of the AuNPs enlarging the particle size of AuNPs and therefore improving the sensitivity by a factor of 10(193)(194)(195).

On the other hand, the reduction of HAuCl4 on the GNP in the presence of NH_2OH or H_2O_2/2-(Nmorpholino) ethanesulfonic acid (MES) demonstrated to decrease the limit of detection in about two orders of magnitude. Recently, it has been presented an enlargement approach based on to the post-assay GNP enlargement on the strip through a catalytic reduction of $HAuCl_4$ in the presence of H_2O_2 which provides the highest enhancement (240-fold) and requires minimal time (1 min) without washing, time-required incubation, or the use of additional equipment(196).

The enhancement of the signal can be also achieved by the production of a detectable compound by the functionalization of the gold nanoparticles with molecules that promote an enzymatic reaction in the presence of substrates. Due to its high catalytic activity, HRP has been widely used for the coating of gold nanoparticles in this kind of assays together with the bioreceptor of the analyte and combined with different substrates such as TMB or AEC(197)(198). After the common performance of the bioassay, the strip is treated with a solution that contains the HRP substrates producing insoluble coloured products on the detection lines.

This HRP-like catalytic activity has been also observed in catalytic metals such as platinum and several works using this metal coating AuNPs have been carried out(199).

4.4.2. Other particles used in LFA

4.4.2.1. Polymeric materials

The first lateral flow immunoassay was fabricated using latex particles as labels and due to their low-cost and versatility they still remain as one the most common options for the development of rapid tests(200)(201). Well stablished protocols for latex particles synthesis can be found in the literature(202). Depending on the final product application particles with different sizes and properties can be prepared including paramagnetism(203) and fluorescence(204). Due to the well-known chemistry of latex surface, protocols for amino carboxyl and thiol functionalization can be easily found. In addition, a huge variety of beads can be found to achieve the properties of interest by means of the incorporation of coloured or/and fluorescent dyes(205).

The labelling with coloured dyes of silica(206) and cellulose beads also achieve this versatility existing decenes of commercially available particles for its application in colour multiplex testing(207).

4.4.2.2. Carbon

The use of carbon for immunochromatographic tests, either as carbon nanoparticles or carbon nanotubes(208)(209), highlight for its good signal-to-noise ratio because of the high contrast between the dark black colour of carbon and the white nitrocellulose membrane background. CNPs are easy to prepare and stable in their conjugated form. They do not require chemical crosslinking but rather direct adsorption of the desired protein and they have a low cost compared to other labels. Carbon nanotubes provide good stability in the time avoiding aggregation but enlarge the time of assay due to their size(210).

4.4.2.3. Fluorescent labels

Fluorescent particles have received great expectations owing to the improvements in the sensitivity in quantitative analysis. Diverse fluorescent reporters have been used for the development of fluorescent lateral flow test such as quantum dots (QDs), up-converting phosphor (UCP) or lanthanide labels among others. Another strategy consists in incorporating fluorescent dyes into other organic/inorganic

nanomaterials, such as silica nanoparticles, liposomes(211)(212) and polystyrene nanoparticles(213).

The fluorescence is mainly originated from the combined aromatic groups or conjugated double bonds in fluorophores(214).

Near infrared radiation (NIR) dyes (excitation/emission peak above 680 nm) are specially interesting for LFA since the strip membrane and sample matrix normally exhibit autofluorescence between 300 and 650 nm.

A remarkable work of NIR-based multiplex lateral flow for the simultaneous detection of four families of antibiotics in milk and the results were in good agreement with that of LC-MS/MS reference method is reference (215).

Quantum dots (QD) are mainly semiconductor III-V and II-VI nanocrystals which are among the most promising fluorescent labels for biomedical diagnosis, molecular imaging and chemical analysis. Depending on the fabrication material and the size they have different emission wavelengths and therefore, different colours(216)(217).

Upconverting phosphor reporters (UCP) are a class of rare-earth containing crystal particles, up-converting photons of lower energy infrared light into higher energy visible light. They have narrow emission bands, long luminescence lifetimes, excellent photostability(218).

Regarding to lanthanide labels, their main advantage is that, unlike organic dyes, they are not affected by strong nonspecific scattering light, such as Tyndall, Raman or Rayleigh scattering, and concentration quenching(217) .

Liposomes can be also used in as signal reporters encapsulating dyes(219). The release of the coloured or fluorescent dye is produced adding surfactants which lyse the membrane. This susceptibility is their main drawback since it decreases the shelf life of the final product.

4.4.2.4. Magnetic particles

The use of magnetic particles is extremely promising for immunochromatography since it allows a previous step of preconcentration of the analyte form a larger matrix (Section xxx) which considerably improve the sensitive of the assay. Moreover, the brown-yellowish colour of magnetic particles makes them colourful labels for lateral flow tests. In addition MPs possess a single magnetic domain that

can be manipulated by an external magnetic field to produce uniform magnetic excitation that can be quantified using a magnetic detection sensor(220).

4.4.2.5. Dendrimers

Dendrimers are synthetic polymeric macromolecules consisting of inner core and peripheral shell are well-designed branching architectures with abundant terminal groups. The modifiable surface of the dendrimers allow conjugation with different molecules, like targeting ligands or drugs(221). These hyperbranched 3D molecules are used in lateral flow, among many other biosensors, improving the sensitivity and reducing nonspecific binding. Dendrimers have also shown high stability and low variability in their response(222).

4.5. Readout systems for lateral flow strips

Lateral flow tests have traditionally generated results in terms of binary YES/NO results that can be read using the naked-eye. If it is true that the information provided by qualitative and semi-quantitative tests is highly valuable for several applications, there is a general demand on moving towards quantitative test with low LODs in order to make effective their real implantation in fields where accurate results are mandatory such as pathogen detection.

Consequently, parallel to the development of new strategies for the detection of analytes on lateral flow strips previously explained, such as the amplification of the signal or the use of other particles, technology to perform the reading and processing of the results has been also developed. In detail, many efforts have been focused on the fabrication of portable devices which do not compromise the concept of point of care especially representative of lateral flow tests. These devices must be also rapid, light-weighted, easy to use and interpret, with automatic data analysis and transmission, robust and economic.

4.5.1. Optical readers

Generally, the instruments detecting colour signals and its software, identify the control and test line position, adjust the background of the strip and interpret the optical density or the grey value as a peak or area integral. This value is thus expressed as a concentration of analyte.

Lateral flow strip readers normally contain a strip holder, where the sample is adjusted depending on its size or the lines position, a light source and image sensors such as a complementary metal oxide semiconductor (CMOS)(223) camera or charge-coupled device (CCD)(224) to capture the images of samples. Other devices do not include an image sensor but an scan (225)(226).

In this case, the colorimetric scanning of the strips is performed by moving the test strip over a light source or vice versa. The detector receives the light reflected on the nitrocellulose as a blank. When the control and test lines pass the light beam, the light reflected decreases due to the absorption/reflection of the nanoparticles, and this quantifiable change is registered and interpreted as a signal proportional to the particles on the bands(227).

4.5.2. Fluorescent readers

Fluorescent readers work with the same principles but in this case the sensor is fluorimetric(228).

Labels in control and test lines are excited at a certain wavelength which enables the emission of a light with longer wavelength from the bands which can be visible or not. This light is then detected and quantified, being proportional to the amount of labels accumulated on control and detection zones. The detection performed from this devices capture fluorescent signal from QDs(229), dye-doped NPs (230) or up-converting NPs(220) among others.

4.5.3. Magnetic readers

Superparamagnetic nanoparticles (MNPs) have sparked great interest as labels lateral flow test. The reading of magnetic signals is associated with a low background due to the negligible magnetic signals detected in biological

samples(231). In addition, the magnetic signals generated do not degrade over a long period allowing the storage for rechecking(232).

The magnetic measurement requires the excitation of the nanoparticles in a magnetic field. Detection is thus performed by exposing a membrane to a group of small coils that reside in between the poles of an electro magnet. The magnetization of the magnetic particles is thereby caused to oscillate at the excitation frequency in the manner of a dipole to create their own fields. These fields are inductively coupled to a sensor in a gradiometer configuration whose signal is then amplified and processed to return a value that indicates the quantity of magnetic particles in the analytical region(233). This system have demonstrated to be able to lower the limit of detection 100 times compared to conventional visual readout of magnetic particles(234).

Table 1. Classification of labels and readers for lateral flow tests.

Optical reader	Fluorescence reader	Magnetic reader
Latex NPs Gold NPs Magnetic NPs Cellulose NPs Silica NPs Carbon NPs and NTs Liposomes Colloidal selenium NPs	Quantum dots Latex NPs Silica NPs Liposomes Upconverting phosphor Lanthanide NPs	Magnetic NPs

5. Final remarks

During last decades, PoC diagnostic tests have allowed to move diagnostic testing more available to the final users. This has been only possible thanks to the advances in key enabling technologies such as biotechnology, nanotechnologies and advanced materials which have produced more sensitive, rapid and specific devices. Moreover, equipment miniaturization and analytical simplification afford the detection of many diseases in remote places.

However, in spite of the many applications of PoC tests, these devices have not reached their full potential. The future of point of care is undoubtedly linked to the advances in each of the scientific disciplines involved in the development.

In this sense, the advent of new technologies and resources for the identification of new biomarkers related with different diseases play a very important role, especially in the early detection of communicable and non-communicable diseases. Screening programs in hospitals and healthcare systems will allow to personalize and administer a specific treatment as soon as possible.

In terms of detection, research continues on the improvement of current platforms and the creation of new ones that improve those costly, time-consuming, and invasive methods currently (235). Consequently, the emphasis of analytical platforms is shifting toward prevention and early detection of diseases and therefore many researchers are exploring the possibility of developing fast, reliable, and non-invasive diagnostic tools that can be used by local physicians at the point-of-care as well as for the management of multiple chronic conditions at home (236)(237).

There is no doubt that, in this sense, advances in complementary technologies such as 3D printing(238), cheap prototyping of electronics together with the miniaturization of readers or potentiostats will be decisive for creating low-cost and sensitive devices that are increasingly variated and that adapt to different needs.

For instance, printed electronics and flexible materials have made possible continuous monitoring for an extended amount of time by wearable PoC device

which allow for continuous chemical sensing in non-invasive samples such as saliva, tears, and sweat. This format of biosensors has received tremendous attention over the past decade not only for being non-invasive, discrete and user-friendly but also for providing valuable real-time information (239). The main interest in wearable biosensors rely on its potential application in the home-based personal management. These devices will provide information of great value which will empower the patients to monitor and manage their own health which would be directly reflected as a lowering health-care costs (240). Recently, it has been reported in literature a needleless temporary tattoo sensor for glucose monitoring in sweat which is in phase I clinical trial (241). Moreover, a new biosensing contact lens capable of detecting glucose levels in patients with diabetes has been also recently reported (242).

In order to maximize the possibilities offered by these devices, they can be wirelessly connected to a drug delivery system that will administer the drug based on the information received in real time (243). This information can also be registered or remotely sent to the doctor in order to adjust the parameters. This is one of the reasons why the current trend in PoC devices is inclined strongly towards smart devices paired with smartphones. However, it is not the only one: a wide range of uses of mobile phone-based technologies have already been developed for the readout of colorimetric, fluorescent, electrochemical tests. As a matter of example, a device for counting blood cells by installing three imaging components on a mobile phone has been developed (244). Other researchers have presented a cost-effective and compact multimodal microscope integrated on a mobile phone that can be used for targeted DNA sequencing and *in situ* point mutation analysis for molecular analysis of tumour tissue morphology (245). In addition, parts of the phone such as the mobile charging connection have been used to connect and embedded circuit and a disposable microfluidic chip for the detection of *Plasmodium falciparum* histidine-rich protein 2, an important biomarker for malaria (246). Mobile phones can be also useful to increase the sensitivity of the devices as they are also used as a microcontroller for hand-held and battery-powered PCR, qPCR and isothermal amplifications (247). Moreover, their use as readers for lateral flow strips could significatively reduce the cost of current LF readers(248).

Driven by all these emerging technologies and the possibilities they offer, the concept ASSURED has been reformulated and the goal is to fabricate REASSURED devices. While maintaining the requirements of ASSURED technology, the concepts of real-time connectivity (R) and ease of specimen collection (E) have been included (249).

Despite there is still room for improvement, these new requirements are a further step to achieve ideal PoC devices. Certainly, the day is not far off when the access of PoC devices would be universal, even in the remotest regions.

6. References

1. Mcpartlin DA, Loftus JH, Crawley AS, Silke J, Murphy CS, Kennedy RJO. ScienceDirect Biosensors for the monitoring of harmful algal blooms. Curr Opin Biotechnol. 2017;45:164–9.
2. De Araujo W, Cardoso TMG, da Rocha RG, Santana MHP, Muñoz RAA, Richter EM, et al. Portable analytical platforms for forensic chemistry: A review. Anal Chim Acta. 2018;1034:1–21.
3. Soares RRG, Ricelli A, Fanelli C, Caputo D, De Cesare G, Chu V, et al. Advances, challenges and opportunities for point-of-need screening of mycotoxins in foods and feeds. Analyst. 2018;143(5):1015–35.
4. Anfossi L., Giovannoli C., Baggiani C. Introductory Chapter: Rapid Test - Advances in Design, Formats, and Detection Strategies. In: Anfonssi L, editor. Rapid Test - Advances in Design, Format and Diagnostic Applications. IntechOpen; 2018. p. 13.
5. Larsson A, Greig-pylypczuk R, Huisman A. The state of point-of-care testing : a european perspective. Ups J Med Sci. 2015;2011(October 2014):1–10.
6. Shaw JL V. Practical challenges related to point of care testing. Pract Lab Med. 2016;4:22–9.
7. Rajan A, Glorikian H. Point-of-care diagnostics : market trends and growth drivers market trends and growth drivers. Expert Opin Med Diagn. 2009;3(1):1–4.
8. Aluisio AR, Waheed S, Cameron P, Hess J, Jacob ST, Kissoon N, et al. Clinical

emergency care research in low- income and middle-income countries : opportunities and challenges. BMJ Glob Heal. 2019;4:1–8.

9. Diseases I. Infectious Diseases, Introduction. In: Kanki P, Grimes DJ, editors. Infectious Diseases. Boston, MA, USA: Springer; 2012. p. 1–6.
10. Ameli J. Communicable Diseases and Outbreak Control. Turkish J Emerg Med. 2015;15(Suppl 1):20–6.
11. Societies F of IR. The Global Impact of Respiratory Disease. Sheffi eld: European Respiratory Society; 2017.
12. Biscevic-Tokic J, Tokic N, Musanovic A. Pneumonia as the most common lower respiratory tract infection. Med Arch. 2013;67(6):442–5.
13. Blasi F, Cosentini R, Migliori GB, Boersma W. Steps forward in LRTI and tuberculosis : update from the ERS Respiratory Infections Assembly. Eur Respir J. 2009;33(6):1448–53.
14. Glaziou P, Sismanidis C, Floyd K, Raviglione M. Global Epidemiology of Tuberculosis. Cold Spring Harb Perspect Med. 2015;5:1–17.
15. Bell LCK, Noursadeghi M. Pathogenesis of HIV-1 and Mycobacterium tuberculosis co-infection. Nat Publ Gr. 2017;
16. Global Health Estimates 2016: Deaths by Cause, Age, Sex, by Country and by Region: 2000-2016. Geneva: World Health Organization; 2018.
17. Harris JB, LaRocque RC, Qadri F, Ryan ET, Calderwood SB. Cholera. Lancet. 2012;379(9835):2466–76.
18. Saha M, Debnath C, Pramanik AK. Review Article Listeria monocytogenes : An Emerging Food Borne Pathogen. Int J Curr Microbiol Appl Sci. 2015;4(11):52–72.
19. Collaborators G 2015 M and C of D. Global , regional , and national life expectancy , all-cause mortality , and cause-specifi c mortality for 249 causes of death , 1980 – 2015 : a systematic analysis for the Global Burden of Disease Study 2015. Lancet. 2016;388:1459–544.
20. Majowicz SE, Musto J, Scallan E, Angulo FJ, Kirk M, Brien SJO, et al. The Global Burden of Nontyphoidal Salmonella Gastroenteritis. Clin Infect Dis. 2010;50:882–9.
21. Shridhar PB, Siepker C, Noll LW, Shi X, Nagaraja TG. Shiga Toxin Subtypes of Non-O157 Escherichia coli Serogroups Isolated from Cattle Feces. Front Cell

Infect Microbiol. 2017;7(121):1–8.

22. Schrank G, Branch-Elliman W. Breaking the Chain of Infection in Older Adults. A Review of Risk Factors and Strategies for Preventing Device-Related Infections. Infect Dis Clin North Am. 2017;31:649–71.
23. Sandle T. History and development of microbiological culture media. J (Institute Sci Technol. 2010;10–4.
24. Ayyash S, Wu W-I, Selvaganapathy PR. Fast and Inexpensive Detection of Bacterial Viability and Drug Effectiveness through Metabolic Monitoring. Sensors. 2016;16:1879.
25. Mishra M, Chauhan P. Applications of Microscopy in Bacteriology. Microsc Res. 2016;4(January):1–9.
26. Frederick K, Ishii M, Qi H, Bajénoff M, Egen JG, Germain RN, et al. Quantifying cellular interaction dynamics in 3-D fluorescence microscopy data. Nat Protoc. 2009;4(9):1305–11.
27. Carr SA, Hemling ME, Bean MF, Roberts GD. Integration of Mass Spectrometry in Analytical Biotechnology ’. Anal Chem. 1991;63:2802–24.
28. Graham DW. MALDI-TOF mass spectrometry : an emerging technology for microbial identification and diagnosis. Front Microbiol. 2015;6:1–16.
29. Yu H, Halonen MJ, Pepper IL. Immunological Methods. In: Pepper IL, Gerba CP, Gentry TJ, editors. Envromental Microbiology. Elsevier Inc.; 2015. p. 245–70.
30. Hibbs AR. Fluorescence Immunolabelling. In: Hibbs AR, editor. Confocal Microscopy for Biologists. New York: Plenum Publishers; 2004.
31. Burry RW. Controls for immunocytochemistry: An update. J Histochem Cytochem. 2011;59(1):6–12.
32. Lin A V. Direct ELISA. In: Hnasko R, editor. ELISA: Methods and Protocols. New York; 2015. p. 61–7.
33. Konstantinou GN. Enzyme-Linked Immunosorbent Assay (ELISA). In: Lin J, Alcoce M, editors. Food Allergens: Methods and Protocols. Springer; 2017. p. 79–94.
34. Shojaeian S, Maslehat Lay N, Zarnani A-H. Detection Systems in Immunohistochemistry. In: Immunohistochemistry. IntechOpen; 2018. p. 13.
35. Vashist SK, Luong JHT. Enzyme-Linked Immunoassays. Handbook of

Immunoassay Technologies. Elsevier Inc.; 2018. 97–127 p.

36. Mahmood T, Yang P. Western Blot : Technique , Theory , and Trouble Shooting. N Am J Med Sci. 2012;4(9):429–34.
37. Renart J, Behrens MM, Fernandez-renart M, Nez JLM. IMMUNOBLOTTING TECHNIQUES. In: Diamandis EP, Christopoulos TK, editors. Immunoassay. 1996. p. 537–54.
38. Skogerboe KJ, West SF, Murllio M, Glass MW, Shaunak S, Taft JF. Genetic Screening of Newborns for Sickle Cell Disease : Correlation of DNA Analysis with Hemoglobin Electrophoresis. Clin Chem. 1991;37(3):454–8.
39. Bailey GS. Ouchterlony Double Immunodiffusion. In: Walker JM, editor. The Protein Protocols Handbook. Humana Press Inc; 2002. p. 0–3.
40. Mancini G, Carbonara AO, Heremans JF. Immunochemical quantitation of antigens by single radial immunodiffusion. Immunochem. 1965;235(2):251–2.
41. Kashyap RS, Agarwal NP, Chandak NH, Taori GM, Biswas SK, Purohit HJ, et al. The application of the Mancini technique as a diagnostic test in the CSF of tuberculous meningitis patients. Med Sci Monit. 2002;8(6):95–9.
42. Maclagan NF. Flocculation tests: chemical and clinical significance. Br Med J. 1948;2(4585):892–6.
43. Wanger A, Chavez V, Huang R, Wahed A, Dasgupta A, Actor J. Antigen and Antibody Testing. In: Microbiology and Molecular Diagnosis in Pathology. Elsevier; 2017. p. 221–32.
44. Wu D, Shen J, Bai H, Yu G. Supramolecular self-assemblies for bacterial cell agglutination driven by directional charge-transfer interactions. Chemcomm. 2018;54:2922–5.
45. Ryu W. Diagnosis and Methods. In: Molecular Virology of Human Pathogenic Viruses. Elsevier Inc.; 2017. p. 47–62.
46. Hage DS, Moser A. Immunoaffinity chromatography: an introduction to applications and recent developments Annette. Bioanalysis. 2010;2(4):769–90.
47. Pray LA. Discovery of DNA Structure and Function : Watson and Crick. Nat Educ. 2019;1(1):100.
48. Jones ME. Albrecht Kossel, a Biographical Sketch. Yale J Biol Med. 1953;26.

49. István H. The tetranucleotide hypothesis : a centennial. Struct Chem. 2009;20:753–6.
50. Cobb M. Oswald Avery , DNA , and the transformation of biology. Curr Biol. 2005;24(2):55–60.
51. Separation T. Chargaff ' s Rules : the Work of Erwin Chargaff. J Biol Chem. 2005;280(24):172–5.
52. Thompson J, Braun G, Tierney D, Wessels L, Schmitzer H. Rosalind Franklin ' s X-ray photo of DNA as an undergraduate optical diffraction experiment. Am Assoc Phys Teach. 2018;86:95–104.
53. Bansal M. DNA structure : Revisiting the Watson – Crick double helix. Curr Sci. 2003;85(11):1556–63.
54. Mullis KB. The Unusual Origin of the Polymerase Chain Reaction. Sci Am. 1990;(April):56–65.
55. Garibyan L, Avashia N. Research Techniques Made Simple: Polymerase Chain Reaction (PCR). J Invest Dermatol. 2013;133(3):1–8.
56. Lorenz TC. Polymerase Chain Reaction : Basic Protocol Plus Troubleshooting and Optimization Strategies. J Vis Exp. 2012;63:1–15.
57. Bachman J. Reverse-Transcription PCR (RT-PCR). In: Methods in Enzymology [Internet]. 1st ed. Elsevier Inc.; 2013. p. 67–74. Available from: http://dx.doi.org/10.1016/B978-0-12-420037-1.00002-6
58. Lee PY, Costumbrado J, Hsu C, Kim YH. Agarose Gel Electrophoresis for the Separation of DNA Fragments. J Vis Exp. 2012;62:1–5.
59. Peirson SN, Butler JN. Quantitative Polymerase Chain Reaction. In: Circadian Rhythms: Methods and Protocols. Humana Press Inc; 2007. p. 349–62.
60. Jalali M, Zaborowska J, Jalali M. The Polymerase Chain Reaction: PCR, qPCR, and RT-PCR. Basic Science Methods for Clinical Researchers. Elsevier Inc.; 2017. 1–18 p.
61. Stefan CP, Chase K, Coyne S, Kulesh DA, Minogue TD, Koehler JW. Development of real-time reverse transcriptase qPCR assays for the detection of Punta Toro virus and Pichinde virus. Virol J. 2016;13(54):1–6.
62. Shahnewaj K, Mannan B, Chowdhury A, Mazumdar RM, Hossain N, Islam S. Nucleic acid amplification : Alternative methods of polymerase chain reaction. J Pharm Bioallied Sci. 2013;5(4):245–53.

63. Guatelli JC, Whitfieldt KM, Kwoht DY, Barringert KJ, Richman DD, Gingeraso TR. Isothermal , in vitro amplification of nucleic acids by a multienzyme reaction modeled after retroviral replication. Proc Natl Acad Sci. 1990;87(March):1874–8.
64. Walker GT, Fraiser MS, Schram JL, Little MC, Nadeau JG, Malinowski DP. Strand displacement amplification-an isothermal, in vitro DNA amplification technique. Nucleic Acids Res. 1992;20(7):1691–6.
65. Zeng L, Mukama O, Mukama O, Lu X, Cao S, Lin D. Strand Displacement Amplification for Multiplex Detection of Nucleic Acids. In: Modulating Gene Expression - Abridging the RNAi and CRISPR-Cas9 Technologies. 2018. p. 61–82.
66. Walker GT, Little MC, Nadeau JG, Shank DD. Isothermal in vitro amplification of DNA by a restriction enzyme / DNA polymerase system. Proc Nati Acad Sci USA. 1992;89:392–6.
67. Vincent M, Xu Y, Kong H. Helicase-dependent isothermal DNA amplification. EMBO Rep. 2004;5(8):795–800.
68. Biomax. Available from: http://www.bio-helix.com/
69. Uphoff TS, Buchan BW, Ledeboer NA. Multicenter Evaluation of the Solana Group A Streptococcus Assay : Comparison with Culture. J Clin Microbiol. 2016;54(9):2388–90.
70. Li J, Macdonald J. Advances in isothermal amplification : Novel strategies inspired by biological processes Biosensors and Bioelectronics Advances in isothermal ampli fi cation : novel strategies inspired by biological processes. Biosens Bioelectron. 2014;64(September):196–211.
71. Notomi T, Okayama H, Masubuchi H, Yonekawa T, Watanabe K, Amino N, et al. Loop-mediated isothermal amplification of DNA. Nucleic Acids Res. 2000;28(12).
72. Tambo M, Id MM, Id DRM. Loop-mediated isothermal amplification (LAMP) and Polymerase Chain Reaction (PCR) as quality assurance tools for Rapid Diagnostic Test (RDT) malaria diagnosis in. PLoS One. 2018;13(12):1–8.
73. Cai S, Kong F, Xu S, Yao C. Real-time loop-mediated isothermal amplification for rapid detection of Enterocytozoon hepatopenaei. PeerJ. 2018;(6:e5993).
74. Carinelli S. Biomarkers detection of global infectious diseases based on

magnetic particles. Universitat Autònoma de Barceloan; 2019.

75. Li J, Stetten F Von, Macdonald J. Review: a comprehensive summary of a decade development of the recombinase polymerase amplification. Analyst. 2019;144(1):31.
76. Zhao G, He H, Wang H. Use of a recombinase polymerase amplification commercial kit for rapid visual detection of Pasteurella multocida. BMC Vet Res. 2019;15(154):1–8.
77. Ali M, Li F, Zhang Z, Zhang K. Rolling circle amplification: A versatile tool for chemical biology, materials science and medicine. Chem Soc Rev. 2014;43:3324.
78. Mabey D, Peeling RW, Ustianowski A, Perkins MD. Diagnostics for the developing world. Nat Rev Microbiol. 2004;2(3):231–40.
79. Food and Drug Administration, 2008. Clinical Laboratory Improvement Amendments of 1988 (CLIA).
80. LaBarre P, Hawkins KR, Gerlach J, Wilmoth J, Beddoe A, Singleton J, et al. A simple, inexpensive device for nucleic acid amplification without electricity-toward instrument-free molecular diagnostics in low-resource settings. PLoS One. 2011;6(5).
81. Yager P, Domingo GJ, Gerdes J. Point-of-Care Diagnostics for Global Health Point-of-Care Diagnostics for Global Health. Annu Rev Biomed Eng. 2008;10:107–44.
82. Lee HH, Allain JP. Improving blood safety in resource-poor settings. Vox Sang Suppl. 2004;87(2):176–9.
83. Gale BK, Jafek AR, Lambert CJ, Goenner BL. A Review of Current Methods in Microfluidic Device Fabrication and Future Commercialization Prospects. Inventions. 2018;3(60).
84. Xianyu Y, Wang Q, Chen Y. Magnetic particles-enabled biosensors for point-of-care testing Yunlei. Trends Anal Chem. 2018;106:213–24.
85. Majidi S, Sehrig FZ, Farkhani SM, Goloujeh MS. Current methods for synthesis of magnetic nanoparticles. 2014;(October):1–13.
86. Shevtsov M, Zhao L, Protzer U. Applicability of Metal Nanoparticles in the Detection and Monitoring of Hepatitis B Virus Infection. Viruses. 2017;9(193).

87. Serve A, Pieler MM, Benndorf D, Rapp E, Wolff MW, Reichl U. Comparison of influenza virus particle purification using novel magnetic sulfated cellulose particles with an established centrifugation method for analytics. Anal Chem. 2015;87(21):10708–11.
88. Patramool S, Bernard E, Hamel R, Natthanej L, Chazal N, Surasombatpattana P, et al. Isolation of infectious chikungunya virus and dengue virus using anionic polymer-coated magnetic beads. J Virol Methods. 2013;193(1):55–61.
89. Carinelli S, Ballesteros CX, Martí M, Alegret S, Pividori MI. Electrochemical magneto biosensor for CD4 count in AIDS diagnosis and monitoring. Biosens Bioelectron. 2015;74:974–80.
90. Gao X, Yao X, Zhong Z, Jia L. Rapid and sensitive detection of Staphylococcus aureus assisted by polydopamine modi fi ed magnetic nanoparticles. Talanta. 2018;186(February):147–53.
91. Liebana S, Brandao D, Cortes P, Campoy S, Alegret S, Pividori MI. Analytica Chimica Acta Electrochemical genosensing of Salmonella , Listeria and Escherichia coli on silica magnetic particles. 2016;904(Anal. Chim. Acta):1–9.
92. Palma R De, Liu C, Barbagini F, Reekmans G, Bonroy K, Laureyn W, et al. Magnetic Particles as Labels in Bioassays : Interactions between a Biotinylated Gold Substrate and Streptavidin Magnetic Particles. J Phys Chem C. 2007;111:12227–35.
93. Jing LAN, Yang C, Zongshan Z. Effective Organochlorine Pesticides Removal from Aqueous Systems by Magnetic Nanospheres Coated with Polystyrene. J Wuhan Technol Univ Sci Ed. 2014;(1):168–73.
94. Price PM, Mahmoud WE, Al-ghamdi AA, Bronstein LM. Magnetic Drug Delivery : Where the Field Is Going. Front Chem. 2018;6:1–7.
95. Panagiotopoulos N, Duschka RL, Ahlborg M, Bringout G, Debbeler C, Graeser M, et al. Magnetic particle imaging : current developments and future directions. Int J Nanomedicine. 2015;10:3097–114.
96. Kozitsina AN, Svalova TS, Malysheva NN, Okhokhonin A V, Vidrevich MB, Brainina KZ. Sensors Based on Bio and Biomimetic Receptors in Medical Diagnostic , Environment , and Food Analysis. Biosensors. 2018;8:1–34.
97. Chang Y, Hong Y, Wei Y, Tai Y. Self-assembled biomimetic monolayers using

phospholipid- containing disulfides. Biomaterials. 2005;26:2313–24.

98. Grinsven BB Van, Eersels K, Akkermans O, Ellermann S, Kordek A, Peeters MM, et al. Label-free detection of Escherichia coli based on thermal transport through surface imprinted. ACS Sensors. 2016;1(9):1140–7.
99. Redeker ES, Eersels K, Akkermans O, Royakkers J, Dyson S, Nurekeyeva K, et al. Biomimetic Bacterial Identi fi cation Platform Based on Thermal Wave Transport Analysis (TWTA) through Surface-Imprinted Polymers. ACS Infect Dis. 2017;3:388–97.
100. Pan J, Chen W, Pan G, Chen W. Chem Soc Rev Molecularly imprinted polymers as receptor mimics for selective cell recognition. Chem Soc Rev Tutor. 2018;47:5574–87.
101. Eersels K, Grinsven B Van, Ethirajan A, Timmermans S, Jimenez K, Bogie J, et al. Selective identification of macrophages and cancer cells based on thermal transport through surface- imprinted polymer layers. ACS Appl Mater Interfaces is. 2013;5(15):7258–67.
102. Marfa J, Pividori MI. Molecularly imprinted polymers for biotin and biotinylated molecules. A promising material for Rapid Diagnostic Tests. 2017.
103. Foguel MV, Thaisa N, Pedro B, Valnice M, Zanoni B, Taboada P. Molecularly imprinted polymer (MIP): a promising recognition system for development of optical sensor for textile dyes. Procedia Technol. 2017;27:299–300.
104. Uzuriaga-Sánchez RJ, Wong A, Khan S, Pividori MI, Picasso G, Sotomayor MDPT. Synthesis of a new magnetic-MIP for the selective detection of 1-chloro-2,4-dinitrobenzene, a highly allergenic compound. Mater Sci Eng C. 2017;74:365–73.
105. Newman JD, Setford SJ. Enzymatic Biosensors. Mol Biotechnol. 2006;32:249.
106. Liu C, Xu C, Xue N, Hai Sun J, Cai H, Li T, et al. Enzyme Biosensors for Point-of-Care Testing. In: MEMS Sensors - Design and Application. 2017.
107. Pisoschi AM. Potentiometric Biosensors : Concept and Analytical Applications-An Editorial. Biochem Anal Biochem. 2016;5(3):19–20.
108. Zuber AA, Elizaveta K, Bachhuka A. Biosensing. Elsevier; 2018. p. 1–21.
109. Takhistov P. Biosensor Technology for Food Processing, Safety and Packaging. In: Handbook of Food Science, Technology, and Engineering.

Taylor & Francis; 2005.

110. Grieshaber D, MacKenzie R, Voros J, Reimhult E. Electrochemical Biosensors - Sensor Principles and Architectures. Sensors. 2008;8:1400–58.
111. Moran KLM, Fitzgerald J, Mcpartlin DA, Loftus JH. Biosensor-Based Technologies for the Detection of Pathogens and Toxins. Vol. 74, Comprehensive Analytical Chemistry. Elsevier Ltd; 2016. 93–120 p.
112. Yoo E, Lee S. Glucose Biosensors: An Overview of Use in Clinical Practice. Sensors. 2010;10:4558–76.
113. Swain GM. Solid Electrode Materials : Pretreatment and Activation. In: Zoski CG, editor. Handbook of Electrochemistry. Elsevier B.V.; 2007.
114. Wang P, Zheng Y, Li B. Preparation and electrochemical properties of polypyrrole / graphite oxide composites with various feed ratios of pyrrole to graphite oxide. Synth Met. 2013;166:33–9.
115. García PG, Torres M, Franco-urquiza EA. Mechanical and thermal behavior dependence on graphite and oxidized graphite content in polyester composites. Polymer (Guildf). 2018;153:9–16.
116. Pividori MI, Alegret S. Electrochemical Genosensing Based on Rigid Carbon Composites . A Review. Anal Lett. 2005;38:2541–65.
117. Brasil PR, Marques DO, Lermo A, Campoy S, Yamanaka H, Alegret S, et al. Double-Tagging Polymerase Chain Reaction with a Thiolated Primer and Electrochemical Genosensing based on Gold Nanocomposite Sensor for Food Safety. Anal Chem. 2009;81(4):1332–9.
118. Fenga PG, Stradiotto R, Pividori I. Silver Nanocomposite Electrode Modified with Hexacyanoferrate . Preparation , Characterization and Electrochemical Behaviour Towards Substituted Anilines. Electroanalysis. 2011;23(5):1100–6.
119. Pumera M, Merkoci A, Alegret S. Carbon nanotube composites for electrochemical sensing. Tokyo, Japan: Digest of Papers Microprocesses and Nanotechnology 2005; 1991.
120. Valle M, Pumera M, Llopis X, Pe B. New materials for electrochemical sensing VI : Carbon nanotubes. 2005;24(9):826–38.
121. Erdem A, Pividori MI, Lermo A, Bonanni A, Alegret S. Genomagnetic assay based on label-free electrochemical detection using magneto-composite

electrodes. Sensors and Actuators. 2006;114:591–8.

122. Taleat Z, Khoshroo A. Screen-printed electrodes for biosensing: a review (2008 – 2013). Microchim Acta. 2014;181:865–91.
123. Garbarino F, Antonio G, Minero S, Rizzi G, Fock J, Fougt M. Biosensors and Bioelectronics Integration of rolling circle amplification and optomagnetic detection on a polymer chip. Biosens Bioelectron. 2019;142(July):111485.
124. Wade D, Diaw PA, Daneau G, Diallo AA. Laboratory and Field Evaluation of the Partec CyFlow MiniPOC for Absolute and Relative CD4 T-Cell Enumeration. PLoS One. 2015;10:1–14.
125. Jung W, Han J, Choi J, Ahn CH. Microelectronic Engineering Point-of-care testing (POCT) diagnostic systems using microfluidic lab-on-a-chip technologies. Microelectron Eng. 2015;132:46–57.
126. Nguyen T, Wolff A, Bang DD. From Lab on a Chip to Point of Care Devices : The Role of Open Source Microcontrollers. Micromachines. 2018;9:403.
127. Hu J, Wang S, Wang L, Li F, Pingguan-murphy B, Jian T, et al. Biosensors and Bioelectronics Advances in paper-based point-of-care diagnostics. Biosens Bioelectron. 2014;54:585–97.
128. Fridley G, Le H, Fu E, Yager P. Controlled release of dry reagents in porous media for tunable temporal and spatial distribution upon rehydration. Lab Chip. 2013;12(21):4321–7.
129. Carrell C, Kava A, Nguyen M, Menger R, Munshi Z, Call Z, et al. Microelectronic Engineering Beyond the lateral fl ow assay : A review of paper-based micro fl uidics. Microelectron Eng. 2019;206(November 2018):45–54.
130. Lam T, Devadhasan JP, Howse R, Kim J. A Chemically Patterned Microfluidic Paper-based Analytical Device (C- μ PAD) for Point-of-Care Diagnostics. Sci Rep. 2017;7:1188.
131. Smith S, Smith S. Printed Paper – Based Electrochemical Sensors for Low-Cost Point-of-Need Applications. Electrocatalysis. 2019;
132. Rafiq M, Kadir A. Lab on a Chip patterning technique. 2012;209–18.
133. Martinez AW, Phillips ST, Nie Z, Cheng C, Carrilho E, Wiley BJ, et al. Programmable diagnostic devices made from paper and tape. 2010;2499–504.

134. Virekunnas L. Colloidal gold and paramagnetic labels in lateral flow assay detecting ricin. 2012;(April).
135. Microfluidic MAP, Strong EB, Knutsen C, Wells JT, Jangid AR, Mitchell ML, et al. Devices (MicroPADs). 2019;
136. Anfossi L, Baggiani C, Giovannoli C, Giraudi G. Lateral Flow Immunoassays for Aflatoxins B and G and for Aflatoxin M1. In: Razzaghi-Abyaneh M, editor. Aflatoxins - Recent Advances and Future Prospects. IntechOpen; 2018. p. 13.
137. Biagini RE, Sammons DL, Smith JP, MacKenzie BA, Striley CAF, Snawder JE, et al. Rapid, sensitive, and specific lateral-flow immunochromatographic device to measure anti-anthrax protective antigen immunoglobulin G in serum and whole blood. Clin Vaccine Immunol. 2006;13(5):541–6.
138. Wang D, Zhu J, Zhang Z, Zhang Q, Zhang W, Yu L, et al. Simultaneous lateral flow immunoassay for multi-class chemical contaminants in maize and peanut with one-stop sample preparation. Toxins (Basel). 2019;11(1):1–11.
139. Akter S, Kustila T, Leivo J, Muralitharan G, Vehniäinen M, Lamminmäki U. Noncompetitive Chromogenic Lateral-Flow Immunoassay for Simultaneous Detection of Microcystins and Nodularin. Biosensors. 2019;9(2):79.
140. Hudson M, Stuchinskaya T, Ramma S, Patel J, Sievers C, Goetz S, et al. Drug screening using the sweat of a fingerprint: Lateral flow detection of ’ " 9 - tetrahydrocannabinol, cocaine, opiates and amphetamine. J Anal Toxicol. 2019;43(2):88–95.
141. Posthuma-Trumpie GA, Korf J, Van Amerongen A. Lateral flow (immuno)assay: Its strengths, weaknesses, opportunities and threats. A literature survey. Anal Bioanal Chem. 2009;393(2):569–82.
142. Thinblueline. https://history.nih.gov/exhibits/thinblueline/timeline.html
143. Simmer HH. The First Experiments to Demonstrate an Endocrine Function of the Corpus Luteum: Part II: Ludwig Fraenkel Versus Vilhelm Magnus. Franz Steiner Verlag. 1972;1:76–99.
144. Iversen E. Papyrus Carlsberg nº VIII. 1939.
145. Olszynko-gryn J. Thin blue lines : product placement and the drama of pregnancy testing in British cinema and television. 2017;50:495–520.
146. Wide L, Gemzell CA. An Immunological Pregnancy Test. Acta Endocrinol (Copenh). 1960;35(II):261–7.

147. Midgley AR. Radioimmunoassay: a method for human chorionic gonadotropin and human luteinizing hormone. Endocrinology. 1966;79(1):10–8.
148. Vaitukaitis JL, Braunstein GD, Ross GT. A radioimmunoassay which specifically measures human chorionic gonadotropin in the presence of human luteinizing hormone. Am J Obstet Gynecol. 1972;113(6):751–8.
149. Wilven M. Testing times. The birth of pregnancy test. Biomed Sci. 2019;18–22.
150. Clearblue. 2019. Available from: https://www.clearblue.com/pregnancy-tests/digital
151. PATH. A HealthTech Historical Profile - Lateral-Flow, Point-of-Care Diagnostic Tests for Infectious Diseases [Internet]. 2005. Available from: www.path.org
152. Koczula KM, Gallotta A. Lateral flow assays. Essays Biochem. 2016;60(June):111–20.
153. Amerongen A, Veen J, Arends H, Koets M. Lateral Flow Immunoassay. In: Handbook of Immunoassay Technologies. Elsevier Inc.; 2018. p. 157–82.
154. Tisone TC, Farrell BO. Manufacturing the Next Generation of Highly Sensitive and Reproducible Lateral Flow Immunoassay. In: Lateral Flow Immunoassay. 2009. p. 131–56.
155. Holstein CA, Chevalier A, Bennett S, Anderson CE, Keniston K, Olsen C, et al. Immobilizing affinity proteins to nitrocellulose : a toolbox for paper-based assay developers. Anal Bioanal Chem. 2016;408(5):1335–46.
156. Quesada-gonzález D, Stefani C, González I, De A, Domingo N, Mutjé P, et al. SC. Biosens Bioelectron. 2019;141:111407.
157. Millipore M. Rapid Lateral Flow Test Strips. Considerations for Product Development Table of Contents. 2013.
158. Sajid M, Daud M. Designs , formats and applications of lateral flow assay : A literature review. J Saudi Chem Soc. 2015;19(6):689–705.
159. Hristov DR, Rodriguez-quijada C, Gomez-marquez J, Hamad-schifferli K. Designing Paper-Based Immunoassays for Biomedical Applications. Sensors. 2019;19(3):554.
160. Lee E, Ah Y, Tae Y, Hammock BD. Competitive immunochromatographic

assay for the detection of the organophosphorus pesticide EPN. Food Agric Immunol. 2013;24(2):129–38.

161. Yang X, Yang J, Wang Y, Li L, Sun Z, Yue Z, et al. A Lateral Flow Immunochromato-graphic Strip Test for Rapid Detection of Oseltamivir Phosphate in Egg and Chicken Meat. Sci Rep. 2018;8(1):16680.
162. Liu J, Hu X, Cao F, Zhang Y, Lu J, Zeng L. Subject Category : Subject Areas : A lateral flow strip based on gold nanoparticles to detect 6-monoacetylmorphine in oral fluid. R Soc open sci. 2018;5(6).
163. Anfossi L, Nardo F Di, Cavalera S, Giovannoli C. Multiplex Lateral Flow Immunoassay : An Overview of Strategies towards High-throughput Point-of-Need Testing. Biosensors. 2019;9(1):2.
164. Kong F-Y, Zhang J-W, Li R-F, Wang Z-X, Wang W-J, Wang W. Unique Roles of Gold Nanoparticles in Drug Delivery, Targeting and Imaging Applications. Molecules. 2017;22:1445.
165. Mahan MM, Doiron AL. Gold Nanoparticles as X-Ray , CT , and Multimodal Imaging Contrast Agents : Formulation , Targeting , and Methodology. J Nanomater. 2018;2018.
166. Wang S, Lu G. Applications of Gold Nanoparticles in Cancer Imaging and Treatment. In: Noble and Precious Metals - Properties, Nanoscale Effects and Applications. IntechOpen; 2017.
167. Carlos F, Franco R, Pedrosa P, Veigas B, Baptista P V. Gold Nanoparticles for DNA/RNA-Based Diagnostics ´. In: Handbook of Nanoparticles. Springer International Publishing; 2016. p. 1339–70.
168. Cordeiro M, Carlos FF, Pedrosa P, Lopez A, Baptista PV. Gold Nanoparticles for Diagnostics : Advances towards Points of Care. Diagnostics. 2016;6:20.
169. Yeh Y-C, Creran B, Rotello VM. NIH Public Access. Nanoscale. 2014;4(6):1871–80.
170. Domènech A. Immunoassaigs de flux lateral per a la seva aplicació en la malaltia celíaca. 2019.
171. Thanh NTK, Maclean N, Mahiddine S. Mechanisms of nucleation and growth of nanoparticles in solution. Chem Rev. 2014;114(15):7610–30.
172. Kimling J, Maier M, Okenve B, Kotaidis V, Ballot H, Plech A. Turkevich Method for Gold Nanoparticle Synthesis Revisited. J Phys Chem B.

2006;100(32):15700–7.

173. Jana NR, Gearheart L, Murphy CJ. Evidence for Seed-Mediated Nucleation in the Chemical Reduction of Gold Salts to Gold Nanoparticles. Chem Mater. 2001;13:2313–22.
174. Zanella R. Metodologías para la síntesis de nanopartículas : controlando forma y tamaño. Mundo Nano. 2012;5(1):69–81.
175. Niu Z, Li Y. Removal and Utilization of Capping Agents in Nanocatalysis Removal and Utilization of Capping Agents in Nanocatalysis. Chem Mater. 2014;26(1):72–83.
176. Malvern Panalytical. 2019. Characterization of Nanoparticle Size and State Prior to Nanotoxicological Studies Using NTA. AZoNano, viewed 22 July 2019
177. Azonano. https://www.azonano.com/article.aspx?ArticleID=2474
178. Razak KA, Makhsin SR, Zakaria ND, Nor NM. Gold nanoparticles for diagnostic development. In: Sustainable Diagnostics for Low Resource Areas. Universiti Sains Malaysia;
179. Ackerson CJ, Powell RD, Hainfeld JF. Site-Specific Biomolecule Labeling with Gold Clusters. Vol. 481, Methods in Enzymology. Elsevier Masson SAS; 2010. 195–230 p.
180. Wang P, Wang X, Wang L, Hou X, Liu W, Chen C. Interaction of gold nanoparticles with proteins and cells. Sci Technol Adv Mater. 2015;16(3):34610.
181. Liu G, Zhang Y, Guo W. Covalent Functionalization of Gold Nanoparticles as Electronic Bridges and Signal Amplifiers Towards an Electrochemical Immunosensor for Botulinum Neurotoxin Type A. Biosens Bioelectron. 2014;61:547–53.
182. Marco M Di, Razak KA, Aziz AA, Devaux C, Borghi E, Levy L, et al. Overview of the main methods used to combine proteins with nanosystems : absorption , bioconjugation , and encapsulation. Int J Nanomedicine. 2010;5:37–49.
183. Aubin-Tam M, Hamad-Schifferli K. Structure and function of nanoparticle – protein conjugates. Biomed Mater. 2008;3:17.
184. Sperling RA, Parak WJ. Surface modification , functionalization and bioconjugation of colloidal inorganic nanoparticles. Phil Trans R Soc A. 2010;368:1333–83.

185. Njoki PN, Lim IS, Mott D, Park H, Khan B, Mishra S, et al. Size Correlation of Optical and Spectroscopic Properties for Gold Nanoparticles. J Phys Chem. 2007;111:14664–9.
186. Storhoff JJ, Lazarides AA, Mucic RC, Mirkin CA, Letsinger RL, Schatz GC. What Controls the Optical Properties of DNA-Linked Gold Nanoparticle Assemblies ? J Am Chem Soc. 2000;122:4640–50.
187. Leuvering J, Thal P, Van der Waart M, Schuurs A. A Sol particle agglutination assay for human chorionic gonadotrophin. J Immunol Methods. 1981;45:183–94.
188. Wielaard F, Denissen A, Van der Veen L, Rutjes I. A sol-particle immunoassay for determination of anti-rubella antibodies ; development and clinical validation. J Virol Methoak. 1987;17:149–58.
189. Fong WK, Modrusan Z, Nevin JPMC, Marostenmaki J, Zin BEN, Bekkaoui F. Rapid Solid-Phase Immunoassay for Detection of Methicillin- Resistant Staphylococcus aureus Using Cycling Probe Technology. J Clin Micriobiology. 2000;38(7):2525–9.
190. Hu J, Wang L, Li F, Han L, Lin M, Lu J. Oligonucleotide-linked gold nanoparticle aggregates for enhanced sensitivity in lateral flow assays. Lab Chip. 2013;13:4352–7.
191. Rivas L, Escosura-muñiz A De, Serrano L, Altet L, Francino O. Triple lines gold nanoparticle-based lateral flow assay for enhanced and simultaneous detection of Leishmania DNA and endogenous control. Nano Res. 2015;1–11.
192. Xu H, Chen J, Birrenkott J, Xiaojun J, Takalkar S, Baryeh K, et al. Gold-Nanoparticle-Decorated Silica Nanorods for Sensitive Visual Detection of Proteins. Anal Chem. 2014;86:7351–9.
193. Panferov VG, Safenkova I V, Byzova NA, Varitsev YA, Zherdev A V, Dzantiev BB, et al. Silver-enhanced lateral flow immunoassay for highly-sensitive detection of potato leafroll virus. Food Agric Immunol. 2017;1–13.
194. Wei Y, Xiao-bing L, Guo-wen L, Bing-bing Z, Yi Z, Tao K. A colloidal gold probe-based silver enhancement immunochromatographic assay for the rapid detection of abrin-a. Biosens Bioelectron. 2011;26(8):3710–3.
195. Linares EM, Kubota LT, Michaelis J, Thalhammer S. Enhancement of the detection limit for lateral fl ow immunoassays : Evaluation and comparison

of bioconjugates. J Immunol Methods. 2012;375(1–2):264–70.

196. Panferov VG, Safenkova I V, Zherdev A V, Dzantiev BB. Post-assay growth of gold nanoparticles as a tool for highly sensitive lateral flow immunoassay . Application to the detection of potato virus X. Microchim Acta. 2018;1–8.
197. Parolo C, Escosura-Muñiz A, Merkoçi A. Enhanced lateral flow immunoassay using gold nanoparticles loaded with enzymes. Biosens Bioelectron J. 2013;40:412–6.
198. Mao X, Ma Y, Zhang A, Zhang L, Zeng L, Liu G. Disposable Nucleic Acid Biosensors Based on Gold Nanoparticle Probes and Lateral Flow Strip. Anal Chem. 2009;81(4):1660–8.
199. Ye H, Xia X. Enhancing the Sensitivity of Colorimetric Lateral Flow Assay (CLFA) through Signal Amplification Techniques. J Mater Chem. 2018;
200. Lee S, Mehta S, Erickson D, Lee S, Mehta S, Erickson D. Two-color lateral flow assay for multiplex detection of causative agents behind acute febrile illnesses. Anal Chem. 2016;88:8359–63.
201. Zhu M, Jia Y, Peng L, Ma J, Li X, Shi F. A highly sensitive dual-color lateral flow immunoassay for brucellosis using one-step synthesized latex microspheres. Anal Methods. 2019;11:2937–42.
202. Cho Y, Shin CH, Han S. Dispersion Polymerization of Polystyrene Particles Using Alcohol as Reaction Medium. Nanoscale Res Lett. 2016;11(46):9.
203. Earl W, Rios AM. Non-specific cell binding characteristics of para-magnetic polystyrene microspheres used for antibody-mediated cell selection. J Immunol Methods. 1989;121:289–94.
204. Juntunen E, Myyryläinen T, Salminen T, Soukka T, Pettersson K. Performance of fluorescent europium (III) nanoparticles and colloidal gold reporters in lateral flow bioaffinity assay. Anal Biochem. 2012;428(1):31–8.
205. Reisch A, Klymchenko AS. Fluorescent Polymer Nanoparticles Based on Dyes : Seeking Brighter Tools for Bioimaging. Small. 2016;12(15):1968–92.
206. Mohammad N, Khorramfar S, Najafi F. Amine-functionalized silica nanoparticle : Preparation , characterization and anionic dye removal ability. Desalination. 2011;279:61–8.
207. Quesada-gonzález D, Merkoçi A. Nanoparticle-based lateral flow biosensors. Biosens Bioelectron. 2015;73:47–63.

208. Abera A, Choi J. Quantitative lateral flow immunosensor using carbon nanotubes as label. Anal Methods. 2010;2:1819–22.
209. Huang Y, Wu T, Wang F, Li K, Qian L, Zhang X, et al. Magnetized Carbon Nanotube Based Lateral Flow Immunoassay for Visual Detection of Complement Factor B. Molecules. 2019;24:2759.
210. Qiu W, Xu H, Takalkar S, Gurung AS, Liu B, Zheng Y, et al. Carbon nanotube-based lateral fl ow biosensor for sensitive and rapid detection of DNA sequence. Biosens Bioelectron. 2015;64:367–72.
211. Edwards KA, Baeumner AJ. Liposomes in analyses. Talanta. 2006;68:1421–31.
212. Zhan W, Bard AJ. Immunoassay of Human C-Reactive Protein by Using Ru (bpy) 32 + -Encapsulated Liposomes as Labels. Anal Chem. 2007;79(2):459–63.
213. Xia X, Xu Y, Zhao X, Li Q. Lateral Flow Immunoassay Using Europium Chelate–Loaded Silica Nanoparticles as Labels. Clin Chem. 2009;182:179–82.
214. Martynov VI, Pakhomov AA, Popova N V, Deyev IE, Petrenko AG. Synthetic Fluorophores for Visualizing Biomolecules in Living Systems. Acta Naturae. 2016;8(31):33–46.
215. Chen Y, Chen Q, Han M, Liu J, Zhao P, He L, et al. Near-infrared fl uorescence-based multiplex lateral fl ow immunoassay for the simultaneous detection of four antibiotic residue families in milk. Biosens Bioelectron. 2016;79:430–4.
216. Rogach A. Semiconductor Nanocrystal Quantum Dots. Vol. XI. 2008. 372 p.
217. Gong X, Cai J, Zhang B. A review for Fluorescent Lateral Flow Immunochromatographic Strip. J Mater Chem B. 2017;
218. Rijke F Van De, Zijlmans H, Li S, Vail T, Raap AK, Niedbala RS, et al. Up-converting phosphor reporters for nucleic acid microarrays. Nat Publ Gr. 2001;19:273–6.
219. Khreich N, Lamourette P, Boutal H, Devilliers K, Créminon C, Volland H. Detection of Staphylococcus enterotoxin B using fluorescent immunoliposomes as label for immunochromatographic testing. Anal Biochem. 2008;377:182–8.
220. Van Dam G, Dood C, Lewis M. A robust dry reagent lateral flow assay for diagnosis of active schistosomiasis by detection of Schistosoma circulating

anodic antigen. Exp Parasitol. 2014;135(2):274–82.
221. Satija J, Sai VVR, Mukherji S. Dendrimers in biosensors: Concept and applications. J Mater Chem. 2011;21(38):14367–86.
222. Bishop JD, Hsieh H V., Gasperino DJ, Weigl BH. Sensitivity enhancement in lateral flow assays: A systems perspective. Lab Chip. 2019;19(15):2486–99.
223. Pilavaki E, Member S, Valente V, Demosthenous A. CMOS Image Sensor for Lateral Flow Immunoassay Readers. IEEE Trans Circuits Syst II Express Briefs. 2018;65(10):1405–9.
224. https://www.genprime.com/poc.
225. https://www.skannex.com/.
226. http://idetekt.com/reader-systems/
227. Faulstich C, Gruler R, Eberhard M, Lentzsch D, Haberstroh K. Handheld and Portable Reader Devices for Lateral Flow Immunoassays
228. https://www.cd-diatest.com/device-reader-of-lateral-flow-tests
229. Qin W, Wang K, Xiao K, Hou Y, Lu W, Xu H, et al. Carcinoembryonic Antigen Detection with " Handing " -Controlled Fluorescence Spectroscopy Using a Color Matrix for Point-of-care Applications. Biosens Bioelectron [Internet]. 2016; Available from: http://dx.doi.org/10.1016/j.bios.2016.10.052
230. ESE-Quant Lateral Flow. https://www.qiagen.com

231. Wang Y, Xu H, Wei M, Gu H, Xu Q, Zhu W. Study of superparamagnetic nanoparticles as labels in the quantitative lateral fl ow immunoassay. Mater Sci Eng C. 2009;29(3):714–8.
232. Xu Q, Xu H, Gu H, Li J, Wang Y, Wei M. Development of lateral fl ow immunoassay system based on superparamagnetic nanobeads as labels for rapid quantitative detection of cardiac troponin I. Mater Sci Eng C. 2009;29(3):702–7.
233. MagnaBioScience. MAR ™ Assay Development System Operator ' s Manual. Vol. 92121. p. 1–41.
234. Zheng C, Wang X, Lu Y, Liu Y. Rapid detection of fi sh major allergen parvalbumin using superparamagnetic nanoparticle-based lateral flow immunoassay. Food Control. 2012;26(2):446–52.
235. Hayes B, Murphy C. Developments in Point-of-Care Diagnostic Technology

for Cancer Detection. Diagnostics. 2018;8(39):1–18.

236. Point-of-care testing : a view of trends and new horizons. 2015;(December).
237. Du Y, Wang ML. State of the art and new perspectives for non- invasive point-of-care testing. Int J Biosens Bioelectron. 2016;1(1):7–9.
238. Chana HN, Tan MJA, Wu H. Point-of-Care Testing: Applications of 3D Printing. Lab Chip. 2017;
239. Killard AJ. 4 - Screen printing and other scalable point of care (POC) biosensor processing technologies. Medical Biosensors for Point of Care (POC) Applications. Elsevier Ltd; 2017. 67–98 p.
240. Wang P, Kricka LJ. Reviews Current and Emerging Trends in Point-of-Care Technology and Strategies for Clinical Validation and Implementation. 2018;000.
241. https://ucsdnews.ucsd.edu/feature/clinical-trial-tests-tattoo-sensor-as-needleless-glucose-monitor
242. Park J, Kim J, Kim S, Cheong WH, Jang J, Park Y, et al. Soft , smart contact lenses with integrations of wireless circuits , glucose sensors , and displays. 2018;1–12.
243. Arefin MS, Redouté J, Yuce MR. 7 - Wireless biosensors for POC medical applications. Medical Biosensors for Point of Care (POC) Applications. Elsevier Ltd; 2017. 151–180 p.
244. Manuscript A. NIH Public Access. 2014;13(7):1282–8.
245. Ozcan A, Yang Z, Tseng D, Ahlford A, Mathot L, Sjo T. Targeted DNA sequencing and in situ mutation analysis using mobile phone microscopy. 2017;1–8.
246. Lillehoj P, Huang M, Truong N, Ho C. Rapid electrochemical detection on a mobile phone Peter. Lab Chip. 2013;13:2950–5.
247. Ahrberg C, Ilic B, Manz A, Neuzil P. Handheld Real-Time PCR Device. Lab Chip. 2016;16:586–92.
248. Ruppert C, Phogat N, Laufer S, Kohl M, Deigner H. A smartphone readout system for gold nanoparticle-based lateral flow assays : application to monitoring of digoxigenin. 2019;
249. Land KJ, Boeras DI, Chen X, Ramsay AR, Peeling RW. control strategies , strengthen health systems and improve patient outcomes. Nat Microbiol. 2019;4.

CHAPTER 2

Objectives

The overall aim of this dissertation is the design and development of strategies, methods and materials to improve the analytical performance and to simplify the analytical procedure in rapid diagnostic tests, including novel solid-phase preconcentration strategies, amplification methods and advanced materials and their integration in different platforms (mainly biosensors based on electrochemical detection and paper-based strips for optical detection). In all instances, the applications selected are focused on communicable diseases, including foodborne pathogens and mycobacteria. In order to achieve this task, the following specific objectives are proposed, as follows:

- Defining the needs of rapid diagnostic test in low-resource settings.
- Synthesis of magnetic molecularly imprinted polymers (magnetic-MIPs) by merging the properties of magnetic actuation and biomimetic bioreceptor using biotin as a template.
- Characterisation of the magnetic-MIPs towards different biotinylated molecules, including small fluorescent dyes, DNA and proteins, and using different readout systems.
- Integration of the magnetic-MIPs in a magneto-actuated immunoassay as a platform for the preconcentration and immobilization of biotinylated DNA.
- Development of a magneto-actuated immunoassay for the detection of biotin in a competitive format using the magnetic-MIP as a platform.
- Design, fabrication and optimization of lateral flow platforms for pathogenic bacteria detection.
- Study of different biotinylated reporters including antibodies and dendrimers as a control line for lateral flow strips and using streptavidin gold nanoparticles as a signal generating systems.
- Comparison of the analytical performance of the lateral flow immunoassay and electrochemical magneto-genosensor in terms of LODs.
- Assessment of the analytical performance of non-conventional configuration of immunochromatography: lateral and vertical flow platforms.
- Study of the efficiency of the preconcentration of bacteria by the integration of magnetic particles.
- Characterization of the analytical performance of electrochemical genosensing for the detection of amplicons obtained by isothermal amplification techniques in order to avoid temperature cycling and simplified the analytical procedure.
- Comparison of the analytical features in terms of rapidity, sensitivity and specificity for the developed strategies.

CHAPTER 3

Comparing nucleic acid lateral and vertical flow configuration for the detection of Mycobacteria fortuitum

3.1. Abstract

This work addresses a method combining immunomagnetic separation (IMS) and paper-based nucleic acid immunochromatography for the sensitive detection of *Mycobacterium fortuitum.* In particular, the preconcentration of the mycobacteria was achieved by using magnetic particles modified with an antibody specific towards mycobacteria. Following the IMS, the bacteria were lysed and the genome was amplified by double-tagging PCR using a set of primers specific for the 16S rRNA gene common to all members of the *Mycobacterium* genus. During the amplification, the amplicons were labelled with biotin and digoxigenin tags. The paper-based immunochromatographic platforms were based on vertical and lateral flow and on the use of streptavidin gold nanoparticles as a signal generating system. The visual readout was achieved when the gold-modified amplicons were captured by the antiDIG antibody in the test line. The analytical performance of both methods, nucleic acid vertical flow (NAVF) and nucleic acid lateral flow (NALF) was discussed and compared. Although NALF showed lower LODs, both NALF and NAVF combined with IMS were able to detect the required LOD in hemodialysis water becoming two promising and useful techniques for the monitoring of water supplies in hemodialysis centers to prevent the exposure of immunosuppressed patients to contaminated sources.

3.2. Introduction

POC testing has skyrocketed in the last decades as a result of the increasing demand for sensitive, specific and fast methods of detection (1-5). These tests have already demonstrated to play a critical role in preventing the transmission of infectious diseases allowing the effective and prompt treatment to illnesses that cannot be made properly without diagnosis in the first place (6). Furthermore, the characteristics of the rapid tests have made grown their interest not only for clinical applications, but also in other fields as food safety (2), emergency testing (3), veterinary (9,10), forensic investigations (11), water and soil quality monitoring (7), among many other applications.

The rapidity, sensitivity and specificity are not the only features that define this tests, but also the simplicity, robustness, portability and low cost (13). These requirements are compatible with the use of paper as substrate for the development of these technologies by providing low-cost and disposable platforms suitable for the use in remote settings (9).

Not surprisingly, different types of rapid tests are based on cellulose with special interest on those based on immunochromatography(10). These devices are built by overlapping a series of pads which enable the flow of sample and reagents due to capillary forces. In the case of lateral flow, the movement of the fluids is produced through the strip, where the lines appear, showing the results of the presence of the analyte of interest (11). Similarly, vertical flow assays are also based on the pass of the sample through a series of layered membranes by gravity while the analytes are captured by biorecognition molecules on the reactive membrane to reveal the result of the test (12).

Despite the fact that immunochromatographic tests have been traditionally used for qualitative and semi-quantitative analysis (13), these technologies have found their way into several quantitative applications (19,20). However, some improvements in terms of sensitivity are still needed. In this regard, the preconcentration of the sample plays an important role to decrease the limits of detection of the technique. The use of magnetic particles modified with biomolecules allows the specific biorecognition, followed by capture, isolation and preconcentration of a huge range of analytes, including cells, proteins and drugs, among others, from a large volume of complex matrix (16–18). For instance, an electrochemical magneto immunosensor based on the magnetic nanoparticles able to detect as low as 1 CFU in 25 mL of milk after 8 h of pre-enrichment was previously reported by our research group (19).

Moreover, in order to achieve the required limits of detection, in many instances, amplification of DNA still remain as an ineluctable procedure for the sensitive detection of some pathogens. Although polymerase chain reaction (PCR) has been traditionally thought as a laboratory technique due to its necessity of facilities such as reliable power supply, nowadays solutions to these barriers can be found in the market thanks to the efforts for fabricating cheap, portable and operated with

batteries thermocyclers (25) as Palm PCR™ (Ahram Biosystems Inc.), Franklin™ (Biomeme), Freedom4 (Ubiquitome) or miniPCR (Amplyus). Moreover, the tagging-PCR procedures paves the way for the immobilization of the amplicon on different functionalized substrates such as magnetic particles, gold or latex nanoparticles among other carriers (26-28).

The integration of IMS, the double-tagging PCR amplification and two different paper-based platforms for immunochromatography are presented in this work for the detection of *Mycobacterium fortuitum*. This is one of the most commonly found mycobacteria in contaminated hemodialysis waters putting the immunocompromised patients at risk. For this reason, it is important to continuously monitor water supplies in hemodialysis centers in order to minimize the exposure of renal transplantation and immunocompromised individuals to contaminated sources (23). In detail, this work presents a comparative study of the two paper-based platform configuration, based on nucleic acid immunochromatography. The role of the IMS was also studied. The preconcentration of the mycobacteria from the samples was achieved by using anti-Mycobacteria antibody functionalized magnetic particles, and the efficiency was evaluated by the comparison with samples preconcentrated by centrifugation.

3.3. Experimental section

3.3.1. Instrumentation and materials

Glass fiber conjugate pad (GFCP083000) as well as cellulose fiber sample pad strips (CFSP203000) were purchased from Millipore. Absorbent pads (CF7) and nitrocellulose membranes (FP120HP) were from GE Healthcare Europe. Whatman® Protran® nitrocellulose membrane used for vertical flow devices (Z670634) was provided by Sigma. Gentle Tape 2.5 cm x 5 m roll was from Leukopor and Miriad RVF cartridges were acquired from Euromedex (Souffelweyersheim, France). Lateral flow strips Adhesive Backing Cards were obtained from Kenosha C.V.(Netherlands). The dispensing of the test and control line was performed using a Lateral Flow Reagent Dispenser from Claremont Bio (Upland, CA) combined with the KDSLegato™ 200 series syringe pump from KD Scientific Inc.(Holliston,MA).

3.3.2. Chemicals and biochemical

InnovaCoat® GOLD 40nm Streptavidin gold nanoparticles (streptAv-AuNPs) were purchased from Innova Biosciences (Cambridge, UK). Dynabeads™ M-280 Tosylactivated magnetic particles (2.8 µm, 30 mg mL^{-1}, 2 x 10^9 MP mL^{-1}) were provided by Invitrogen Dynal AS (Oslo, Norway).

Guinea Pig Antibody to Mycobacterium (MBS315001) was from MyBioSource (San Diego, CA). All buffer solutions were prepared with Milli-Q water and all other reagents were in analytical reagent grade (supplied from Sigma). The composition of these solutions were: conjugate diluting buffer (2 mmol L^{-1} borate pH 7, 10 % w/v sucrose); running buffer (0.01 mol L^{-1} phosphate buffer pH 7.4, 1% BSA, 0.05 % Tween 20); borate buffer (0.1 mol L^{-1} boric acid, pH 8.5); Ammonium sulphate ($(NH_4)_2SO_4$ 3 mol L^{-1} in borate buffer); blocking buffer (PBS 0.5% BSA: 10 mmol L^{-1} phosphate, 0.5% w/v BSA, pH 7.4); washing buffer (PBS 0.1% BSA: 10 mmol L^{-1} phosphate, 0.1% w/v BSA, pH 7.4).

3.3.3. Oligonucleotides sequences

The oligonucleotides were obtained from Sigma (Berlin, Germany). These sequences, complementary to the region of 16S rRNA gene (accession no. (16S rRNA gene) AY457066) common to all members of the genus Mycobacterium, were selected from the previous work published by Richardson and coworkers (29).

Biotin (BIO) and digoxigenin (DIG) were used as double labels, both inserted in 5' end of the primers. The primer sequences as well as the tags used for the PCR amplification are shown in Table 1.

Table 3.1. Sequences of the set of primers for the double-tagging PCR amplification for the detection of *Mycobacterium fortuitum.*

Strain	Gene	Primer sequence(5'-3')	Type	5'-Labels	Size (bp)
Mycobacterium Fortuitum	*16s*	ACCACGCATTTCATGGTGT	Reverse	Biotin	278
		ACTTGCGCTTCGTCCCTAT	Forward	Digoxigenin	

3.3.4. Preparation of the devices in vertical flow configuration

The different pads conforming the system were assembled and placed in the cartridge as it is shown in Figure 1. After that, 0.5 µL of the anti-digoxigenin antibody (1 mg mL^{-1}) and the positive control biotinylated reporter (1 mg mL^{-1}) were deposited on the nitrocellulose membrane and were then dried at RT for 30 min. Furthermore, the streptAv-AuNPs were diluted 5 times in conjugate diluting buffer, embedded in the glass fiber conjugate pads and then dried for 3h at RT. Finally, the glass fiber was placed on the corresponding well of the device, in direct contact with the test and control area of the nitrocellulose.

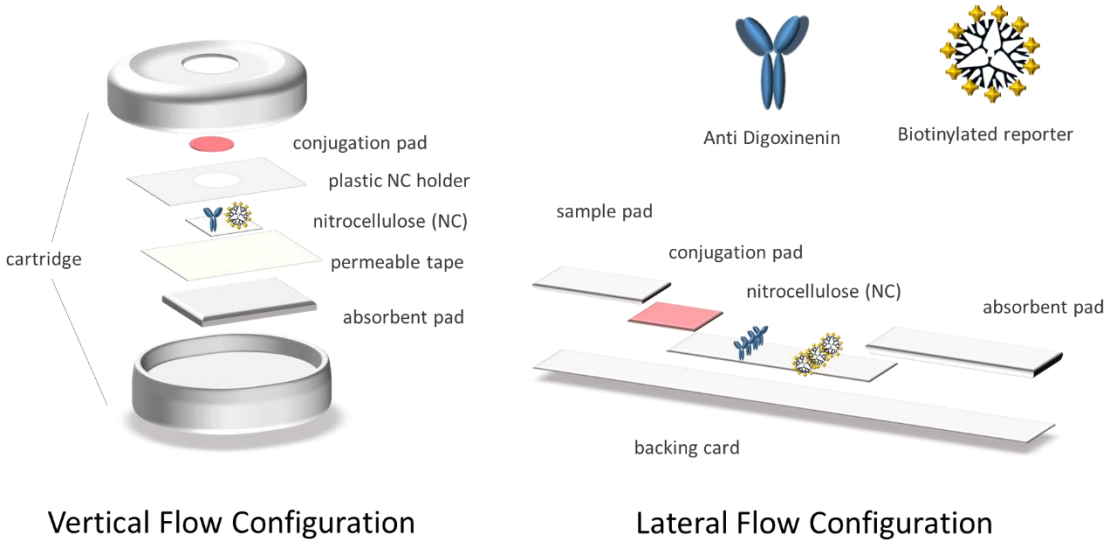

Figure 3.1. Schematic representation of the components forming the vertical and lateral flow immunoassay.

3.3.5. Preparation of devices in lateral flow configuration

The cellulose fiber sample pads were soaked into sample pad buffer. The streptAv-AuNPs were then diluted 10 times in conjugate diluting buffer and embedded in the glass fiber conjugate pads. All the pads were dried for 3h at RT. The antibody (1 mg mL^{-1}) and the positive control biotinylated reporter (1 mg mL^{-1}) were dispensed on the nitrocellulose membrane and dried at RT for 1h. Finally, the strips were assembled on the adhesive backing card as it is shown in Figure 1.

3.3.6. Covalent immobilization of antibodies on magnetic particles

Guinea pig antibody to *Mycobacterium fortuitum* was covalently coupled on tosyl activated magnetic particles (tosyl-MPs) as described in Figure 2 A.

A volume of 35 µL of tosyl-MP was washed twice with 1 mL of borate buffer. Afterwards, 20 µg of antibody and 100 µL of ammonium sulphate buffer was added in borate buffer performing a total volume of 240 µL.

MPs were incubated under continuous agitation for a total reaction time of 18 h at 37 ºC. After incubation, MPs were separated with a magnet and the supernatant was removed. After that, 1 mL of phosphate blocking buffer was added to the suspension and incubated under shaking for 2 h at 37 ºC, in order to block the remaining tosyl groups of the magnetic particles.

Finally, the antibody functionalized-magnetic microparticles were washed and resuspended in phosphate storage buffer to reach a concentration of 5.3 mg mL^{-1} and were then stored at 4 ºC for further use.

3.3.7. Bacterial strain and culture

Mycobacterium fortuitum subsp. Fortuitum ATCC® 6841™ strain was grown in trypticase soy broth (TSB) supplemented with 0.025% Tween 20 under continuous agitation at 37 °C for 72 h. After that, serial dilutions from the culture were performed in hemodyalisis water. Hemodialysis water was used since NTM are associated with infection arising from contamination of water in hemodialysis patients. The hemodialysis water was kindly provided by the Servei de Nefrologia, Hospital Parc Taulí Sabadell. 100 µL of each dilution was spread onto Tryptic Soy Agar plates. After incubating the plates at 37 ºC for 24 h, the culture colonies on the plates were counted to estimate the number of viable bacteria in CFU mL^{-1}.

3.3.8. Immunomagnetic separation and DNA extraction

The magnetic separation of the mycobacteria was performed in order to preconcentrate the bacteria from high volume of sample, in order to improve the LODs. 20 µL of the antibody functionalized-magnetic particles was added to 1 mL of each mycobacteria samples (ranging from 0 to 10^6 CFU mL^{-1}) and were incubated by stirring at RT for 60 min.

Afterwards, the bacteria attached to the MPs were separated with a magnet and the supernatant was removed. Then, MPs were washed with PBST (X3) and water (X1) under shaking for 1 min at RT and 700 rpm.

The particles were separated with a magnet and resuspended in 50 µL of Tris-EDTA (TE) buffer for DNA extraction. The suspension was then kept in a boiling water bath for 10 min. After cooling on ice for 5 min, 2 µL of the supernatant was used directly for the amplification.

In order to assess the efficiency of the preconcentration with magnetic particles, a parallel extraction of DNA from the same solutions was performed with no magnetic preconcentration. In this case, 1 mL of each one of the dilutions of mycobacteria were centrifuged at 12000 g for 15 min, the liquid cultures were removed, and the pellet was resuspended in 1 mL of water. After a second centrifugation at 12000 g for 15 min, the suspension was kept in a boiling water bath for 10 min. After cooling on ice for 5 min, the samples were centrifuged and 2 µL of the supernatant was used for the amplification samples.

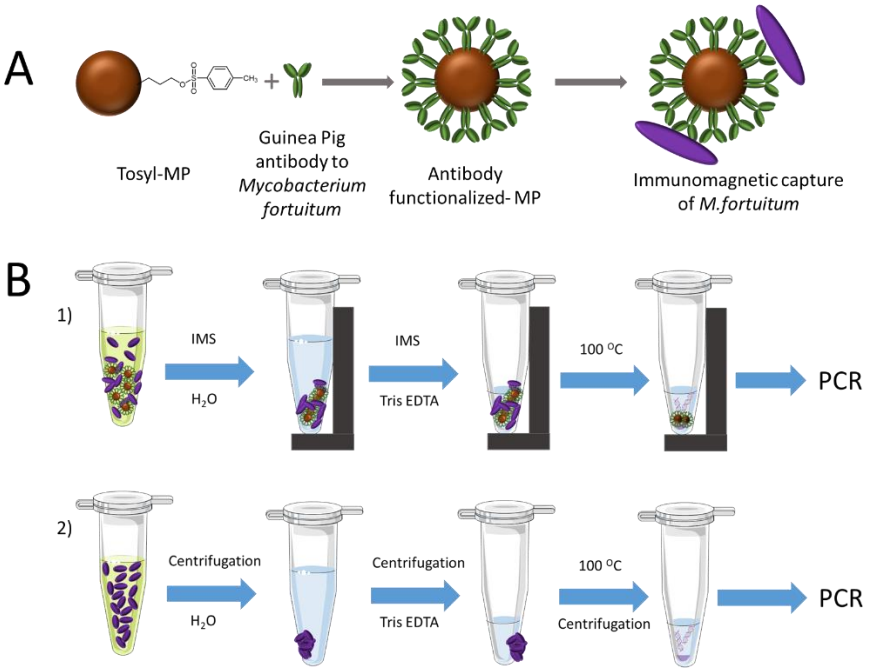

Figure 3.2. A) Covalent immobilization of the antibody specific to *Mycobacterium fortuitum* on Tosyl-MP. B) 1. Immunomagnetic separation of Mycobacteria from culture media dilutions and DNA extraction. 2. DNA extraction of mycobacteria from culture dilutions

3.3.9. Double-tagging PCR

A set of primers tagged with biotin and digoxigenin respectively was used for the amplification and the double-tagging of the extracted DNA. The PCR was performed in 15 µL of reaction mixture containing 2 µL of the extracted DNA. Each reaction contained 250 µmol L^{-1} of each deoxynucleotide triphosphate (dATP, dGTP, dCTP, and dTTP), 100 nmol L^{-1} of the double-tagged set of primers and 3 U of Taq polymerase. The reaction was carried out in *Taq* DNA Polymerase PCR 1x Buffer (Biotools) containing 7.5 mM Tris HCl (pH 9.0), 0.2 mM $MgCl_2$, 5 mM KCl, 2 mM $(NH_4)_2SO_4$. The amplification mixtures were treated, with an initial step at 95 ºC for 5 min followed by 40 cycles at 95 ºC for 40 s, 60 ºC for 30 s, and 72 ºC for 2 min, and a last step of 10 min at 72 ºC. The resulting samples were stored at 4 ºC.

3.3.10. Nucleic acid vertical flow

The procedure for the detection of Mycobacteria by NAVF is schematically described in Figure 3A. The amplicon solutions obtained from the double-tagging PCR were diluted in 75 µL of running buffer and deposited on the sample zone. After 20 seconds, 75 µL of running buffer were added in order to drag the remaining streptAv-AuNPs to the absorbent pad. The streptAv-AuNPs thus reacted with the biotin (BIO-tag) of the amplicons. As the products moved towards the nitrocellulose, the streptAv-AuNPs/amplicons were captured by the digoxigenin (DIG-tag) on the test dot, containing the antibody antiDIG. A valid test was considered when the streptAv-AuNPs also reacted with a biotinylated reporter located on the control dot. After one minute, the remaining streptAv-AuNPs migrated to the absorbent pad and the visual readout was achieved. For the quantification of the optical signal, the images were processed with ImageJ software(NHI).

3.3.11. Nucleic acid lateral flow

The procedure for the detection of Mycobacteria by NALF is schematically described in Figure 3B. The amplicon solutions obtained from the double-tagging PCR amplifications was diluted in 100 µL of PBS running buffer and deposited on the sample zone. After 1 min, 100 µL of running buffer were added in order to transport

the remaining streptAv-AuNPs up to the absorbent pad. Similarly, to the vertical flow immunoassay, the streptAv-AuNPs reacted with the biotin of the amplicons (BIO-tag). When streptAv-AuNPs/amplicon moved through the nitrocellulose, the specific antibody antiDIG on the test line reacted with the DIG-tag of the amplicons. The remaining streptAv-AuNPs flow through the nitrocellulose up to the control line where are captured by the biotinylated reporter used as a positive control. After 10 min the test reveal the lines and the test is ready for the interpretation of the results. For the quantification of the intensity of the signal, the resulting images were processed with ImageJ software(NHI).

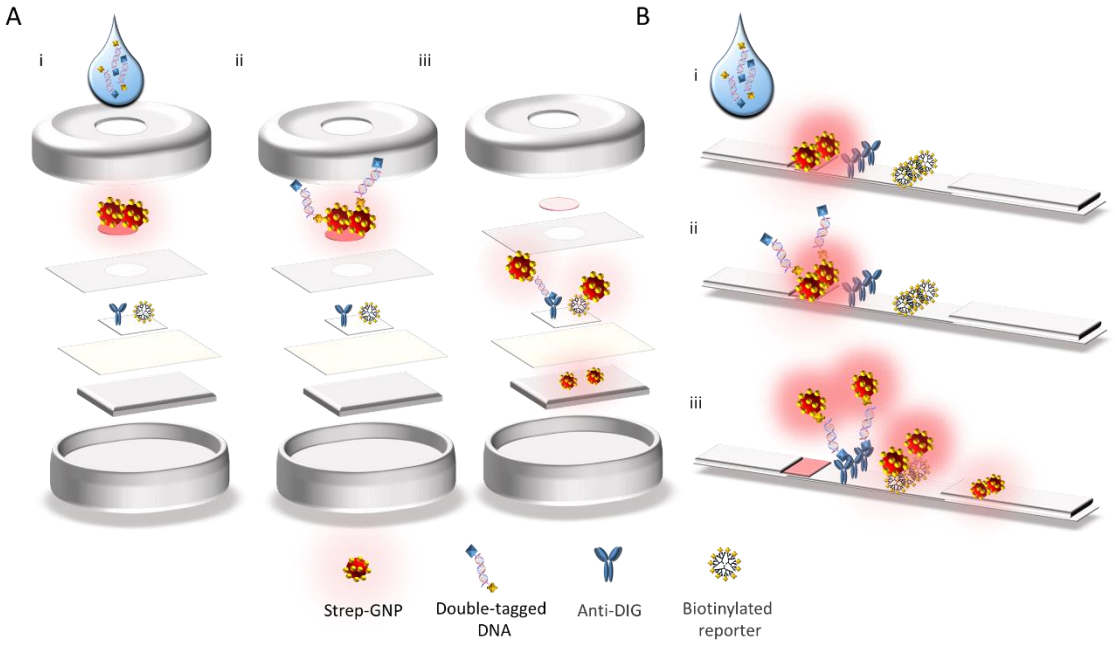

Figure 3.3. Schematic representation of Nucleic Acid Vertical Flow (A) and Nucleic Acid Lateral Flow (B): i) Deposition of the amplicons in the sample zone ; ii) Streptavidin Gold nanoparticles (streptAv-AuNPs) captured by the biotin tag of the amplicon; iii) streptAv-AuNPs Amplicon capture in the test zone (dot or line, respectively) by the anti-DIG antibody and capture of gold nanoparticles by the biotinylated reporter. The remaining streptAv-AuNPs flow up to the absorbent pad.

3.4. Results

3.4.1. Double-tagging PCR

The double-tagging PCR procedure was firstly studied by end-point PCR and agarose gel electrophoresis and the results are shown in Fig. 3.4. The resulting bands showed a MW as expected for the 16S fragment (277 bp).

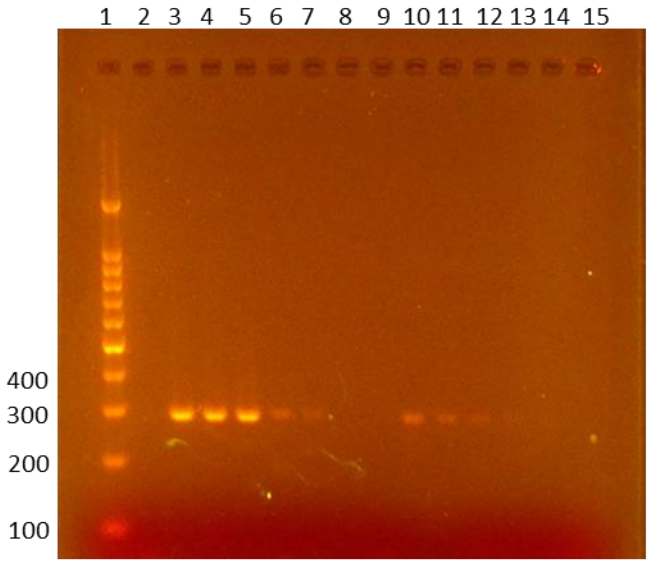

Figure 3.4. Gel electrophoresis. Lane 1 is the molecular weight marker. Lanes 3 to 8 were obtained by the double tagging PCR combined with IMS. Lane 2 is the negative control of this procedure and correspond to 0 CFU mL^{-1}. Lanes 3 to 8, ranging from 10^6 to 10^1 CFU mL^{-1}. Lane 9 correspond to 0 CFU mL^{-1}. Lanes from 10 to 15 are the samples resulting from the double tagging PCR combined with centrifugation, instead of IMS, from10^6 to 10^1 CFU mL^{-1}. Lane 9 is the negative control of this procedure and correspond to 0 CFU mL^{-1}

The relative intensities of the bands can be correlated with the individual performance of each set of primers depending on the initial concentration of DNA as well as the amplicon length.

It can be observed that the amplification resulting of the samples magnetically preconcentrated is much higher than the procedure performed by centrifugation. An expected decrease in the signal is also observed when lowering the concentration of the bacteria.

3.4.2. Nucleic acid vertical flow

Figure 3.5 shows the results obtained by NAVF, while Figure S3.2 (Supp data) shows the original cartridge. Regarding the performance of the device, it is important to highlight that the readout can be achieved in only 1 min. The results of the tests can be read with the naked eye but the measurement of the intensity of the dots using the image processing program ImageJ allows the quantification and an enhanced evaluation of the data. After processing the images resulting from the addition of the amplicons to the detection area of the devices, the intensity of color produced for each concentration of mycobacteria was quantified, and the results are shown in Figure S3.3.

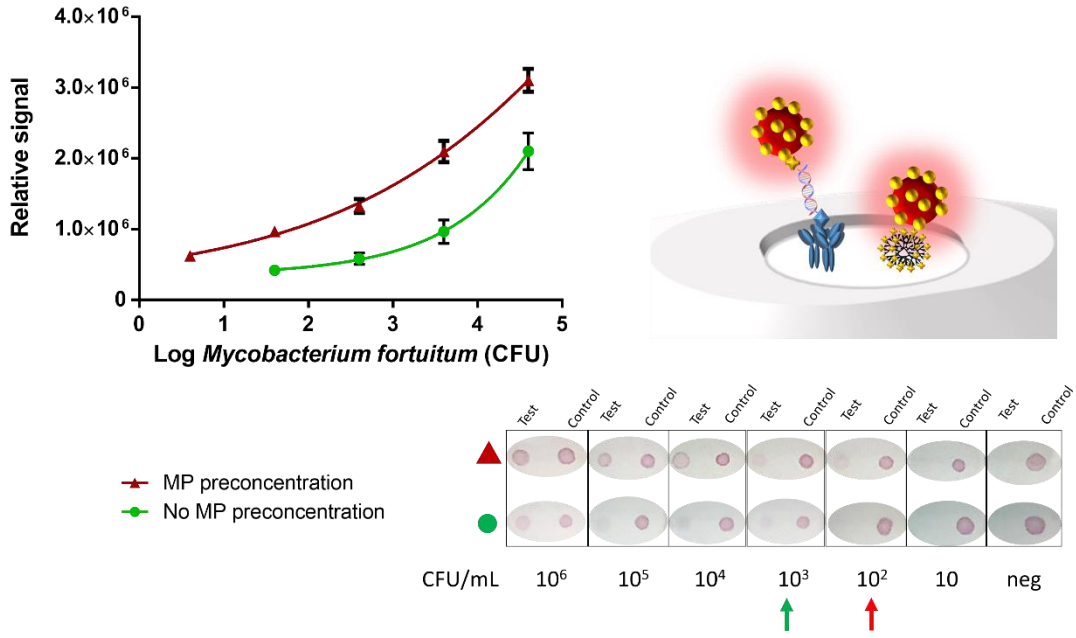

Figure 3.5. Results obtained for the NAVF for different amount of *Mycobacteria Fortuitum* with previous magnetic preconcentration (▲) and with no magnetic preconcentration (●).

The relative areas obtained after were fitted using a nonlinear regression (Four Parameter logistic Equation– GraphPad Prism Software) (R^2=0.9881 for MP preconcentrated samples and 0.9620 for non magnetically preconcentrated samples). The results are shown in figure 3.5 as well as the results of reproducibility can be found in Supporting information (Figure S3.4). The NAVF method was able to visually detect signals as low as 4 CFU in 2 µL (100 CFU mL^{-1}) of extracted DNA. This strategy showed better results than those obtained from the method without

previous preconcentration, obtaining a result of 40 CFU in 2 µL (1000 CFU mL^{-1}) of extracted DNA. This difference could be attributed to lower performance of bacteria preconcentration obtained by centrifugation process compared to IMS provided by the high affinity and specificity of the immobilized antibody. Therefore, the magnetic preconcentration step improved an order of magnitude the detection of *Mycobacteria fortuitum.*

3.4.3. Nucleic acid lateral flow immunoassay

The results combining double-tagging PCR and lateral flow immunoassay with followed the IMS of the mycobacteria (or alternatively, the classical centrifugation) were quantified as previously described for NAVF. The readouts in this instance were obtained after 15 from the addition of the sample on the strip.

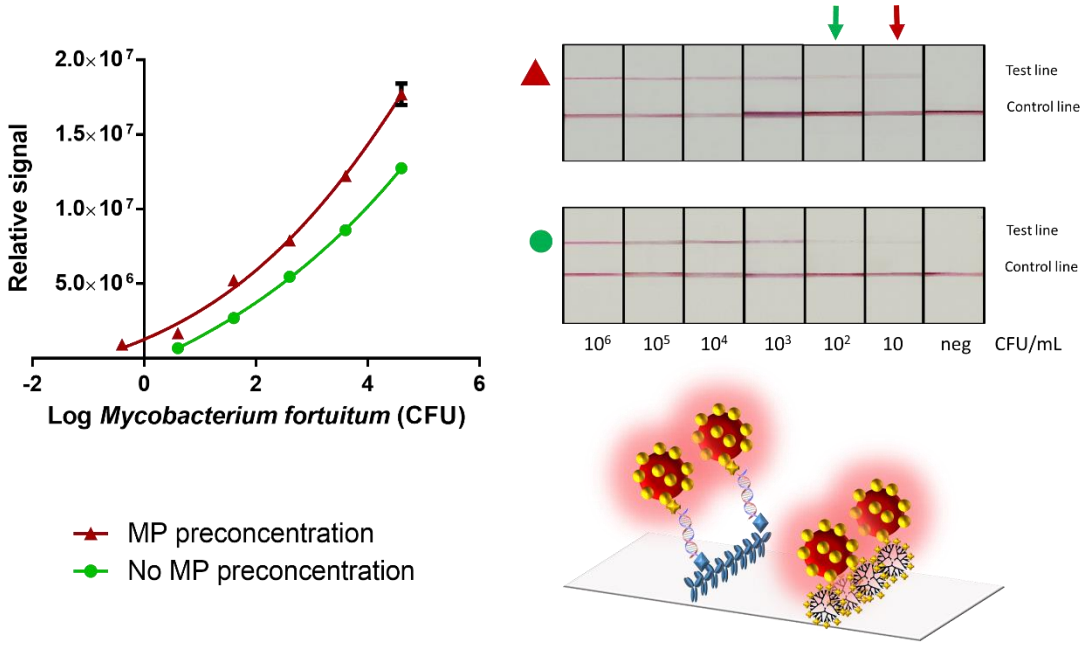

Figure 3.6. Results obtained for the NALF for different amount of *Mycobacteria Fortuitum* with previous magnetic preconcentration (▲) and with no magnetic preconcentration (●).

The results for both approaches, IMS/NALF compared to the common procedure based on centrifugation are shown in Figure 3.6. In this case, the relative areas obtained were also fitted using a nonlinear regression (Four Parameter logistic Equation– GraphPad Prism Software) (R^2=0.9949 for IMS/NALF and 0.9445 for NALF).

The LOQ of the curve for the procedure combining IMS was 0.4 CFU in 2 µL of extracted DNA (10 CFU mL^{-1}), 10 times lower than the value obtained from samples separated by centrifugation (4 CFU in 2 µL of extracted DNA, 100 CFU mL^{-1}), being results in agreement with those obtained by NAVF.

Furthermore, the comparison of the analytical performance of NAVF compared to NALF showed an improved result for NALF. The better LOD of lateral flow format can be attributed to the fact that, due to the configuration of the assay, all the gold nanoparticles, as well as the samples, are forced to pass by the test and control lines, ensuring a major contact of the reagents and providing much more opportunities for reaction. Unlikely, although much more rapid since the flow are also move by gravity, in the vertical flow format some reagents including gold nanoparticles and sample, can pass by the membrane without reacting with the control and test dots. This fact provides variability and adds difficulty to obtain the quantitative detection of analytes.

For this reason, it can be though that in order to ensure the detection of all the content of the sample, lateral flow would be the best candidate. However, the time of detection and the amount of materials required for NAVF makes this format very attractive for applications that require qualitative results ensuring in any case the correct performance to reach the proper LOQ for each necessity. Moreover, Hook's effect (a phenomenon that is caused by the presence of excess amount of antibodies preventing agglutination), which can lead to inaccurate results in lateral flow assays, is also eliminated in the vertical flow configuration.

3.5. Conclusions

The increasing need for analysis of challenging samples in low-resource settings, has increased the interest for commercial solutions and for the development of PoC devices. On the other hand, in the face of the increasing demand for decentralized infectious disease testing, researchers have step up their efforts to provide solutions that meet the features required according the guidelines published by WHO and defined by the acronym ASSURED ((A) Affordable, (SS) Sensitive, Specific, (U) User-friendly, (R) Rapid and Robust, (E) Equipment free, and (D) Deliverable to those who need it. In this line, the combination of technologies with a proven performance

record in life science research, such as immunoassays or PCR amplification, with the use of smartphone and tablets as readers leads to portable and cheaper devices.

In this work, the combination of double-tagged PCR and nucleic acid vertical flow platform for *Mycobacteria fortuitum* detection is presented and compared with a conventional format based on lateral flow.

In detail, Mycobacteria DNA was amplified by using a set of primers for 16S rRNA gene common to all members of the genus *Mycobacterium* and the signal was also amplified at the same time by labelling with biotin and digoxigenin in order to achieve a visual readout by NAVF or NALF using both gold nanoparticles as signal generating system. Moreover, the performance obtained by the preconcentration of the sample using magnetic particles was also evaluated. The fact of including immunomagnetic separation provided results as greater as one order of magnitude compared to the same method of analysis with centrifugation instead of magnetic preconcentration. The results obtained from these two methods were discussed and compared. NALF showed a better sensitivity being able to detect as low as10 CFU mL^{-1} when the IMS was included in the procedure in front of the 100 CFU mL^{-1} when IMS was not included. The LOD of NAVF was also improved (100 CFU mL^{-1}) when the IMS was performed, again 10 times lower than the LOD obtained with NAVF with samples preconcentrated by centrifugation. The results of NALF are comparable to those obtained in literature (13 CFU mL^{-1}) using a magneto-ELISA(25), and represents a great improvement in terms of time with respect to conventional methods, which require at least 72 hours to detect rapid growing mycobacteria. On the other hand, the time of assay for vertical flow format was only 1 minute in front of the 15 min needed to obtain the results by using lateral flow format. Furthermore, the volume of reagents needed for the assay was significantly lower thus reducing the cost of the product. Although both platforms have differences, both methods presented in this study were able to detect concentrations of this important pathogen in application such as dialysate fluid (<200 CFU mL^{-1}). This is one of the most commonly found mycobacteria in contaminated hemodialysis waters placing the immunocompromised patients at risk. For this reason it is important to continuously monitor water supplies in hemodialysis centers in order to minimize the exposure of renal transplantation and immunocompromised individuals to contaminated sources (30).

3.6. Acknowledgements

This work was funded by the Ministry of Economy and Competitiveness (MINECO), Madrid (Project ASSURED, BIO2013-41242-R). Financial support from the projects BFU2011-23478, CTQ2014-53662-P, CTQ2014-51912-REDC (Ministry of Economy and Competitiveness, MICINN, Madrid) and 2014SGR572, 2014SGR572, 2014SGR1105 (DURSI-Generalitat de Catalunya) are also gratefully acknowledged.

3.7. Supplementary information

3.7.1. Double-tagging PCR

The PCR reaction was carried out in a thermal cycler Primus 25. The detailed conditions for the double-tagging PCR is presented in Table S3.1 and schematically shown in Figure S3.1.

Table S3.1. Thermal cycler conditions for the double-tagging PCR

	Initial step	**DNA denaturation**	**Annealing**	**Extension**	**Last step**
	1 cycle	**40 cycles**			**1 cycle**
Temperature (ºC)	**95**	**95**	**60**	**72**	**4**
Time (s)	**300**	**40**	**30**	**120**	**300**

The performance of the multiplex double-tagging PCR was analyzed with conventional agarose gel electrophoresis on 2% agarose gel in TAE buffer containin 1 × GelRed dye. A molecular weight (MW) marker consisting of DNA fragments ranged from 100 to 1000 base pair (bp) was used as size amplicon control. The DNA bands were visualized by UV transillumination (FastGene FAST Digital System).

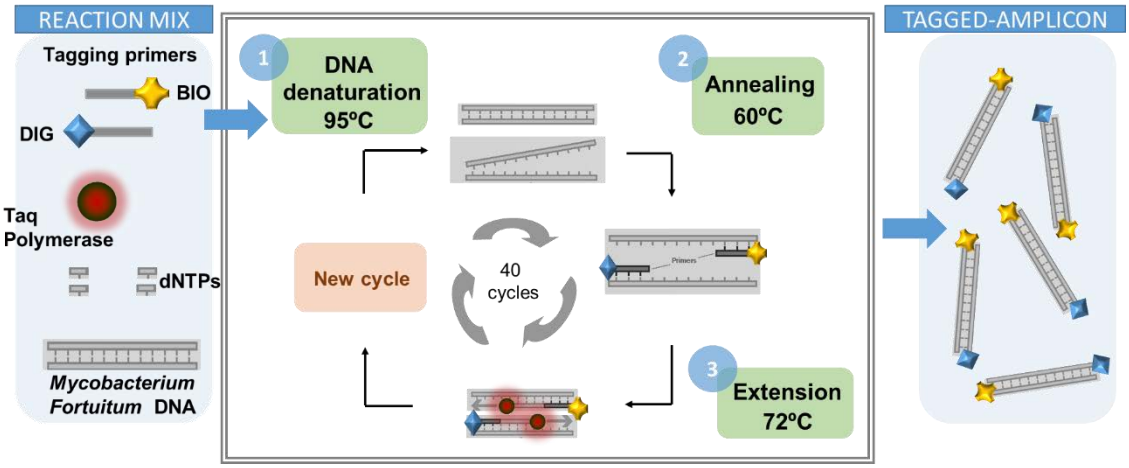

Figure S3.1. Schematic representation of the double-tagging PCR amplification, in order to obtain the double-tagged amplicon labelled with biotin and digoxigenin from mycobacteria DNA.

3.7.2. Readout

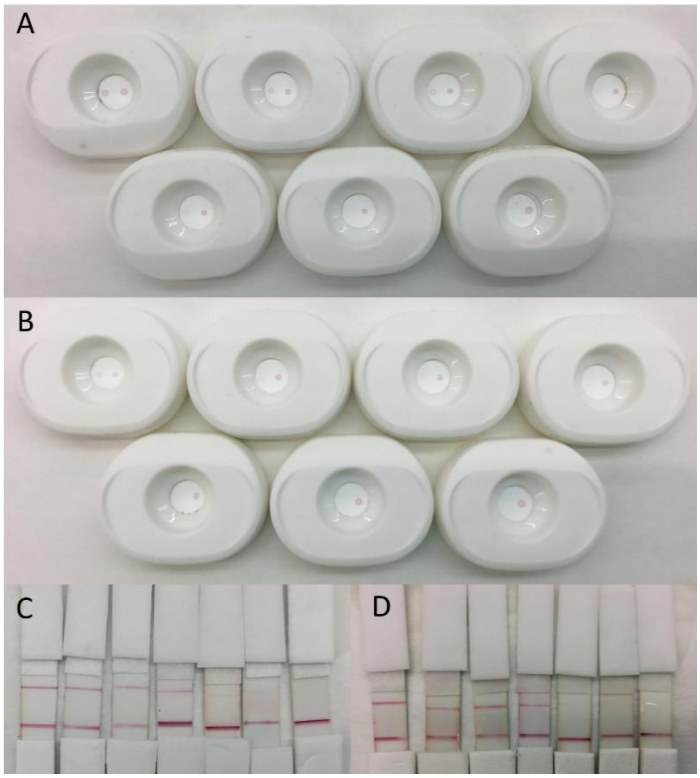

Figure S3.2. (A) Image from results obtained from NAVF with previous immunomagnetic separation of mycobacteria. (B) Image from results obtained from NAVF with no IMS. (C) Image from results obtained from NALF with previous immunomagnetic separation of mycobacteria. (D) Image from results obtained from NALF with no IMS.

Table S3.1. Results obtained from ImageJ processing of the images.

CFU/mL	VF/IMS	VF	LF/IMS	LF
10^6	3103850	2098781	18289510	12747360
10^5	2097775	963717	12219430	8584016
10^4	1324749	582529	7901137	5482610
10^3	967009	419508	5249225	2708974
10^2	622769		1697548	697820
10^1			943376	
0				

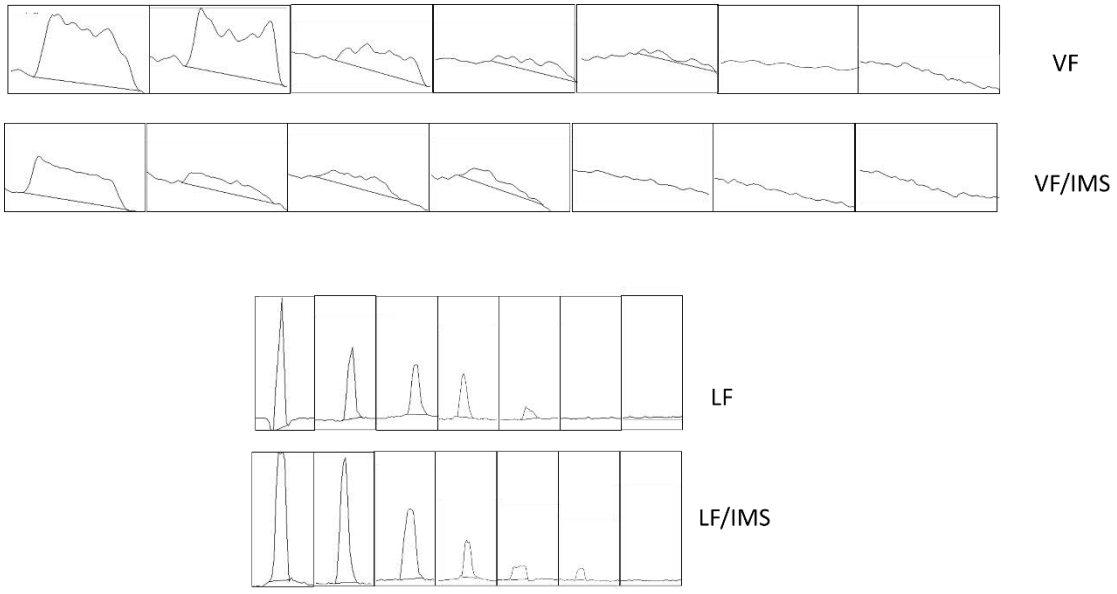

Figure S3.3. (A) Image of peaks resulting of the image processing with the software ImageJ

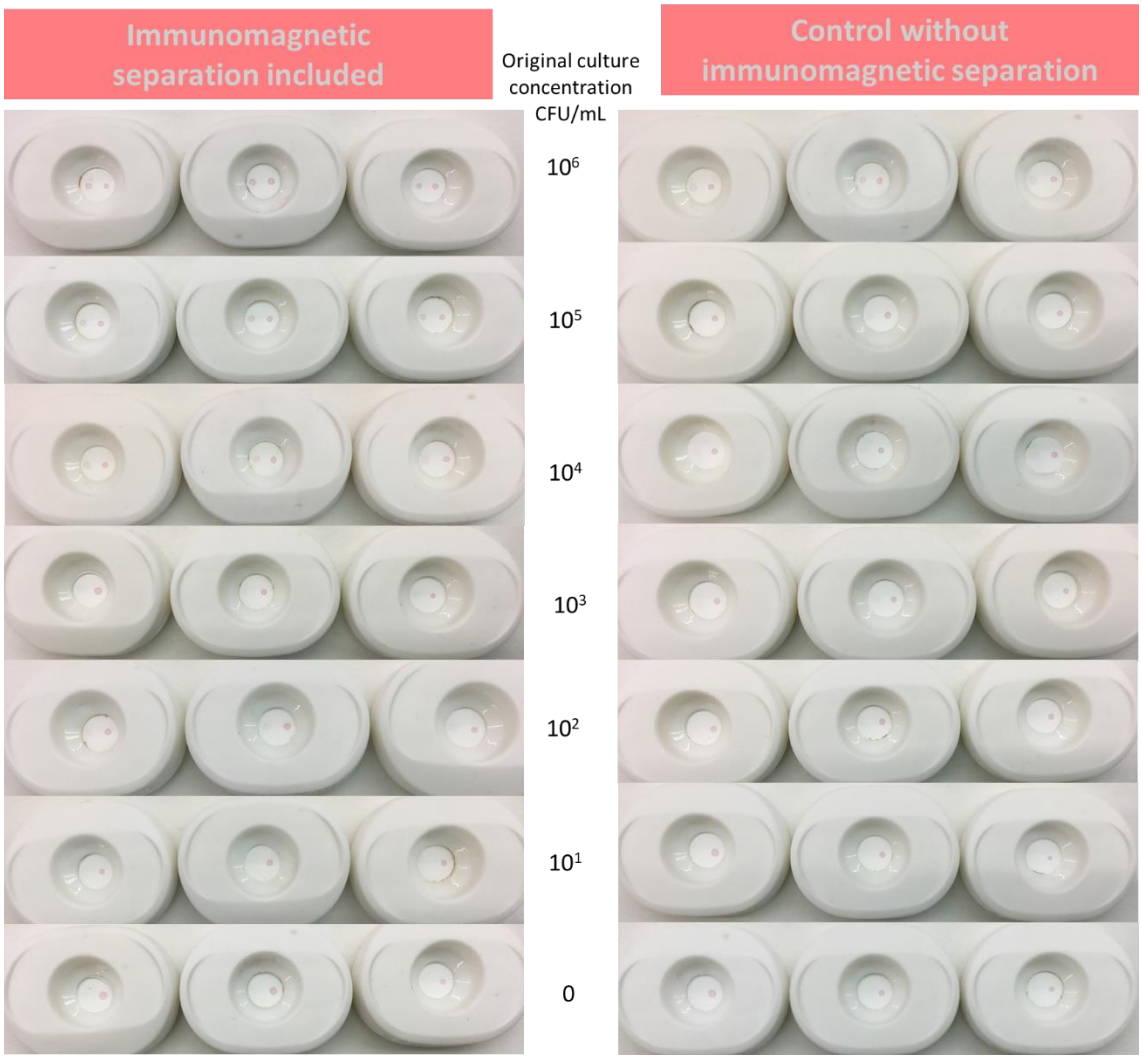

Figure S3.4. Image from reproducibility results obtained from NAVF with and without previous immunomagnetic separation of mycobacteria.

5.7.3. rRNA sequence of Mycobacterium fortuitum

The position of the set of primers are highlighted in red (Reverse BIO-primer) and blue (Forward DIG-primer). AY457066.1 Mycolicibacterium fortuitum subsp. fortuitum DSM 46621 = ATCC 6841 strain CIP 104534 16S ribosomal RNA gene, partial sequence

TAGAGTTTGATCCTGGCTCAGGACGAACGCTGGCGGCGTGCTTAACACATGCAAGTCGAACGGAAAGGCCC
TTCGGGGTACTCGAGTGGCGAACGGGTGAGTAACACGTGGGTGATCTGCCCTGCACTTTGGGATAAGCCTG
GGAAACTGGGTCTAATACCGAATATG**ACCACGCGCTTCATGGTGT**GTGGTGGAAAGCTTTTGCGGTGTG
GGATGGGCCCGCGGCCTATCAGCTTGTTGGTGGGGTAATGGCCTACCAAGGCGACGACGGGTAGCCGGCCT
GAGAGGGTGACCGGCCACACTGGGACTGAGATACGGCCCAGACTCCTACGGGAGGCAGCAGTGGGGAATA
TTGCACAATGGGCGCAAGCCTGATGCAGCGACGCCGCGTGAGGGATGACGGCCTTCGGGTTGTAAACCTCT
TTCA**ATAGGGACGAAGCGCAAGT**GACGGTACCTATAGAAGAAGGACCGGCCAACTACGTGCCAGCAGCC

GCGGTAATACGTAGGGTCCGAGCGTTGTCCGGAATTACTGGGCGTAAAGAGCTCGTAGGTGGTTTGTCGC
GTTGTTCGTGAAAACTCACAGCTTAACTGTGGGCGTGCGGGCGATACGGGCAGACTAGAGTACTGCAGGG
GAGACTGGAATTCCTGGTGTAGCGGTGGAATGCGCAGATATCAGGAGGAACACCGGTGGCGAAGGCGGGT
CTCTGGGCAGTAACTGACGCTGAGGAGCGAAAGCGTGGGGAGCGAACAGGATTAGATACCCTGGTAGTCC
ACGCCGTAAACGGTGGGTACTAGGTGTGGGTTTCCTTCCTTGGGATCCGTGCCGTAGCTAACGCATTAAGT
ACCCCGCCTGGGGAGTACGGCCGCAAGGCTAAAACTCAAAGGAATTGACGGGGGCCCGCACAAGCGGCGGA
GCATGTGGATTAATTCGATGCAACGCGAAGAACCTTACCTGGGTTTGACATGCACAGGACGACTGCAGAG
ATGTGGTTTCCCTTGTGGCCTGTGTGCAGGTGGTGCATGGCTGTCGTCAGCTCGTGTCGTGAGATGTTGGG
TTAAGTCCCGCAACGAGCGCAACCCTTGTCTCATGTTGCCAGCACGTTATGGTGGGGACTCGTGAGAGACT
GCCGGGGTCAACTCGGAGGAAGGTGGGGATGACGTCAAGTCATCATGCCCCTTATGTCCAGGGCTTCACAC
ATGCTACAATGGCCGGTACAAAGGGCTGCGATGCCGTGAGGTGGAGCGAATCCTTTCAAAGCCGGTCTCAG
TTCGGATCGGGGTCTGCAACTCGACCCCGTGAAGTCGGAGTCGCTAGTAATCGCAGATCAGCAACGCTGCG
GTGAATACGTTCCCGGGCCTTGTACACACCGCCCGTCACGTCATGAAAGTCGGTAACACCCGAAGCCGGTG
GCCTAACCCTTGTGGAGGGAGCCGTCGAAGGTGGGATCGGCGATTGGGACGAAGTCGTAACAAGGTAGCC
GTA

3.8. References

1. Chen H, Liu K, Li Z, Wang P. Point of care testing for infectious diseases. Clin Chim Acta [Internet]. 2019;493:138–47. Available from: https://doi.org/10.1016/j.cca.2019.03.008

2. Primiceri E, Chiriacò MS, Notarangelo FM, Crocamo A, Ardissino D, Cereda M, et al. Key enabling technologies for point-of-care diagnostics. Vol. 18, Sensors. 2018. p. 3607.

3. Di Serio F, Lovero R, Leone M, De Sario R, Ruggieri V, Varraso L, et al. Integration between the Tele-Cardiology Unit and the central laboratory: Methodological and clinical evaluation of point-of-care testing cardiac marker in the ambulance. Clin Chem Lab Med. 2006;44(6):768–73.

4. Schlacks S, Vishkautsan P, Butkiewicz C, Shubitz L. Evaluation of a commercially available, point-of-care Coccidioides antibody lateral flow assay to aid in rapid diagnosis of coccidioidomycosis in dogs. Med Mycol [Internet]. 2019;0:1–5. Available from: https://academic.oup.com/mmy/advance-article/doi/10.1093/mmy/myz067/5520381

5. Cummins B, Ligler FS, Walker GM. Point-of-Care Diagnostics for Niche Applications. Biotechnol Adv. 2016;34(3):161–76.

6. Na JY. Point-of-care hemoglobin A1c testing in postmortem examination. Forensic

Sci Med Pathol. 2018;14(3):322–6.

7. Kolm C, Martzy R, Führer M, Mach RL, Krska R, Baumgartner S, et al. Detection of a microbial source tracking marker by isothermal helicase-dependent amplification and a nucleic acid lateral-flow strip test. Sci Rep. 2019;9(1):1–9.

8. Anfossi L., Giovannoli C., Baggiani C. Introductory Chapter: Rapid Test - Advances in Design, Formats, and Detection Strategies. In: Anfonssi L, editor. Rapid Test - Advances in Design, Format and Diagnostic Applications. IntechOpen; 2018. p. 13.

9. Singh AT, Lantigua D, Meka A, Taing S, Pandher M, Camci-Unal G. Paper-based sensors: Emerging themes and applications. Sensors (Switzerland). 2018;18:1–22.

10. O'Farrell B. Evolution in Lateral Flow–Based Immunoassay Systems. Lateral Flow Immunoassay. Humana Press; 2009. 1–33 p.

11. Amerongen A, Veen J, Arends H, Koets M. Lateral Flow Immunoassay. In: Handbook of Immunoassay Technologies [Internet]. Elsevier Inc.; 2018. p. 157–82. Available from: http://dx.doi.org/10.1016/B978-0-12-811762-0.00007-4

12. Chen P, Gates-Hollingsworth M, Pandit S, Park A, Montgomery D, AuCoin D, et al. Paper-based Vertical Flow Immunoassay (VFI) for detection of bio-threat pathogens. Talanta [Internet]. 2019;191(August):81–8. Available from: https://doi.org/10.1016/j.talanta.2018.08.043

13. Posthuma-Trumpie GA, Korf J, Van Amerongen A. Lateral flow (immuno)assay: Its strengths, weaknesses, opportunities and threats. A literature survey. Anal Bioanal Chem. 2009;393(2):569–82.

14. Miočević O, Cole CR, Laughlin MJ, Buck RL, Slowey PD, Shirtcliff EA. Quantitative Lateral Flow Assays for Salivary Biomarker Assessment: A Review. Front Public Heal [Internet]. 2017;5. Available from: http://journal.frontiersin.org/article/10.3389/fpubh.2017.00133/full

15. Jekarl DW, Choi H, Kim ES, Lee S, Park H, Kim M, et al. Analytical evaluation and clinical application of insulin and C-peptide by a whole blood , lateral flow , point of care (POC) assay system. Scand J Clin Lab Invest [Internet]. 2019;79(0):1–7. Available from: https://doi.org/10.1080/00365513.2019.1627575

16. Castilho MDS, Laube T, Yamanaka H, Alegret S, Pividori MI. Magneto Immunoassays for Plasmodium falciparum Histidine-Rich Protein 2 Related to Malaria based on Magnetic Nanoparticles. Anal Chem. 2011;83:5570–7.

17. Carinelli S, Martí M, Alegret S, Pividori MI. Biomarker detection of global infectious diseases based on magnetic particles. N Biotechnol. 2015;32(5):521–32.

18. Saiyed Z, Telang S, Ramchand C. Application of Magnetic Techniques in the Fields of Drug Discover y and Biomedicine Application of Magnetic Techniques in the Fields of Drug Discover y and Biomedicine. Biomagn Res Technol. 2004;1:1–8.

19. Brandão D, Liébana S, Campoy S, Alegret S, Pividori MI. Immunomagnetic separation of Salmonella with tailored magnetic micro and nanocarriers. A comparative study. Talanta [Internet]. 2015;143:198–204. Available from: http://dx.doi.org/10.1016/j.talanta.2015.05.035

20. Lermo A, Campoy S, Barb J, Hern S, Alegret S, Pividori MI. In situ DNA amplification with magnetic primers for the electrochemical detection of food pathogens. Biosens Bioelectron. 2007;22:2010–7.

21. BenAissa A, Jara JJ, Sebastián RM, Vallribera A, Campoy S, Pividori MI. Biosensors and Bioelectronics Comparing nucleic acid lateral fl ow and electrochemical genosensing for the simultaneous detection of foodborne pathogens. Biosens Bioelectron [Internet]. 2017;88:265–72. Available from: http://dx.doi.org/10.1016/j.bios.2016.08.046

22. Low K, Rijiravanich P, Kaur K, Singh B, Surareungchai W, Yean CY. An Electrochemical Genosensing Assay Based on Magnetic Beads and Gold Nanoparticle-Loaded Latex Microspheres for Vibrio cholerae Detection. J Biomed Nanotechnol. 2015;11:702–10.

23. Malvern Panalytical. 2019. Characterization of Nanoparticle Size and State Prior to Nanotoxicological Studies Using NTA. AZoNano, viewed 22 July 2019

24. Richardson ET, Samson D, Banaei N. Rapid identification of Mycobacterium tuberculosis and nontuberculous mycobacteria by multiplex, real-time PCR. J Clin Microbiol. 2009;47(5):1497–502.

25. Fernanda M, Bundalian R, Laube T, Julián E, Luquin M, Valnice M, et al. Magneto-actuated immunoassay for the detection of Mycobacterium fortuitum in hemodialysis water. Talanta [Internet]. 2016;153:38–44. Available from: http://dx.doi.org/10.1016/j.talanta.2016.02.041

26. Roshdi Maleki M, Moaddab SR, Samadi Kafil H. Hemodialysis waters as a source of potentially pathogenic mycobacteria (PPM).Desalin Water Treat. 2019;152:168–73.

CHAPTER 4

Comparing nucleic acid lateral flow and electrochemical genosensing for the simultaneous detection of foodborne pathogens

Ben Aissa A, Jara JJ, Sebastián RM, Vallribera A, Campoy S, Pividori MI

Biosens Bioelectron. 2017 Feb 15;88:265-272

4.1 Abstract

Due to the increasing need of rapid tests for application in low resource settings, WHO summarized their ideal features under the acronym ASSURED (Affordable, Sensitive, Specific, User-friendly, Rapid & Robust, Equipment-free, Delivered to those who need it). In this work, two different platforms for the rapid and simultaneous testing of the foodborne pathogens *E.coli O157:H7* and *Salmonella enterica*, in detail a nucleic acid lateral flow and an electrochemical magneto genosensor are presented and compared in terms of their analytical performance. The DNA of the bacteria were amplified by polymerase chain reaction using a quadruple-tagging set of primers specific for *E. coli eaeA gen* (151 bp) and *Salmonella enterica yfiR gen* (375 bp). During the amplification, the amplicons were labelled at the same time with biotin/digoxigenin or biotin/fluorescein tags, respectively. The nucleic acid lateral flow assay was based on the use of streptavidin gold nanoparticles for the labelling of the tagged amplicon from *E. coli* and *Salmonella*. The visual readout was achieved when the gold-modified amplicons were captured by the specific antibodies. The features of this approach are discussed and compared with an electrochemical magneto genosensor. Although nucleic acid lateral flow showed higher limit of detection, this strategy was able to clearly distinguish positive and negative samples of both bacteria being considered as a rapid and promising detection tool for bacteria screening.

4.2. Introduction

The polymerase chain reaction (PCR)(1,2) has found widespread application in many areas including the diagnostic of infectious diseases. As main advantages, the PCR can improve test sensitivity up to 100-fold over immunoassays and with much more rapid turnaround times compared with classical culturing. However, PCR requires thermocycling platforms, trainee personnel, and infrastructure including reliable power supply, which can be a barrier for its application in some low-resource settings(3). To overcome this issue, recent work has focused on PCR platforms that are cheap, portable and operated with batteries(4) that are now commercialized, including Palm PCR™ (Ahram Biosystems Inc.), Freedom4 (Ubiquitome), miniPCR (Amplyus), among others. The detection of PCR products can be easily achieved by electrochemical genosensing(5). Since this early report, novel routes based on tagging-PCR procedures to increase the sensitivity of the electrochemical detection and, at the same time to achieve the immobilization of the amplicon on different platforms were explored(6,7). Among this platforms, the magnetic particles (MPs) greatly enhance the performance of the biological reaction by increasing the surface area, improving the washing steps and, importantly, minimizing the matrix effect (8). MPs also

allow reduction of reaction times and reagent volumes. In addition, MPs can be easily magneto-actuated using permanent magnets(9). Recently, a triple-tagging multiplex PCR amplification strategy for the simultaneous electrochemical genosensing of foodborne pathogens was reported (10). In this work, a set of tagging primers were selected for the specific multiplex amplification of the bacteria, being one of the primers for each set (the forward primers) labelled with fluorescein (FLU), biotin (BIO) and digoxigenin (DIG) coding for *Salmonella*, *Listeria* and *E. coli*, respectively, while the reverse primers are not labelled. Afterwards, silica magnetic particles were used as a platform for the immobilisation by physical adsorption of the amplicons which were further labelled with three different specific antibodies (conjugated with horseradish peroxidase, HRP), in three separated reaction chambers for each pathogen: antiFluorescein-HRP (antiFLU-HRP) coding for *Salmonella*, streptavidin-HRP (strepAv-HRP) coding for *Listeria,* and antiDigoxigenin-HRP (antiDIG-HRP) coding for *E. coli,* respectively. Magnetic actuation in three differentiated magneto-electrodes for each pathogen was then performed. As a main advantage of this approach, the use of the same electrochemical reporter (HRP) allowed the simultaneous electrochemical detection in an array of electrodes to be performed in the same electrochemical cell, by using the same substrate and mediator for the enzyme. Recently, there have been significant developments in the detection of amplicons directly without the need of an instrument or gel electrophoresis(11,12) using, for instance, lateral-flow assay (LFA)(13,14). This technology introduced in 1988 by Unipath is the most common commercially available point of care (PoC) diagnostic format. The LFA incorporates porous membranes, antibodies, and a visible signal-generating system (commonly colloidal gold or dyed polystyrene or latex spheres). It depends upon fluid migration or flow technology(15,16). LFAs are currently used for qualitative –and to some extent quantitative– monitoring in non-laboratory environments. Although there are many commercial available examples for biomedical diagnosis including the pregnancy test, other applications are still under development(17). Lately, many methodological improvements have been done(18), although in general the sensitivity observed for this technology should be improved(19,20).

This work addresses, for first time, the simultaneous detection of two of the most important foodborne pathogens, *Salmonella enterica* and *E. coli O157:H7* (21,22) based on the quadruple-tagging PCR amplification of DNA and by comparing two different approaches for the readout: electrochemical magneto-genosensing and NALF. A set of tagged primers for the quadruple-tagging PCR were selected for the amplification of yfiR (375 bp) and eaeA (151 bp) genes specific for *Salmonella* and *E. coli,* respectively. During PCR, the DNA of each pathogen is amplified and double-labelled at the same time by BIO/FLU and BIO/DIG tags.

In the electrochemical magneto-genosensor strategy, the BIO tags, carried by the reverse primers, is common for both pathogens and used for the immobilization of the amplicons on streptavidin-magnetic particles (streptAv-MPs), while the FLU and DIG-tags, carried by the forward primers, are used for the labelling with the specific antibodies, antiFLU-HRP and antiDIG-HRP, coding for *Salmonella* and *E. coli,* respectively, and performed in two separated reaction chambers. The simultaneous electrochemical readout of the two pathogens is based on HRP as electrochemical reporter and performed in the same electrochemical cell, as previously reported (10). On the contrary, in the NALF strategy, the common BIO-tag is used for the labelling and the visual readout based on streptavidin-gold nanoparticles (streptAv-AuNPs), while FLU and DIG tags, for capturing the amplicon in separated location on the strip by the specific antibodies antiFLU, coding for *Salmonella*, and antiDIG, coding for *E. coli*. The analytical performance of the NALF test and the electrochemical magneto-genosensor are discussed and compared. The NALF test showed promising features, including outstanding limit of detection (LOD) for bacteria screening of the most relevant pathogens in food.

4.3. Experimental section

4.3.1. Instrumentation and materials

Glass fiber conjugate pad (GFCP083000) and cellulose fiber sample pad strips (CFSP203000) were purchased from Millipore. Adhesive Backing Cards were obtained from Kenosha C.V. (Netherlands) and nitrocellulose membranes (FP120HP) as well as the absorbent pads (CF7) were purchased from GE Healthcare Europe. Lateral Flow Reagent Dispenser from Claremont Bio (Upland, CA) combined with the KDS Legato™ 200 series syringe pump from KD Scientific Inc. (Holliston, MA) was used to dispense the test and control line. Electrochemical measurements were performed with a LC-4C amperometric controller (BAS Bioanalytical Systems Inc., U.S.) and Autolab PGSTAT Eco-chemie, using magneto-electrodes based on graphite-epoxy composite (m-GEC) as working electrodes(23).

4.3.2. Chemicals and biochemicals

Dynabeads streptavidin magnetic beads (Prod. N° 112.06) (streptAv-MPs) were purchased from Invitrogen Dynal AS (Oslo, Norway). InnovaCoat® GOLD 40nm Streptavidin gold nanoparticles (streptAv-AuNPs) were purchased from Innova Biosciences (Cambridge, UK). Anti-digoxigenin (11214667001) (antiDIG), anti-fluorescein (11426320001) (antiFLU), anti-digoxigenin-POD (11426346910) (antiDIG-HRP) and anti-fluorescein-POD

(11426346910) (antiFLU-HRP) were purchased from Roche Diagnostics. The buffer solutions were prepared with milliQ water and all other reagents were in analytical reagent grade (supplied from Sigma and Merck). The composition of these solutions is described in Supp. data.

4.3.3. Preparation of the lateral-flow strips

The streptAv-AuNPs were diluted 8 times in conjugate diluting buffer and embedded in the glass fiber conjugate pads. The cellulose fiber sample pads were then soaked into sample pad buffer. The pads were then dried for 3 h at RT. The antibodies and the positive control biotinylated reporter were dispensed on the nitrocellulose membrane and were then dried at RT for 1 h. Finally, the strips were assembled in the usual way on the adhesive backing card.

4.3.4. Bacterial strains, growth conditions and DNA extraction

The bacterial strains *Salmonella enterica serovar* Typhimurium (ATCC® 700720™) and *E. Coli* O157:H7 (clinical isolate supplied by Hospital of Bellvitge, Barcelona, Spain) were grown in Luria Bertani (LB) broth or agar plates for 18 h at 37 °C. The lysis of the bacteria, DNA extraction and purification was performed according to the kit manufacturer (DNeasy Tissue and Blood Kit, Qiagen). The extraction and purification efficacy was evaluated by spectrophotometric analysis as UV absorption at 260 nm.

4.3.5. Oligonucleotides sequences

The oligonucleotides were obtained from TIB- Molbiol GmbH (Berlin, Germany). These primers were selected for the amplification of *yfiR* (375 bp) and *eaeA* (151 bp) gene fragments specific to *S. Typhimurium* and *E. coli*, respectively(24). Each set of primer was double tagged in 5′ end with BIO/FLU and BIO/DIG (Table 4.1).

Table 4.1. Sequences of the set of primers for the quadruple-tagging PCR amplification for the simultaneous detection of *Salmonella* and *E. coli*.

STRAIN	GENE	PRIMER SEQUENCE (5'-3')	TYPE	5'-LABELS	SIZE (bp)
S. enterica	*yfiR*	GTCACGGAAGAAGAGAAATCCGTACG	Forward	Fluorescein	375
		GGGAGTCCAGGTTGACGGAAAATTT	Reverse	Biotin	
E. coli	*eae*A	GGCGGATAAGACTTCGGCTA	Forward	Digoxigenin	151
		CGTTTTGGCACTATTTGCCC	Reverse	Biotin	

4.3.6. Quadruple-tagging PCR

The quadruple-tagging PCR was achieved by a set of four tagging primers for the amplification of the *yfiR* (375 bp), and *eaeA* (151 bp) genes, being the primers for each set labelled with FLU/BIO and DIG/BIO coding for *Salmonella* (S) and *E. coli* (C), respectively (Table 4.1). During the amplification, the amplicons were labelled at the same time with BIO/FLU for *Salmonella* (S) and BIO/DIG for *E. coli* (C). The PCR was performed by using 100 ng of chromosomal DNA of each microorganism in the PCR mixture. Moreover, the negative controls were also included, in which no DNA template was added to the PCR mixture. The Expand High Fidelity PCR System kit (Roche Molecular Biochemicals) was used for performing the PCR reaction in a thermal cycler (Product Nº 2720, Applied Biosystems, Life Technologies Corporation) (as shown in Table S4.1 and Figure S4.1, Supp. Data). The performance of the quadruple-tagging PCR were analysed with conventional agarose gel electrophoresis on 4% agarose gel containing 0.5 x Tris-acetate-EDTA (TAE) and ethidium bromide staining, using HinfI digested ϕ174 DNA as a molecular weight marker, as shown in Figure S4.2.

4.3.7. Simultaneous detection of *Salmonella* and *E. coli* by quadruple-tagging PCR and electrochemical magneto-genosensing assay

The detailed procedure for the simultaneous detection of *Salmonella* and *E. coli* is described in Supp. data and schematically shown in Figure 4.1. Briefly, after the quadruple-tagging PCR, the product was divided in two separated reaction chambers. The common BIO-tag was used for the immobilization of the amplicons on streptavidin-magnetic particles (streptAv-MPs), while the FLU and DIG-tags allowed the labelling by the specific antibodies, antiFLU-HRP and antiDIG-HRP, coding for *Salmonella* and *E. coli*, respectively. The procedure comprised the following steps: (i) immobilization and preconcentration of the tagged amplicons on streptAv-MPs, based on the BIO-tag of the amplicons and (ii)

incubation with the electrochemical reporters, in detail AntiFLU–HRP, and AntiDIG–HRP coding for *Salmonella* (FLU-tag), and *E. coli* (DIG-tag), respectively, in two different incubation chambers; (iii) magnetic actuation by an array of two working electrodes (one coding for *E. coli*, while the other for *Salmonella*), which contain a small magnet (m-GEC) (23); (iv) amperometric readout using the m-GEC electrodes polarized at -0.100V (vs. Ag/AgCl), under enzyme saturation conditions in PBSE buffer, upon the addition of hydroquinone (1.81 mM) and hydrogen peroxide (4.90 mM). More details about the amperometric determination are provided in Supp. data (Figure S4.3). Further characterization of the magneto electrodes (including reproducibility of the construction, renewal and reusability, and stability are also detailed in Supp. data, Figures S4.4, S4.5 and S4.6. The steady-state current was used for the electrochemical signal plotted in further results shown in Figs. 2 and 3. In order to determine the LODs, a calibration curve was performed with increasing amount of *E. coli* and *Salmonella* amplicon. The specificity of the assay was performed by challenging all possible combinations, including i) the binary combinations (S/C), and ii) the single combinations (S; C), as well as a negative control.

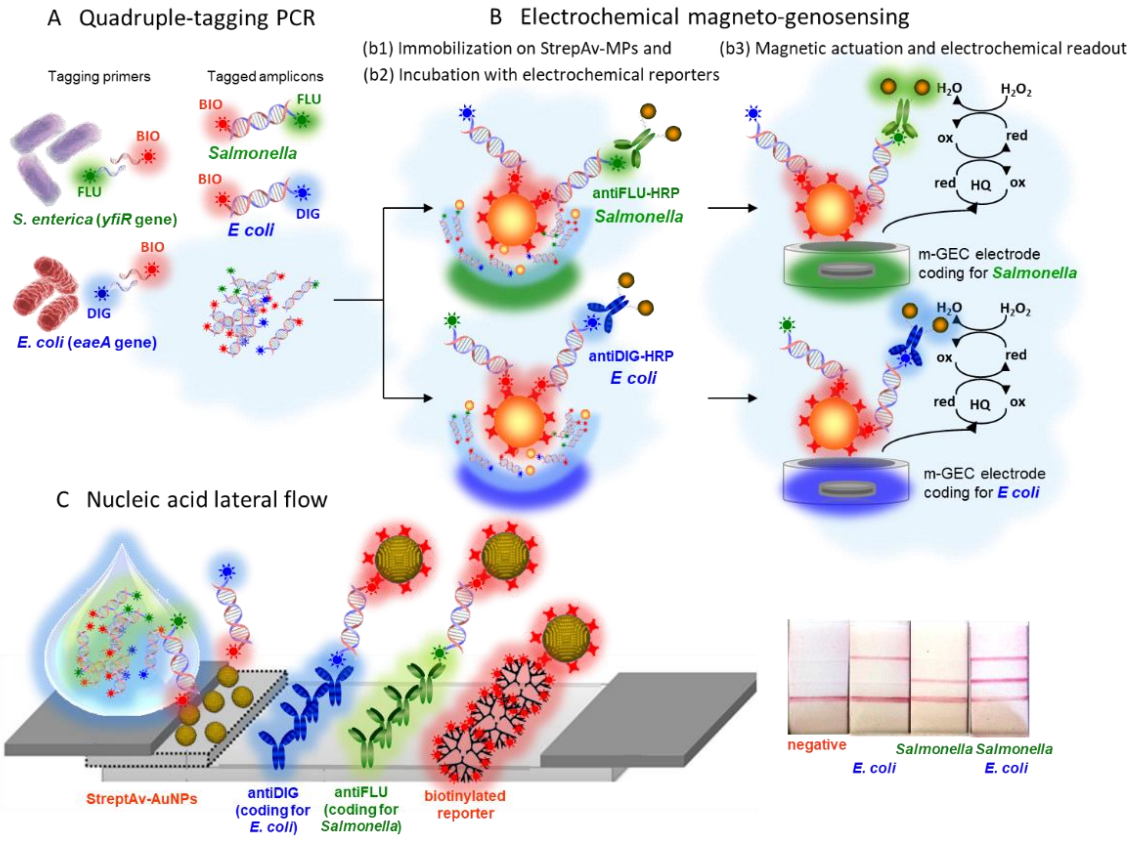

Figure 4.1. Schematic representation of the simultaneous detection of *Salmonella* and *E. coli* by (A) Quadruple-tagging PCR followed by either (B) Electrochemical magneto-genosensing on streptAv-MPs or (C) Nucleic acid lateral flow.

4.3.8. Simultaneous detection of *Salmonella* and *E. coli* by quadruple-tagging PCR and nucleic acid lateral flow assay

The procedure for the simultaneous detection of *Salmonella* and *E. coli* by NALF is schematically described in Figure S4.7, Supp. data. Different amounts of the tagged amplicons were diluted in 150 µL of running buffer and the mixed was added to the sample pad (Figure S4.7, panel b1). After 5 min, 100 µL of running buffer were added in order to drag the remaining streptAv-AuNPs to the absorbent pad. The streptAv-AuNPs thus reacted with the common BIO-tag of the amplicons from *E. coli* and *Salmonella* (Figure S4.7, panel b2). As the products moved along the strip, the streptAv-AuNPs/amplicons were captured by the specific antibodies (antiDIG coding for *E. coli* and antiFLU coding for *Salmonella*) in separated location on the strip (Figure S4.7, panel b3). A valid test was considered when the remaining streptAv-AuNPs reacted with a biotinylated reporter used as a positive control at the control line. The visual readout was thus achieved as well as the interpretation of the results (Figure S4.7, panel b4, Supp. Data). For the quantification of the optical signal, the images were taken with FastGene FAST Digital System and the resulting images were processed with ImageJ software (NHI). In order to determine the LODs, a calibration curve was performed with increasing amount of *E. coli* and *Salmonella* amplicon. The specificity of the magneto-genosensors coding for each bacteria, *Salmonella* (S) and *E. coli* (C) was performed by challenging all possible combinations, including i) the binary combinations (S/C), and ii) the single combinations (S;C), as well as a negative control. To come up with the stability and repeatability study, nine strips were prepared and evaluated along 15 days. They were protected from light and moisture by wrapping them in aluminum foil and kept in a zip plastic bag with silica gel. Four of them were kept at room temperature (RT), while other two were kept at 4ºC.

4.4. Results and Discussion

4.4.1. Quadruple-tagging PCR

The end-point amplicons studied by agarose gel electrophoresis are shown in Figure S4.2 (Supp. Data). Two separated bands, related to each fragment target gene, in detail *S. enterica yfiR* gene fragment (375 pb) and *E. coli eaeA* gene fragment (151 bp) were observed in lane 4, corresponding to the expected amplicon size when compared with the molecular weight markers in lane 5 (in base pairs). The single combinations are shown in lanes 2 and 3. The negative control with no DNA template is also shown in Fig. S2, lane 1. This control is mandatory since it can detect the presence of primer secondary structures (including hairpins, self and cross dimmers, produced by inter and intramolecular interactions

between the primers), which can adversely affect primer template annealing, by reducing the availability of primers to the reaction leading to poor or no yield of the product. Moreover, such undesirable products carrying tags can also be non-specifically amplified, leading to false positive results. As expected, no undesirable amplification in the negative control was observed. Moreover, each target bacteria produced a specific band relative to its correspondent amplicon, showing the PCR outstanding specificity. The relative intensities of the bands can be correlated with the individual performance of each set of primers, and the amplicon length, since as higher the amplicon length is, greater the signal will be, due to ethidium bromide staining (24).

4.4.2. Simultaneous detection of *Salmonella* and *E. coli* by quadruple-tagging PCR and electrochemical magneto-genosensing assay

The LOD of the method was firstly calculated by serial dilution of the tagged-amplicon in single combinations, and the results are shown in Figure 4.2. For *E. coli*, the amplicon ranging from 0.0 to 0.52 ng was processed by using antiDig–HRP as electrochemical reporter (while keeping the *Salmonella* in 0.0 ng). In the case of *Salmonella*, the amplicon ranging from 0.0 to 0.74 ng was processed by using antiFLU-HRP as electrochemical reporter (while keeping the *E. coli* in 0.0 ng). In both cases, the electrochemical signal was fitted using a nonlinear regression (Four Parameter logistic Equation– GraphPad Prism Software) (R^2=0.9973 and 0.9927 for *E. coli* and *Salmonella*, respectively). The LOD was calculated for *E. coli*, by processing the negative control samples (n=6) obtaining a mean value of 0.540 μA with a standard deviation (SD) of 0.052. The cut-off value was then determined with a one-tailed t test at a 95% confidence level (t=2.015), giving a value of 0.645 μA. The LOD was found to be 0.083 ng in 140 μL of sample (0.59 pg μL^{-1}). The LOD was calculated for *Salmonella*, by processing the negative control samples (n=6) obtaining a mean value of 0.455 μA with SD of 0.052. The cut-off value was then determined with a one-tailed t test at a 95% confidence level (t=2.015), giving a value of 0.561 μA. The LOD was found to be 0.105 ng in 140 μL of sample (0.75 pg μL^{-1}).

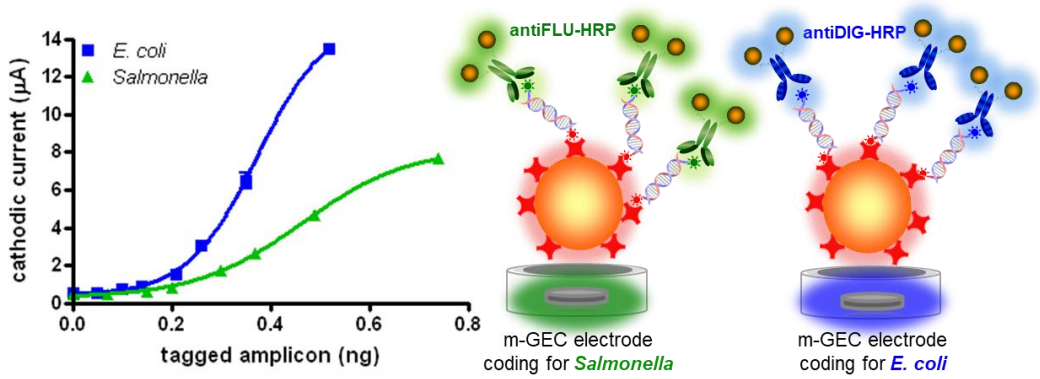

Figure 4.2. Electrochemical responses for the electrochemical magneto genosensing at amplicon amounts in single combinations ranging from (■) 0.0 to 0.52 ng of *E. coli* amplicon (while keeping the *Salmonella* in 0.0 ng) using 60 µg AntiDIG–HRP and (▲) 0.0 to 0.74 ng of *Salmonella* amplicon (while keeping the *E. coli* in 0.0 ng) using 60 µg AntiFLU-HRP. The error bars show the standard deviation for n = 3. The negative controls are also shown (n=6).

Figure 4.3 shows the simultaneous detection of *E. coli* (Figure 4.3, panel A) and *Salmonella* (Figure 4.3, panel C) by quadruple-tagging PCR followed by electrochemical magneto-genosensing on streptAv-MPs. The LOD of the method was calculated in three replicates of each serial dilution of the tagged-amplicon in the binary combinations. For *E. coli*, the amplicon ranging from 0.0 to 0.52 ng was processed by using antiDig–HRP as electrochemical reporter (while keeping the *Salmonella* in 0.74 ng). On the contrary, for *Salmonella*, the amplicon ranging from 0.0 to 0.74 ng was processed by using antiFLU-HRP as electrochemical reporter (while keeping the *E. coli* in 0.52 ng). In both instances, the electrochemical signal was fitted using a nonlinear regression (Four Parameter logistic Equation– GraphPad Prism Software) (R^2=0.9958 and 0.9910 for *E. coli* and *Salmonella*, respectively). The LOD were calculated as above, obtaining similar values than those for the single combinations shown in Figure 4.2: 0.092 ng in 140 µL of sample (0.66 pg μL^{-1}) for *E. coli* (when *Salmonella* is also present at high concentration level), and 0.164 ng in 140 µL of sample (1.17 pg μL^{-1}) for *Salmonella* (when *E. coli* is also present at high concentration level), highlighting the robustness and specificity of the method. However, the specificity of the magneto-genosensors coding each bacterium, *Salmonella* (S) and *E.coli* (C), was further studied in three replicates by challenging all possible combinations of the amplicons, including i) the binary combinations (S/C), ii) the single combinations (S; C), as well as the negative control, with the two electrochemical reporters (antiFLU-HRP and antiDIG–HRP, respectively). As observed in Figure 4.3, panels B and D, each of the electrodes only detected one of the two pathogen, even in the presence/or absence of the other one. For instance, in the electrode coding for *E. coli* (Figure 4.3, panel B), the mean value for the electrochemical signal obtained for *E. coli* (C) (13.47 µA, CV% 3.0), is almost the same when *Salmonella* is

also present (S/C) (13.35 µA, CV% 3.8), while when *E. coli* is absent (negative control) (0.58 µA, CV% 7.8), the signal is equal even in the presence of *Salmonella* (S) at high concentration level (0.51 µA, CV% 6.0) (Figure 4.3, panel B). Similar results were obtained in the case of *Salmonella* (Figure 4.3, panel D), since the mean value for *Salmonella* (S) (7.53 µA, CV% 4.3), is almost the same when *E. coli* is also present (S/C) (7.68 µA, CV% 2.5), while when *Salmonella* is absent (negative control) (0.45 µA, CV% 4.6), the signal is equal even in the presence of *E. coli* (C) (0.49 µA, CV% 8.1), highlighting the specificity of both, the quadruple-tagging PCR, as well as the electrochemical detection.

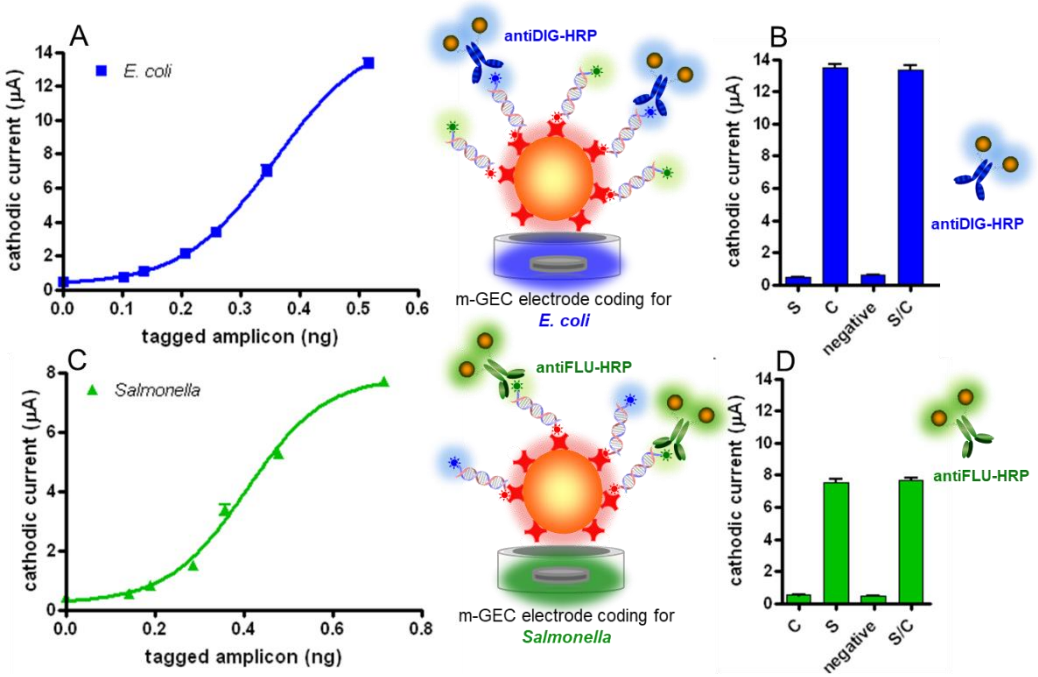

Figure 4.3. Electrochemical responses for the simultaneous electrochemical magneto genosensing at amplicon amounts in binary combinations ranging from (■) 0.0 to 0.52 ng of *E. coli* amplicon (A) (while keeping the *Salmonella* at high amount of 0.72 ng) using 60 µg AntiDIG–HRP and (▲) 0.0 to 0.72 ng of *Salmonella* amplicon (C) (while keeping the *E. coli* in 0.52 ng) using 60 µg AntiFLU-HRP. Panel (B) and (D) show the specificity study for i) the binary combinations (S/C), and iii) the single combinations (S; C), challenged towards (B) 60 µg AntiDIG-HRP coding for *E. coli* and (D) 60 µg AntiFLU–HRP coding for *Salmonella*. In all cases (B and D), an amplicon amount of 0.52 and 0.72 ng, respectively for *E. coli* and *Salmonella*. The error bars show the standard deviation for n=3. The negative controls are also shown (n=3).

Hence, the results suggest that this approach was able to clearly distinguish between the two different bacteria and their single and binary combinations, with outstanding repeatability. The stability of the magneto-genosensing approach is determined by the stability of the reagents (PCR mix, antibodies and strepAv-MPs), that should be kept at 4ºC

as recommended by the manufacturers. As the m-GEC electrode is not biologically-modified, they were storage at RT. Further details about reproducibility of the construction, renewal and reusability, and stability of the m-GEC electrodes are provided in Supp. data, Figures S4.4, S4.5 and S4.6.

4.4.3. Simultaneous detection of *Salmonella* and *E. coli* by quadruple-tagging PCR and nucleic acid lateral flow assay

The detection of *Salmonella* and *E. coli* by quadruple-tagging PCR followed by NALF was performed as schematically shown in in Figure S4.7 (supp. Data). The total assay time is less than 15 min. The results of the tests can either be estimated with the naked eye or by measuring the intensity of the red bands with the software ImageJ. The LOD of the method was calculated by serial dilution of the tagged-amplicon in single combinations, and the results are shown in Figure 4.4, panel A. For *E. coli*, the amplicon was ranging from 0.0 to 103 ng while for *Salmonella*, from 0.0 to 143 ng.

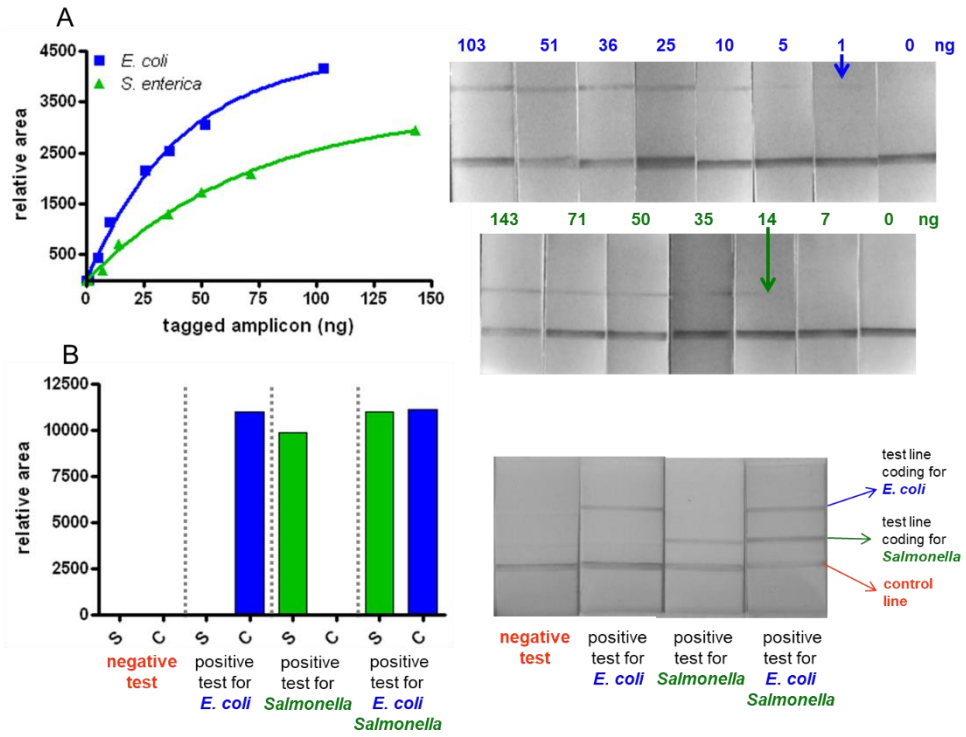

Figure 4.4. (A) Results obtained for the NALF at amplicon amounts in single combinations ranging from (■) 0.0 to 103 ng of *E. coli* amplicon (while keeping the *Salmonella* in 0.0 ng) and (▲) 0.0 to 143 ng of *Salmonella* amplicon (while keeping the *E. coli* in 0.0 ng). The corresponding images of the strips are also shown. (B) Results obtained in single and binary combination, with an amount of amplicon of 51 ng of *E.coli* and 71 ng of *Salmonella*.

The relative areas obtained by processing the images were fitted using a nonlinear regression (Four Parameter logistic Equation– GraphPad Prism Software) (R^2=0.9952 and 0.9958 for *E. coli* and *Salmonella*, respectively). The NALF approach was able to visually detect (signalling by arrows in Figure 4.4) as low as 5.2 ng in 150 µL of sample (LOD = 34 pg μL^{-1}) for *E. coli* and 14.3 ng in 150 µL of sample (LOD = 95 pg μL^{-1}) for *Salmonella*.

The Figure 4.4, panel B, shows the specificity study for the simultaneous detection of *E. coli* and *Salmonella*, in single and binary combination, with an amount of amplicon of 51 ng of *E.coli* and 71 ng of *Salmonella,* as well as the negative control. As can be observed, the negative control only provided signal in the control line, as expected. No cross-reaction of the signal-generating system (strept(Av)-AuNPs) were thus observed with the specific antibodies (antiDIG coding for *E. coli* and antiFLU coding for *Salmonella*) located on the test lines of the strip. Furthermore, for samples containing exclusively the *Salmonella* amplicon, only the antiFLU test line provided a positive signal. No cross-reaction of the BIO/FLU double-tagged *Salmonella* amplicon was thus observed with the antiDIG antibody located in the test line coding for *E. coli*. Similarly, for samples containing only the BIO/DIG double-tagged *E. coli* amplicon, no cross-reaction was observed in the antiFLU test line coding for *Salmonella*. Finally, the binary combination provided signals in both test lines, coding for *Salmonella* and *E. coli.* Hence, the results suggest that this approach was able to clearly distinguish between the different bacteria and their single and binary combinations.
The stability of the strips was evaluated along 15 days, by keeping the strips protected from light and moisture, at RT and at 4ºC. The results for the binary combination containing 51 ng of *E.coli* and 71 ng of *Salmonella* are shown in Figure 4.5. The interday stability study during 15 days, showed CV% of 12.3, 12.7 and 7.8 % for *E. coli*, *Salmonella* and the positive control line, respectively (n=9). The repeatability of the NALF assay was study with the strips recently prepared (numbered as 1, 2 and 3, Figure 4.5), showing CV% of 4.5, 7.3 and 8.8 %, for *E. coli*, *Salmonella* and the positive control line, respectively, suggesting also a good reproducibility in the preparation of the strips (n=3). Furthermore, no significant differences in signals were observed when the strips were storage at RT or 4ºC. The CV% for the strips (n=3) kept for 1 week at RT (Nº 4 and 5) and 4ºC (Nº 6), were 5.4, 5.9 and 7.8 % for *E. coli*, *Salmonella* and the positive control, while also similar CV% (7.1, 3.0 and 5.3 %) were obtained when the strips were kept for 2 weeks (nº 7, 8 and 9). The results are also similar to the strips recently prepared (Nº 1, 2 and 3), suggesting that they can be storage either at RT or 4ºC without any loss in the activity, at least for 15 days. Although it is known that the biological reagents can be housed in the lateral flow strips at RT without loss of activity before an expiration date (for instance, the commercial available pregnancy tests),

further studies should be done for longer storage period. Finally, it is important to highlight that none of the NALF assays performed in this work provided invalid results, since in all cases the line corresponding to the positive control was observed.

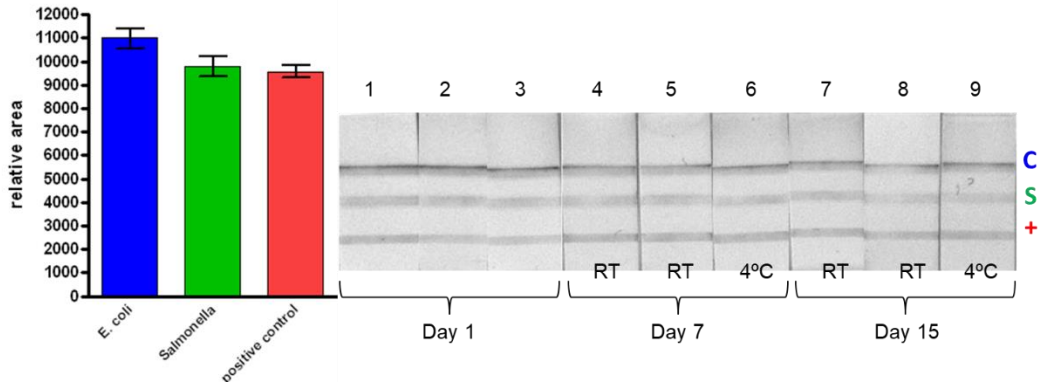

Figure 4.5. Stability and repeatability study of the NALF, for the binary combination containing 51 ng of *E.coli* and 71 ng of *Salmonella*. The corresponding images of the strips are also shown. n=9.

4.5. Conclusions

Concerns about food safety have increased in more affluent societies. The Center for Disease Control and Prevention estimates that only in the United States each year roughly 48 million people get sick from a foodborne illness. Contamination can occur during production, processing, distribution or preparation. For this reason, it is extremely important the detection at any point of the food chain production with rapid and reliable techniques. Beside this, it is important to highlight the burden of foodborne diseases in the developing world, where the facilities and equipments for the detection of pathogens combined with the lack of availability of essential medicines and supplies for treatment make increase the case fatality rate. According to World Health Organization, billions of people are at risk and it is estimated that 1 in 10 people fall ill every year and 420000 die as a result of consuming contaminated food. Recent guidelines published by WHO recommend that diagnostic devices for developing countries to be ASSURED being this acronym defined by (A) Affordable, (SS) Sensitive, Specific, (U) User-friendly, (R) Rapid and Robust, (E) Equipment free, and (D) Deliverable to those who need it. In this work, two methods (electrochemical genosensors and NALF) following these recommendations are compared, demonstrating to be promising candidates for the detection of *Salmonella* and *E. coli* at low-resource settings. The specificity was studied obtaining outstanding results with both methods, being able to clearly distinguish between the different bacteria and their single and binary combinations. Among the two methods, it has to be highlighted the simplicity, low cost and the rapidness

of lateral flow. Qualified personal is not required and the results can be read with the naked eye in less than 15 min unlike the electrochemical magneto genosensor which the time of assay is 2 hours. Nevertheless, the electrochemical magneto genosensor showed a higher sensitivity and noticeable improved limits of detection, being the LODs as low as 83 pg of *E.coli* PCR amplicon (0.59 pg μL^{-1}) and 105 pg for *Salmonella (*0.75 pg μL^{-1}) compared with 5.2 ng (34 pg μL^{-1}) and 14.3 ng (95 pg μL^{-1}) for *E.coli* and *Salmonella,* respectively, visually detected by the NALF approach. Furthermore, the electrochemical magneto genosensor provides quantitative results. Although both methods require PCR for amplification, reliable thermocyclers that are cheap, portable and operated with batteries are now in the market, which can easily be adapted in resource-constrained settings to meet the demands for ASSURED diagnosis recommended by WHO.

4.6. Acknowledgments

This work was funded by the Ministry of Economy and Competitiveness (MINECO), Madrid (Project ASSURED, BIO2013-41242-R). Financial support from the projects BFU2011-23478, CTQ2014-53662-P, CTQ2014-51912-REDC (Ministry of Economy and Competitiveness, MICINN, Madrid) and 2014SGR572, 2014SGR572, 2014SGR1105 (DURSI-Generalitat de Catalunya) are also gratefully acknowledged.

4.7. Supporting information

4.7.1. Buffers and solutions

All buffer solutions were prepared with milli-Q water and all other reagents were in analytical reagent grade (supplied from Sigma and Merck). The composition of these solutions are:

- *conjugate diluting buffer* (2 mmol L^{-1} borate pH 7, 10 % w/v sucrose).
- *sample pad buffer* (0.01 mol L^{-1} phosphate buffer pH 7.4, 1% BSA, 0.05 % Tween 20).
- *running buffer* (0.01 mol L^{-1} phosphate buffer pH 7.4, 1% BSA, 0.05 % Tween 20).
- *5 x SSC* (0.75 mol L^{-1} NaCl, 75 mmol L^{-1} trisodium citrate, pH 7.0).
- *Tris buffer* (0.1 mol L^{-1} Tris, 0.15 mol L^{-1} NaCl, pH 7.5).
- *blocking Tris buffer* (2 % w/v BSA, 0.1 % w/v Tween 20, 5 mmol L^{-1} EDTA, 0.1 mol L^{-1} Tris, 0.15 mol L^{-1} NaCl, pH 7.5).
- *PBSE buffer* (0.1 mol L^{-1} phosphate buffer, 0.1 mol L^{-1} KCl, pH 7.0).

4.7.2. Quadruple-tagging PCR

The PCR reaction was carried out in a thermal cycler (Product Nº 2720, Applied Biosystems, Life Technologies Corporation). The detailed conditions for the quadruple-tagging PCR is presented in Table S4.1 and schematically shown in Figure S4.2.

Table S4.1. Thermal cycler conditions for the quadruple-tagging PCR

	Initial step	DNA denaturation	Annealing	Extension	Last step
	1 cycle	40 cycles			1 cycle
Temperature (°C)	95	95	60	72	72
Time (sec)	600	20	30	30	420

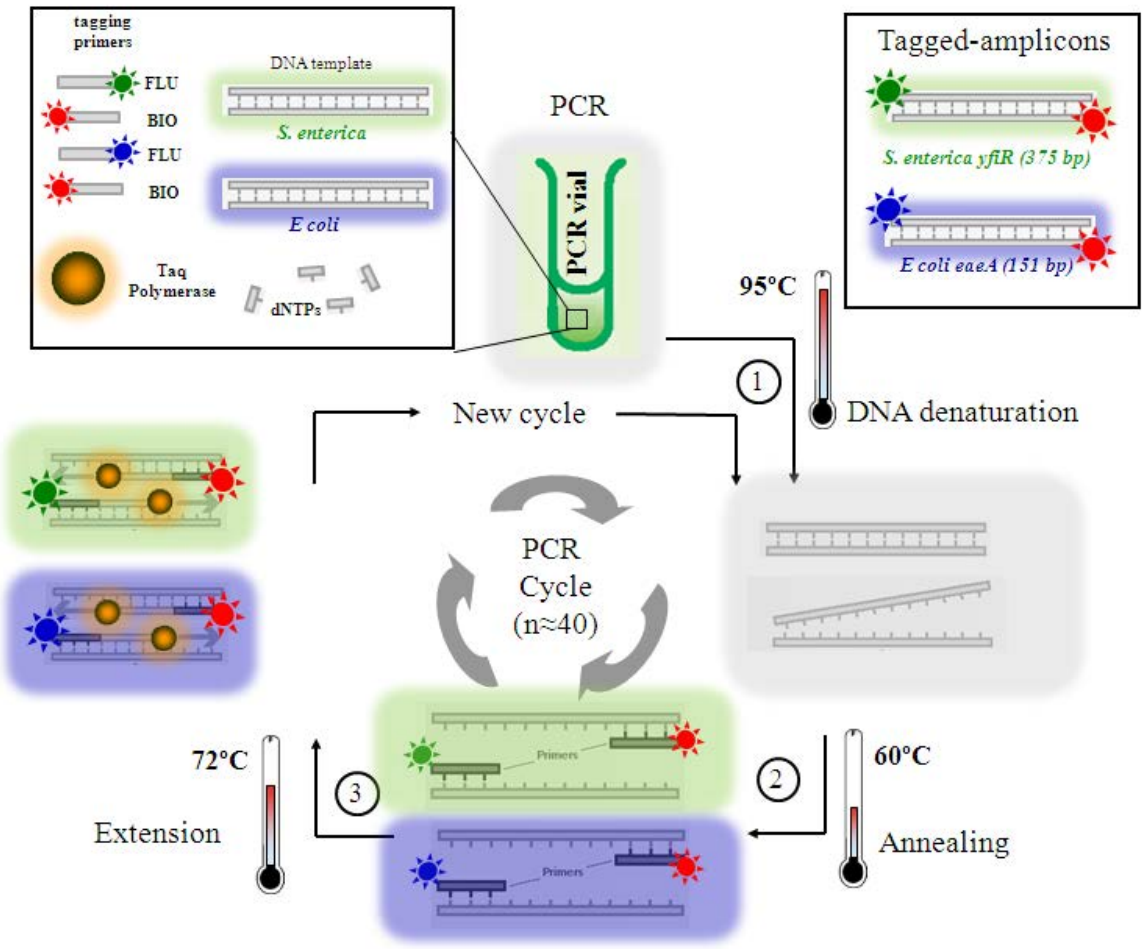

Figure S4.1. Schematic representation of the quadruple-tagging PCR amplification, in order to obtain the double-tagged amplicon labelled with biotin and digoxigenin for *E. coli* and with biotin and fluorescein for *S. enterica*.

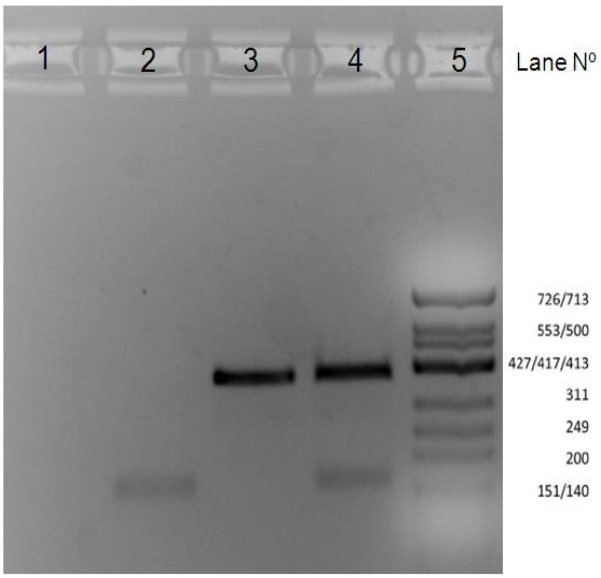

Figure S4.2. Gel electrophoresis of the quadruple-tagging PCR. The amplification bands correspond to *S. enterica yfiR* gene fragment (375 pb) and E*. coli eaeA* gene fragment (151 bp). Lane 1 is the negative control in which no DNA template has been added to the PCR mixture, while lane 2 and 3 show the single combination, and lane 4 the binary combination. HinfI digested ϕ174 DNA was used as a molecular weight marker, ranging from 726 to 140 bp.

4.7.3. Simultaneous detection of S. enterica and E. coli by quadruple-tagging PCR and electrochemical magneto-genosensing assay

The procedure for the simultaneous detection of *S. enterica* and *E. coli* is schematically shown in Figure 4.1. The product quadruple-tagging PCR was divided in two separated reaction chambers, for each pathogens, one coding for *E. coli* and the other for *Salmonella*. The common BIO-tag was used for the immobilization of the amplicons on streptavidin-magnetic particles (streptAv-MPs), while the FLU and DIG-tags allowed the labelling by the specific antibodies, antiFLU-HRP and antiDIG-HRP, coding for *Salmonella* and *E. coli*, respectively. The procedure in each chamber comprises the following steps: (i) immobilization and preconcentration of the tagged amplicons on streptavidin-MPs ($6.2\ 10^6$) in Eppendorf tubes with the diluted amplicon in 5 x SSC for 30 min at 42 ºC at a final volume of 140 µL, followed by two washing steps (140 µL of 5 x SSC) for 2 min at 42 ºC; (ii) incubation with the electrochemical reporters by using antiDIG-HRP (60 µg) (coding for *E. coli*) and antiFLU-HRP (60 µg) (coding for *Salmonella*) in blocking Tris buffer at a final volume of 140 µL for 30 min at 42 ºC, followed by two washing steps (140 µL Tris buffer) for 2 min at 42 ºC. After each incubation or washing step, the MPs were separated from the

supernatant on the side wall by placing the Eppendorf tubes in a magnet separator until the beads were migrated to the tube sides and the liquid was clear, iii) magnetic actuation by an array of two modified working electrodes (one coding for *E. coli*, whole the other coding for *Salmonella*, respectively), by dipping the magneto electrode (m-GEC) inside the reaction tube; (iv) amperometric readout was performed in a electrochemical cell containing 20 mL of PBSE buffer (0.1 mol L^{-1} phosphate buffer, 0.1 mol L^{-1} KCl, pH 7.0) and 1.81 mmol L^{-1} hydroquinone with a platinum auxiliary electrode (Crison 52-67 1), a double junction Ag/AgCl reference electrode (Orion 900200) with 0.1 mol L^{-1} KCl as the external reference solution and the m-GEC electrodes polarized at -0.100 V (vs. Ag/AgCl), under continuous magnetic stirring. When a stable baseline was reached, H_2O_2 was added into the electrochemical cell to a final concentration of 4.90 mmol L^{-1}, and the current was measured until the steady state current was reached.

The electrochemical magneto-genosensing strategy is based on amperometry, in the presence of hydrogen peroxide (H_2O_2) as a substrate of the enzyme and hydroquinone (HQ) as mediator to shuttle electrons between the m-GEC electrode and the horseradish peroxidase enzyme (HRP). The respective antibodies labelled with HRP were used as electrochemical reporter, since they coupled to the DIG and FLU tags of double tagged amplicons. The mediator was regenerated by applying a reduction potential on the surface of the electrode being the current measured directly proportional to the concentration of HRP, when saturated substrate (H_2O_2) conditions were used, as shown in Figure S4.3.

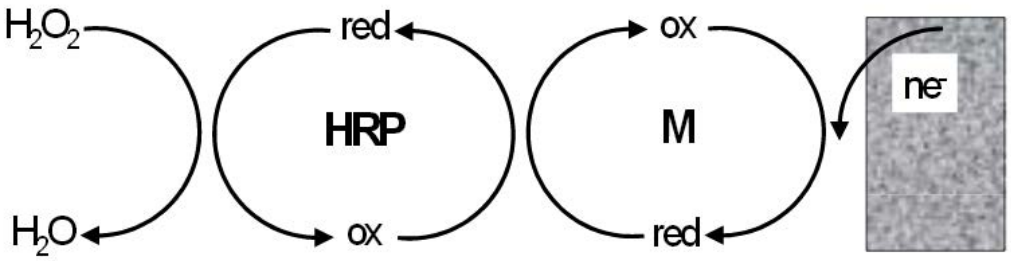

Figure S4.3. Enzymatic mechanism of the HRP enzyme in the surface of the m-GEC electrode, using H_2O_2 as a substrate of the enzyme and hydroquinone as a mediator.

In each measurement a steady-state current was obtained normally after 1 min of hydroquinone (1.8×10^{-3} mol L^{-1}) and hydrogen peroxide (4.9×10^{-3} mol L^{-1}) addition in phosphate buffer (PBSE), as mediator and substrate for the enzyme HRP respectively. After each use, the surface of the m-GEC electrodes were renewed by a simple polishing procedure, wetted with double-distilled water, and then thoroughly smoothed with abrasive paper and then with alumina paper (polishing strips 301044-001, Orion) (25).

4.7.4. Characterization of the m-GEC electrodes and selection of the applied potential for the amperometric measurements

The characterization of a batch of 3 electrodes used in this work (and prepared as detailed in Zacco et al., 2006) as well as the selection of the applied potential for the amperometric readout was performed by cyclic voltammetry. The three-electrode setup (Ag/AgCl as reference electrode, the platinum as auxiliary electrode and m-GEC electrodes as working electrode) was immersed into the electrochemical cell containing 20 mL of phosphate buffer (PBSE) and the CVs were recorded from -1.00 V to +1.00 V, at a scan rate of 100 mV/s. Figure S4.4 shows the typical cyclic voltammograms obtained with the batch of 3 m-GEC electrodes, upon the addition of hydroquinone (1.8×10^{-3} mol L^{-1}) in phosphate buffer solution (PBSE). Outstanding reproducibility in the preparation of the m-GEC electrodes was achieved. According to Figure S4.4, a potential of -0.100 V corresponding to the reduction of the mediator was chosen for the amperometric readout in further experiments.

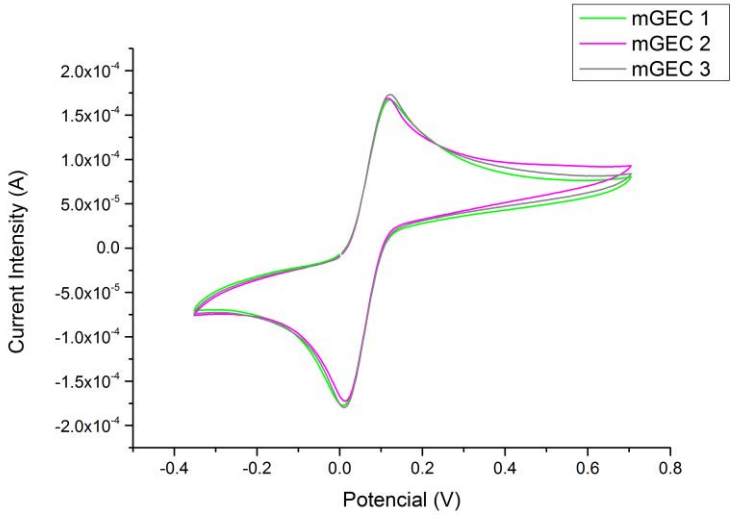

Figure S4.4. Typical cyclic voltammograms of a batch of 3 m-GEC electrodes upon the addition of 1.8 10^{-3} mol L^{-1} of hydroquinone in phosphate buffer pH= 7.0 vs. Ag/AgCl reference electrode.

4.7.5. Renewal and reusability of the m-GEC electrodes

After each use, the surface of the m-GEC electrode was renewed by a simple polishing procedure, wetted with double-distilled water, and then thoroughly smoothed with abrasive paper and then with alumina paper (polishing strips 301044-001, Orion). Figure S4.5 shows the cyclic voltammograms obtained before and after the renewal of an m-GEC electrode, upon the addition of hydroquinone (1.8×10^{-3} mol L^{-1}) in phosphate buffer solution (PBSE). No significant differences were observed with the same electrode submitted to the renewal processes of the surface by polishing.

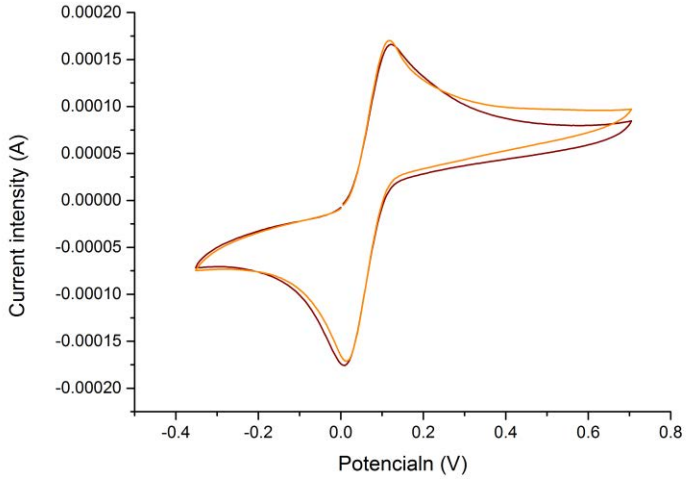

Figure S4.5. Cyclic voltammograms obtained before (brown) and after (orange) the renewal of the m-GEC electrode upon the addition of 1.8 10^{-3} mol L^{-1} of hydroquinone in phosphate buffer pH= 7.0 vs. Ag/AgCl reference electrode.

4.7.6. Stability study of the m-GEC electrodes

Moreover, stability of materials of mGEC electrodes was tested over a period of 180 days and no significant differences were observed. Figure S4.6 shows the cyclic voltammograms obtained on different days during 6 months and no significant differences were observed with the same electrode during this period of time.

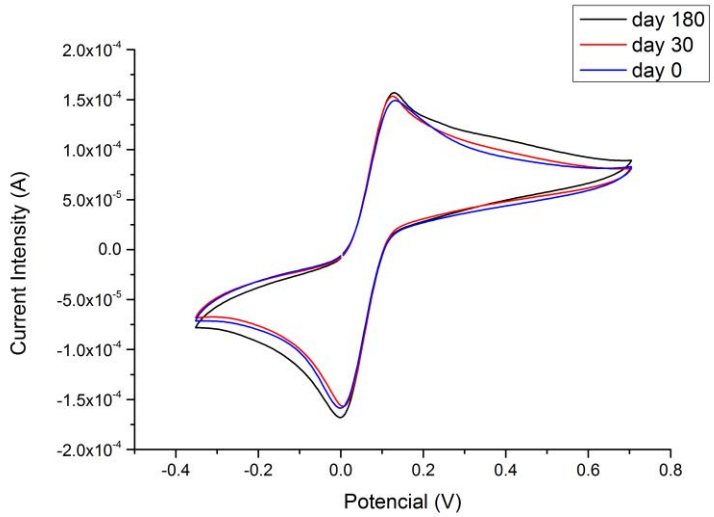

Figure S4.6. Cyclic voltammograms obtained over a period of 6 months upon the addition of 1.8 10^{-3} mol L^{-1} of hydroquinone in phosphate buffer pH= 7.0 vs. Ag/AgCl reference electrode.

4.7.7. Simultaneous detection of *Salmonella* and *E. coli* by quadruple-tagging PCR and nucleic acid lateral flow assay

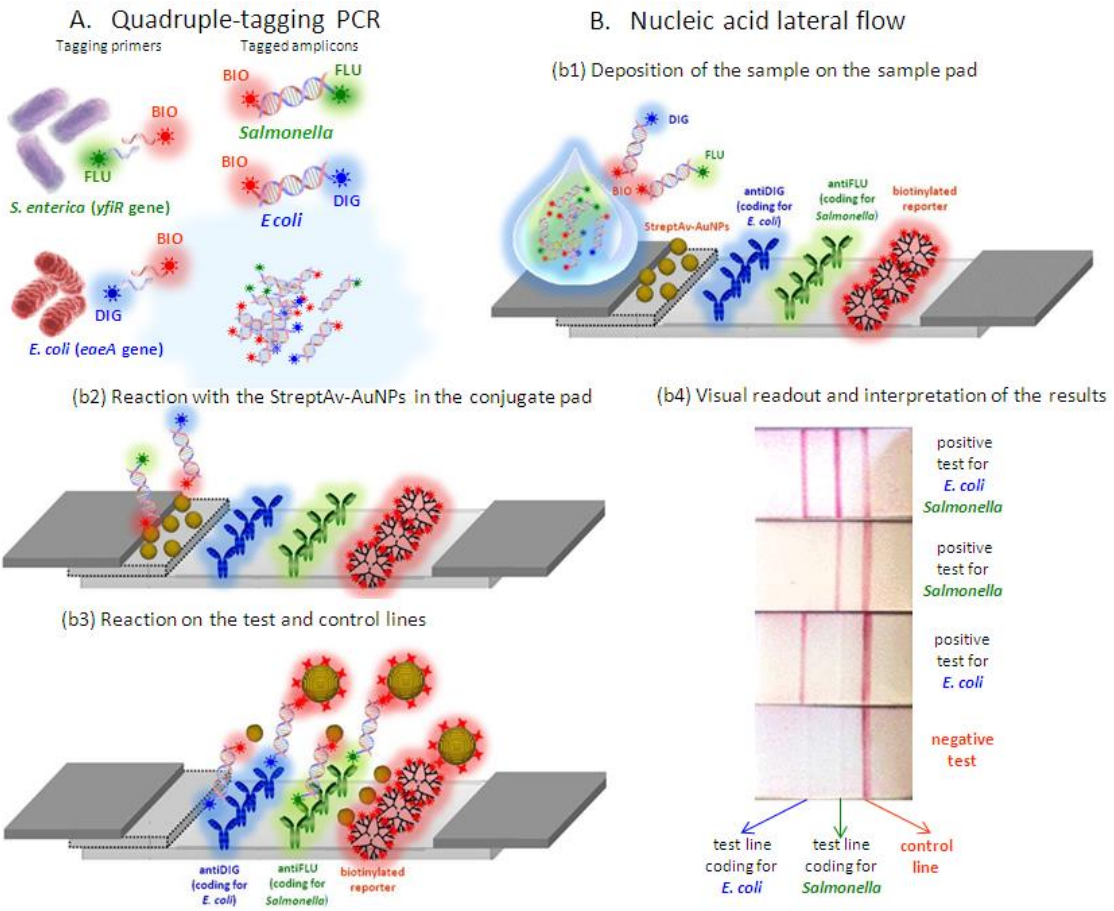

Figure S4.7. Schematic representation of the quadruple-tagging PCR amplification, in order to obtain the double-tagged amplicon labelled with biotin and digoxigenin for *E. coli* and with biotin and fluorescein for *S. Enteric*, and the detailed steps for the simultaneous detection of *Salmonella* and *E. coli* by the Nucleic acid lateral flow.

4.8. References

1. Mullis KB, Faloona FA. [21] S p e c i f i c S y n t h e s i s o f D N A in Vitro v i a a Polymerase-Catalyzed Chain Reaction. Methods Enzymol. 1987;155:335–50.
2. Saik RK, Gelfand DH, Stoffel S, Scharf SJ, Higuchi R, Horn GT, et al. Primer-Directed Enzymatic Amplification of DNA with a Thermostable DNA Polymerase. 1988;239(1986):487–91.
3. Urdea M, Penny LA, Olmsted SS, Giovanni MY, Kaspar P, Shepherd A, et al. Requirements for high impact diagnostics in the developing world. Nature. 2006;444:73–9.
4. Marx V. PCR heads into the field. Nat Methods. 2015;12(5):393–7.
5. Pividori MI, Merkoçi A, Barbe J, Alegret S. PCR-Genosensor Rapid Test for Detecting Salmonella. Electroanalysis. 2003;15:1815–23.

6. Lermo A, Campoy S, Barb J, Hern S, Alegret S, Pividori MI. In situ DNA amplification with magnetic primers for the electrochemical detection of food pathogens. Biosens Bioelectron. 2017;22(2007):2010–7.

7. Brasil PR, Marques DO, Lermo A, Campoy S, Yamanaka H, Alegret S, et al. Double-Tagging Polymerase Chain Reaction with a Thiolated Primer and Electrochemical Genosensing based on Gold Nanocomposite Sensor for Food Safety. Anal Chem. 2009;81(4):1332–9.

8. Alegret S, Pividori MI, Lermo A, Zacco E, Barak J, Delwiche M, et al. Biosensors and Bioelectronics Towards Q-PCR of pathogenic bacteria with improved electrochemical double-tagged genosensing detection. 2008;23:1805–11.

9. Brandao D, Liébana S, Pividori MI. Multiplexed detection of foodborne pathogens based on magnetic particles. N Biotechnol [Internet]. 2015;32(5):511–20. Available from: http://dx.doi.org/10.1016/j.nbt.2015.03.011

10. Brandão D, Liébana S, Campoy S, Cortés MP, Alegret S, Pividori MI. Simultaneous electrochemical magneto genosensing of foodborne bacteria based on triple-tagging multiplex amplification. Biosens Bioelectron [Internet]. 2015;74:652–9. Available from: http://dx.doi.org/10.1016/j.bios.2015.07.008

11. Niemz A, Ferguson TM, Boyle DS. Point-of-care nucleic acid testing for infectious diseases. Trends Biotechnol. 2011;29(5):240–50.

12. Tomita N, Mori Y, Kanda H, Notomi T. Loop-mediated isothermal amplification (LAMP) of gene sequences and simple visual detection of products. Nat Protoc. 2012;3(5):877–82.

13. Carter DJ, Cary RB. Lateral flow microarrays : a novel platform for rapid nucleic acid detection based on miniaturized lateral flow chromatography. Nucleic Acids Res. 2007;35(10).

14. Singh J, Sharma S, Nara S. Evaluation of gold nanoparticle based lateral flow assays for diagnosis of enterobacteriaceae members in food and water. FOOD Chem [Internet]. 2014;170:470–83. Available from: http://dx.doi.org/10.1016/j.foodchem.2014.08.092

15. Chun P. Colloidal Gold and Other Labels for Lateral Flow Immunoassays. In: Lateral Flow Immunoassay. New York: Humana Press; 2009. p. 75–93.

16. Farrell BO, Immunoassays C. Evolution in Lateral Flow – Based Immunoassay Systems. In: Lateral Flow Immunoassay. New York: Humana Press; 2009. p. 1–33.

17. Gubala V, Harris LF, Ricco AJ, Tan MX, Williams DE. Point of Care Diagnostics : Status and Future. Anal Chem. 2012;84:487–515.

18. Posthuma-trumpie GA, Korf J. Lateral flow (immuno) assay : its strengths , weaknesses , opportunities and threats . A literature survey. Anal Bioanal Chem. 2009;569–82.

19. Seo K, Holt PS, Stone HD, Gast RK. Simple and rapid methods for detecting Salmonella enteritidis in raw eggs. Int J Food Microbiol. 2003;87:139–44.

20. Moongkarndi P, Rodpai E, Kanarat S. Evaluation of an immunochromatographic assay for rapid detection of Salmonella enterica serovars Typhimurium and Enteritidis. J Vet Diagnostic Investig. 2011;23(4):797–801.

21. WHO. WHO estimates of the global burden of foodborne diseases. Foodborne disease burden epidemiology reference group 2007-2015. Switzerland: WHO Library Cataloguing-in-Publication Data; 2015.

22. Altekruse SF, Cohen ML, Swerdlow DL, Control D. Emerging Foodborne Diseases. Emerg Infect Dis. 1997;3(3):285–93.

23. Pividori MI, Alegret S. Electrochemical Genosensing Based on Rigid Carbon

Composites . A Review. Anal Lett. 2005;38:2541–65.

24. Kawasaki S, Horikoshi N, Okada Y, Takeshita K, Sameshima T, Kawamoto S. Multiplex PCR for Simultaneous Detection of Salmonella spp ., Listeria monocytogenes , and Escherichia coli O157 : H7 in Meat Samples. 2005;68(3):551–6.

25. Zacco E, Adrian J, Galve R, Marco M, Alegret S, Pividori MI. Electrochemical magneto immunosensing of antibiotic residues in milk. 2007;22:2006–7.

CHAPTER 5

Magnetic molecularly imprinted polymer for the isolation and detection of biotin and biotinylated biomolecules

Ben Aissa A, Herrera-Chacon A, Pupin RR, Sotomayor MDPT, Pividori MI

Biosens Bioelectron. 2017 Feb 15;88:101-108

5.1. Abstract

Magnetic separation based on biologically-modified magnetic particles is a preconcentration procedure commonly integrated in magneto actuated platforms for the detection of a huge range of analytes. However, the main drawback of this material is their stability and high cost. In this work, a novel hybrid molecularly-imprinted polymer with magnetic properties is presented with affinity towards biotin and biotinylated biomolecules. During the synthesis of the magneto core-shell particles, biotin was used as a template. The characterization of this material by microscopy techniques including SEM, TEM and confocal microscopy is presented. The application of the magnetic-MIPs for the detection of biotin and biotinylated DNA in magneto-actuated platforms is also described for the first time. The magnetic-MIP showed a significant immobilization capacity of biotinylated molecules, giving rise to a cheaper and a robust method (it is not required to be stored at 4º C) with high binding capacity for the separation and purification under magnetic actuation of a wide range of biotinylated molecules, and their downstream application including determination of their specific targets.

5.2. Introduction

Since the early reports on magnetic separation technology(1), magnetic particles (MPs) have been used as a powerful and versatile preconcentration tool in a variety of analytical and biotechnology applications(2). This technology has been widely incorporated for researchers worldwide in classical methods, in molecular tools (PCR, immunoassays) and in emerging technologies including biosensors(3) and microfluidic devices with application ranging from biomarker detection of infectious diseases(4) foodborne pathogens(5), among many others. Magnetic particles have been commercially available for many years and are widely used in laboratories to extract desired biological components from a fluid. They consist of an inorganic core of magnetic materials coated with polymer to confer stability (such as polystyrene, dextran, polyacrylic acid, or silica), which can be modified with functional groups (such as amino and carboxylic acids) to make subsequent conjugations easier. Hence, magnetic particles can be coupled to ligands, including peptides, small molecules, proteins, antibodies, and nucleic

acids. Among the different biological biomolecules, strept(avidin)-modified MPs are highly implemented due to the specific interaction with biotin and biotinylated biomolecules. Avidin and streptavidin bind four moles of biotin per mole of protein with an extraordinary affinity (Ka = 10^{15} M^{-1})(6). Some applications in which the strept(avidin)-biotin interaction has been used include ELISA, immunohistochemical staining, Western, Northern and Southern blotting, immunoprecipitation, cell-surface labeling, affinity purification, fluorescence-activated cell sorting (FACS), among many others(7). The valeric acid side chain of the biotin molecule can be derivatized to incorporate various reactive groups that are used to attach biotin to other molecules, including peptides, antibodies, enzymes, receptors, nucleic acids, without significantly altering their biological activity(6). To take advantages of this interaction for separation, purification of biotinylated biomolecules, as well as for the downstream application, there are many commercial available avidin/streptavidin magnetic particles, for example, Streptavidin MagBeads (GenScript), Dynabeads® (Dynal), hyBeads® Streptavidin (Hyglos), Adembeads (Ademtech), among others. The use of MPs greatly improves the performance of the biological reaction by increasing the surface area, improving the washing steps and, importantly, minimizing the matrix effect. MPs also allow reduction of reaction times and reagent volumes. In addition, MPs can be easily magneto-actuated using permanent magnets(8). In particular, super paramagnetic particles are highly attractive due to their capability to magnetise under a magnetic field. Thus, the particles can be separated easily from the liquid phase with a small magnet, but can be redispersed immediately after the magnet is removed. Several procedures may be used for subsequent final detection, such as conventional culturing, microscopy, impedance technology, ELISA, latex agglutination or DNA hybridization involving amplification techniques.

Beside the amazing properties of MPs, the main drawback of the biologically-modified MPs is their high cost and low stability. Molecularly Imprinted Polymers (MIPs) are synthetic biomimetic materials mimicking biological receptors(9,10). They are highly cross-linked macromolecular structures towards the template which is then extracted after polymerization, originating cavities (binding sites) complementary to the template molecule(11) and acting as plastic antibodies(12). Although MIPs have in general lower affinity and selectivity compared to the

biological counterparts, they show important technological features: i) they can be easily and affordably synthesized on a animal-free large scale procedures, and ii) they show high chemical and mechanical stability, allowing to work in harsh conditions (pH, temperature, solvents). Due to their wide range of applications, the synthesis of streptavidin-mimicking molecularly imprinted polymers has been previously reported by using different monomers and biotin as a template(13–15).

This paper described the synthesis of magneto-actuated molecularly imprinted polymers (magnetic-MIPs) using biotin as a template, as well as the separation of biotin and biotinylated biomolecules, and the downstream applications including detection with different readouts. The preparation of the magnetic-MIP is based on a core-shell synthesis in which the core was made of magnetite recovered by a shell of the MIP(16). In this instance, biotin was used as a template in order to separate and detects biotin and biotinylated biomolecules. This material showed the synergic advantages of MIPs and MPs, including low cost of production, stability and magnetic actuation. The characterization of the material was performed by SEM and TEM. The binding capacity towards biotin and biotinylated biomolecules including enzymes, dendrimers and DNA is demonstrated and compared with the corresponding magnetic-NIP (non-imprinted polymers), showing promising features for their integration in magneto-actuated approaches.

5.3. Experimental section

5.3.1 Instrumentation

The SEM images were taken with the scanning electron microscope EVO MA-10 (with EDS Detector, Oxford LINCA). The TEM images were taken with the transmission electron microscope JEM-2011 (with EDS Detector Oxford LINCA). The confocal fluorescence images were taken with the TCP-SP5 Leica Microscope. Optical measurements were performed on a TECAN Sunrise microplate reader with Magellan v4.0 software. The PCR reaction was carried out in a thermal cycler (Applied Biosystems, Life Technologies Corporation). Further description is provided in Supp data.

5.3.2 Chemicals and Biochemicals

The reagents for the synthesis of the magnetic particles based on biotin molecularly imprinted polymer (magnetic-MIP) and the corresponding NIP were purchased from Sigma Aldrich®, while 2,2'azobisisobutyronitrile (AIBN), from Fisher®. ELISA Substrate kit (Prod. Nº. 34021) was purchased from Thermo Scientific. The streptavidin labeled with cyanine 5 dye (Strep-Cy5) was purchased from Life Technologies (Prod No. SA-1011), while the fluorescent dye ATTO 665-biotin, from Sigma Aldrich (Prod No. 01376). The reagents for the magneto actuated immunoassay were biotin-HRP (Fisher Scientific, Prod. Nº 10324693) and antiDIG-HRP (anti-digoxigenin-POD Fab fragments, Roche Diagnostics, Prod. Nº 11207733910). All buffer solutions were prepared with milliQ water and all other reagents were in analytical reagent grade (supplied from Sigma and Merck). The composition of these solutions is described in Supp. Data, Table S5.1. The primers for the double-tagging PCR of *E. coli* were obtained from TIB-Molbiol GmbH (Berlin, Germany), and the sequences are detailed in Supp. Data, Table S5.2.

5.3.3 Synthesis of the magnetic molecularly imprinted polymer (magnetic-MIP) for biotin

The preparation of the magnetic-MIP (schematized in Figure S5.1) was based on a core-shell synthesis in which the core was made of magnetite recovered by a shell of the MIP using biotin as a template (17). The core-shell synthesis(18), with slight modifications is described in detail in Supp. data. (and Figures S5.1 to S5.4 therein). The magnetic-MIP and NIP were dried at 40º C under vacuum and conserved in room temperature until their use. For all the studies of binding, hydration of the MIP in aqueous solution was performed. First of all, a suspension of 17.6 mg magnetic-MIPs (and NIPs) in 3200 µL of TRIS buffer pH 7.4 was prepared achieving thus a concentration of 5.5 mg mL^{-1}. The suspension was stirred by vortexing for 3 min. The magnetic-MIP can be easily separated with the help of a magnet (as shown in Supp. data, Figure S5.5). Finally, the tube was stored at 4ºC at least for 24 h to achieve hydration of the material.

5.3.4 SEM and TEM study of the magnetic-MIP

The characterization of the products of the synthesis was performed by scanning electron microscopy (SEM) operated at 3 kV and transmission electron microscopy, (TEM) operated at 200kV. After each step of the core-shell synthesis, the product was collected and characterized by SEM and TEM, as detailed in Supp. Data. Energy dispersive X-ray spectroscopy detector (EDS) was also used for the elemental analysis.

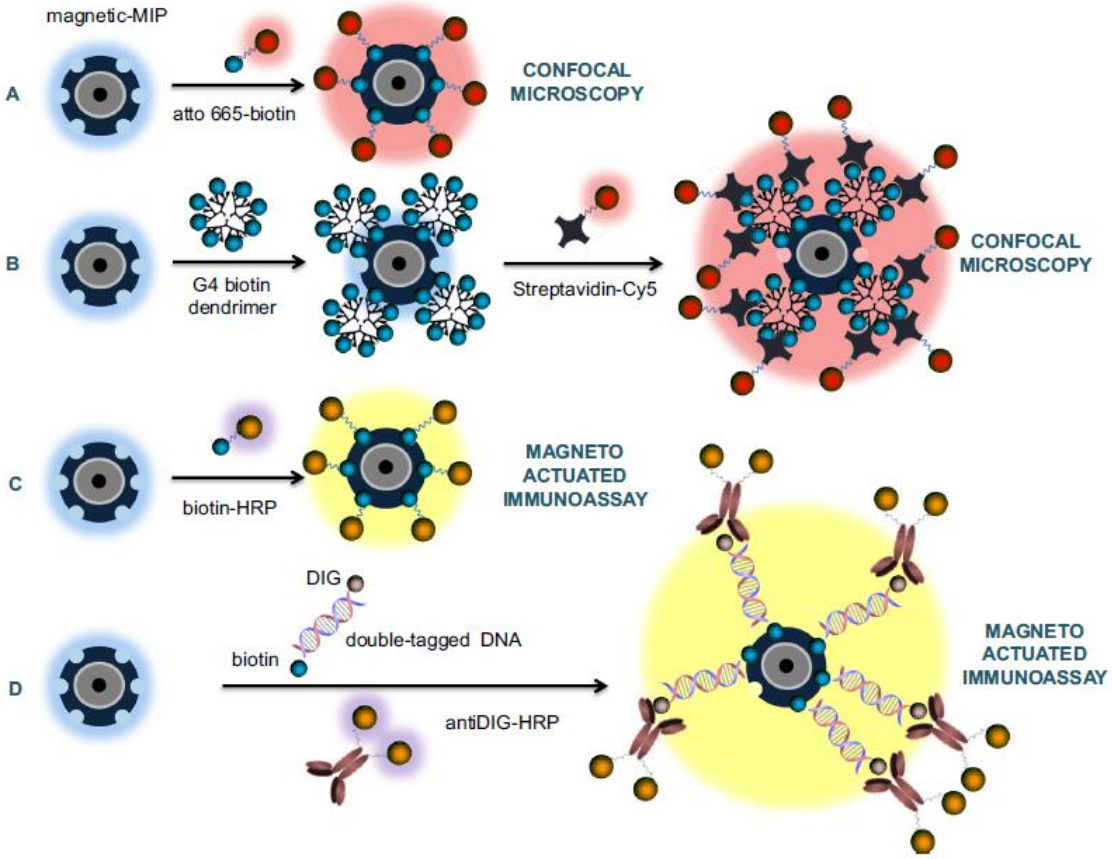

Figure 5.1. Schematic representation for the characterization of the binding of biotinylated biomolecules on the magnetic-MIP. (A) atto665-biotin; (B) G4biotin-dendrimer, followed by the incubation with streptavidin-Cy5. In(A)and(B), the characterization was performed by confocal microscopy. (C) biotin-HRP; (D) double-tagged DNA with biotin for the immobilization on the magnetic-MIP and with digoxigenin for the further reaction with antiDIG-HRP antibody. In (C) and (D), the optical readout was achieved upon the addition of the substrate for the HRP in a magneto-actuated immunoassay.

5.3.5 Characterization of the binding of biotinylated biomolecules by confocal microscopy

The evaluation of the binding of biotinylated biomolecules tagged with fluorophores (including atto 665-biotin and a G4 biotinilated dendrimer conjugated with streptavidin-Cy5) were performed by confocal microscopy, as schematically shown in Figure 5.1, panels A and B, respectively. In the first experiment, the magnetic-MIP was reacted with atto 665-biotin. To achieved this 0.2 mg of magnetic MIPs and 1 µL of biotin-Atto 665 (1 mg mL^{-1}) were incubated in 200 µL TRIS buffer pH 7.4 for 30 min with shaking at 37 ºC. A washing step was then performed for 5 min in TRIS buffer pH 7.4. The negative control was performed with the magnetic-MIP without the addition of the conjugate. Another experiment was performed by the incubation of the magnetic-MIP with a G4 biotinylated dendrimer (96 biotin molecules per molecule of dendrimer) followed by the incubation with streptavidin-Cy5. In this approach, 10 µL of biotinylated dendrimer (1 mg mL^{-1} in 2% DMSO) and 2 mg of magnetic-MIPs were incubated in 200 µL TRIS buffer pH 7.4 for 30 min with shaking at 37 ºC. The magnetic-MIP was separated from the supernatant with a magnet. After that, 200 µL of streptavidin-Cy5 (2 µg mL^{-1}) was added and the mixture was incubated again for 30 min at 37 ºC, followed by a washing step. The negative control was similarly performed but avoiding the addition of the biotinylated dendrimer. In both cases, the images were scanned in two dimensions along x and y axes by using the laser AOTF at a wavelength of 633 nm whereas the emission was captured in the range of 645 to 785 nm.

5.3.6 Characterization of the binding of biotin-HRP by a magneto-actuated immunoassay

The binding of biotinylated biomolecules tagged with HRP as optical reported (including biotin-HRP and double-tagged DNA conjugated with an antibody antiDIG-HRP) were evaluated by a magneto-actuated immunoassay, as schematically shown in Figure 5.1, panels C and D, respectively. The magneto-actuated immunoassay for biotin-HRP (Figure S5.6, Supp. data) was performed in 96-well microtiter plates and involved the following steps: (A) Incubation with

biotin-HRP conjugate. In this step, the magnetic-MIP (0.55 mg per well) was incubated with 100 µL of biotin-HRP (ranging from 0 to 100 ng mL^{-1}) in TRIS buffer pH 7.4 for 30 min with shaking at room temperature. (B) Washing step with 100 µL of TRIS buffer pH 7.4 for 5 min. (C) Optical readout with 100 µL of substrate solution (0.004 % v/v H_2O_2 and 0.01 % w/v TMB in citrate buffer) incubated for 30 min at RT under dark conditions. The enzymatic reaction was stopped by adding 100 µL of H_2SO_4 (2 mol L^{-1}). The absorbance measurement of the supernatants was thus performed with the microplate reader using a 450 nm filter. After each incubation or washing step, a 96-well magnet plate separator was positioned under the microtiter plate until pellet formation on the bottom corner, followed by supernatant separation.

As the pH and the buffer composition is an important parameter for the binding, beside TRIS buffer pH 7.4, different buffer composition and pH, summarized in Table S5.1, were tested, including citrate pH 6.4 and 7.4, phosphate pH 6.4 and 7.4, borate pH 7.4 and 8.4, and TRIS pH 7.4 and 8.4. The assay was performed by using the different buffers a similar manner as above, but by using 0.33 mg per well of the magnetic-MIP.

5.3.7 Characterization of the binding of double-tagged DNA from *E. coli* O157:H7 by a magneto-actuated immunoassay

The double-tagged DNA from *E. coli* O157:H7 was achieved by PCR performed with a double-tagging set of primers for the amplification of the *eaeA* (151 bp) gene fragment specific to *E. coli*(19), being each primer labeled in 5' with biotin (to achieve the immobilization on the magnetic-MIP) and digoxigenin (for the optical readout by using the optical reporter antiDIG-HRP), as schematically shown in Figure 5.1, panel D. The detailed conditions for the double-tagging PCR is presented in Supp. data and Figures therein, including the bacterial strain, growth condition and DNA extraction, safety considerations, the sequence of the tagging-primers (Table S5.2), and the procedure for the double-tagging PCR (Table S5.3 and Figure S5.7). The detection of the double-tagged DNA amplicon was performed in a magneto-actuated immunoassay (Figure S5.8, Supp. data.) in 96-well microtiter plates, involving the following steps: (A) One-step incubation with

double-tagged amplicon and AntiDigoxigenin-HRP conjugate.

In this step, the magnetic-MIP (0.55 mg per well) was incubated with 50 µL of amplicon (ranging from 0 to 206 ng mL^{-1}) and 1.35 µg of antiDIG-HRP in TRIS 0.05 % Tween buffer solution pH 7.4 for 30 min with shaking at room temperature. (B) A washing step with with 100 µL of TRIS buffer pH 7.4. (C) Optical readout as previously described for biotin-HRP.

5.3.8 Quantification of biotin based on a competitive magneto-actuated immunoassay

The quantification of biotin was performed by a competitive magneto-actuated immunoassay in two steps, as shown in Figure S5.21 (Supp. Data), in which biotin competes with biotin-HRP for the binding sites of the magnetic-MIP. The competitive magneto-actuated immunoassay for biotin was performed in 96-well microtiter plates and involved the following steps: (A) Incubation with biotin-HRP conjugate. In this step, the magnetic-MIP (0.55 mg per well) was incubated with 100 µL of biotin-HRP (100 ng mL^{-1}) in TRIS buffer pH 7.4 for 30 min with shaking at room temperature. (B) Washing step with 100 µL of TRIS buffer pH 7.4, for 5 min. (C) Competitive reaction with 100 µL of biotin, ranging from from 0.2 pg mL^{-1} to 1.9 ng mL^{-1} in TRIS buffer pH 7.4 for 30 min with shaking at room temperature, followed by a washing step as above. (D) Optical readout as previously described for biotin-HRP. Different competition formats were tested as detailed in Supp data, including a i) one-simultaneous competition step (30 min) (Figure S5.15); ii) one consecutive-competition step by the incubation of biotin (30 min) and biotin-HRP (30 min) (Figure S5.17); iii) one consecutive-competition step by the incubation of biotin-HRP (30 min) and biotin (30 min) (Figure S5.19).

5.4 Results and discussion

5.4.1 SEM and TEM study of the magnetic-MIP

The characterization of the products of the synthesis was performed by scanning electron microscopy (SEM) and transmission electron microscopy (TEM). After each step of the core-shell synthesis, the product was collected and submitted to SEM, TEM and elemental analysis. The results for each synthetic step are presented

in Supp. Data, Figure S5.9 for Fe_3O_4 , Figure S5.10 for Fe_3O_4@SiO_2, Figure S5.11 for Fe_3O_4@SiO_2-MPS, and finally, Figure S5.12 for the magnetic-MIP and NIP. Figure 5.2 shows comparatively the aspect of the magnetic-MIP (panel A) and the magnetic-NIP (panel B). As shown, during the polymerization of the MIP, the polymer includes many nanoparticles of magnetite in the structure, in agreement with the observed high magnetization of the material. It is important to highlight from the TEM images the different porosity pattern of the magnetic-MIP compared with the corresponding NIP. The porosity can be attributed to the cavities towards the biotin template which were achieved during the template extraction. Other characterization of the material was previously performed, including FTIR, magnetic hysteresis, XRD, SEM and N2-sorption measurements(18).

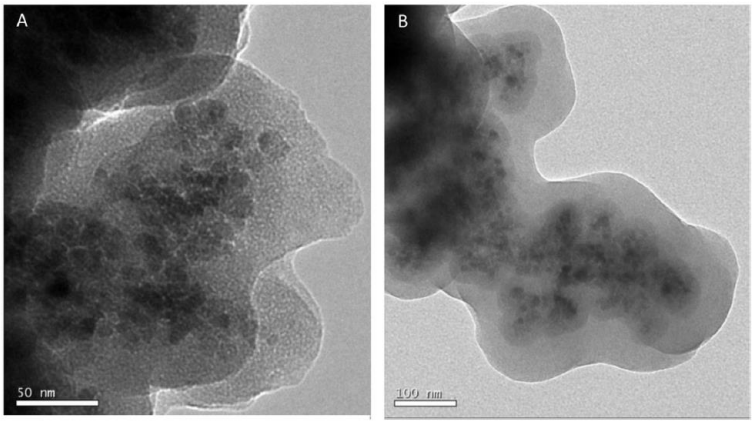

Figure 5.2. Comparatively study at high resolution of Magnetic MIP (A) and NIP (B) by TEM operated at 200kV.

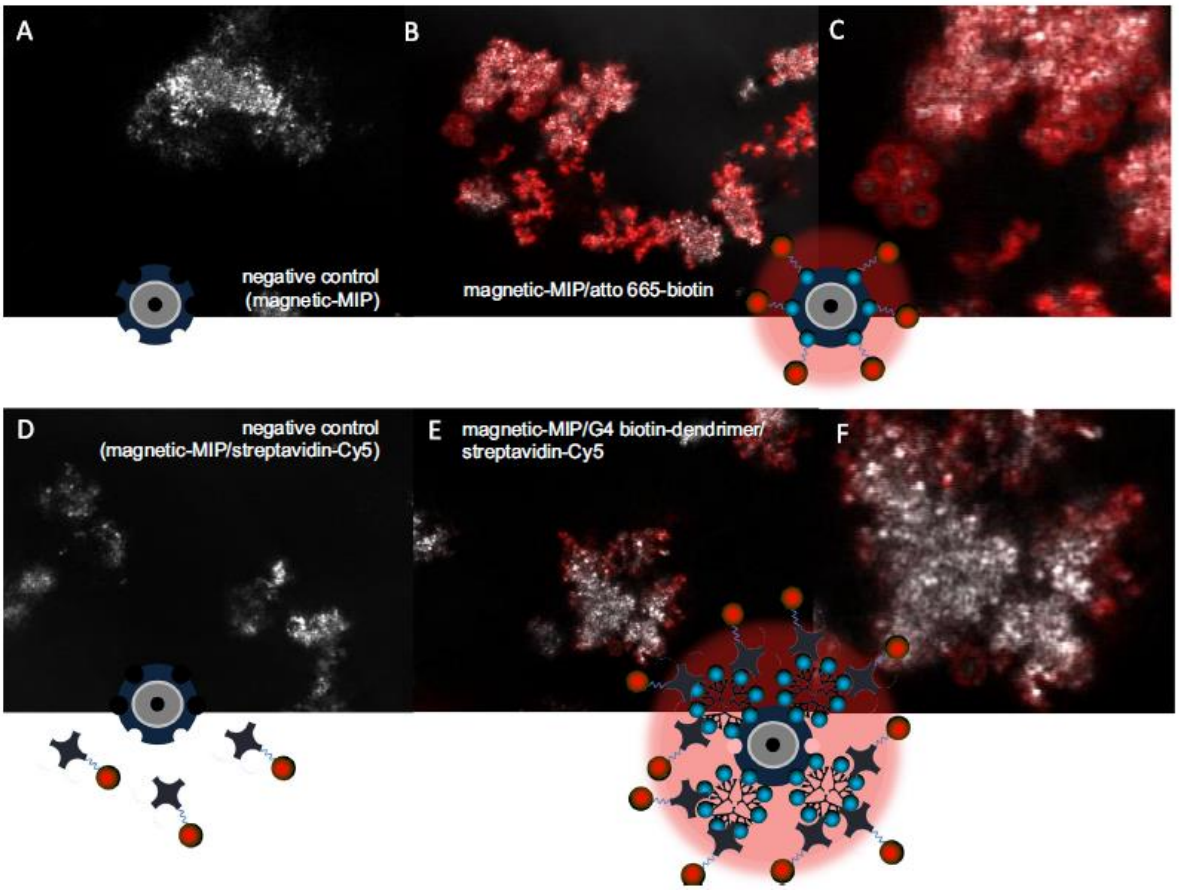

Figure 5.3. Characterization of the binding of biotinylated biomolecules on the magnetic-MIP by confocal microscopy. The binding on the magnetic-MIP of atto 665-biotin is shown in panels B and C, as well as the negative control (panel A). The binding of a G4 biotin dendrimer, followed by the incubation with streptavidin-Cy5 is shown in panels E and F, as well as the negative control (panel D).

5.4.2 Characterization of the binding of biotinylated biomolecules by confocal microscopy

The binding of biotinylated biomolecules of different molecular weights tagged with fluorophores (including atto 665-biotin and a G4 biotinilated dendrimer conjugated with streptavidin-Cy5) were studied by confocal microscopy, as schematically shown in Figure 5.1, panels A and B, respectively. In the first experiment (Figure 5.3, Panels B and C, as well as the negative control, panel A), the magnetic-MIP was attached with atto 665-biotin (M_w 1046 g mol^{-1}), a small molecule that can freely enters in the cavities of the magnetic-MIPs. This experiment suggests a high binding capacity of the magnetic-MIP towards the

biotinylated dye, since the material is completely embedded of dye.

The other experiment (Figure 5.3, Panels E and F, as well as the negative control, panel D) was performed by the incubation of the magnetic-MIP with a much bigger molecule, a G4 biotinylated dendrimer (M_w 69,406.98 g mol^{-1}), followed by the incubation with streptavidin-Cy5. In this instance, due to the size of the biotinylated-dendrimer, the binding pattern shows that the dendrimer cannot freely enters in the interior of the magnetic-MIP, since the fluorescence pattern is shown mainly in the external part of the polymer. From the negative control shown in panel D, which was similarly performed but avoiding the addition of the biotinylated dendrimer, it is important to highlight the specificity of the magnetic-MIP towards biotin, since no binding is observed when the magnetic-MIP is incubated only with the streptavidin-Cy5. The confocal study suggests that the binding capacity of the material depends on the size of the biotinylated molecule, since smaller molecules can easily enter in the structure of the magnetic-MIPs.

5.4.3 Characterization of the binding of biotin-HRP by a magneto-actuated immunoassay

The evaluation of the binding of biotinylated biomolecules tagged with HRP as optical reported was firstly performed with biotin-HRP (as schematically shown in Figure S5.6, Supp. Data), and the results are comparatively shown for the magnetic-MIP and NIP in Figure 5.4.

The results were fitted adjusted to a nonlinear regression (one site-binding/hyperbola, GraphPad Prism Software) (R^2=0.9575 and 0.8907 for the magnetic-MIP and NIP, respectively) for the separation and detection of biotin-HRP in one step from 6.125 to 100 ng mL^{-1}. As shown in Figure 5.4, the magnetic-MIP is able to attach a noticeable higher concentration of biotin-HRP compared with the magnetic-NIP, highlighting the specificity of the material. The one-site binding Equation [Y=Bmax X/(Kd+X)] used for fitting the data describes the binding of a ligand to a receptor that follows the law of mass action, being Bmax the absorbance at maximal binding, and Kd, the concentration of ligand required to reach half-maximal binding. After normalization of the results, the LOD was calculated as the 10 % of the maximal value, and was found to be 1.054 ng mL^{-1} (1.054 ppb) for

biotin-HRP. As it is a saturation binding experiment, in order to obtain the Kd^{app}, the data were transformed to molar concentration (as shown in Figure S5.13, Supp data), and the value was found to be Kd^{app} =2.32 10^{-9} mol L^{-1} (Ka = 4.3 10^{8} M^{-1}). The binding capacity of the material was calculated from the value of the Kd^{app}, and following the equation: Fractional occupancy = [biotin-HRP] /[biotin-HRP]+Kd Taking into account that the occupancy of the binding sites rises to 90% when the ligand concentration equals 9 times the Kd, and up to 99 % when the ligand concentration equals 99 times the Kd, the binding (90 %) was found to be 0.919 µg mL^{-1} (2.09 10^{-8} mol L^{-1}) while the binding (99 %) was 10.118 µg mL^{-1} (2.30 10^{-7} mol L^{-1}). As 0.55 mg of magnetic MIP was used per assay at a volume of 100 µL, the binding capacity (90 %) and (99%) of the magnetic-MIPs towards biotin-HRP was found to be 0.16 and 1.84 mg biotin-HRP/g of magnetic-MIPs, respectively.

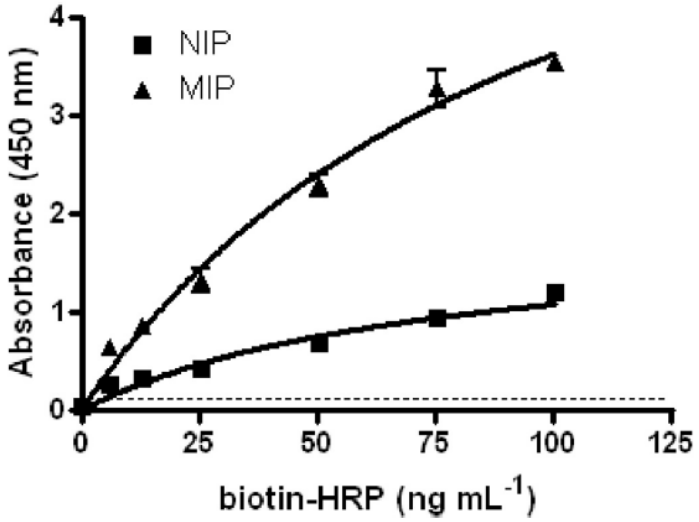

Figure 5.4. Characterization of the binding of biotin-HRP on the magnetic-MIP by magneto-actuated immunoassay in one step, in concentration range from 6.125 to 100 ng/mL of biotin-HRP and a fixed amount of 0.55 mg of magnetic-MIP. Error bar illustrates the standard deviation for the samples (n=3), using de magnetic-MIP (▲). The results obtained using non-imprinted polymers NIP (■) under analogous conditions are also shown.

Finally, as the pH and the buffer composition is an important parameter for the binding, beside TRIS buffer pH 7.4, different buffer composition and pH, summarized in Table S5.1, were tested, including citrate pH 6.4 and 7.4, phosphate pH 6.4 and 7.4, borate pH 7.4 and 8.4, and TRIS pH 7.4 and 8.4, as shown in Figure

S5.14, Supp. data. Although the non-specific binding of biotin-HRP on the magnetic-NIP was essentially the same under different pHs and composition of buffer, improved binding for biotin-HRP on the magnetic-MIP was achieved by using citrate and TRIS buffer over phosphate and borate, specially with TRIS pH 7.4, which was used in all the experiments performed in this work.

5.4.4 Characterization of the binding of double-tagged DNA from *E. coli* O157:H7 by a magneto-actuated immunoassay

The characterization of a double-tagged DNA amplicon from *E. coli* O157:H7 obtained by double-tagging PCR(20) was also performed by a magneto-actuated immunoassay, as schematically shown in Figure S5.8. During PCR, the amplicon was double-tagged with biotin for binding with the magnetic-MIP and digoxigenin to achieve the optical readout based on antiDigoxigenin-HRP. The magneto-actuated immunoassay was performed in a one incubation step of the double-tagged amplicon, the antiDigoxigenin-HRP and the magnetic-MIP, and results are comparatively shown for the magnetic-MIP and NIP in Figure 5.5.

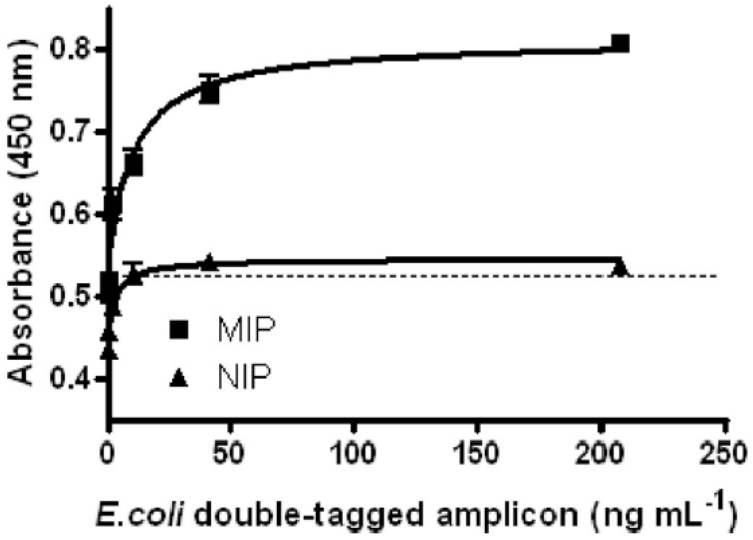

Figure 5.5. Characterization of the binding of the double-tagged DNA from *E. coli* O157:H7 obtained by PCR and a double-tagging set of primers for the amplification of the eaeA (151 bp) gene fragment, on the magnetic-MIP by magneto-actuated immunoassay in one step, in concentration range from 0 to 206.8 ng mL^{-1} and a fixed amount of 0.55 mg of magnetic-MIP and 1.35 µg of antiDIG-HRP. Error bar illustrates the standard deviation for the samples (n=3), using de magnetic-MIP (▲). The results obtained using non-imprinted polymers NIP (■) under analogous conditions are also shown.

The results were fitted to a nonlinear regression (two site-binding/hyperbola, GraphPad Prism Software) for the separation and detection of double-tagged amplicon in one step (30 min) from 0 to 206.8 ng mL^{-1}. As shown in Figure 5.5, the magnetic-MIP is able to attach a noticeable higher concentration of double-tagged amplicon compared with the magnetic-NIP, highlighting the specificity of the material. Moreover, the nonspecific binding of antidigoxigenin-HRP antibody was also extremely low. For this system, the LOD was estimated by processing the negative control samples (n=3), containing all the components except the double-tagged amplicon, obtaining a mean value of 0.504 AU with a SD of 0.006_6. The cut-off values were then determined with a one-tailed t test at a 95% confidence level, giving a value of 0.523 AU (shown in Figure 5.5, as the dotted lines). The LOD was found to be 1.28 ng mL^{-1}, much lower than the values for a similar system for *E. coli* O157:H7 amplicon in silica magnetic particles recently reported for our group (27 ng mL^{-1}) (20).

5.4.5 Quantification of biotin based on a competitive magneto-actuated immunoassay

The quantification of biotin was performed by a competitive magneto-actuated immunoassay. Firstly, different competition formats were tested as detailed in Supp data, including a i) one-simultaneous competition step (30 min) (Figure S5.15); ii) one consecutive-competition step by the incubation of biotin (30 min) and biotin-HRP (30 min) (Figure S5.17); iii) one consecutive-competition step by the incubation of biotin-HRP (30 min) and biotin (30 min) (Figure S5.19). The results are respectively shown in Supp. Data for i) (Figure S5.16), ii) (Figure S5.18) and iii) (Figure S5.20). None of the format showed a real competition, except for the iii) one consecutive-competition step by the incubation of biotin-HRP (30 min) and biotin (30 min) at low concentration range. That's why in order to favor the competition, a washing step was included in betweens, in a two-competition step format (Figure S5.21), in which the magnetic-MIP was firstly incubated with biotin-HRP for 30 min, followed by washing and by a second incubation with biotin ranging from 0 to 1.90 ng mL^{-1} for 30 min. The raw data is shown in Figure S5.22 (Supp data), in which a competition results was clearly obtained. In this experiment only one replicate was rejected among 56 replicates,

showing an outstanding reproducibility. The results were normalized to obtain the main parameters of competition (including IC50 and LOD) and the standard curve was fitted (R^2 = 0.9782) to a four-parameter logistic equation according to $y=\{(A-B)/[1 + 10 \exp((\log C-\log X)\times D)]\}+ B$, where A is the maximal absorbance, B is the minimum absorbance, C is the concentration producing 50% of the maximal absorbance, X is the biotin concentration and D is the slope at the inflection point of the sigmoid curve. The results are shown in Figure 5.6.

The LOD value was obtained as 90% of A value, being as low as 0.857 pg mL^{-1} (0.857 ppt). The LOQ was also calculated being 2.352 pg mL^{-1}, and the dynamic range was found to be from 2.352 pg mL^{-1} to 0.330 ng mL^{-1}. The IC50 was found to be as low as 0.017 ng mL^{-1}. The LOD was much lower than those previously obtained (20 ng mL^{-1}) with a similar system but by using streptavidin magnetic particles(21).

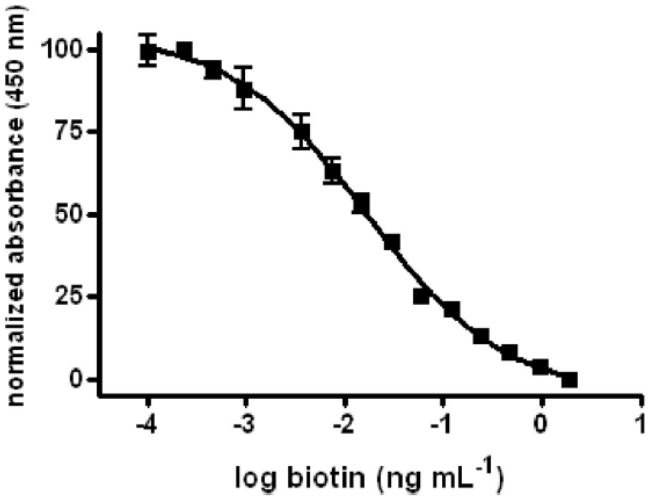

Figure 5.6. Fitted curve adjusted to a nonlinear regression (Sigmoidal dose-response with variable slope) of the raw data for the competition assay in two steps (as schematically shown in Figure S5.21), performed by the incubation of the magnetic-MIP (0.55 mg per well) with 100 µL of biotin-HRP (100 ng mL-1) for 30 min, followed by washing and a second incubation with biotin ranging from 0 pg/mL to 1.90 ng mL-1 for 30 min, under shaking in TRIS buffer pH 7.4 at room temperature. Error bar illustrates the standard deviation for the samples (n=4). Only one replicate was rejected among 56 replicates.

5.5. Conclusions

This work addresses the synthesis and characterization of a hybrid molecularly-imprinted polymer towards biotin (and biotinylated biomolecules) with magnetic properties, as an alternative for the well-known streptavidin magnetic particles. The main advantages of this material is, beside the magnetic properties, the possibility to be stored at room temperature without loss of the activity. It should be also highlighted that the cost of synthesis at laboratory scale is almost 300 times lower than the price of the streptavidin-MPs from a commercial source. Moreover, it is demonstrated that can be coupled with different readouts system, including fluorescence measurements. It should be pointed-out that the fluorescence readout cannot be easily performed with commercial streptavidin magnetic particles, since, as they are recovered in most of the cases with polystyrene, they provide a broad fluorescence spectra, overlapping the signal of fluorescence tags(22). The material is also compatible with magneto ELISA-like procedures using enzymatic activity and optical readout. When coupled in a magneto-ELISA-like procedure for the detection of an amplicon coming from PCR, the LOD was found to be 1.28 ng mL^{-1}. Impressive LODs (0.857 pg mL^{-1}) and reproducibility were also achieved for the detection of biotin in a competitive-like format. Although the affinity is lower than for the natural system biotin-strept(avidin) (Kd =10^{-14} mol/L), it shows a good affinity towards biotinylated biomolecules, such as biotin-HRP (Kd= 2.32 10^{-9} mol L^{-1}) and high binding capacity of 0.16 (90 %) and 1.84 (99%) mg biotin-HRP/g of magnetic-MIPs, respectively. Further work will be focused on other downstream applications of the material as well as biocompatibility studies.

5.6. Acknowledgments

Ministerio de Economía y Competitividad (MINECO), Madrid (BIO2013-41242-R) and National Council for Scientific and Technological Development (CNPq) Brazil (Processes 4004759/2012-4, 303979/2012-7 and 151525/2013-7) are acknowledged

5.8. Supporting information

5.7.1. Buffers and solutions

All buffer solutions were prepared with milli-Q water and all other reagents were in analytical reagent grade (supplied from Sigma and Merck). The composition of these solutions is summarized in Table S5.1.

Table S5.1. Composition of the buffers

Buffer	pH	Composition
Citrate	6.4	0.04 M of citrate, 0.15 M NaCl, 0.05 % Tween
Citrate	7.4	0.04 M of citrate, 0.15 M NaCl, 0.05 % Tween
PBS	6.4	0.1 M Na_2HPO_4 , 0.15 M NaCl, 0.05 % Tween
PBS	7.4	0.1 M Na_2HPO_4 , 0.15 M NaCl, 0.05 % Tween
Borate	7.4	0.1 M H_3BO_3 , 0.15 M NaCl, 0.05 % Tween
Borate	8.4	0.1 M H_3BO_3 , 0.15 M NaCl, 0.05 % Tween
TRIS	7.4	0.1 M TRIS, 0.15 M NaCl, 0.05 % Tween
TRIS	8.4	0.1 M TRIS, 0.15 M NaCl, 0.05 % Tween

5.7.2. Instrumentation

The SEM images were taken with the scanning electron microscope EVO MA-10 (resolution: 3 nm at 30kV; acceleration voltage: from 0.2 to 30 kV; EDS Detector Oxford LINCA). E5000 Sputter Coater Polaron Equipment Limited metallizer and K850 Critical Point Drier Emitech (Ashford, UK) were used for sample treatment. The TEM images were taken with the transmission electron microscope JEM-2011 (Resolution: 0.18 nm at 200 kV; acceleration voltage: 80 - 200 kV; EDS Detector Oxford LINCA). The confocal fluorescence images were taken with the TCP-SP5 Leica Microscope, being the images processed with the Imaris X64 v.6.2.0 software (Bitplane, Switzerland). Optical measurements were performed on a TECAN Sunrise microplate reader with Magellan v4.0 software. The data were analyzed using the Graph Prism software (GraphPad Software, San Diego, CA). Polystyrene microtiter plates were purchased from Nunc (Maxisorb, Roskilde, DK). The PCR reaction was carried out in a thermal cycler (Product Nº 2720, Applied Biosystems, Life Technologies Corporation). All the incubations and washing steps were performed on microtiter plates under shaking conditions using a Minishaker

MS1 (IKA, Germany). Temperature-controlled incubations with Eppendorf tubes were performed in an Eppendorf Thermomixer compact. Magnetic separation during the washing steps was performed using a magnetic separator Dynal MPC-S (Product Nº 120.20D, Dynal Biotech ASA, Norway).

5.7.3. Synthesis of the magnetic MIPs and NIPs

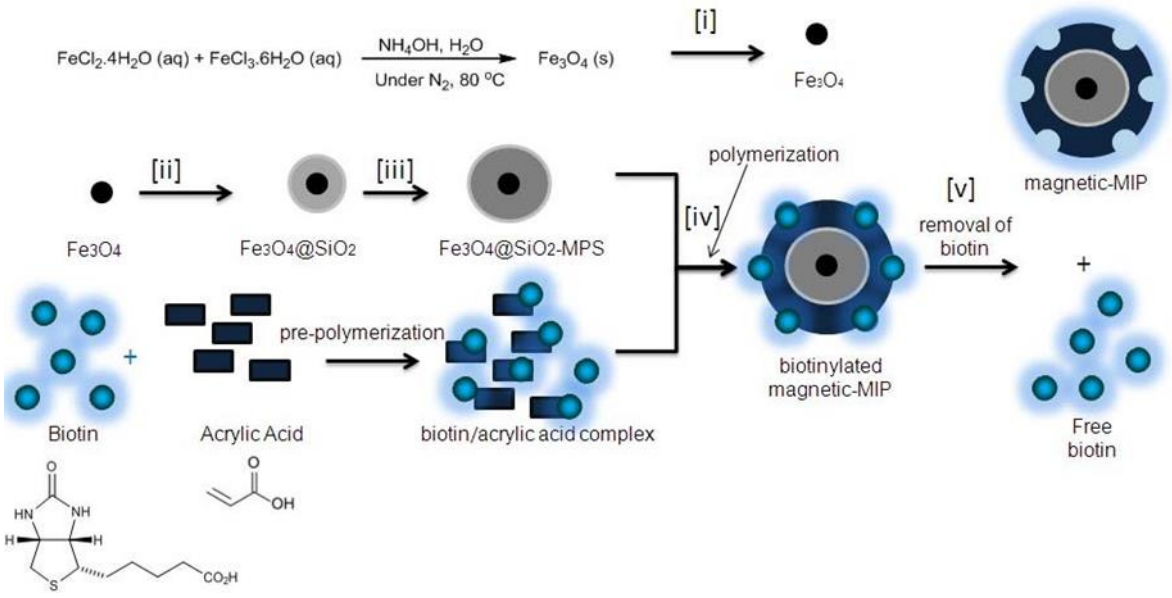

Figure S5.1. Schematic representation for the synthesis of the magnetic particles based on biotin molecularly imprinted polymer (magnetic-MIP).

5.7.4. Synthesis of magnetite nanoparticles

The preparation of Fe_3O_4 was performed by co-precipitation of a Fe^{2+}/Fe^{3+} mixed solution prepared from iron salts (as shown in Figure S5.2, panel A) by dissolving 3.44 g of $FeCl_2.4H_2O$ and 9.44 g of $FeCl_3.6H_2O$ in 160 mL of water under nitrogen with vigorous magnetic stirring and heating by controlling the pH with a pH-meter. When the solution reached 70-80ºC, 60 mL of NH_4OH were added drop by drop using a 25 mL burette for 30-45 min to achieve a pH 9-10 (25). The black precipitate was then separated with a magnet followed by gently washing with water. The obtained product is dried at 50ºC for 24 h and collected for SEM and TEM analysis.

5.7.5. Synthesis of Fe_3O_4@SiO_2 particles

The Fe_3O_4 nanoparticles were modified with tetraethoxy silane (TEOS), also named tetraethyl orthosilicate, (as shown in Figure S5.2, panel B) to achieve an amorphous layer of SiO_2 with OH groups for further reactions (26). 600 mg of Fe_3O_4 nanoparticles were dispersed in 80 mL of ethanol and 8 mL ultrapure water under ultrasonication for 15 min in a round bottom flask of 250 mL. After that, 10 mL of NH_4OH and 4 mL of TEOS were added. The mixture was reacted for 12 h at room temperature with mechanically stirring. The product was separated again with a magnet and washed with water. After that the product was dried at 50 ºC for 24 h and collected for SEM and TEM analysis.

(A)

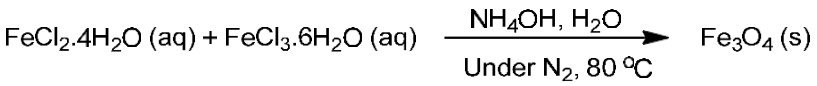

(B)

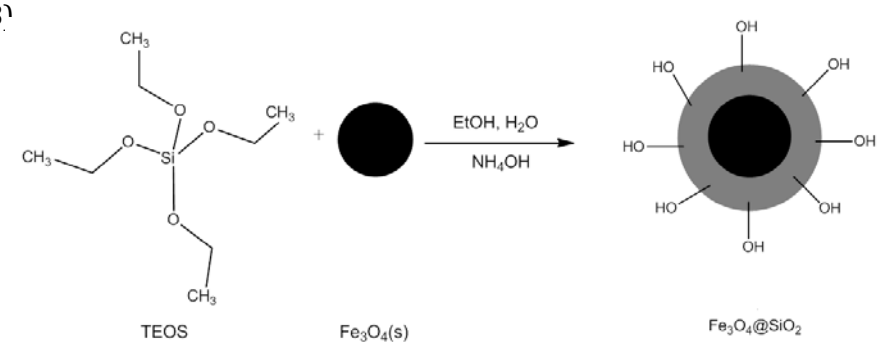

Figure S5.2. Synthesis of magnetite (A) and Fe_3O_4@SiO_2 nanoparticles (B).

5.7.6. Synthesis of Fe_3O_4@SiO_2-MPS MPs

The following step is the reaction of the hydroxyl modified MPs prepared in the previous step (Fe_3O_4@SiO_2), with acrylic group containing silanizating agent, such as 3-methacryloxypropyltrimethyloxysilane (MPS), as schematically shown in Figure 3, to provide activated C=C groups for further copolymerization in the following step. 500 mg of the Fe_3O_4@SiO_2 were dispersed in 100 mL of anhydrous toluene and 10 mL of MPS in a three neck round bottom flask (Figure S5.3). The mixture was allowed to react for 12 h under nitrogen. The product was separated again with a magnet and gently washed with water. Then the product is dried at 50ºC for 24 h, and collected for SEM and TEM analysis.

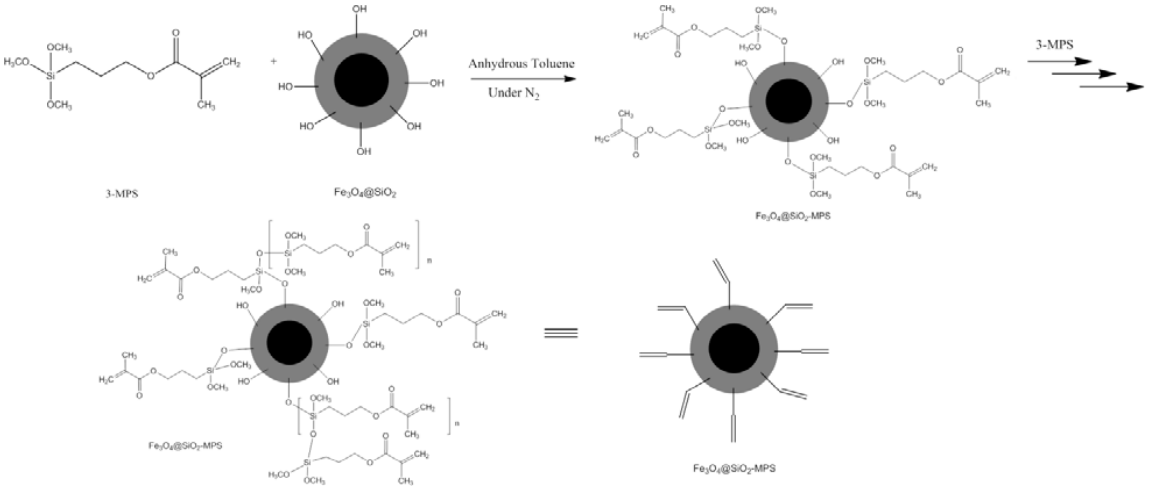

Figure S5.3. Synthesis of Fe_3O_4@SiO_2-MPS

5.7.7. Prepolymerization of the template biotin

Previous to the synthesis of the magnetic-MIP with affinity towards biotin, a pre-polymerization step of biotin (0.2 mmol) and the monomer acrylic acid (0.8 mmol) is required as is schematically shown in Figure S5.4. The reagents were dissolved in 30 mL of ethanol under magnetic stirring for 12 h at 25ºC. The solution was covered to avoid the evaporation of the solvent. Similarly, the NIPs were prepared without the presence of the template biotin. During this step, non-covalent weak interactions between the template and the monomer, mainly hydrogen bonds, electrostatic and hydrophobic interactions are formed maintaining a complex between biotin and acrylic acid, as schematized in Figure S5.4.

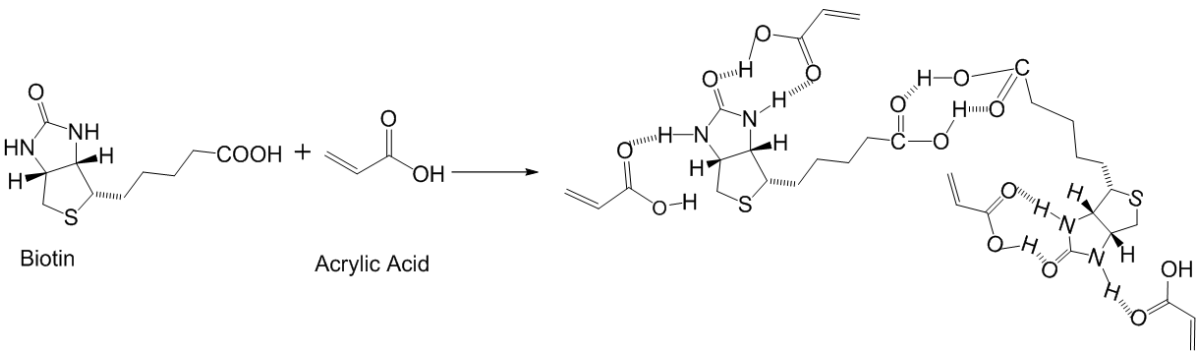

Figure S5.4. Pre-polymerization step between the monomer and the template, showing the weak interactions established between acrylic acid and biotin.

5.7.8. Polymerization

During this step, the silanized MPs containing the functional monomer (acrylic acid), in the presence of the pre-polymerized template biotin, a crosslinking monomer, (ethylene glycol dimetacrilate, EGDMA), a radical initiator, (AIBN) were polymerized in a porogenic solvent. The pre-polymerization mixture was transferred to a round ball. After that, 200 mg of Fe_3O_4.SiO2-MPS were added and allowed to react under mechanical stirring for 3 h. 4.0 mmol of EGDMA and 0.05 mmoL of AIBN were added and the mixture was treated with ultrasounds in a water bath for 5 minutes, under N_2. The reaction was kept at 60ºC under nitrogen gas for 7 h.

5.7.9. Washing steps and biotin removal

The biotin extraction was done using a Soxhlet extraction and methanol:acetic acid 9:1 as extracting solvent. The solution was changed every 12 hours during three days to ensure the complete removal of biotin. The magnetic-NIP was treated in the same way.

5.7.10. Preparation of magnetic-MIP suspension

The magnetic-MIP and NIP were dried at 40º C under vacuum and conserved in room temperature until their use. For all the studies of binding, hydration of the MIP in aqueous solution was performed. First of all, a suspension of 17.6 mg magnetic-MIPs (and NIPs) in 3200 µL of TRIS buffer pH 7.4 was prepared achieving thus a concentration of 5.5 mg mL-1. The suspension was stirred for 3 min. The magnetic-MIP can be easily separated with the help of a magnet (as shown in Supp. data, Figure S5.5). Finally, the tube was stored at 4ºC at least for 24 h to achieve hydration of the material.

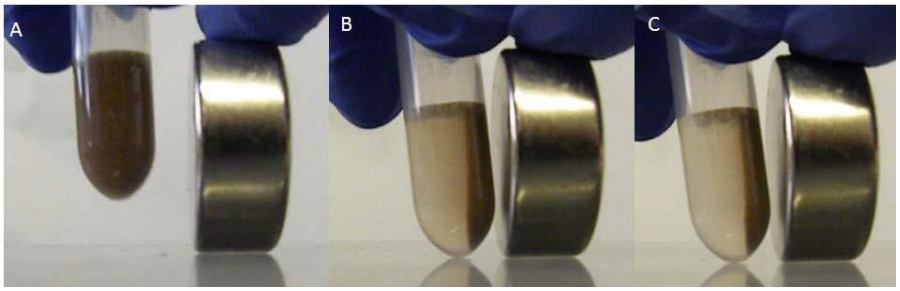

Figure S5.5. Magnetic actuation of the magnetic-MIP in TRIS buffer at t=0 (panel A), after 5 seconds (panel B) and after 30 seconds (Panel C).

5.7.11. Characterization of the binding of biotin-HRP by a magneto-actuated immunoassay

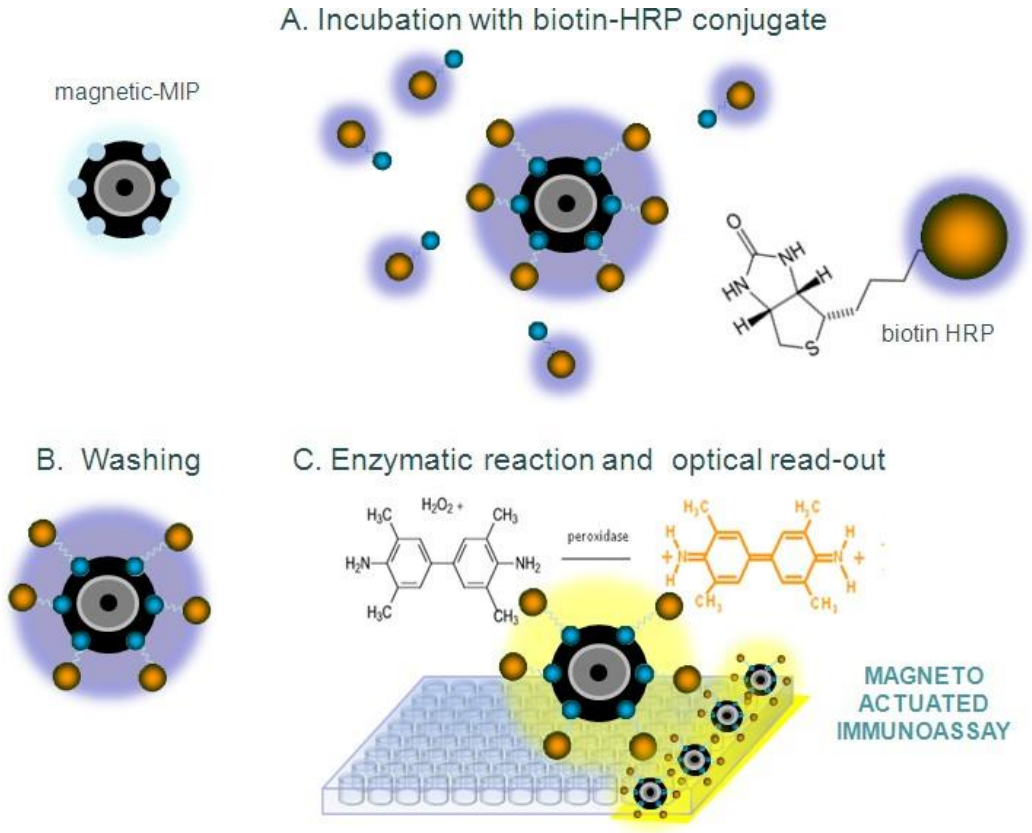

Figure S5.6. Schematic procedure for the magneto-actuated immunoassay based on magnetic-MIP for the detection of biotin-HRP.

5.7.12. Characterization of the binding of double-tagged DNA from *E. coli O157:H7* by a magneto-actuated immunoassay

5.7.12.1. Bacterial strain, growth condition and DNA extraction

The *E. coli* O157:H7 (clinical isolate supplied by Hospital of Bellvitge, Barcelona, Spain) was grown in Luria Bertani (LB) broth or agar plates for 18 h at 37 ºC. The lysis of the bacteria, DNA extraction and purification was performed according to the kit manufacturer (DNeasy Tissue and Blood Kit, Qiagen). The extraction and purification efficacy was evaluated by spectrophotometric analysis as UV absorption at 260 nm.

5.7.12.2. Safety considerations

All the procedures involved the manipulation of human cells were handled using Biosafety Level 2 Laboratory (BSL-2) and containment. All works were performed in a Biosafety cabinet, and all material decontaminated by autoclaving or disinfected before discarding in accordance with U.S. Department of Health and Human Services guidelines for level 2 laboratory Biosafety.

5.7.12.3. Sequence of the tagging-primers

The primers for the double-tagging PCR of *E. coli* were selected for the amplification of *eaeA* (151 bp) gene fragments specific to *E. coli* (27). The oligonucleotides were respectively tagged in 5' end with biotin (for the binding with the magnetic-MIP) and digoxigenin, for the optical readout using and antiDIG-HRP optical reporter. The primer sequences, as well as the tags used for the double-tagging PCR are shown in Table S5.2.

Table S5.2. Triple-tagging set of primers for the PCR amplification of *E.coli O157:H7*.

STRAIN	GENE	PRIMER SEQUENCE (5'-3')	TYPE	5'-LABELS	SIZE (bp)
E. coli	*eae*A	GGCGGATAAGACTTCGGCTA	Forward	Digoxigenin	151
		CGTTTTGGCACTATTTGCCC	Reverse	Biotin	

5.7.12.4. Double-tagging PCR

The PCR reaction was carried out in a thermal cycler (Product Nº 2720, Applied Biosystems, Life Technologies Corporation). The detailed conditions for the double tagging PCR is presented in Table S5.3 and schematically shown in Figure S5.6.

Table S5.3 Thermal cycler conditions for the double-tagging PCR

	Initial step	**DNA denaturation**	**Annealing**	**Extension**	**Last step**
	1 cycle	40 cycles			1 cycle
Temperature (°C)	95	95	60	72	72
Time (sec)	600	20	30	30	420

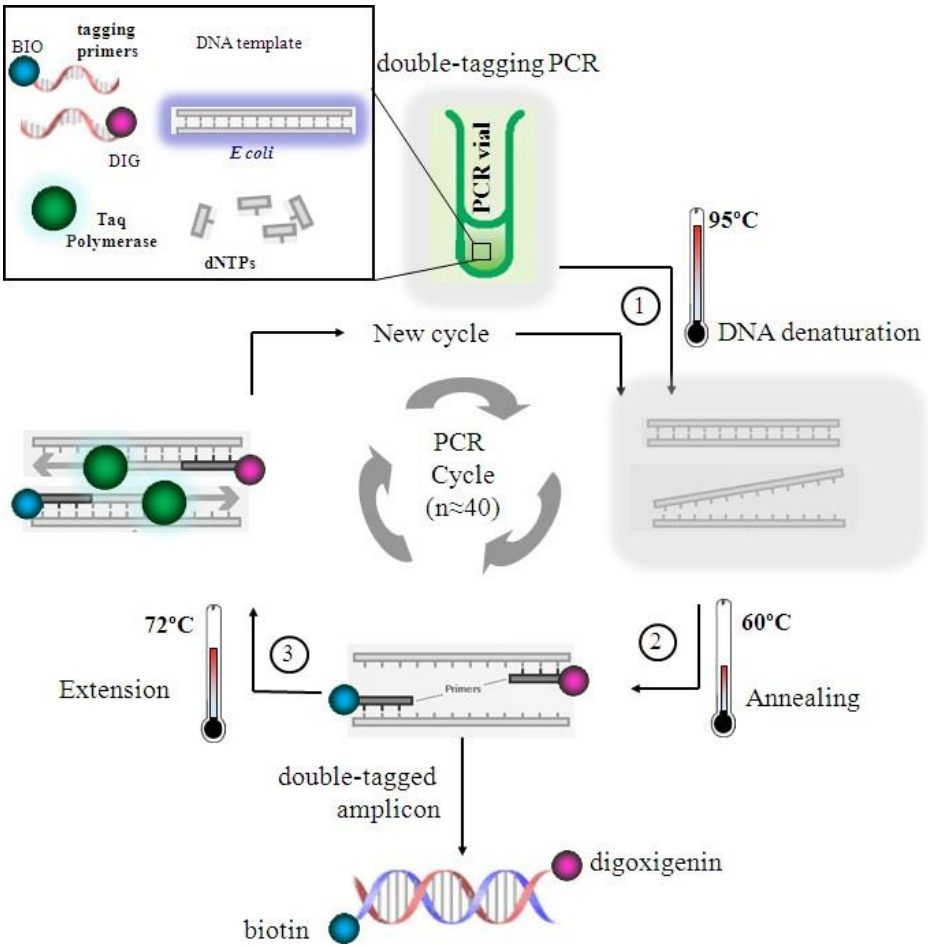

Figure S5.7. Schematic representation of the double-tagging PCR amplification, in order to obtain the double-tagged amplicon labelled with biotin and digoxigenin from *E. coli* chromosomal DNA.

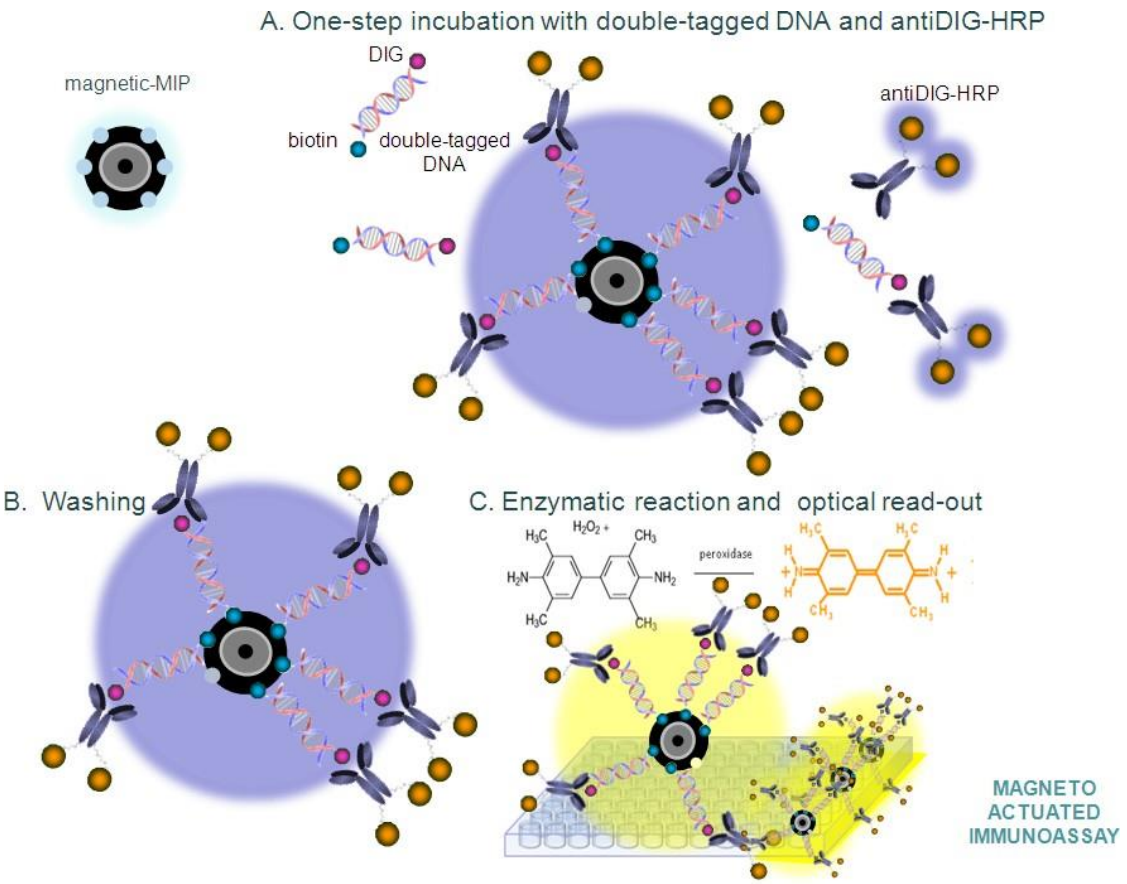

Figure S5.8. Schematic procedure for the magneto-actuated immunoassay based on magnetic-MIP for the detection of double-tagged DNA.

5.7.13. Results and discussion

5.7.13.1. *SEM and TEM study of the magnetic-MIP*

The characterization of the products of the synthesis was performed by scanning electron microscopy (SEM) operated at 3 kV and transmission electron microscopy, (TEM) operated at 200kV. After each step of the core-shell synthesis, the product was collected and characterized by SEM and TEM. Aluminum stubs were used as a support for SEM. A conductive carbon-tape was then printed in the surface. A small amount of sample was sprinkled into the surface. Then, the conductive carbon-tapes were metalized by an Au-Pd alloy (80:20) during 4 min adding a layer of approximately 15 to 20 nm on the sample. For TEM, 2 mg of the sample was suspended in 1 mL of ethanol. Then, the samples were sonicated for 2 min. One drop of each sample was sprinkled in a Cu-grid. Energy dispersive X-ray spectroscopy detector (EDS) was also used for the elemental analysis.

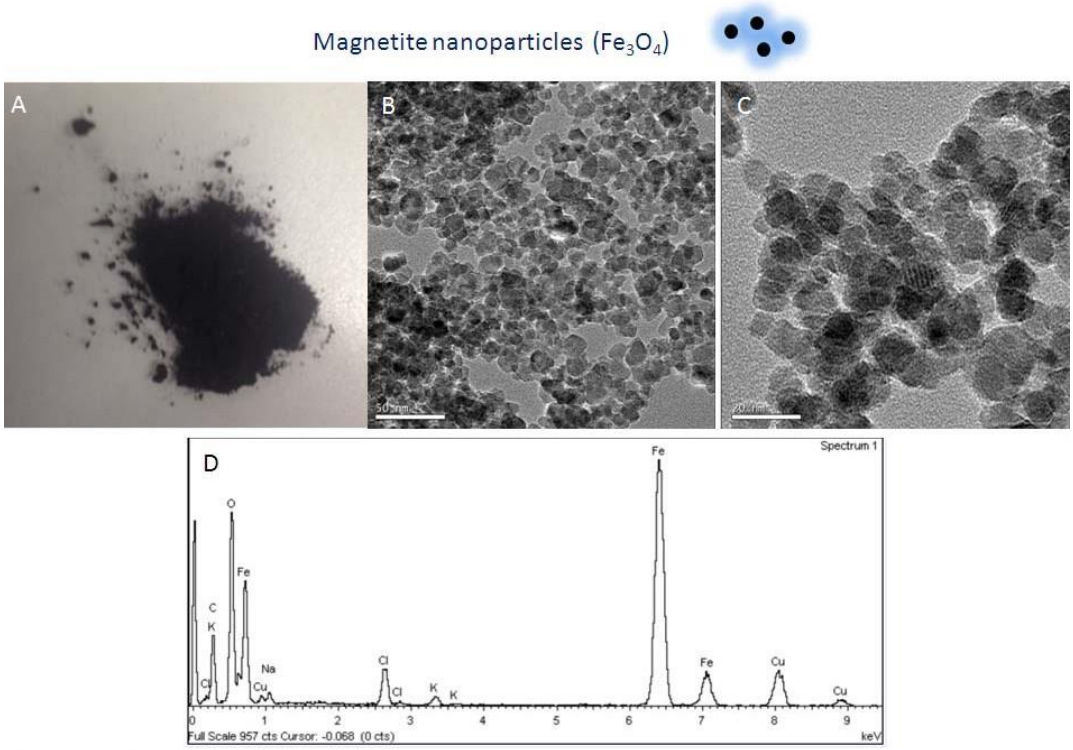

Figure S5.9. Study of magnetite particles (Fe_3O_4). (A) macroscopic aspect; (B and C) TEM at different resolution levels; (D) Elemental analysis

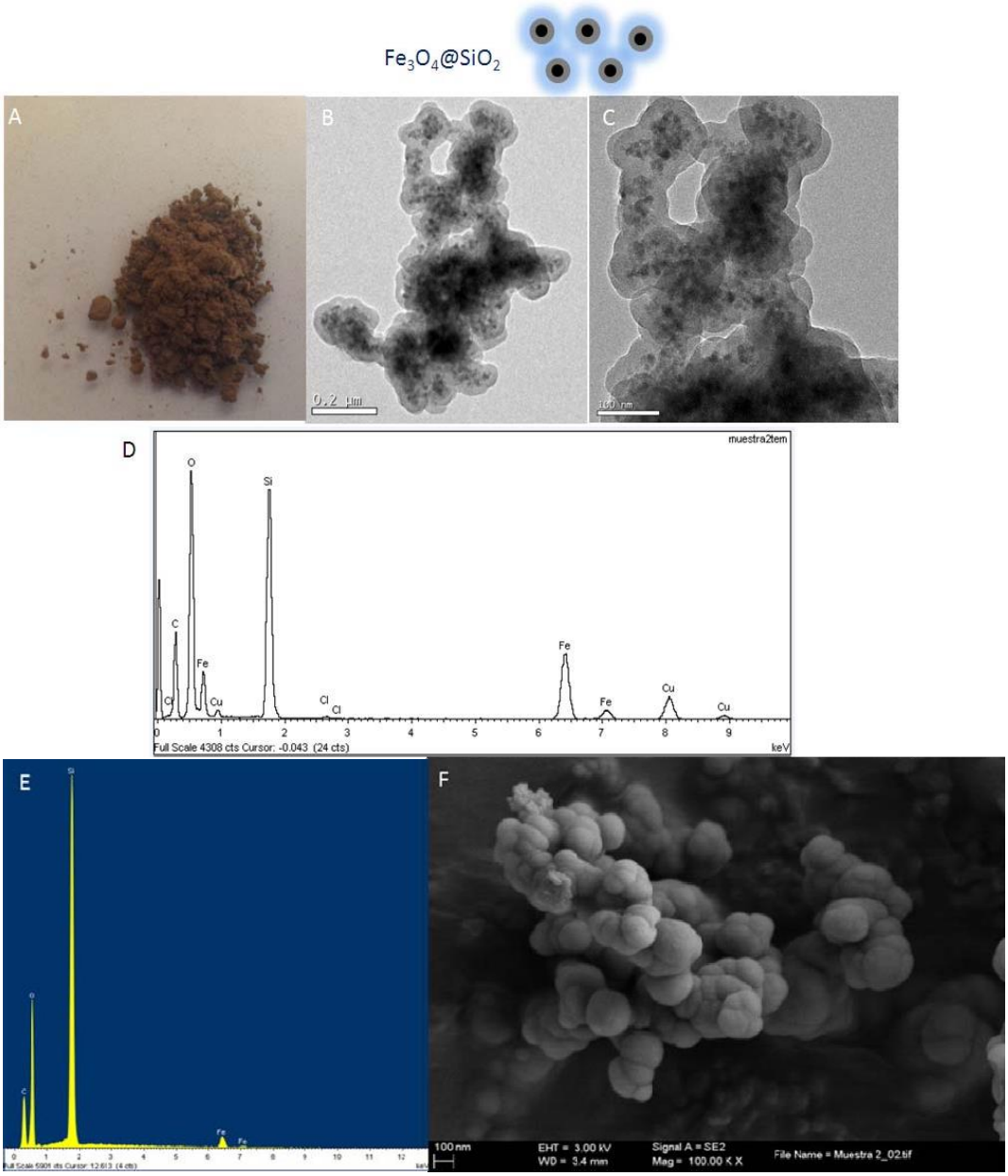

Figure S5.10. Study of Fe_3O_4@SiO_2 magnetic particles (A) macroscopic aspect; (B and C) TEM images at different resolution levels and (D) the corresponding elemental analysis; (E) Elemental analysis and (F) SEM image.

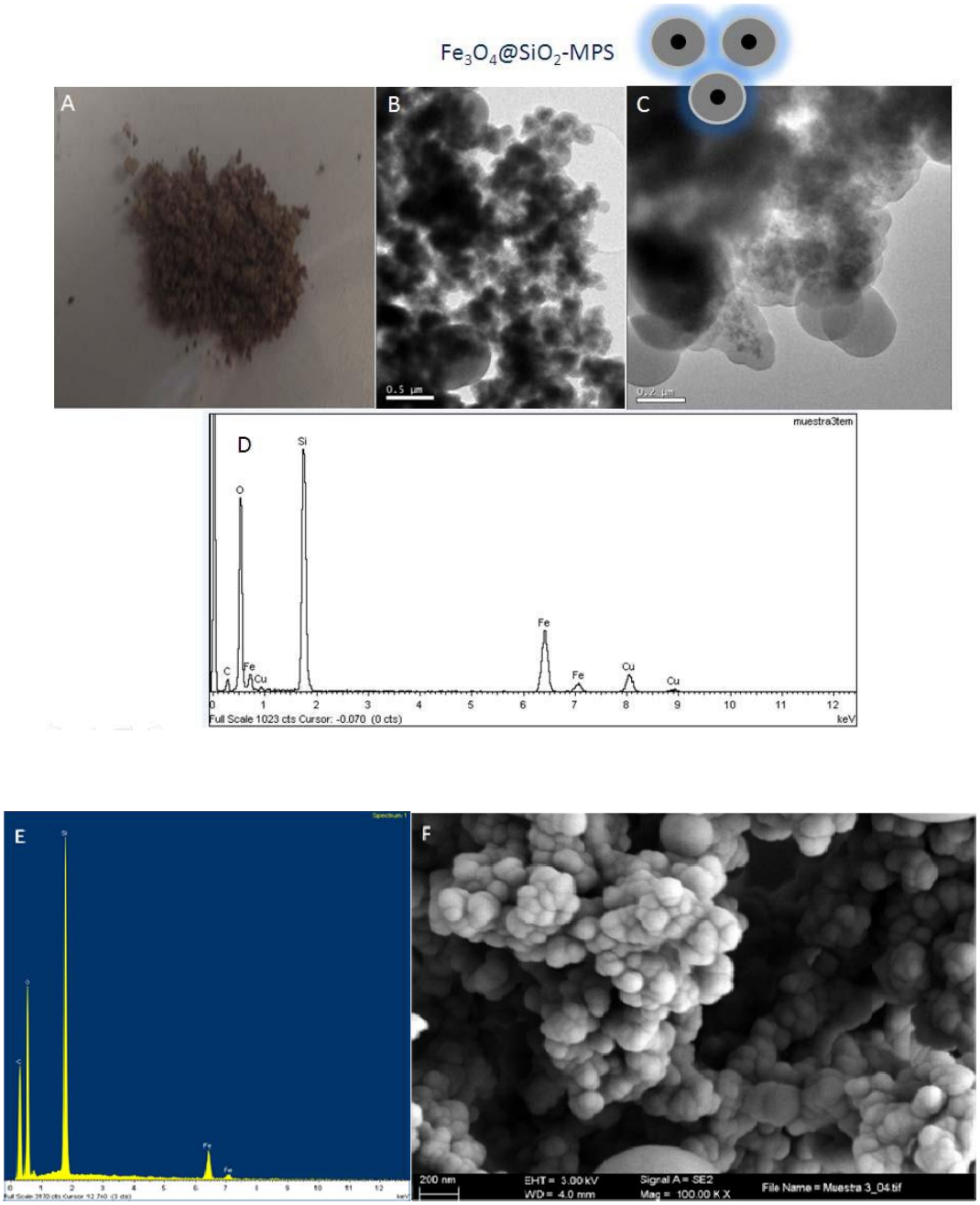

Figure S5.11. Study of Fe_3O_4@SiO_2-MPS nanoparticles (A) macroscopic aspect; (B and C) TEM images at different resolution levels and (D) the corresponding elemental analysis; (E) Histograms; (F) Elemental analysis and (G) SEM image.

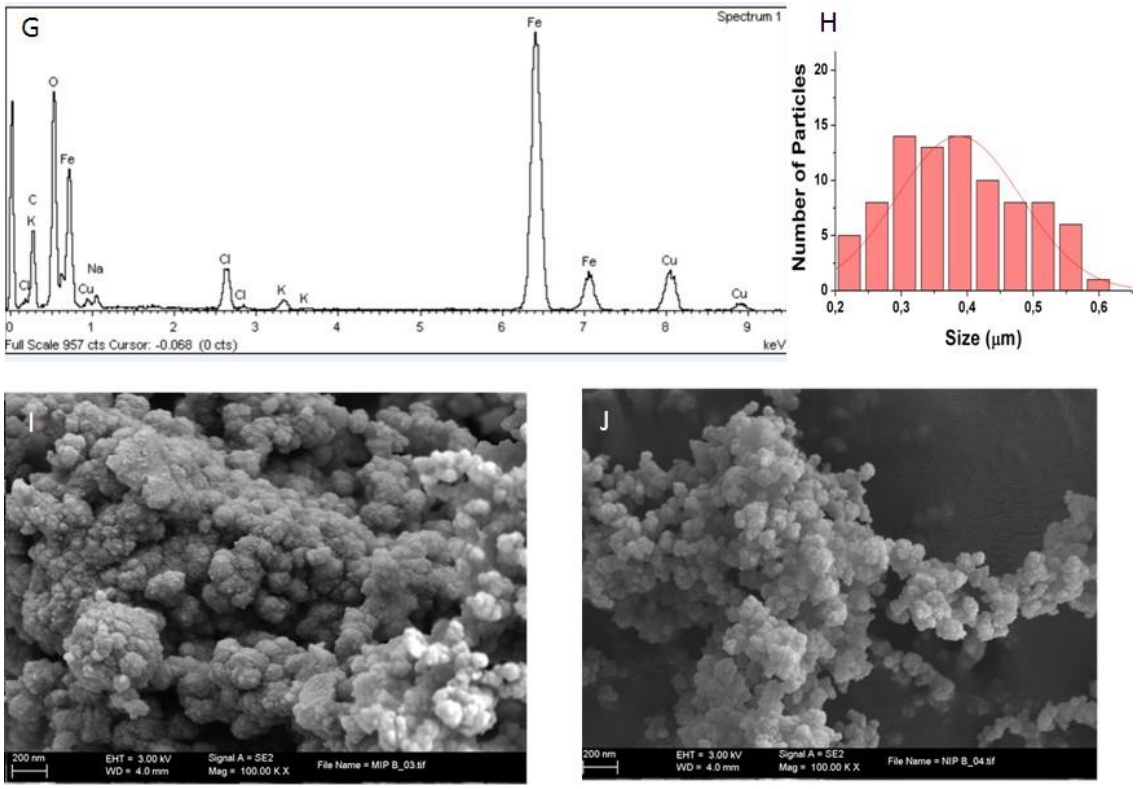

Figure S5.12. Study of Magnetic MIP and NIP macroscopic aspect for MIP and NIP, (A and B) respectively; TEM images at different resolution levels for MIP (C, D) and NIP (E, F) and (G) the corresponding elemental analysis for MIP; SEM image for MIP (I) and NIP (J). The histogram corresponding for size distribution of the magnetic MIP (taken from panel I) is shown in panel H.

5.7.13.2. Characterization of the binding of biotinylated biomolecules by confocal Microscopy

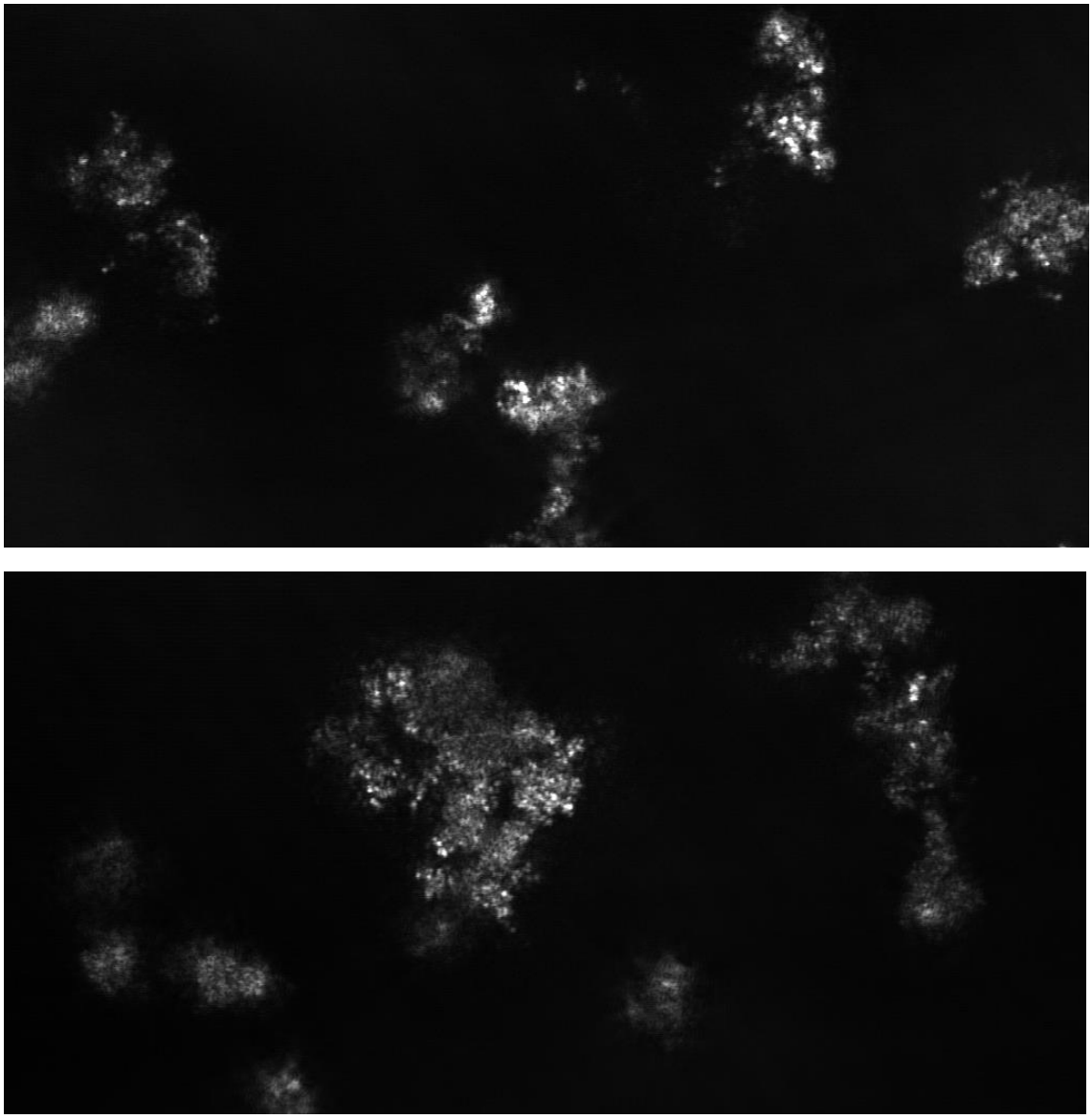

Figure S5.13. Characterization of the non-specific adsorption of streptavidin-Cy5 on the magnetic-MIP of binding of biotinylated biomolecules on the magnetic-MIP by confocal microscopy.

5.7.13.3. Characterization of the binding of biotin-HRP by a magneto-actuated immunoassay

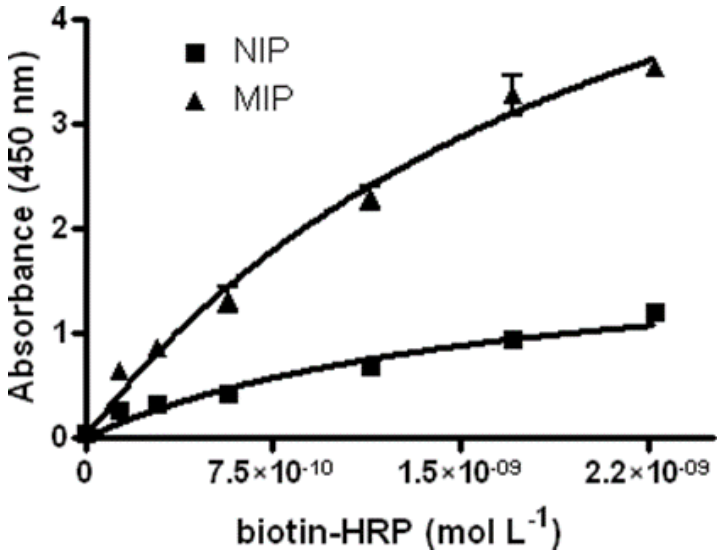

Figure S5.14. Characterization of the binding of biotin-HRP on the magnetic-MIP by magneto-actuated immunoassay in one step, in concentration range from 1.39 10^{-10} to 2.84 10^{-9} M of biotin-HRP and a fixed amount of 0.55 mg of magnetic-MIP. The negative controls are also shown. Error bar illustrates the standard deviation for the samples (n=4), using de magnetic-MIP (▲). The results obtained using non- imprinted polymers NIP (■) under analogous conditions are also shown.

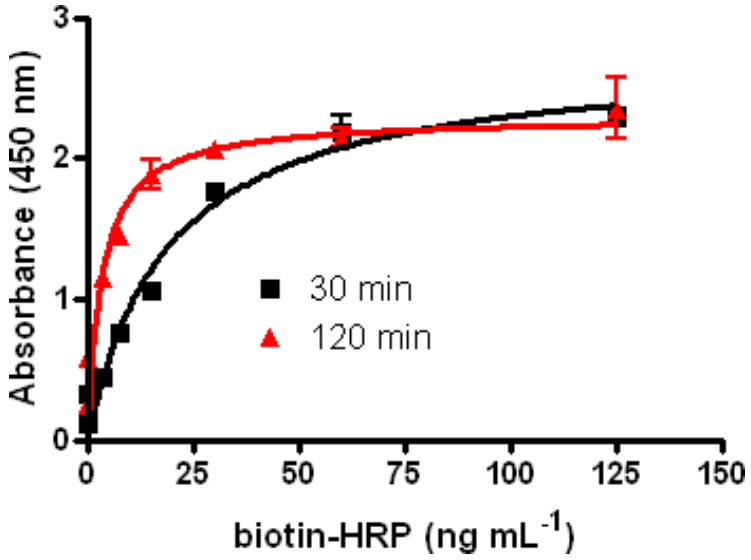

Figure S5.15. Study of the incubation time for the binding of biotin-HRP on the magnetic-MIP by magneto-actuated immunoassay in one step, in concentration range from 0 to 125 ng mL^{-1} of biotin-HRP and a fixed amount of 0.33 mg of magnetic-MIP. The negative controls are also shown. Error bar illustrates the standard deviation for the samples (n=3), upon 30 (■) and 120 minutes (▲) of incubation time.

Table S5.4 Comparison of binding at incubation times of 30 and 120 minutes

Concentration Biotin-HRP (ng mL^{-1})	**Mean value (a.u.) (30 min)**	**SD**	**Mean value (a.u.) (120 min)**	**SD**	**% binding**
125	2.289	0.103	2.356	0.300	97.1
60	2.187	0.194	2.142	0.121	102.1
30	1.768	0.001	2.064	0.195	85.7
15	1.053	0.003	1.892	0.150	55.6
7.7	0.755	0.077	1.447	0.005	52.2
3.8	0.441	0.081	1.152	0.028	38.3
0.375	0.321	0.075	0.577	0.020	55.7
0.187	0.118	0.004	0.250	0.053	47.3

5.7.13.4. Study of pH and the buffer composition

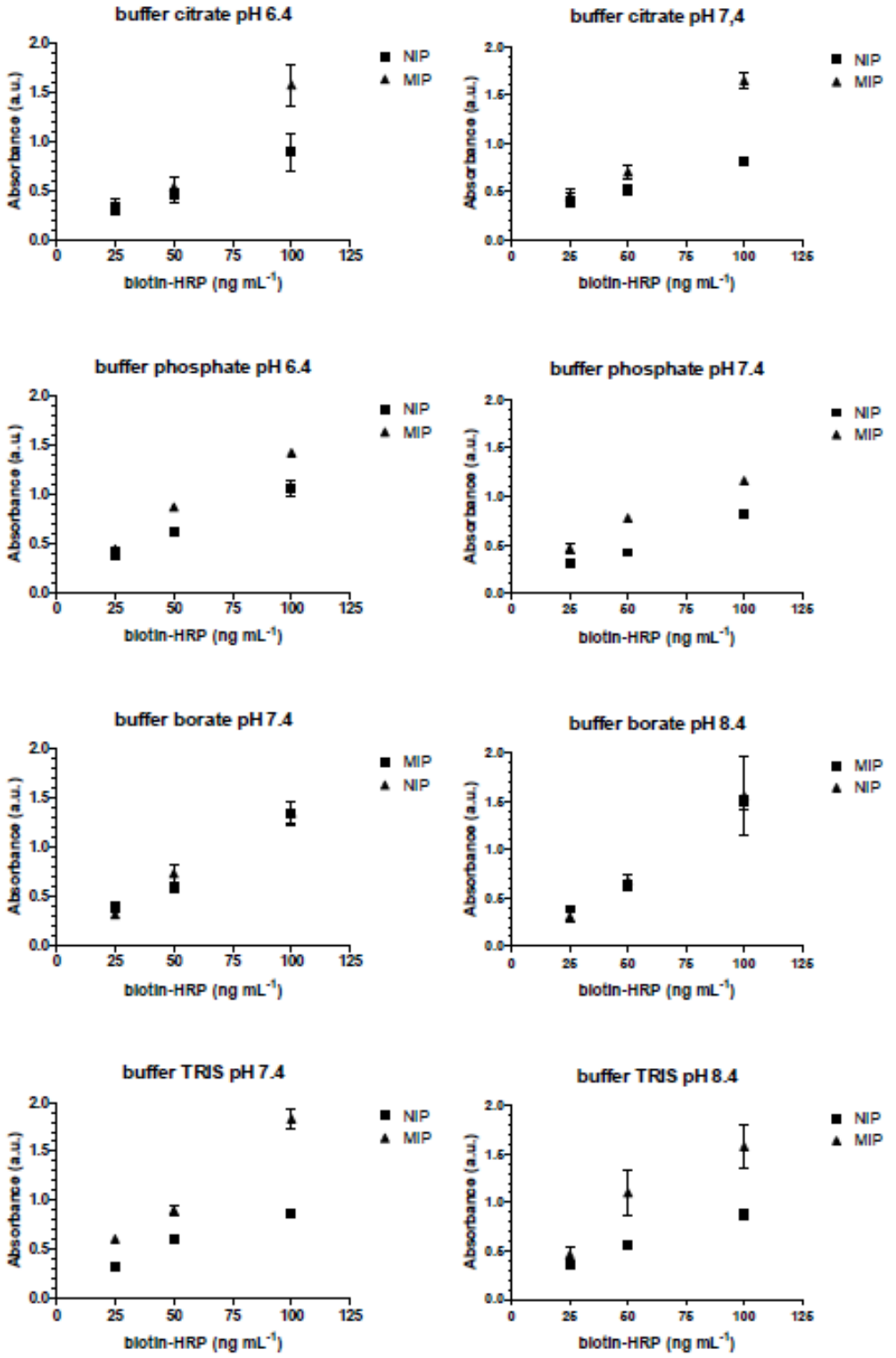

Figure S5.16. Characterization of the binding of biotin-HRP on the magnetic-MIP by magneto-actuated immunoassay in one step performed under different buffers compositions and pH, in concentration range from 25, 50, and 100 ng mL^{-1} of biotin-HRP and a fixed amount of 0.33 mg of magnetic-MIP per assay. Error bar illustrates the standard deviation for the samples (n=3), using de magnetic-MIP (▲). The results obtained using non-imprinted polymers NIP (■) under analogous conditions are also shown

5.7.13.5. Quantification of biotin based on a competitive magneto-actuated immunoassay

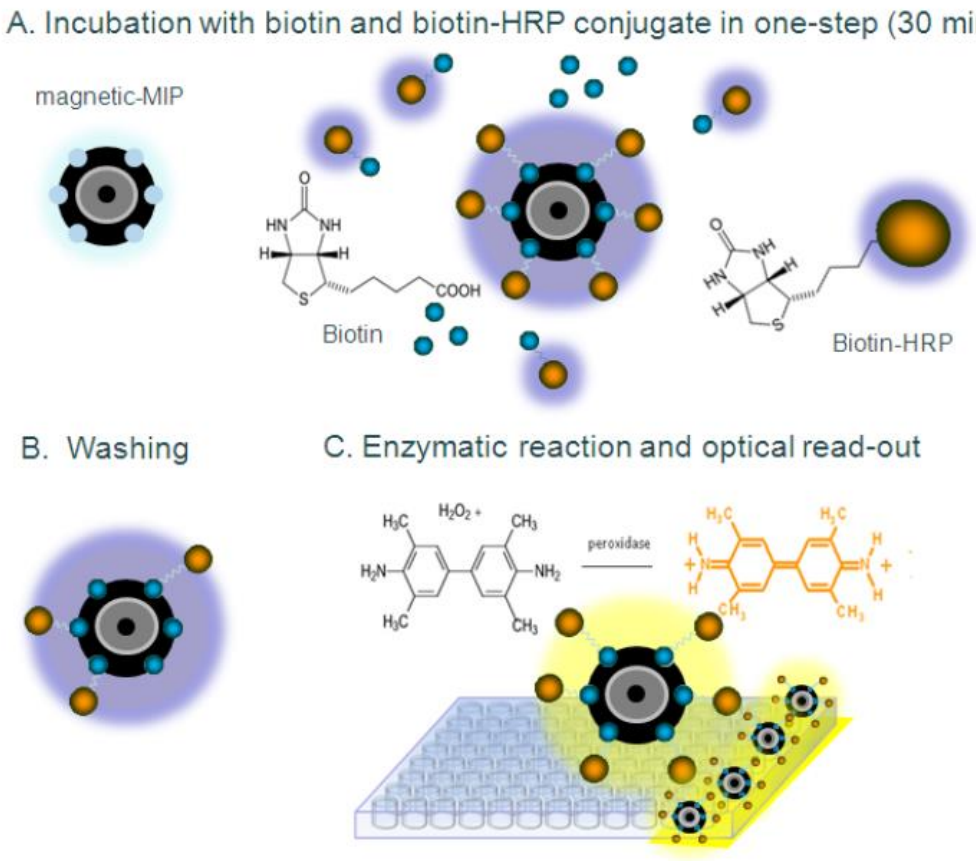

Figure S5.17. Schematic procedure for the competitive magneto-actuated immunoassay based on magnetic-MIP for the detection of biotin in a one simultaneous-competition step between biotin and biotin-HRP (30 min).

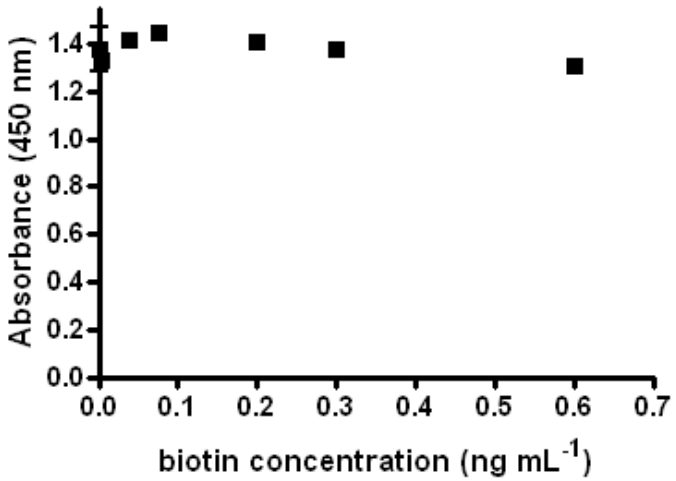

Figure S5.18. Raw data for the competition assay in one-simultaneous competition step (30 min) (as schematically shown in Figure S5.17), performed by the incubation at the same time of the magnetic-MIP (0.55 mg per well) with 100 µL of biotin-HRP (100 ng mL^{-1}) with biotin ranging from 0 to 0.7 ng mL^{-1} for 30 min under shaking in TRIS buffer pH 7.4 at room temperature. Error bar illustrates the standard deviation for the samples (n=3).

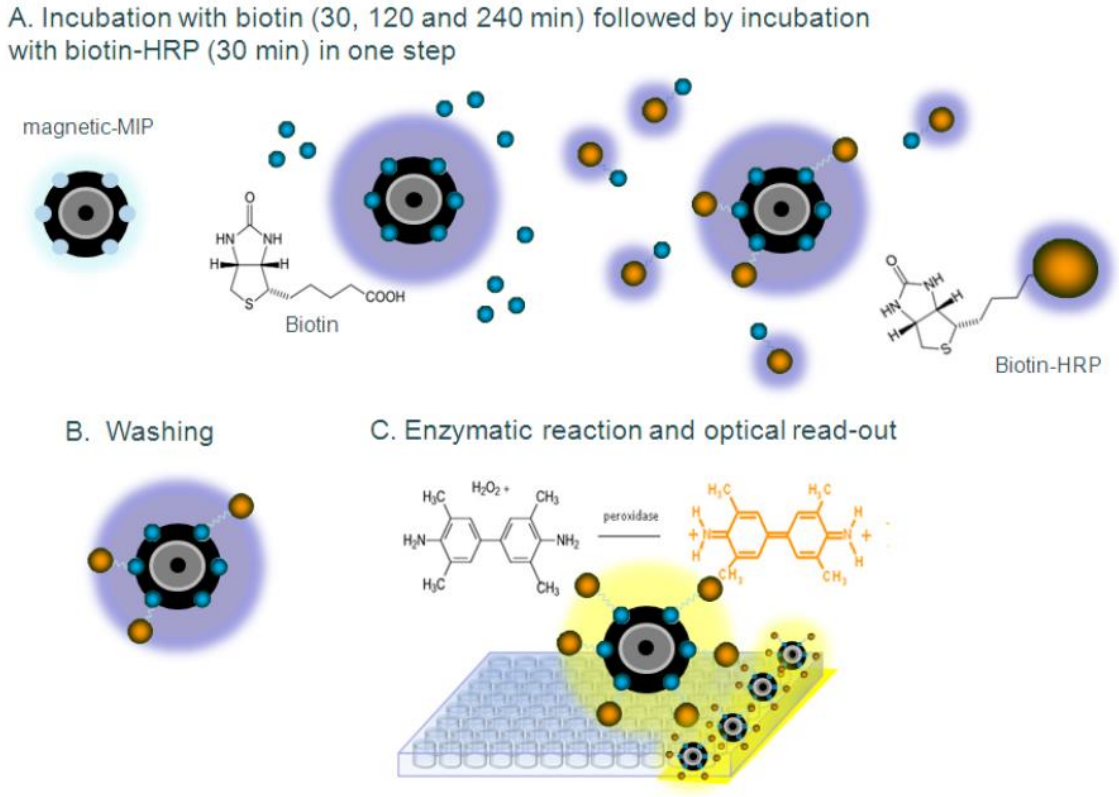

Figure S5.19. Schematic procedure for the competitive magneto-actuated immunoassay based on magnetic-MIP for the detection of biotin in a one consecutive-competition step by the incubation of biotin (30, 120 and 240 min) and biotin-HRP (30 min).

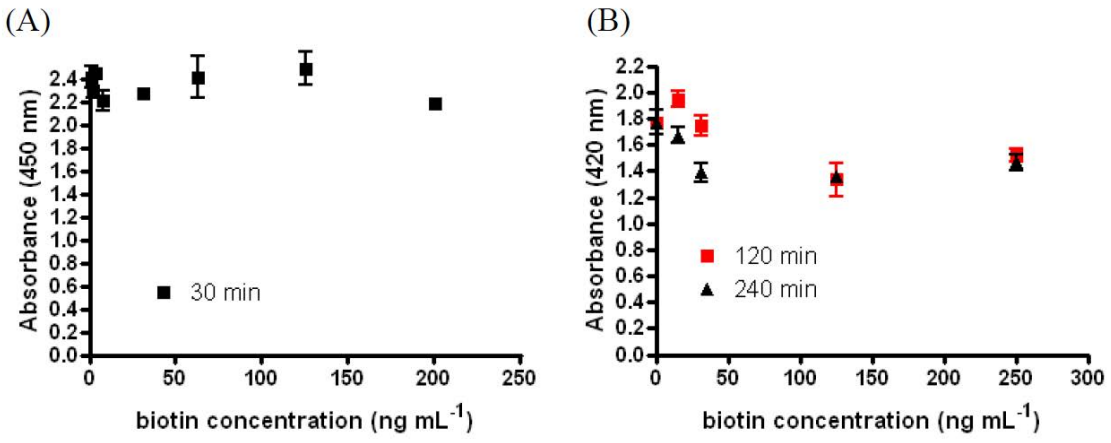

Figure S5.20. Raw data for the competition assay in one consecutive-competition step as schematically shown in Figure S5.19), performed by the incubation of the magnetic-MIP (0.55 mg per well) with biotin ranging from 0 to 250 ng mL^{-1} for 30 min (panel A) and 120 and 240 minutes (panel B) followed by the incubation of 100 µL of biotin-HRP (100 ng mL^{-1}) for further 30 min, under shaking in TRIS buffer pH 7.4 at room temperature. Error bar illustrates the standard deviation for the samples (n=3).

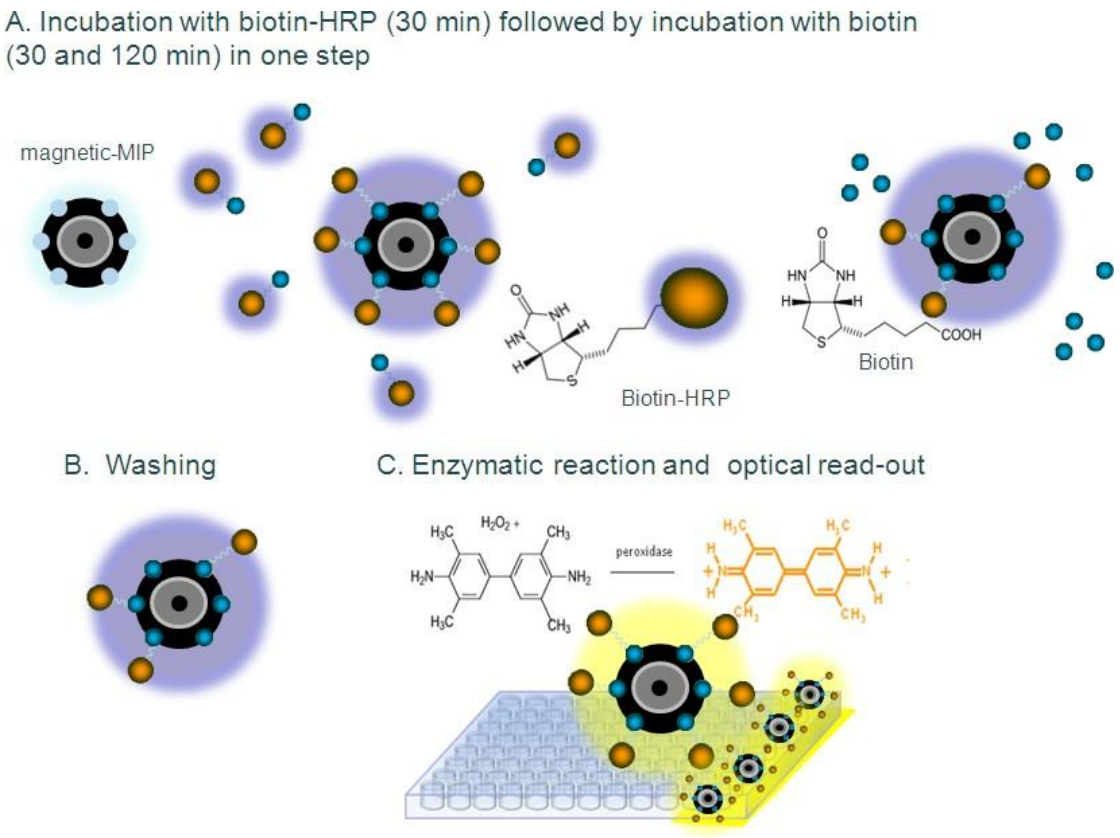

Figure S5.21. Schematic procedure for the competitive magneto-actuated immunoassay based on magnetic-MIP for the detection of biotin in a one consecutive-competition step by the incubation of biotin-HRP (30 min) and biotin (30 min).

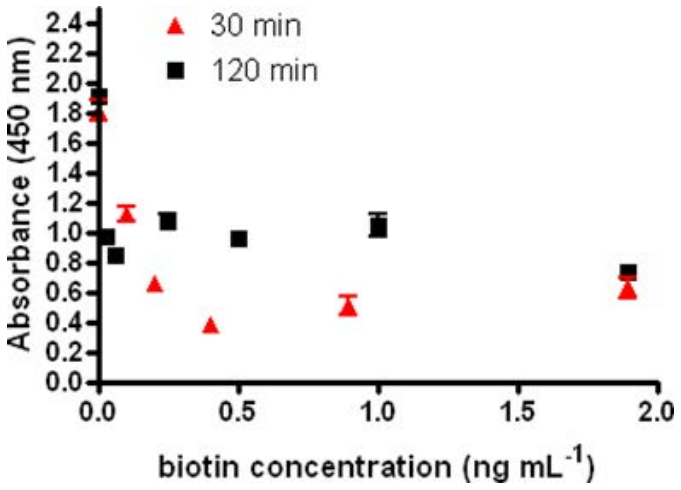

Figure S5.22. Raw data for the competition assay in one consecutive-competition step (as schematically shown in Figure S5.21), performed by the incubation of the magnetic-MIP (0.55 mg per well) with 100 µL of biotin-HRP (100 ng mL^{-1}) for 30 min, followed by the incubation with biotin ranging from 0 to 2 ng mL^{-1} for further 30 and 120 min, under shaking in TRIS buffer pH 7.4 at room temperature. Error bar illustrates the standard deviation for the samples (n=3).

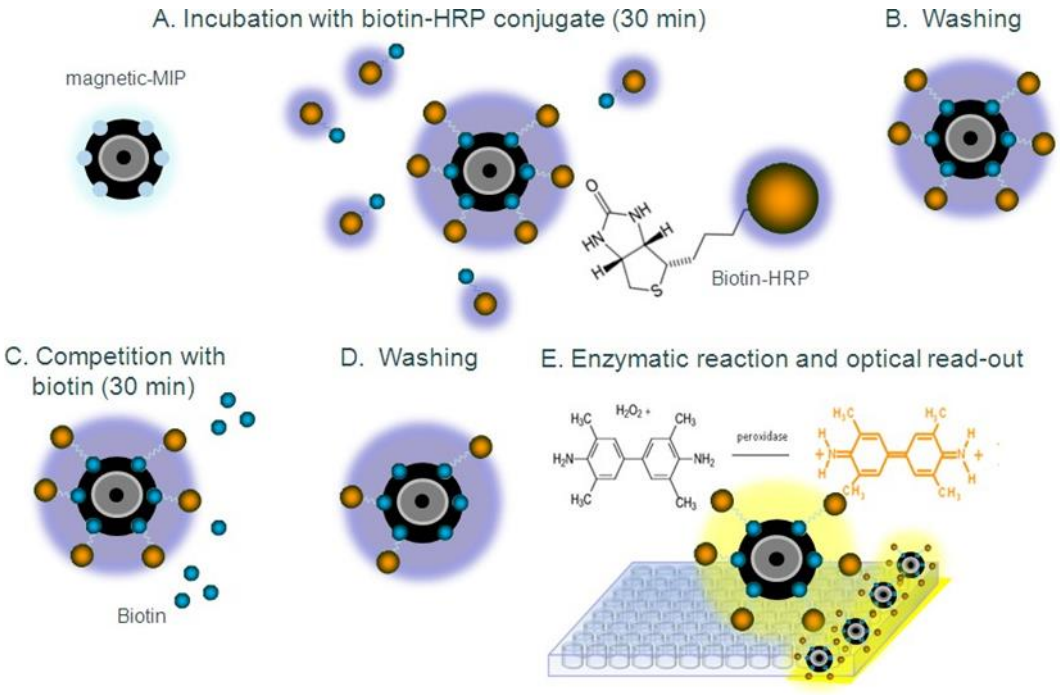

Figure S5.23. Schematic procedure for the competitive magneto-actuated immunoassay based on magnetic-MIP for the detection of biotin in two steps.

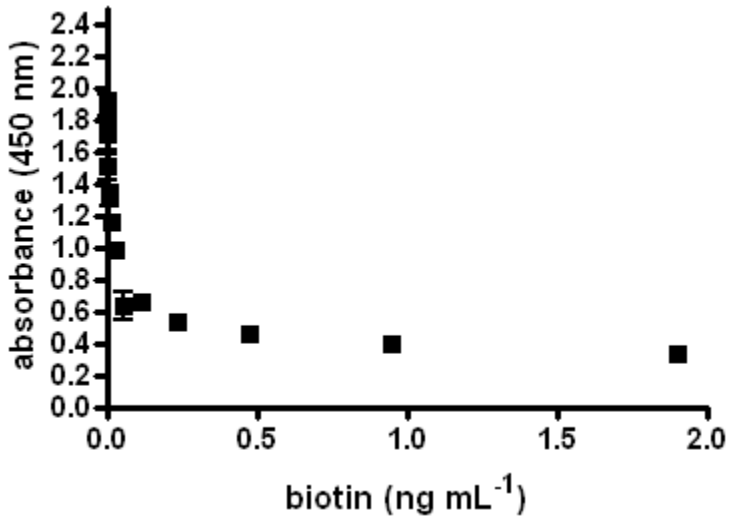

Figure S5.24. Raw data for the competition assay in two-competition step (60 min) (as schematically shown in Figure S5.9), performed by the incubation of the magnetic-MIP (0.55 mg per well) with 100 µL of biotin-HRP (100 ng mL^{-1}) for 30 min, followed by washing and a second incubation with biotin ranging from 0 pg/mL to 1.90 ng mL^{-1} for 30 min, under shaking in TRIS buffer pH 7.4 at room temperature. Error bar illustrates the standard deviation for the samples (n=4). Only one replicate was rejected among 56 replicates.

5.7.13.6. Characterization of the binding of double-tagged DNA from E. coli O157:H7 by a magneto-actuated immunoassay

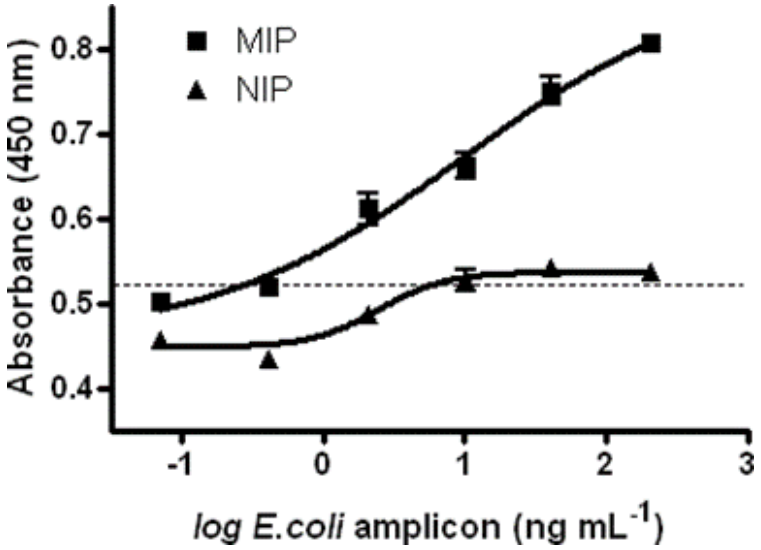

Figure S5.25. Fitted curve adjusted to a nonlinear regression (Sigmoidal dose-response with variable slope) for the binding of the double-tagged DNA from *E. coli* O157:H7 obtained by PCR and a double-tagging set of primers for the amplification of the *eaeA* (151 bp) gene fragment, on the magnetic-MIP by magneto-actuated immunoassay in one step, in concentration range from 0 to 206.8 ng mL^{-1} and a fixed amount of 0.55 mg of magnetic-MIP and 1.35 µg of antiDIG-HRP. Error bar illustrates the standard deviation for the samples (n=4), using de magnetic-MIP (■). The results obtained using non-imprinted polymers NIP (▲) under analogous conditions are also shown.

5.8. References

1. Brandão, D., Liébana, S., Pividori, M. I., 2015a. New Biotechnol. 32, 511-520.

2. Brandão, D., Liébana, S., Campoy, S., Cortes, M.P., Alegret, S, Pividori, M.I., 2015b.

Biosensors and Bioelectronics 74, 652–659.

3. Brandão, D., Liébana, S., Campoy, S., Alegret, S, Pividori, M.I., 2015c. Talanta 143, 476 198–204

4. Carinelli, S., Martí, M., Alegret, S., Pividori, M. I., 2015. New Biotechnol. 32, 521-532.

5. Chen, L., Zhang, X., Sun, L., Xu, Y., Zeng, Q., Wang, H., Xu, H., Yu, A., Zhang, H.,

6. Ding, L., 2009. Journal of Agricultural and Food Chemistry 57, 10073–10080. 480 Haupt, K., 2010. Nature Mater. 9, 612-614.

7. Kergaravat, S.V., Gómez, G.A., Fabiano, S.N., Laube T.I, Pividori, M.I., Hernández,

S.R., 2012. Talanta 97, 484–490.

8. Liébana, S., Brandão, D., Alegret, S., Pividori, M. I., 483 2014. Anal Methods 6, 8858-8873.

9. Meier, T. and Fahrenholz, F., Eds, 1996. A Laboratory Guide to Biotin-Labeling in

Biomolecule Analysis. Verlag Basel, Berlin.

10. Moreno-Bondi, M.C., Navarro-Villoslada, F., Benito-Pena, E., Urraca, J.L., 2008. Curr

Anal Chem 4:316-340

11. Piletska, E., Piletsky, S., Karim, K., Terpetschnig, E., Turner, A., 2004. Analytica

Chimica Acta 504, 179–183.

12. Pividori, M.I., Alegret, S., 2005. Analytical letters 38, 2541-2565.

13. Pividori, M.I., Taboada Sotomayor, M.P., European Patent, PCT/EP2016/062021.

14. Reddy, L.H., Arias, J.L., Nicolas, J., Couvreur, P., 2012. Chem Rev 112, 5818–5878.

15. Zacco, E., Pividori, M.I., Alegret, S., Galve, R., Marco, M.P., 2006. Anal Chem 78, 494 1789-1798.

16. Rembaum, A., Yen, R.C.K, Kempner, D.H., Ugelstad, J., 1982. J Immunol Methods 52,

496,341-351.

17. Savage, D., Mattson, G., Desai, S., Nielander, G., Morgensen, S., Conklin, E.,1992.

18. Avidin-Biotin Chemistry: A Handbook. Pierce Chemical Company, Rockford, Illinois,

U.S.A.

19. Vlatakis, G., Andersson, L.I., Müller, R., Mosbach, K., 1993. Nature 361, 645–647.

20. Ramstrom, O., Mosbach, K., 1999. Curr. Opin. Chem. Biol. 3, 759-764.

21. Takeuchi, T., Dobashi, A, Kimura, K, 2000. Anal. Chem. 72, 2418–2422.

22. Uzuriaga-Sánchez, R.J., Khan, S., Wong, A., Picasso, G., Pividori, M.I., Maria Del

23. Taboada Sotomayor, M.P., 2016. Food Chemistry 190, 460–467.

24. Wiklander, J., Karlsson, B.C.G., Aastrup, T., Nicholls, I.A., 2011. Anal Bioanal Chem 506 400, 1397–1404.

25. Kang, Y.S., Risbud, S., Rabolt, J.F., Stroeve, P., 1996. Chem. Mater. 8, 2209-2211.

26. Kim, J., Lee, J.E., Lee, J., Yu, J.H., Kim, B.C., An, K., Hwang, Y., Shin, C.-H., Park,

J.-G., Kim, J.. 2006. J. Am. Chem. Soc. 128, 688-689

27. Kawasaki, S., Horikoshi, N., Okada, Y., Takeshita, K., Sameshima, T., Kawamoto, S.,

2005. J. Food Protect. 68,551–556.

CHAPTER 6

Electrochemical genosensing of E. coli based on padlock probes and isothermal amplification

6.1. Abstract

Isothermal amplification techniques are nowadays emerging for the detection of pathogenic bacteria in low resource settings, where many infectious diseases are endemic and the lack of reliable power supply, trained personnel and specialized facilities are critical barriers to polymerase chain reaction. This work addresses the detection of *E. coli* based on DNA isothermal amplification and electrochemical genosensing on disposable electrodes by square-wave voltammetry. In this approach, the bacterial DNA is preconcentrated using a specific magnetic probe and then amplified on the magnetic particles by rolling circle amplification (RCA) by a padlock probe. Two different electrochemical readout methods for the RCA amplicons are tested. The first one relied on the labelling of the magnetic RCA product with a digoxigenin probe followed by the incubation with antiDIG-HRP antibody as electrochemical reporter. In the second case, the direct detection with an HRP-probe was performed. This last strategy showed better analytical performance, achieving a limit of detection of as low as 6.7 amol in 120 min and avoiding the use of thermocyclers or any other bench top equipment.

6.2. Introduction

Escherichia coli is the most common enteric Gram-negative bacteria. From a clinical perspective, *E. coli* strains can be classified as commensal strains, intestinal pathogenic strains, and extraintestinal pathogenic *E. coli* (ExPEC)(1)(2). ExPEC infections are often originated from the normal intestinal flora. In this instance, the bacteria colonize the intestine and then are transferred to an extraintestinal site where it causes infection (3). ExPEC, can cause a wide spectrum of illnesses in humans, including neonatal meningitis, sepsis, pneumonia, surgical site infections (4)(5), being, the most common the urinary tract infection (UTI)(6). *E. coli* is responsible of the 90 % of all urinary tract infections in ambulatory and hospital settings. These infections cause morbidity in all age groups and can be categorized according to the clinical syndrome, as cystitis, pyelonephritis, catheter-related infection, or asymptomatic bacteriuria (7)(8)(9).

Importantly, UTIs caused by ExPEC represents a large burden in terms of health care costs (10). Only in US, there are 6-8 million of uncomplicated cystitis, 250,000 pyelonephritis which 100,000 require hospitalization, and 1-1.5 million episodes of catheter-associates UTI reported cases per year, resulting in an estimated cost of billions of dollars annually (11).

Furthermore, this problem has increased in the last years due to the antimicrobial resistance developed among *E. coli* strains (13-16).

The incidence and the cost related to these infections would be reduced if rapid tests for the strained causative bacteria were widely available for the accurate and rapid diagnosis. Conventional microbiological techniques are currently the gold standard for identification of pathogenic bacteria, although they are time-consuming (13). Several approaches for rapid detection usually include immunoassays and polymerase chain reaction (PCR). However, PCR analysis requires thermo-cycling instruments and trained personnel.

This work addresses the detection of *Escherichia coli* based on DNA isothermal amplification (14) using padlock probes and electrochemical genosensing on commercial screen-printed electrodes by square-wave voltammetry. Padlock probes are long oligonucleotides, whose ends are complementary to adjacent target sequences. Upon hybridization to the target, both ends are brought into contact, allowing circularization by a DNA ligase(15). Circularization by ligation requires that both target complementary probe arms hybridize to the target sequence with perfect match (16) (17). The high discrimination rate of DNA ligase provides an outstanding specificity.

Moreover, this approach can be integrated with magnetic separation for a further increase of the sensitivity, by using a capture olignucleotide coupled to magnetic particles. In this work, a capture oligonucleotide was designed as such that it binds to a specific sequence of the target DNA downstream (5´). The biotinylated capture probe is then bind to streptavidin-modified magnetic particles. The incorporation of magnetic particles to the assay allow the use of high concentration of padlock probes, which reduces the assay and ligation time from hours to several minutes. Once the ligation is finished, the unreacted padlock probes are easily removed by magnetic separation. Subsequently, the circularized padlock probe can serve as template for rolling circle amplification (RCA)(18). RCA is an isothermal reaction,

therefore making it advantageous for the application in point of care diagnostics. In this isothermal amplification, the phi29 polymerase continuously copies the circle (circularized padlock) in a rolling circle amplification reaction. Amplification of padlock probes by RCA is exclusive to circularized probes which add another step of specificity.

The amplified single strand product consists of hundreds of concatemerized padlock probe copies that can be labelled with a short tagged oligonucleotide that hybridized to the repetitive detection tag sequence introduced in the padlock probe backbone. In this work, two different electrochemical readout methods for the RCA amplicons were tested. Diagnostic applications outside a laboratory environment are enabled by portable biosensors devices. The rapidity of the electrochemical readout, the simplicity and economical potentiostat and the use of disposable commercially available screen-printed electrode make this strategy an exciting alternative for bacteria detection at practitioner site.

6.3. Experimental section

6.3.1. Instrumentation

The electrochemical measurements were performed on carbon screen-printed electrodes (ref. DRP-110) using a portable bipotentiostat DRP-STAT200 operated by DropView 2.2 for instrument control and data acquisition (Dropsens, Spain). Fluorescently labelled rolling circle products were detected using Aquila 400 (Q-linea AB, Sweden).

6.3.2. Chemicals and biochemicals

Streptavidin magnetic particles (MPs) (Dynabeads® MyOne Streptavidin T1 Prod. No. 65601) were purchased from Life Technologies. Synthetic DNA and padlock probe were from Sigma Aldrich and Cy3 labelled detection probes were produced by Integrated DNA technologies (Begium). Peroxidase-modified probes were provided by Biomers, Germany. T4 ligase and phi29 DNA polymerase as well as its corresponding buffer (33 mmol L^{-1} Tris-acetate pH 7.9, 10 mmol L^{-1} magnesium acetate, 66 mmol L^{-1} potassium acetate, 0.1% Tween-20, 1 mmol L^{-1} DTT) came

from Thermo Fisher Scientific. T4 ligase reaction buffer (66 mmol L^{-1} Tris-HCl pH 7.5, 10 mmol L^{-1} DTT, 10 mmol L^{-1} $MgCl_2$) was purchased from DNA Gdansk. The other buffer solutions were prepared with Milli-Q water and all other reagents were in analytical reagent grade (supplied from Sigma and Merck). The composition of these solutions were: phosphate buffer for electrochemical measurement (ePBS): 0.1 mol L^{-1} Na_2HPO_4, 0.1 mol L^{-1} NaCl; hybridization buffer A: 6,6 mmol L^{-1} Tris-acetate pH 7.9, 2 mmol L^{-1} magnesium acetate, 13 mmol L^{-1} potassium acetate, 0.02% Tween-20, 0.2 mmol L^{-1} DTT; hybridization buffer B: 20 mmol L^{-1} EDTA, 40 mmol L^{-1} Tris-HCl, 2.8 mol L^{-1} NaCl, and 0.2% Tween-20; hybridization buffer C: 20 mmol L^{-1} EDTA, 40 mmol L^{-1} Tris-HCl, 2.8 mol L^{-1} NaCl, 0.2% Tween-20, 30 mM trisodium citrate and 40% formamide; hybridization buffer D: 40 mM Tris-HCl pH 8.3, 50 mM KCl, 20 mM $MgCl_2$, 1 mM NAD, 0.02% Triton® X-100 and washing buffer: 10 mmol L^{-1} Tris-HCl pH 7.5, 5 mmol L^{-1} EDTA, 0.1% Tween-20 and 0.1 mol L^{-1} NaCl.

6.3.3. Design of the padlock, capture and readoutprobes

A padlock probe is a linear, 89-pb long, oligonucleotide that consists of four aligned segments: two complementary sequences located at the 5' and 3' ends (indicated as a1 and a4 in Figure 6.1, panel A) which hybridized the target. The selected target sequence is specific for *Escherichia coli* 16S ribosomal gene (the most conserved regions among the *E. coli* genome, Genbank accession Nº CP016182.2).

After hybridization of both ends of the padlock probe to the target sequence for *E. coli* (Figure 6.1, panel B) and further ligation (panel C), the linear probe is then converted to a DNA circle (panel D). The padlock probe also comprises two sequences located in the centre (a2 and a3, in Figure 6.1, panel A), non-complementary to the target but which hybridize with the readout probes, modified with different tags for indirect (digoxigenin) and direct (Cy3 and HRP) labelling and to achieve fluorescence and electrochemical readouts.

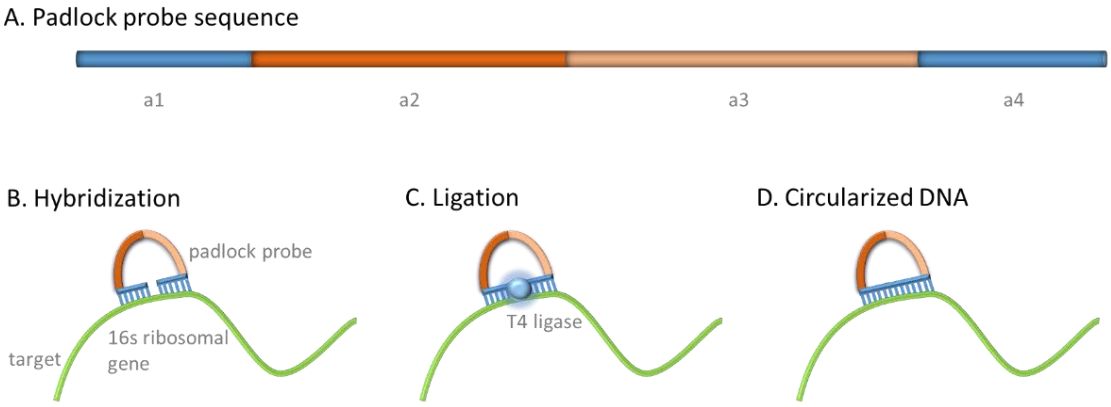

Figure 6.1. (A) Design of the specific padlock probe for the detection of *E. coli* comprising two complementary sequences to the target (a1 and a4) and two sequences (a2 and a3) to achieve the readout. (B) Hybridization of the padlock probe to the 16S ribosomal *E. coli* gene. (C) Ligation by the T4 DNA ligase enzyme. (D) Circularized DNA templates obtained after ligation of the padlock probes and used for the rolling circle amplification.

In order to achieve the target isolation and preconcentration based on magnetic actuation, a biotinylated capture probe, was designed to hybridize a specific sequence located downstream of the *E.coli* recognition sequence. Thus, streptavidin-magnetic particles can bind to the biotinylated probe and preconcentrate the sample as shown Figure 6.2, panel B.

Finally, synthetic target for *Escherichia coli* 16s rRNA was designed. Table 6.1 summarizes the oligonucleotide sequences used in this study.

Table 6.1. Oligonucleotide sequences used in this study.

Description	Sequence	Label
Padlock probe	[Phos]GTTACCCGCAGAAGAAGAGTGTACCGACCTCAGT ATCTTGCGACGTCAGTGGATAGTGTCTTACACGATTT ATACCTTTGCTCATTGAC	none
16s ribosomal *E.coli* synthetic target	TAACGCTTGCACCCTCCGTATTACCGCGGCTGCTGGCACG GAGTTAGCCGGTGCTTCTTCTGCGGGTAACGTCAATGAGCA AAGGTATTAACTTTACTCCCTTCC	none
Capture probe	CTCTCTCTCTCGTGCCAGCAGCCGCGGTAATACGGAGGG TGCAAGCGTTA	5' Biotin (magnetic separation)
Readout probe 1	CTTGCGACGTCAGTGGATAGTGTCTTACACGATTT	5' HRP (direct electrochemical readout)
Readout probe 2	AGAGTGTACCGACCTC	5' HRP (direct electrochemical readout)

Readout probe 3	CTTGCGACGTCAGTGGATAGTGTCTTACACGATTT	5' Cy3 (direct fluorescence readout)
Readout probe 4	AGAGTGTACCGACCTC	5' Cy3 (direct fluorescence readout)
Readout probe 5	CTTGCGACGTCAGTGGATAGTGTCTTACACGATTT	5' DIG (indirect readout)

6.3.4. Optimization of the rolling circle amplification

Different parameters were firstly evaluated. To achieve that, a dilution series of 16s ribosomal *E.coli* synthetic target was performed from 10 amol to 100 fmol, in order to optimize conditions for the rolling circle amplification based on fluorescent readout. Padlock probe ligation mix was added to each sample, comprising 10 nmol·L $^{-1}$ padlock probe, 0.2 mg mL^{-1} BSA, 0,68 mmol L^{-1} ATP, 1x T4 ligase reaction buffer and 5 U T4 ligase (Figure S6.2, panel A). The reaction was incubated at 37 °C for 15 min.

After that, RCA mix containing 1x phi29 DNA polymerase buffer, 125 µM dNTPs, 0.2 mg ml $^{-1}$ BSA and 6 U phi29 DNA polymerase was added to the circularized DNA and RCA was performed at 37°C for 60 min (Figure S6.2, panel B).

Rolling circle products cannot be resolved by gel electrophoresis due to the broad smear of the high molecular weight DNAs. As a control of the RCA process, the Aquila 400 amplified single molecule counter (Q-linea, Uppsala) based on fluorescence readout was used to count the RCA products. This method was also used to achieve the optimal conditions of hybridization: RCA products were fluorescently labelled by using different binding temperatures (45 min at 37ºC with a previous binding step of 2 min at 75ºC or directly 45 min at 37ºC without a range of detection oligo concentrations (from 10mM to up to 25 mM) and different buffer solutions (section 6.3.2: buffers A,B,C,D) as described in supporting information. Finally, 20 µL of the total sample was analysed using the Aquila 400 amplified single molecule counter (Figure S6.2, panel D).

6.3.5. Rolling circle amplification on streptavidin magnetic particles and electrochemical genosensing

In order to achieve the preconcentration of the rolling cycle products (RCPs) on streptavidin magnetic particles, in this case each sample of DNA target was incubated for 20 min with 50 nmol L^{-1} with the biotinylated capture probe (Table 6.1). This reaction was performed in padlock probe ligation mix comprising 10 nmol L^{-1} padlock probe, 0.2 mg mL^{-1} BSA, 0,68 mmol L^{-1} ATP, 1x hybridization buffer and 5 U T4 ligase (Figure 6.2, panel A). Afterwards, 4 µL magnetic particles were added to the ligation reaction mixture and incubated for 5 min at room temperature (RT) under rotation, coupling the biotinylated target/padlock probe complex to the magnetic particles via biotin-streptavidin bond (Figure 6.2, panel B). The mix was removed and the particles were washed once in washing buffer. After that RCA mix, containing 1x phi29 DNA polymerase buffer, 125 µM dNTPs, 0.2 mg ml^{-1} BSA, and 6 U phi29 DNA polymerase, was added to the particles and RCA was performed at 37°C for 60 min (Figure 6.2, panel C).

6.3.6. Evaluation of the electrochemical readout approach

In order to optimize the electrochemical detection of rolling circle amplification products (RCPs), two different electrochemical readout methods for the RCA amplicons on MPs were tested. The first one relied on the indirect labelling of the magnetic RCA product with a digoxigenin probe (readout probe 5, Table 6.1) followed by the incubation with antiDIG-HRP antibody as electrochemical reporter. In the second case, the direct detection with an HRP-probe (readout probe 1, Table 6.1) was performed.

In both instances, 16s ribosomal *E.coli* synthetic target (100 fmol) was incubated for 20 min at 55 °C with 50 nmol L^{-1} of biotinylated capture oligo in padlock probe ligation mix. Negative controls were prepared also prepared**.** After that, the sample was immobilized on magnetic particles and the circularized bacterial DNA was submitted to the rolling circle amplification as described above.

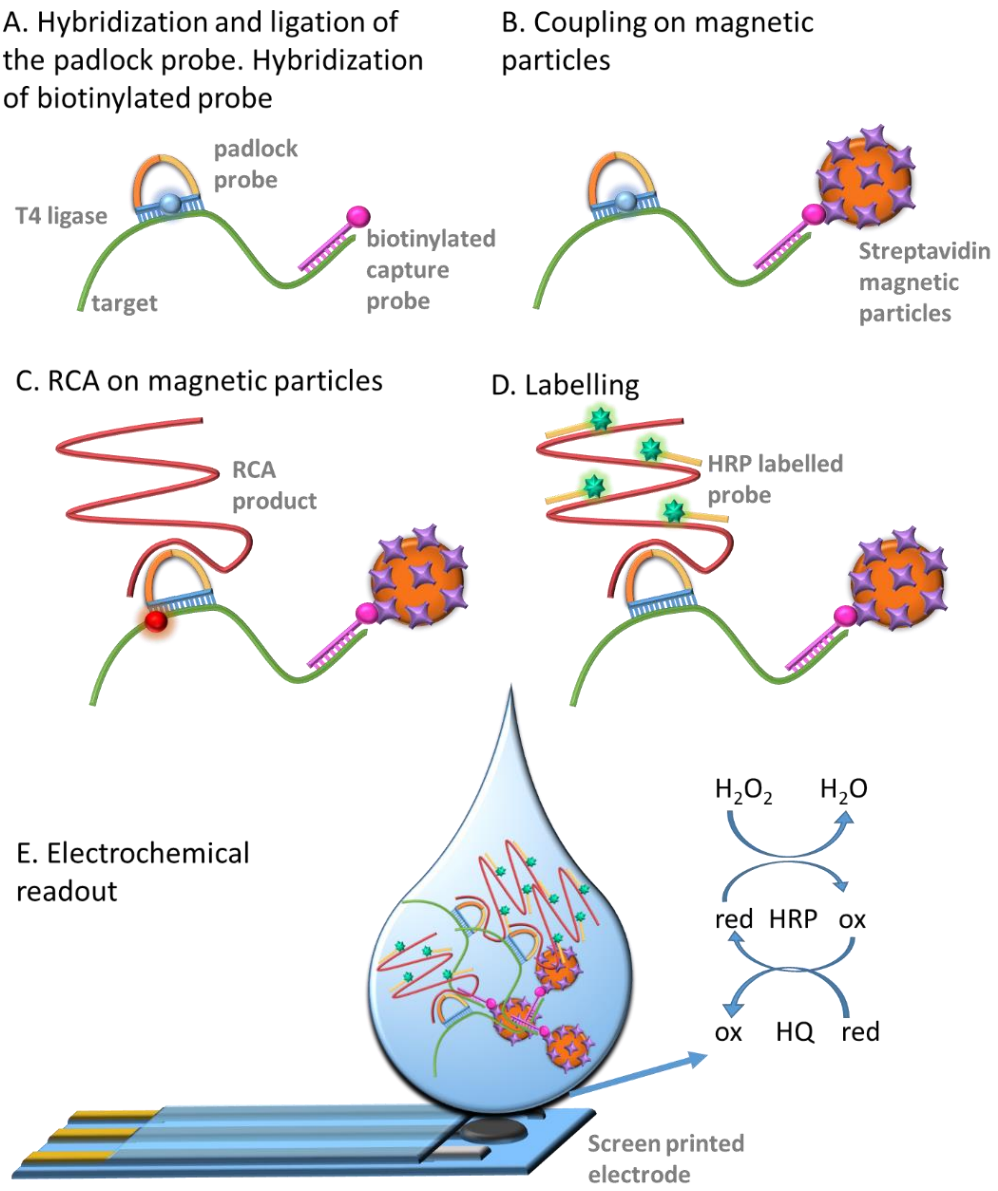

Figure 6.2. Schematic representation of the electrochemical genosensing for the rolling circle amplification products detection on streptavidin-MP. (A) A specific biotinylated capture oligo is hybridized to the DNA target and the padlock probe is hybridized on the DNA target for further ligation (B) The DNA target is coupling on streptavidin magnetic particles; (C) RCA on the streptavidin-MP; (D) Hybridization with the readout probe (HRP labelled in this case) acting as electrochemical reporter; (E) Electrochemical detection by square wave voltammetry upon addition of the mediator HQ and the substrate H_2O_2 for the HRP on screen-printed electrodes.

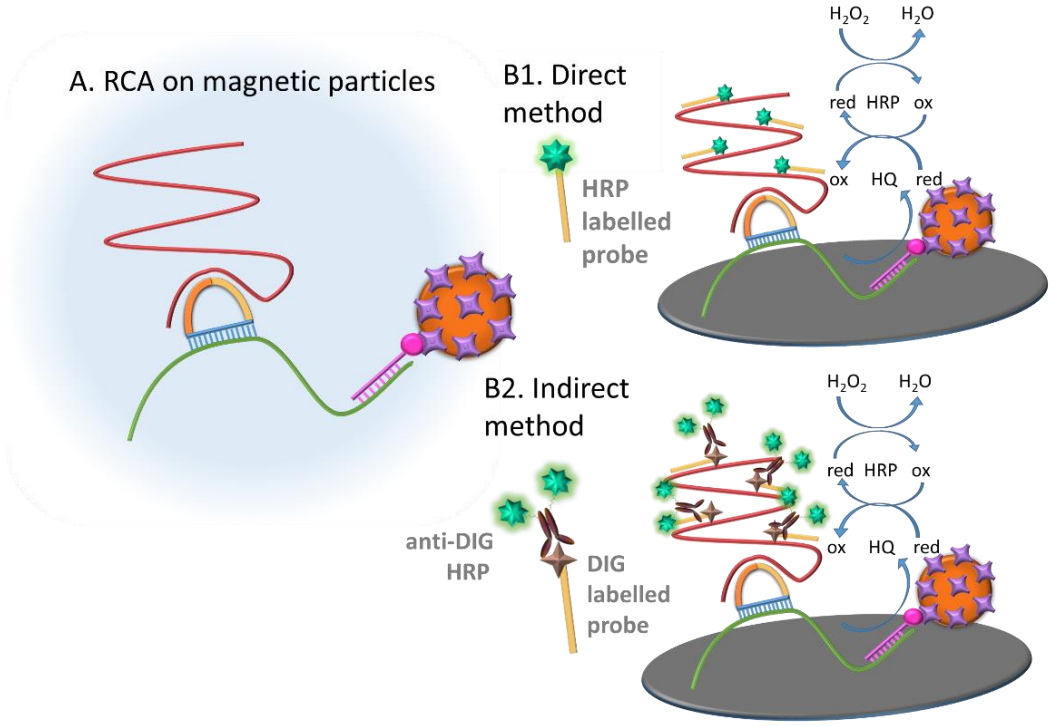

Figure 6.3. Schematic representation of the electrochemical genosensing of *E.coli* by rolling circle amplification. A) RCA on the streptavidin-MPs; B1) Hybridization with the readout probe (digoxigenin labelled) and incubation with the electrochemical reporter antiDIG-HRP; B2) Hybridization with the readout probe (HRP labelled) acting as electrochemical reporter. In both cases, the electrochemical determination is performed by square wave voltammetry upon addition of the mediator HQ and the substrate H_2O_2 for the HRP.

The RCPs attached to the streptavidin-MPs (Figure 6. 3, panel A) were then hybridized with a labelled complementary oligonucleotide (readout probes). In the direct labelling, this procedure was performed by the incubation with the readout probe 1 labelled with HRP (20 nmol L^{-1}) in hybridization buffer A at 37 °C for 45 min (Figure 6.3, panel B1). The indirect labelling was performed by the incubation with the readout probe 5 labelled with digoxigenin (20 nmol L^{-1}) in the same hybridization buffer A at 37 °C for 45 min. After that, to come up with the indirect label, a further incubation step was performed with antidig-HRP antibody in PBS buffer with 1% BSA at 37 °C for 30 min (Figure 6. 3, panel B2). In both instances, the bacterial labelled RCA products were washed (x3) to remove the unbound reagents. After each incubation or washing step, a magnetic separator was positioned under the tubes until pellet formation on the tube side wall, followed by supernatant separation.

Finally, the measurement of RCPs attached on the streptavidin-MPs was performed on carbon screen-printed electrodes with a portable bipotentiostat connected by a universal USB port to a laptop computer operated by a battery. For this, each sample was resuspended in 60 µL of 0.25 mmol L^{-1} H_2O_2 and 1 mmol L^{-1} of hydroquinone (Figure 6. 3, panel E). After 2 min of reaction, the solution was added to the electrode surface and measured by SWV. The potential range was 0.1 to -0.7 V with potential step and amplitude of 10 mV and frequency of 1 Hz. The maximal signal obtained in the peaks was used for the electrochemical signal plotted in results shown in Fig.5. A full description of the procedure basis is provided in Supp. Data

6.3.7. Electrochemical genosensing of *E. coli*

The electrochemical genosensing of the RCPs was performed by the hybridization with the readout probe 1 (Table 6.1) labelled with HRP (20 nmol L^{-1}) (as schematized in Figure 6.2, panel E) in hybridization buffer A for 45 min at 37°C, followed by washing steps under magnetic actuation, to eliminate the excess of readout probe.

The electrochemical genosensor was evaluated for the detection of *Escherichia coli*. For that, rolling circle amplified DNA coming from an overnight culture of *E. coli* DH5α were electrochemically measured. The bacteria E. coli was routinely grown in sterile liquid Luria Bertani (LB) broth for 18 h at 37 ºC under aerobic conditions. After that, serial dilutions from the culture were performed and 100 µL of each dilution was spiked on LB agar plates. After incubating the plate at 37 ºC for 24 h, the culture colonies on the plates were counted to estimate the number of viable bacteria in CFU mL^{-1}.

On the other hand, cells from 1 mL of each sample were lysed and the DNA was extracted. The liquid cultures were removed with centrifugation at 12000 *g* for 15 min and 1 mL of sterile water was added to the pellet. A second centrifugation was performed at 12500 *g* for 15 min, and the cells were resuspended in 50 µL of Tris-EDTA (TE) buffer and then kept in a boiling water bath for 10 min. After cooling on ice for 5 min, the samples were centrifuged at 12500 g for 5 min, and 10 µL of the supernatant was used directly for the amplification (Figure S6.5).

6.4. Results and Discussion

6.4.1. Optimization of the rolling circle amplification

Different experimental conditions were optimized, including the sequence of the detection probe and its concentration, the labelling temperature and the hybridization buffer. The results are shown in Supporting information (Figure S6.1) The best results were obtained using 20 nmol L^{-1} of redout 3 detection oligo at 37ºC for 45 min in buffer A.

6.4.2. Evaluation of the electrochemical readout approach

Different approaches for the labelling of the RCPs were comparatively evaluated, as schematically shown in Figure 6.3. The first one relied on the indirect labelling of the magnetic RCA product with a digoxigenin probe (readout probe 5, Table 6.1) followed by the incubation with antiDIG-HRP antibody as electrochemical reporter. On the other hand, the direct labelling consists in the hybridization with a readout probe modified with a bulky tag (HRP) (readout probe 1). The RCPs on the magnetic particles were electrochemically detected. Negative controls for each method were also tested. The results are shown in Figure 6.4.

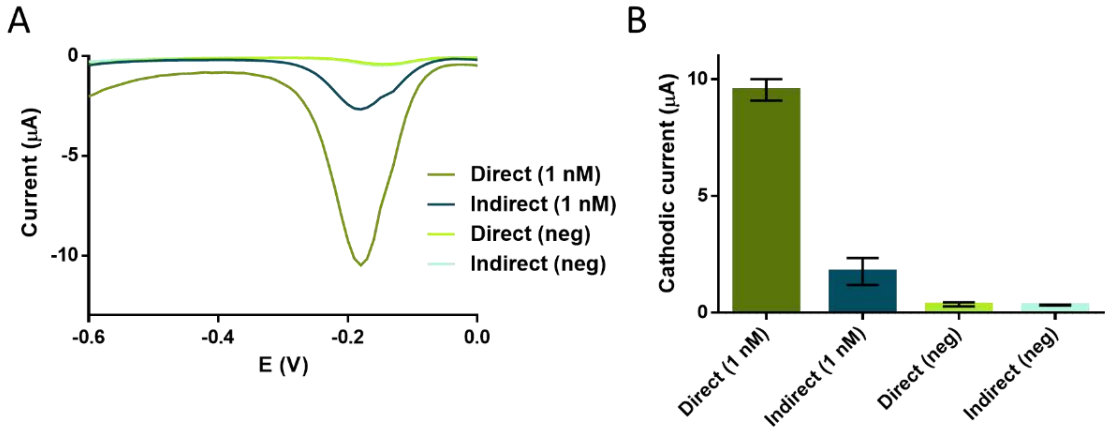

Figure 6.4. Electrochemical signals for the rolling circle amplification and electrochemical genosensing on m-GEC electrodes by using direct and indirect readout systems. For both systems, 1 nmol of circularized bacterial DNA were used, except for the negative controls. A) Raw square wave voltammetry data. B) Graph bars of the SWV maximal signal. The bars represent the mean value of the maximal signal and the error bars, the standard deviation for n=3. Medium: phosphate buffer.

Mediator: hydroquinone 1 mmol L^{-1}. Substrate: H_2O_2 0.25 mmol L^{-1}. The potential range was 0.1 to -0.7 V with potential step and amplitude of 10 mV and frequency of 1 Hz.

Although a higher hybridization rate was expected for readout probe 5, the digoxigenin tag seems to be hindered for the further recognition of the antibody, providing thus poorer performance than the readout probe 1. For the concentration of 100 fmol of circularized bacterial DNA, a mean value of 9.52 µA/SD 0.4 µA (direct labelling), 1,76 µA/SD 0.5 µA (indirect labelling) were obtained. The mean values for the background signals were 0.32 µA/SD 0.02 µA (for direct labelling), 0.42 µA/SD 0.09 µA (for indirect labelling). The signal-to-background ratios were 29.75 and 4.19 for direct and indirect labelling, respectively, confirming an increased performance of the direct labelling for the detection of the RCPs. It is important to highlight that the RCPs were previously described as a blob of DNA in which some of the repeated hybridization sequences might be in the interior, and thus being less accessible for further reactions. This direct readout system was thus used in further experiments.

6.4.3. Rolling circle amplification on streptavidin magnetic particles and electrochemical genosensing

To determine the performance and limit of detection (LOD) of electrochemical genosensing of RCA products, RCA was performed on a serial dilution of 16s ribosomal *E.coli* synthetic target, ranging from 10 amol to 100 fmol, and detected by square wave voltammetry. The results are shown in Figure 6.5.

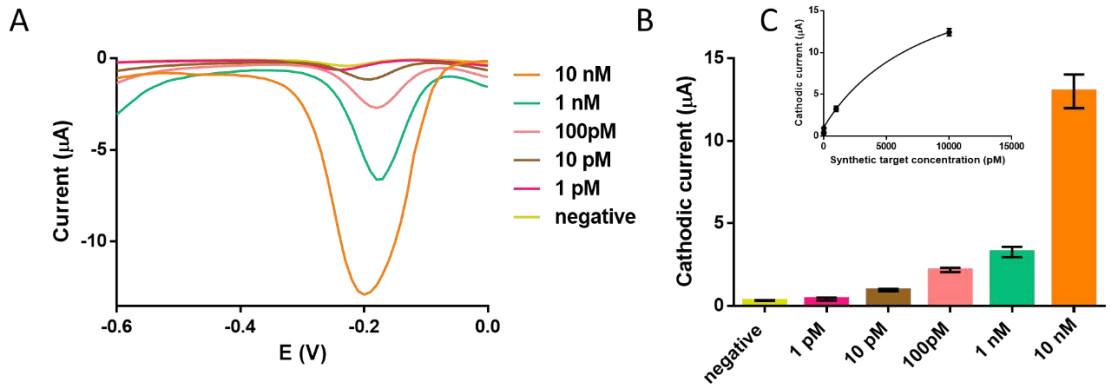

Figure 6.5. SWV voltragramms and electrochemical signal for the rolling circle amplification. 16s ribosomal *E.coli* synthetic target ranging from 10 amol to 100 fmol was used, except for the negative controls. Medium: phosphate buffer. Mediator: hydroquinone 1.0 mmol L^{-1}. Substrate: H_2O_2 0.25

mmol L^{-1}. The SWV conditions were: potential range from 0 to -0.7 V, potential step and amplitude of 10 mV and frequency of 1 Hz. A) Square wave voltammograms; B) Graph bars of the SWV maximal signal. The bars represent the mean value of the maximal signal and the error bars, the standard deviation for n=3. The negative controls are also shown (n=6). C) Fitted curve adjusted to a nonlinear regression: two site binding (hyperbola).

The maximal signals obtained in the voltagramms are presented in Figure 6. 5, panel A. The electrochemical signal was fitted using a nonlinear regression (Two site binding –hyperbola - GraphPad Prism Software) (R^2 =0.9965), as shown Figure 6.5, panel B. The LOD was estimated by fitting the raw data using a nonlinear regression (Four Parameter logistic Equation– GraphPad Prism Software) (R^2 =0.9852), as shown in Figure 6.5, panel C, by processing the negative control samples (n=6) obtaining a mean value of 0.32 μA with a standard deviation (SD) of 0.02. The cut-off value was then determined with a one-tailed t test at a 95% confidence level (t=2.015), giving a value of 0.36 μA. The LOD was found to be 6.69 amol in 10 μL of sample.

It is important to highlight that the limit of detection reached in this work with the electrochemical detection is similar or even improved than other reported bacterial detection methods where the rolling circle is used for the signal amplification(19).

Further improvement of the LOD of *E.coli* at clinically relevant levels, a further improvement in the LOD can be achieved by re-amplification of the RCA products by C2CA(20).

6.4.4. Electrochemical genosensing of *E. coli*

Finally, the electrochemical system was evaluated with *E. coli*. With this purpose, rolling circle amplified DNA from an overnight culture of *E. coli* DH5α were detected. The samples were treated as explained in the experimental section.

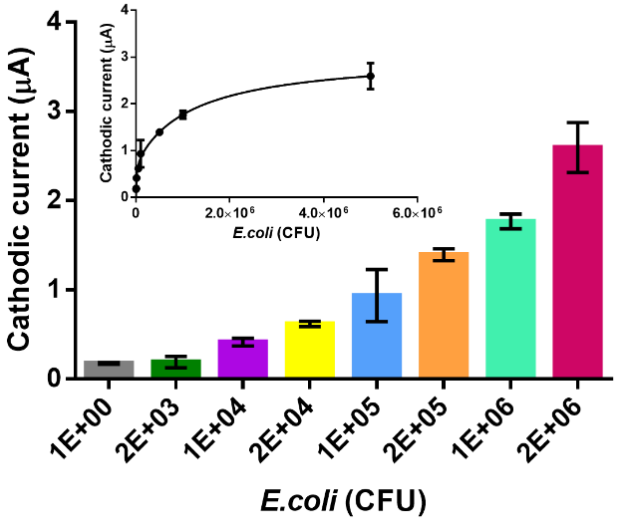

Figure 6.6. Rolling circle amplification and electrochemical genosensing of *E. coli* samples. The plots show the SWV maximal signal. The bars represent the mean value of the maximal signal and the error bars, the standard deviation for n=3. Media: phosphate buffer. Mediator: hydroquinone 1.0 mmol L^{-1}. Substrate: H_2O_2 1.8 mmol L^{-1}. The potential range was 0.1 to -0.7 V with potential step and amplitude of 10 mV and frequency of 1 Hz.

As it was described above, the denatured *E coli* was incubated at the same time with the padlock and capture probe, which was after coupled to 4 µL of streptavidin-magnetic particles for 5 min at RT. Then, the sample-bead complex was washed in order to eliminate the padlock excess and to remove the bacterial matrix, and resupended in RCA mix for the isothermal amplification. RCA was performed for 60 min at 37 ºC. A negative control without E coli DNA, which had the same treatment as the positive sample, was processed. Finally, the rolling circle products were labelled with readout probe 1.

Figure 6.6 shows the maxima signal obtained in the voltagramms for the E coli. The LOD was found to be $10^{4.3}$ CFU mL^{-1}. According to these results, it was demonstrated that the system presented in this performance of the genosensing strategy combined with the rolling circle amplification offers a sensitive method for the bacterial detection to be applied in infection diagnosis.

6.5. Conclusions

The demands on point of care devices to be low cost, user friendly and rapid with high sensitivity and specificity is the major challenge in the development of new diagnostic tests. With recent advances in molecular methods, the combination of

isothermal amplification with electrochemical sensor is a highly suitable approach to reach this objective.

This work reports an electrochemical bacterial DNA detection using padlock probes and the subsequent amplification with rolling circle amplification as a powerful combination for highly specific and sensitive *E coli* DNA detection that can be applied in clinical diagnosis. We demonstrate that isothermal amplification of *E. coli* on magnetic particles and electrochemical genosensing can be used for bacterial detection. The incorporation of magnetic particles in the assay brings several advantages due to their very large surface to volume ratio facilitating high capture efficiencies and higher reaction kinetics. Another important advantage is the easy washing procedure simplifying and reducing the assay time. The specificity provided by the ligation of the padlock probes and the isothermal nature of the rolling circle amplification make it an attractive method for the application in molecular diagnostic assay. Moreover, the use of electrochemical readout offers a robust test that requires minimal training for final user and provide rapid results for taking action immediately, for example prescribing correctly the treatment with antibiotics at the first visit to the doctor.

6.6. Acknowledgments

This work was funded by the Ministry of Economy and Competitiveness (MINECO), Madrid (Projects Sens4All BIO2016-75751-R).

6.7. Supplementary Material

6.7.1. Optimization of the rolling circle amplification

Labelling temperature optimization

A binding step at high temperatures is usually included during the hybridization process due to its demonstrated improvement in terms of time. For the present application the labelling incubation must be kept under 37 ºC due to the degradation of the enzyme HRP produced above this temperature. In order to evaluate the effect on the yield of the labelling, 20 µL of RCP were incubated in hybridization buffer with 25 nmol L^{-1} of readout 4. In the first case, the mix was incubated at 75ºC for 2

min, after that another incubation at 37 ºC for 45 min was performed. The procedure in the second case was exactly the same but for the binding step, the labelling consisted in one only incubation at 37 ºC for 45 min. Results are shown in Figure S6.1 A. The highest yield of labelling was obtained when the binding step was included, however, the labelling was also produced when only an incubation at 37ºC for 45 min was performed.

Detection oligo concentration

Concentrations ranging from 10 to 25 nmol L^{-1} of the readout probe were studied in order to evaluate its influence during the labelling process. In Figure S6.1 (panel C) it can be observed that the best results were obtained with the concentration of 20 nmol L^{-1}. The oligo concentration of 25 nmol L^{-1} seemed to saturate the system and probably the labelling was not so efficient. Moreover, the excess of brightness produced with higher concentrations of fluorophore could affect the readout and could lead to lower counting of molecules.

Hybridization buffer

Four hybridization buffers were studied for the labelling process. The composition of these solutions can be found in the experimental section 6.3.2. Buffer A exhibits the best results for labelling at 37ºC for 45 min with 20 nmol L^{-1} of detection oligo (Figure S6.1 D).

Comparison of sequences of detection probe

A comparison of 2 different readout probes labelled with Cy3 was performed. Slightly better results were obtained when the second readout probe was used (Figure S6.1 B). It allowed the monitorization of the RCA products using Cy3 labelling at the same time that the electrochemical reporter.

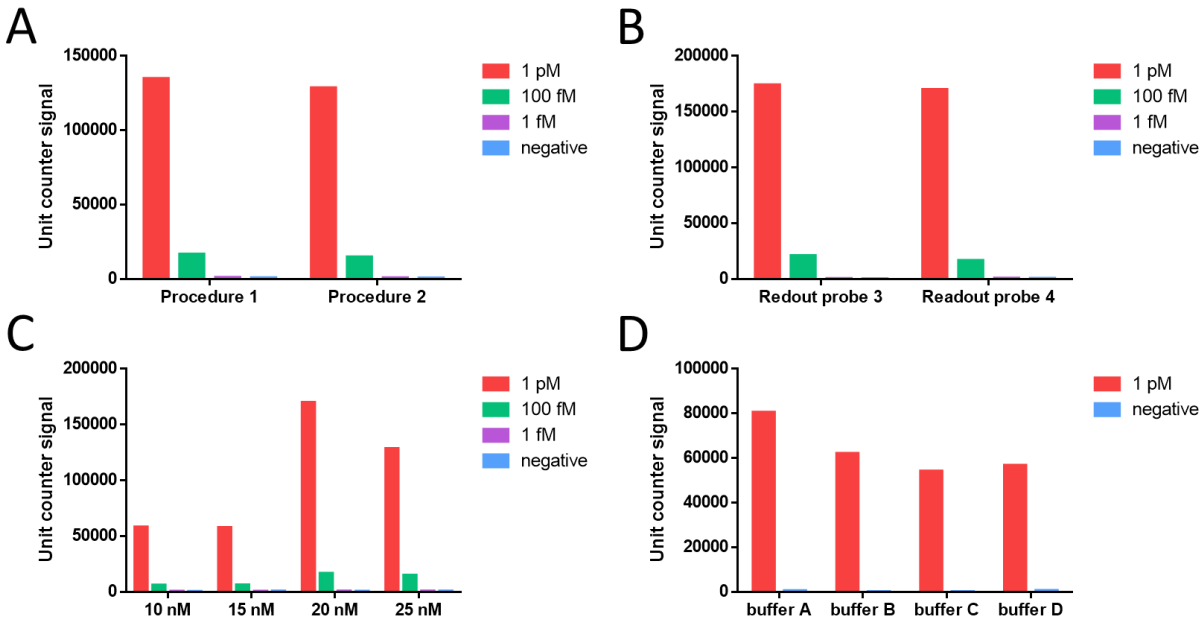

Figure S6.1. Graph bars of the Unit counter signal for each of the labelling optimization. A: Labelling temperature optimization (procedure 1: incubation at 75ºC for 2 min + 37 ºC for 45 min; procedure 2: incubation at 37 ºC for 45 min)*; B:* Comparison of sequences of detection probe.*; C:* Detection oligo concentration*; D:* Hybridization buffer.

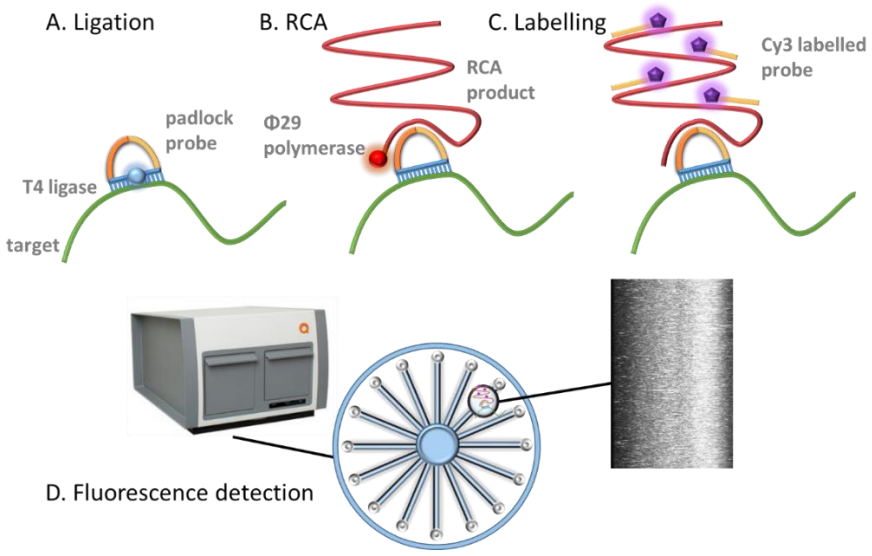

Figure S6.2. Schematic representation of fluorescent detection of the rolling circle amplification products. (A) Padlock probe is hybridized on the bacterial DNA target, followed by ligation; (B) Rolling cycle amplification (C) Hybridization with the Cy3 readout probe acting as fluorescent reporter; (D) Detection with Aquila 400 detection equipment.

6.7.2. Electrochemical readout

Carbon screen-printed electrodes were purchased from Dropsens, Spain (ref. DRP-110). These electrodes are printed using ceramics as a substrate and the electrochemical cell consists on a circular 4mm carbon working electrode, an auxiliary electrode made of carbon as well and silver as a reference electrode. The small dimensions of this electrodes (L 33 x W 10 x H 0.5 mm) make them ideal to work with the small volumes required in this work. The electrodes were connected to the boxed connector for SPE (Ref. DSC) which operates as an interface between the electrodes and the portable bipotentiostat (DRP-STAT200, DropSens, Spain) (Figure S6.3). The square wave voltammetry (SWV) measurements were performed in a laptop computer operated by the battery, in which the portable bipotentiostat was connected by a universal USB port.

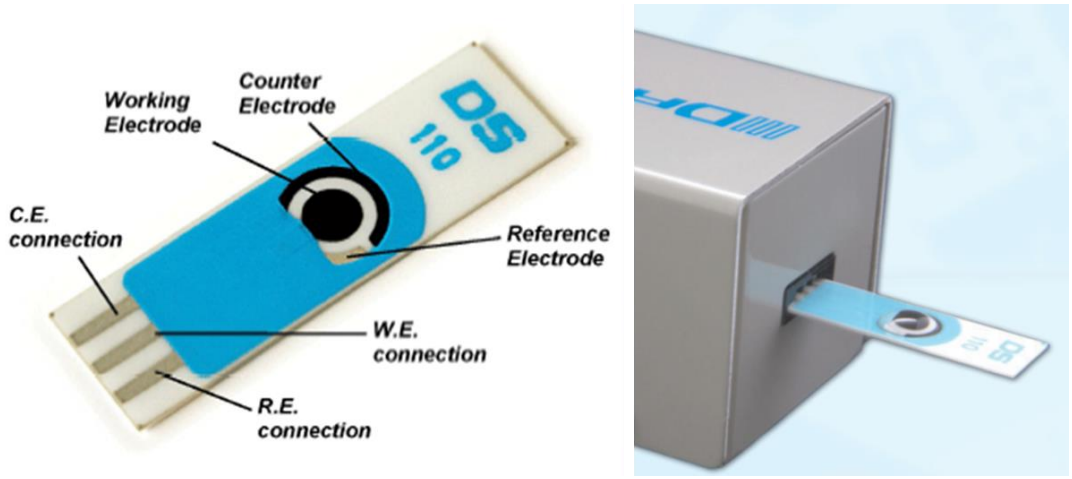

Figure S6.3. Configuration of the commercial screen-printed electrodes used in this work and image of the Boxed Connector for Screen-Printed Electrodes. It can be apreciated the drop on the Surface of the working carbón electrode (images obtained from Dropsens (website:http://www.dropsens.com/en/screenprinted_electrodes_pag.html).

The electrochemical readout was based on square wave voltammetry, in the presence of hydrogen peroxide (H_2O_2) as a substrate and hydroquinone (HQ) as mediator and the horseradish peroxidase enzyme (HRP) conjugated to the readout probes 1 and 2, which were used as electrochemical reporters. The sequences of these oligonucleotides are as follows:

Readout probe 1: HRP-CTTGCGACGTCAGTGGATAGTGTCTTACACGATTT

Readout probe 2: HRP-AGAGTGTACCGACCTC

Readout probe 1 and 2 are complementary to the products of the rolling circle amplification (RCA), as shown in Figure 6.2, panel D.

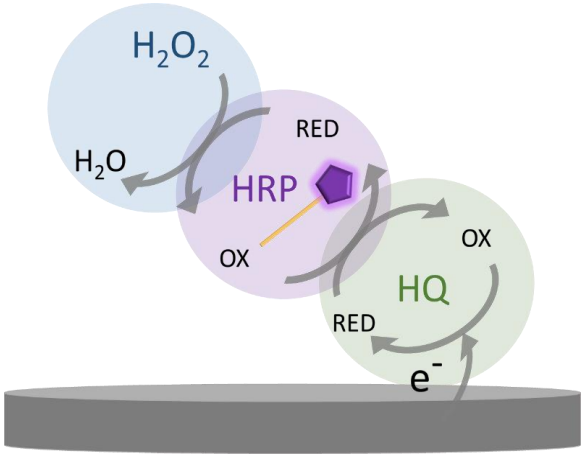

Figure S6.4. Enzymatic mechanism of the HRP enzyme conjugated to the readout probes on the surface of the carbon screen-printed electrode, upon addition of H_2O_2 as a substrate and hydroquinone (HQ) as a mediator.

Due to its high turnover range, horseradish peroxidase enzyme increases the sensitivity of the method amplifying the electrochemical signal. HRP is oxidized catalysing the reduction of hydrogen peroxide to water in the presence of hydroquinone. On the other hand, HRP is reduced again by oxidating hydroquinone to benzoquinone. Therefore, the final readout at the surface of the screen-printed electrode is based on the reduction of the benzoquinone (the oxidized form of HQ) by SWV.

For the square wave voltammetry measurements, 60 µL hydrogen peroxide 0.25 mmol L^{-1} and hydroquinone 1 mmol L^{-1} was added to the sample as substrate and mediator for the HRP enzyme conjugated to the readout probes (as shown in Figure 6.2, panel E). After 2 min of enzymatic reaction, the solution was transferred to the surface of the screen-printed electrode. The potential range used was from 0 to -0.7 V, with a potential step and amplitude of 10 mV, and frequency of 1 Hz. The data were recorded and processed using DropView 2.2 software. The resulting signal is directly proportional to the concentration of HRP, since the enzyme is working at saturation conditions. Hence the higher the hybridization with the readout HRP probe, the higher the cathodic signal.

6.7.3. *E. coli* DNA extraction

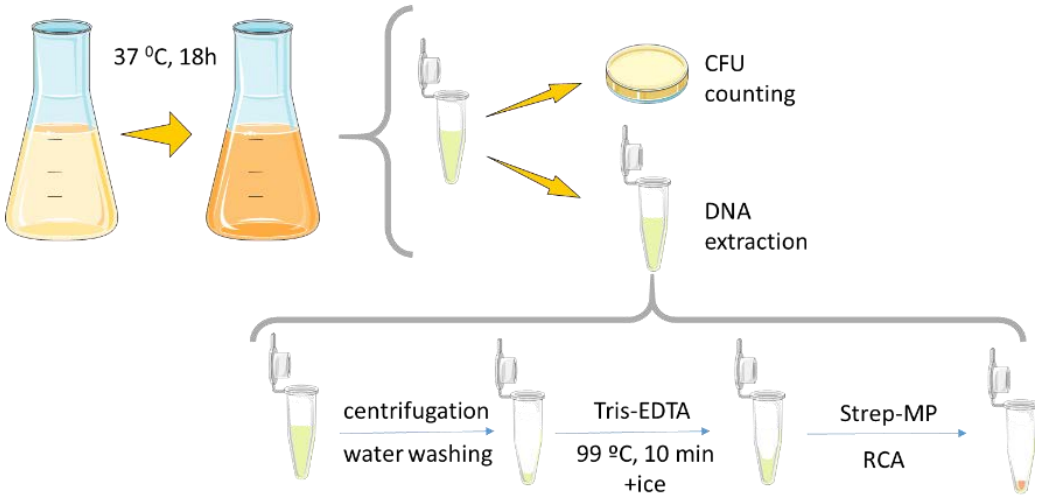

Figure S6.5. *E.coli* culture and DNA extraction process.

6.8. References

1. Russo TA, Johnson JR. Proposal for a New Inclusive Designation for Extraintestinal Pathogenic Isolates of Escherichia coli: ExPEC . J Infect Dis. 2002;181(5):1753–4.

2. Coenye T, Lipuma JJ. [Frontiers in Bioscience 8, e55-67, January 1, 2003] MOLECULAR EPIDEMIOLOGY OF. Front Biosci. 2003;8(4):55–67.

3. George DB, Manges AR. A systematic review of outbreak and non-outbreak studies of extraintestinal pathogenic Escherichia coli causing community-acquired infections. Epidemiol Infect. 2010;138(12):1679–90.

4. Bonacorsi S, Bingen E. Molecular epidemiology of Escherichia coli causing neonatal meningitis. Int J Med Microbiol. 2005;295(6–7):373–81.

5. Breland EJ, Eberly AR, Hadjifrangiskou M. An Overview of Two-Component Signal Transduction Systems Implicated in Extra-Intestinal Pathogenic E. coli Infections. Front Cell Infect Microbiol [Internet]. 2017;7(May):1–14. Available from: http://journal.frontiersin.org/article/10.3389/fcimb.2017.00162/full

6. Russo TA, Johnson JR. Medical and economic impact of extraintestinal infections due to Escherichia coli: Focus on an increasingly important endemic problem.

Microbes Infect. 2003;5(5):449–56.

7. Aggarwal S, Singh H. Approach to urinary tract infections. Indian J Nephrol. 2010;20(2):118.

8. Bergsten G, Wullt B, Svanborg C. Escherichia coli, fimbriae, bacterial persistence and host response induction in the human urinary tract. Int J Med Microbiol. 2005;295(6–7):487–502.

9. Castaño A, Maurer MS. HHS Public Access. 2015;20(2):163–78.

10. Biran D, Ron EZ. Extraintestinal pathogenic escherichia coli. Curr Top Microbiol Immunol. 2018;416(2):149–61.

11. Simmering JE, Tang F, Cavanaugh JE, Polgreen LA, Polgreen PM. The increase in hospitalizations for urinary tract infections and the associated costs in the United States, 1998-2011. Open Forum Infect Dis. 2017;4(1):1–7.

12. Von Baum H, Marre R. Antimicrobial resistance of Escherichia coli and therapeutic implications. Int J Med Microbiol. 2005;295(6–7):503–11.

13. Cho IH, Ku S. Current technical approaches for the early detection of foodborne pathogens: Challenges and opportunities. Int J Mol Sci. 2017;18(10).

14. Zhao Y, Chen F, Li Q, Wang L, Fan C. Isothermal Amplification of Nucleic Acids. Chem Rev. 2015;115(22):12491–545.

15. Lizardi PM, Huang X, Zhu Z, Bray-Ward P, Thomas DC, Ward DC. Mutation detection and single-molecule counting using isothermal rolling-circle amplification. Nature Genetics. 1998. p. 225–32.

16. Henriksson S, Nilsson M. Single-Cell Analysis. Andersson-Svahn H, Lindström S, editors. Hatfield, Hertfordshire, AL10 9AB, UK: Humana Press; 2012. 95–103 p.

17. Antson D-O. PCR-generated padlock probes detect single nucleotide variation in genomic DNA. Nucleic Acids Res. 2002;28(12):58e – 58.

18. Yong Zhang D, Brandwein M, Chun Hung Hsuih T, Li H. Amplification of target-specific, ligation-dependent circular probe. Gene. 1998;211(2):277–85.

19. Russell C, Welch K, Jarvius J, Cai Y, Brucas R, Nikolajeff F, et al. Gold Nanowire Based Electrical DNA Detection Using Rolling Circle Ampli fi cation. ACSNano. 2014;(2):1147–53.

20. Carinelli S, Kühnemund M, Nilsson M, Pividori MI. Yoctomole electrochemical genosensing of Ebola virus cDNA by rolling circle and circle to circle amplification. Biosens Bioelectron [Internet]. 2017;93(October 2016):65–71. Available from: http://dx.doi.org/10.1016/j.bios.2016.09.099

CHAPTER 7

Conclusions

Communicable disease prevention and control relies, to a large extent, on effective and early detection systems. Chain of infection is interrupted if the pathogen agent is detected enabling the isolation and treatment of the affected individuals or eliminating the infection focus.

Conventional methods for the detection of pathogens, such as microbiological culture, are usually time-consuming, laborious, non-amenable to developing point-of-care diagnostic tools, and need skilled personnel.

Many efforts have been made on the development of new technologies to simplify the analytical procedure in order to overcome these limitations. Among the different approaches, biosensors, specially based on electrochemical detection, are promising devices, by combining the sensitivity of the electrochemical readout with the inherent specificity of a biological receptor. Interestingly, the electrochemical signal can be easily achieved with hand-held equipment operated by batteries, as is the case of the most popular commercial example: the glucometer. Other rapid test platforms compatible with low-resource settings are the paper-based lateral or vertical flow, made of inexpensive materials. In this instance, and similarly as the most popular point of care device, the pregnancy test, the results can be read by the naked-eye and are very easy to interpret.

The integration of materials with advanced properties in rapid tests, as is the case of the nanoparticles, has been demonstrated to improve the analytical features of these kind of devices. The improvements in the limit of detection are not only due to the labelling ability (as in the case of the gold nanoparticles) but also to the possibility of isolation or preconcentratation of the analyte from larger volumes of samples (as is the case of magnetic particles).

Despite these progress, nucleic acid amplification techniques are still necessary to reach the challenging limits of detection required for the detection of some pathogens (often few bacteria in large amount of a complex sample). Although different companies have developed portable, battery-powered thermocyclers, it appears that isothermal amplification techniques are good candidates to bring sensitive diagnostic tests in places where the electricity can be a barrier.

Therefore, the present dissertation was focused on key cross-cutting technological challenges that have been identified as technology bottlenecks in rapid diagnostic

test, including the isolation of targets from complex specimens by novel solid-phase preconcentration strategies and advanced materials including magnetic molecularly-imprinted polymeric particles, the enhancement of the analytical signal by isothermal amplification techniques of nucleic acid targets, and their integration in different platforms (mainly biosensors based on electrochemical detection and paper-based strips for optical detection) to achieve analytical simplification.

In order to obtain affordable rapid tests, the design, optimization and fabrication of paper-based devices were considered in chapters 4 and 5 for the detection of pathogenic bacteria in lateral flow format and the non-conventional vertical flow format. These platforms were combined with immunomagnetic preconcentration, double tagging PCR for the detection of *Mycobacterium fortuitum* in haemodialysis water.

The immunomagnetic separation of the mycobacteria from the sample provided results as greater as one order of magnitude compared to the same method of analysis with using centrifugation. This result is due to the fact that they have a very large surface to volume ratio facilitating high capture efficiencies and higher reaction kinetics. Moreover, the washing steps are easier to perform simplifying and reducing the assay time. Regarding to the performance of the different devices, lateral flow showed better LODs, although the time of assay for vertical flow format is only 1 minute compared to the 15 min needed to obtain the results by using lateral flow format. Furthermore, the volume of reagents needed for the vertical flow assay was significantly lower thus reducing the cost of the product. However, it is important to note that both methods, nucleic acid lateral and vertical flow were able to detect concentrations of interest in haemodialysis water.

A nucleic acid lateral flow for the simultaneous detection of *E. coli* and *Salmonella* was also compared with an electrochemical genosensor in chapter 5. Both methods showed similar analytical performance, being able to clearly distinguish between the different bacteria and their single and binary combinations. Although the electrochemical magneto genosensor showed a higher sensitivity and noticeable improved limits of detection, it has to be highlighted the simplicity, low cost and the rapidness of lateral flow. Moreover, the readout equipment can be completely avoided.

In chapter 6 a method for the electrochemical detection of *E. coli* using screen printed electrodes and isothermal amplification is presented. The bacterial DNA was preconcentrated using a specific magnetic probe and then amplified on the magnetic particles by rolling circle amplification (RCA) using a padlock probe. Two different electrochemical readout methods for the RCA amplicons were tested. The first one relied on the labelling of the magnetic RCA product with a digoxigenin probe followed by the incubation with antiDIG-HRP antibody as electrochemical reporter. In the second case, the direct detection with an HRP-probe was performed. This last strategy showed better analytical performance, achieving a limit of detection of as low as 6.7 amol of synthetic DNA and $10^{4.3}$ CFU mL^{-1} of *E.coli* in 120 min and avoiding the use of thermocyclers. This limit of detection could be probably improved by re-amplification of the RCA products by circle-to-circle amplification (C2CA).

Finally, advanced biomimetic materials based magnetic molecular imprinted polymers for the detection of biotinylated molecules were synthesised to be a robust and cheap alternative to the magnetic particles for their use in magneto-actuated assays. It is important to highlight that the cost of synthesis at laboratory scale is almost 300 times lower than the price of the streptavidin-MPs from commercial sources. The resulting material as well as the corresponding non-imprinted polymer were characterized by microscopy techniques including SEM and TEM. These techniques demonstrated the presence magnetite in both materials whereas big porosities corresponding to biotin cavities were only found in magnetic-MIP. Moreover, confocal microscopy demonstrated high binding capacity of the magnetic-MIP towards the biotinylated dye, since the material was completely embedded of the dye.

It is also important to highlight that the confocal study suggested that the binding capacity of the material depends on the size of the biotinylated molecule, since smaller molecules can easily enter in the structure of the magnetic-MIP.

The synthesised material was applied to magneto ELISA for the detection of an amplicon from PCR and for the detection of biotin in a competitive-like format. It showed a surprising good affinity towards biotinylated biomolecules.

In conclusion, the procedures and materials presented in this work are suitable for the rapid and sensitive detection of pathogens. Since screening assays are used on large sample populations, the cost of the assays has been an important factor in order to adjust the strategies presented in this work. The simplicity, cheapness and sensitivity of these technologies flow allow to screen-out of negative samples and thereby to isolate negative from presumptive infected samples. Moreover, the aim of all these technologies is to be applied in other devices meeting the needs of different applications.

CHAPTER 8

Science communications

8.1 List of Publications

Magnetic molecularly imprinted polymer for the isolation and detection of biotin and biotinylated biomolecules

A Ben Aissa, A Herrera-Chacon, RR Pupin, M Sotomayor, MI Pividori. *Biosensors and Bioelectronics* 88, 101-108, 2017

Comparing nucleic acid lateral flow and electrochemical genosensing for the simultaneous detection of foodborne pathogens

A. Ben Aissa, JJ Jara, RM Sebastián, A Vallribera, S Campoy, MI Pividori. *Biosensors and Bioelectronics* 88, 265-272, 2017

Assessment of molecularly imprinted polymers (MIPs) in the preconcentration of disperse red 73 dye prior to photoelectrocatalytic treatment.

JH Franco, A Ben Aissa, GG Bessegato, LM Fajardo, MVB Zanoni, MI Pividori, MDPT Sotomayor. *Environmental Science and Pollution Research* 24 (4), 4134-4143

Magneto actuated biosensors for foodborne pathogens and infection diseases affecting global health

MI Pividori, A Ben Aissa, D Brandao, S Carinelli, S Alegret. *Biosensors for Security and Bioterrorism Applications*, 83-114, 2016

8.2 Conferences and congresses

- Biosensors 2018. 28th Anniversary World Congress on Biosensor. 12-15 June 2018. Miami, FL, USA.
- XXXVI Reunión bienal de la RSEQ. 25-29 June 2017. Sitges, Spain
- Setena edició de les Jornades Doctorals del Departament de Química de la Universitat Autònoma de Barcelona. 31 May- 2 June 2017. Bellaterra, Spain.
- 5th International Conference on Bio-sensing Technology. 7-10 May 2017. Riva del Garda, Italy.

- Biosensors 2016. 26th Anniversary World Congress on Biosensor. 25-27 May 2016. Gothenburg, Sweden.
- XX SIBEE "XX Simpósio Brasileiro de Eletroquímica e Eletroanalítica". 17-21 August 2015. Uberlandia, Brasil.
- XX Trobada Transfrontera de Sensors I Biosensors Conference. 1-2 October 2015. Perpignan, France.

8.3. Workshops and courses

- 4th Bioanalytical Nanotechnology school (www.bantschool.org). 25-29 January 2016. São Luís, Maranhão, Brasil.

- Summer school "Magnetic particles based platforms and bioassays". 30th June-3rd July, 2014. Bellaterra, Spain.

8.4. Others merits

- Second award "VII Jornades Doctorals del Departament de Química", Universitat Autònoma de Barcelona. June 2017